Stability and Chaotic Behavior of Various Populations using Mathematical Modelling and Numerical Simulation

THESIS

Submitted in partial fulfilment of the requirements for the degree of

DOCTOR OF PHILOSOPHY

by

SAJAN
(2018PHXF0433P)

Under the Supervision of

PROF. BALRAM DUBEY

BIRLA INSTITUTE OF TECHNOLOGY AND SCIENCE, PILANI

OCTOBER, 2023

BIRLA INSTITUTE OF TECHNOLOGY & SCIENCE, PILANI

CERTIFICATE

This is to certify that the thesis titled **"Stability and Chaotic Behavior of Various Populations using Mathematical Modelling and Numerical Simulation"** submitted by **Mr. Sajan**, ID No. **2018PHXF0433P** for the award of Ph.D. of the institute embodies original work done by him under my supervision.

Signature of the Supervisor
Name: **PROF. BALRAM DUBEY**
Designation: **Professor**

Date: **October 2023**

Acknowledgments

First and foremost, I sincerely thank my Ph.D. supervisor, Prof. Balram Dubey, who has mentored me throughout this entire process and has been an incredible source of moral support, inspiration, and devotion. His support of my original study and fresh concepts will undoubtedly help me to succeed in the long run.

I am grateful to BITS Pilani's Vice-Chancellor, Director, Dean Academic (AGSRD), and Registrar for allowing me to obtain a challenging position in an area that suited my qualifications and allowed me to apply my skills to establish my merit. They also gave me access to facilities required for research and a healthy atmosphere, for which I am grateful.

I owe a note of appreciation to Prof. Devendra Kumar, Head of the Department of Mathematics, and to Ex-HoD Prof. B. K. Sharma for allowing me to work in this department and helping me complete this work on schedule and through the entire process. I want to thank the whole faculty and staff of the mathematics department for their unwavering support and sincere interest in their students' learning.

I am also thankful to the doctoral advisory committee (DAC) members Prof. Ashish Tiwari and Prof. B. K. Sharma for their valuable comments and constructive suggestions during my Ph.D. research work.

I wish to express my sincere thanks to the late Prof. J. B. Shukla, IIT Kanpur, India, for his significant contribution to enrich my understanding of mathematical modeling in ecology. I thank Dr. Sourav Kumar Sasmal, IIT Roorkee, for his invaluable discussions and research ideas.

I heartily thank my respected senior, Dr. Ankit Kumar, who helped and inspired me throughout my research. I would also like to thank my beloved juniors Ashvini, Anshu, Arjun, and Masoom, with whom I discussed essential concepts and learned many things.

I am very thankful to my senior, Dr. Kapil Kumar Chaudhary, who always cared for me like a brother and supported me emotionally when needed. I also thank my batchmates who made this journey enjoyable and to all my lab mates for supporting me directly or indirectly.

I acknowledge my sincere thank to my respected father, Mr. Darshan Lal Phutela; mother, Mrs. Urmila Rani; elder brother (Lovepreet); sister-in-law (Preet), and my loving nephew (Diljaan) for their enormous love, unquestioning support. I don't envisage a life without their love and blessings.

I thank my wife, Poonam, whom I may have neglected way too much during my research work, for her continual support and love.

I am thankful to Council of Scientific and Industrial Research (CSIR), New Delhi for financial assistance as a part of this work.

Place: BITS Pilani
Date: October 2023

Sajan
(Department of Mathematics)

Abstract

One of the most fundamental ecological connections that exist in nature is the prey-predator relationship. The survival of the species and the balance of ecosystems depend on this interaction. The prey-predator interaction is crucial to ecology for various reasons, some of which are described herein. Population Control: predators help in population control by reducing the number of prey species. Without predators, prey species populations could increase out of control, resulting in overgrazing, deforestation, and other detrimental effects on the ecosystem. Food Web: a crucial part of the food web is the link between prey and predator. The absence of a predator can have a cascading effect on the ecosystem as a whole. Co-evolution: a struggle for survival between prey and predators. To avoid being eaten, prey species develop defence mechanisms like camouflage, while predators develop tactics to counter these defence mechanisms. Both species' evolution is driven by this process, resulting in the emergence of sophisticated structures and behaviours.

One of nature's most well-known examples of the predator-prey dynamic is the link between phytoplankton and zooplankton. Growing phytoplankton populations also enhance zooplankton populations because they give them more food. As a result of zooplankton eating more phytoplankton, their abundance declines. As zooplankton populations increase, so does their need for food, which eventually causes a fall in zooplankton populations due to a lack of food. In turn, this enables phytoplankton to recover and grow once more. Since both groups depend on one another for existence, this interaction is essential to preserving the equilibrium of aquatic ecosystems. The marine and freshwater food chains would be significantly impacted if either population were to go extinct, devastatingly impacting the entire ecosystem.

Many environmental factors can impact the prey-predator relationship in different scenarios. Some of these are; fear induced by the predator in prey, the antipredator behaviour shown by prey against a predator in response to the induced fear, additional food to predator, the toxic chemicals released by dense phytoplanktons, carry-over effects of the induced fear, the presence of seasonality in the physical parameters, different types of time lags. All the above-mentioned ecological components play a significant role in deciding the dynamics of a prey-predator system, particularly in a phytoplankton-zooplankton system. Considering all these assertions, we have proposed and investigated some prey-predator models as an ordinary differential equation with or without time delays, incorporating several physical parameters. We have analysed the dynamics of these models using the stability theories of non-delayed and delayed models, bifurcation theory, chaos theory, and theory used to deal with seasonal models. Extensive numerical

simulations are done to validate theoretical results. We divide this thesis into six chapters, whose abstracts are given below.

In Chapter 1, we have presented a brief introduction about the problems on which we have worked. It consists of some biological preliminaries, functional response with its major types, mathematical definitions and tools which are used frequently throughout this thesis. A quick overview to the bifurcation theory, delay differential equations, and non-autonomous differential equations is also included in this chapter.

Recent studies demonstrate that the density of prey population is not only affected by direct killing by the predator, but the fear in prey caused by predator also reduces it by cutting down the reproduction rate of prey community, and prey shows anti-predator behavior in response to this fear. Taking these facts in account, in Chapter 2, we propose a prey-predator model with fear in prey due to predator and anti-predator behavior by prey against the predator with fear response delay and gestation delay. It is assumed that the predator consumes prey via simplified Holling type IV functional response. We evaluate the equilibrium points and study the local and global stability behavior of the system around them. It is observed that our system undergoes Hopf-bifurcation with respect to the fear parameter. Moreover, the system shows the attribute of bi-stability involving two stable equilibriums. Further, we study the dynamics of the delayed system by incorporating fear response delay and gestation delay. We observe that the delayed system suffers Hopf-bifurcation with respect to both delays. Using the normal form method and center manifold theory, the direction and stability of Hopf-bifurcation are studied. Chaotic behavior for delayed system is observed for large values of fear response delay.

Phytoplankton-zooplankton dynamical interactions have significant effects on terrestrial as well as aquatic animals. Both these planktons collectively form the base for various food chains operating under the water. Phytoplankton acts as a prime food for zooplankton, where fish and large marine animals consume both these planktons. Thus, phytoplankton-zooplankton interaction is a topic of high interest among the interrelationships related to marine habitats. In Chapter 3, we attempt to study the dynamics of a three-dimensional system with three types of plankton; non-toxic phytoplankton, toxic producing phytoplankton, and zooplankton. We assume that both non-toxic and toxic phytoplankton are consumed by zooplankton via Beddington–DeAngelis and general Holling type IV responses, respectively. We also incorporate gestation delay and toxic liberation delay in zooplankton's interactions with non-toxic and toxic-phytoplanktons correspondingly. Firstly, we have studied the well-posedness of the system. Then we analyze all the possible equilibrium points, their local and global asymptotic behaviour. Further, we assessed the conditions for the occurrence of Hopf-bifurcation and transcritical bifurcation. Using the normal form method and center manifold theorem, the conditions for stability and direction of Hopf-bifurcation are also studied. Various time-series, phase

portraits, and bifurcation diagrams are plotted to confirm our theoretical findings. From the numerical simulation, we observe that a limited increase in inhibitory effect of toxic phytoplankton against zooplankton can support zooplankton's growth, and rising predator's interference can also boost zooplankton expansion in contrast to nature of Holling type IV and Beddington–DeAngelis responses, respectively. Next, we notice that on variation of toxic liberation delay, the delayed system switches its stability multiple times, and becomes chaotic. Further, we draw Poincare section and evaluate maximum Lyapunov exponent in order to verify the delayed system's chaotic nature.

In Chapter 2 we studied the prey-predator model with fear in prey due to predator and anti-predator behavior and in Chapter 3 we studied the dynamics of a three-dimensional system with three types of plankton; non-toxic phytoplankton, toxic producing phytoplankton, and zooplankton. Now, in Chapter 4, we propose to explore the dynamics of a phytoplankton-zooplankton-fish system, with fear-induced birth rate reduction in the middle predator by the top predator and an additional food source for the top predator fish. Phytoplankton-zooplankton and zooplankton-fish interactions are handled using Holling type IV and II responses, respectively. Firstly, we prove the well-posedness of the system, followed by results related to the existence of possible equilibrium points. Conditions under which a different number of interior equilibria exist are also derived. We also show this existence numerically by varying the intrinsic growth rate of phytoplankton species which demonstrates model's vibrant nature from mathematical point of view. Further, we did the local and global stability analysis around the above equilibrium points, the transversality conditions for the occurrence of Hopf bifurcation and transcritical bifurcation are established. We observe numerically that for low levels of fear, the system behaves chaotically, and as we increase the fear parameter, the solution approaches to a stable equilibrium by the route of period halving. The chaotic behavior of the system at low levels of fear can also be controlled by increasing the quality of additional food. To corroborate our findings, we constructed several phase portraits, time-series graphs, one and two-parametric bifurcation diagrams. Computation of largest Lyapunov exponent and sketch of Poincare map verify the chaotic character of the proposed system. On varying the parametric values, the system exhibits phenomena like, multistability and the enrichment paradox which are the basic qualities of non-linear models.

Due to induced fear of predation, there can be a reduced reproduction rate of zooplankton species, and the effect of this non-lethal interconnection can be carried over to subsequent seasons or generations. In the Chapter 5, we tend to analyse the role of fish-induced fear in zooplankton with its carry-over effects (COEs) and a corresponding discrete delay (COE delay) in a phytoplankton-zooplankton-fish population model. We use Holling type IV and II functional responses to model the phytoplankton-zooplankton and zooplankton-fish interplay,

respectively. In the well-posedness of the present biological system, firstly, we evaluate an invariant set in which the solutions of the model remain bounded. Then we prove its persistence under some ecologically well-behaved conditions. Next, we establish the conditions under which the different feasible equilibrium points exist; the existence of various interior equilibria is also set up here. To study the system's dynamical behavior, local and global stability analyses for the equilibria mentioned above are also discussed. Further, the theoretical conditions for Hopf and transcritical bifurcations in non-delayed and delayed models are determined. Impacts of non-lethal parameters, fear, and its carry-over effects, on the population densities are studied analytically and supported numerically. For intermediate values of COEs parameter, we notice that the system behaves chaotically, and decreasing (or increasing) it to low (or high) values, solution converges to interior equilibrium point through period-halving. Calculation of the largest Lyapunov exponent and drawing of Poincar'e map validate the chaotic nature of the system. The chaos for medium values of COEs parameter can also be controlled by decreasing the fear parameter. Next, we numerically validate the theoretical result for transcritical bifurcation. We also note that our system shows the phenomenon of enrichment of paradox, and the attribute of multistability. In the delayed model, we observe that increasing delay can eliminate chaotic oscillations through amplitude death phenomenon.

The environmental toxins released by different external sources also affect the phytoplankton-zooplankton dynamics. In Chapter 6, we proposed a model to explore the kinetics of a nutrient-phytoplankton-zooplankton-environmental toxins (NPZT) system. The defence mechanism of phytoplankton against zooplankton is reflected through modified Holling type IV response, whereas the consumption of nutrients by phytoplankton is outlined by Holling type II response. The external toxins are assumed to have the capability of reducing the birth rate of phytoplankton species after coming into contact with their cells. To make our model more pragmatic, seasonal variation in the parameters is also taken into account. Firstly, we do the analysis related to the autonomous model (non-seasonal) like; its boundedness, existence of equilibrium points, their stability analysis, and occurrence of Hopf-bifurcation. Further, for the non-autonomous model (seasonal), we analyze the existence of positive periodic solution, its global stability. Through numerical simulations, we observe that for the non-seasonal model, increasing the rate of suppressing phytoplankton's growth by environmental toxin, and rate at which environmental toxin is added to system make it unstable through Hopf-bifurcation. These oscillations can be removed by raising phytoplankton's inhibitory effect against zooplankton, and this increment also leads to the extinction of the zooplankton population, making zooplankton free equilibrium a stable one. Both models, non-seasonal as well as seasonal manifest different types of multistability, and this is an exciting character associated with non-linear models. We also note that the inclusion of seasonality in our system promotes the coexistence of all populations. Further, through numerical simulations, we show that making some of the parameters seasonal

can cause the emergence of chaos in the system. To verify chaos, we sketch the Poincaré map and evaluate the maximum Lyapunov exponent. The seasonal model also shows the switching of stability through different periodic and chaotic windows on varying the maximum intrinsic growth rate for phytoplankton, and contact rate between environmental toxin and phytoplankton. To substantiate our results, we picture several time-series graphs, basins of attraction, one and two-parametric bifurcation diagrams. Thus we expect that the present work can assist biologists and mathematicians in studying nutrient-plankton systems in a more detailed and realistic manner. This study can also help researchers in the estimation of non-seasonal as well as seasonal parameters while studying these types of complex non-linear models.

Contents

List of Figures

List of Tables

Dedicated To

My Parents, for always supporting me

My Wife, for encouraging me to complete this thesis

Chapter 1

Introduction

1.1 General introduction and literature review

The dynamics of an ecosystem, which provides information about the population increase within that specific ecological community, is a crucial component of an ecosystem. The basis for ecological research is the investigation of prey-predator interactions. Because they offer a framework for comprehending how populations of predators and prey interact with one another and their environment, these models are crucial to ecology. A system of ordinary differential equations or delay differential equations, which are often nonlinear and can exhibit a wide range of behaviours, such as oscillations, bifurcations, and chaos, can be used to model the dynamics of the populations. Strategies for managing pest populations are also developed using prey-predator models. Prey-predator models can assist in the understanding of the effects of pesticide use on both predator and prey populations, as well as the development of more environmentally sustainable pest management methods. Investigating this connection enables us to reveal numerous ecological phenomena. The rate of progress for these individuals depends on a number of factors, including age, weather conditions, the carrying capacity of the infrastructure, and how each specie interacts with the others. This motivates us to research the variables that influence system complexity. First of all, Malthus [1] is credited with having done it. His theory was largely built around the idea that population growth is exponential since it is proportional to the current population. Due to the fact that each habitat has a finite capacity to support its inhabitants, this assumption became the main point of criticism for his hypothesis. After that, Verhulst [2] proposed the logistic growth model in which he incorporated the intraspecific interactions between the members of the population. Population dynamics made significant progress in Lotka's later publication, Elements of Physical Biology [3]. He presented the prey-predator model as a set of two non-linear differential equations that describe the interaction of two species. The work of Lotka was then expanded upon by Volterra in his book [4]. The prey-predator model's beginnings and early studies are briefly discussed in [5]. Every element of

living things exhibits prey-predator interactions, which motivates us to investigate their many subsets. This system became a focal point of ecological research as a result of the inspiration. Several academicians have conducted extensive research in this area, which include [6, 7, 8, 9, 10].

How the predator consumes the prey is a crucial issue in a prey-predator system. Since a change in how they interact might alter the system's dynamics as a whole. We can study the dynamics of the model more realistically by using the term "Functional response," which provides the predator's per capita eating rate on prey. There are many different kinds of functional responses and a significant amount of study has been done employing them, Holling type II in [11], Holling type III in [12], Holling type IV in [13], Beddington-DeAngelis in [14], Crowley-Martin in [15, 16], Hassell-Varley in [17], Leslie–Gower in [18].

Every biological phenomenon includes a time delay. Ecology, population biology, and epidemiology are just a few of the many disciplines in that delay differential equations (DDEs) have applications. DDEs can be used to demonstrate the impact of delay in an ecological model. The nature of delayed models is significantly more realistic. Comparatively speaking, a delay differential equation exhibits substantially more complicated behaviour. By including temporal delays into ecological models using delay differential equations, it is possible to portray biological events more accurately and realistically. These models can aid in our comprehension of the dynamics of ecological systems and help us anticipate how they will respond to environmental change. One of the key properties of DDEs is their propensity to exhibit complicated dynamics, such as oscillations, chaos, and bifurcations. These dynamics might be the result of the interplay between the time delay and the other model parameters. There are different kinds of delay that can be used in a prey-predator model to make it more sound, like; gestation delay[15], negative-feedback delay [19], maturation delay [20, 21]. A comprehensive detail about delay differential equations is present in the literature [22]. Gakkhar and Singh [23] investigated the complex kinetics of a prey-predator system with Holling type II response with the inclusion of multiple delays. They explored the existence of periodic solution through Hopf bifurcation and the chaotic dynamics of the delayed system. Banerjee and Takeuchi [21] studied a stage structured prey-predator model with maturation delay. They argued that although the inclusion of delay in most of the prey-predator models make them unstable, but they showed how the introduction of a delay in their model made it stable. They evaluated the conditions for oscillatory and stable coexistence of prey and predator in presence of weak as well strong Allee effect.

The steady states of dynamical systems undergo both qualitative and quantitative changes, which are explained by the bifurcation theory. The primary types of local bifurcations are Hopf, transcritical, saddle-node, Bogdanov-Takens, Bautin bifurcation whereas homoclinic, and heteroclinic are global bifurcations [24]. The solutions of chaotic systems are particularly sensitive to the initial population densities, for instance, and the chaos theory reveals many new elements

of a chaotic system and explains its different unusual behaviours. The fundamental difficulties in managing a chaotic system are the rapid changes in population densities of participating species that might occur as a result of chaos in a dynamical model. This makes it exceedingly difficult to predict how the chaotic model will behave. Hastings *et al.* [25] provided fine detail regarding chaos theory and its elements, such as a weird attractor, Poincar'e map, Lyapunov exponents, etc. Many methods [26] , including the determination of the Lyapunov exponent, the power spectral density, the fractal dimension of the map, and the recurrence plot, are used to demonstrate the presence of chaos in a system.

Since it is essential for both the predator and the prey to survive, induced fear is a critical part of the predator-prey relationship. Prey animals frequently experience fear-induced reactions, which aid them in spotting and avoiding predators while aiding predators in effectively pursuing and catching their prey. The role of induced fear in the predator-prey relationship has been the subject of various research. Lima and Dill [27] investigated the effect of predator-induced fear on the foraging behavior of prey. Their study discovered that when prey animals perceive the presence of a predator or the threat of an approaching attack, they alter their foraging behaviour. Caro [28] examined the role of coloration in predator-prey relationships. According to this study, many prey species have evolved colours that resemble their surroundings, making them less detectable to predators. The bright and noticeable coloration of some prey species, on the other hand, has developed to serve as a warning to predators of their unappealing or poisonous nature. Furthermore, a study by Kats and Dill [29] shows that chemical signals play an important role in predator-prey interactions. According to their work, prey species can recognize chemical signals given off by predators and modify their behaviour accordingly. For instance, a predator's scent may compel prey to cease foraging, seek cover, or freeze, decreasing their visibility to the predator. Wang *et al.* [30] worked on a prey-predator model in which they modelled the induced fear in the form of a mathematical function, having certain properties. Their mathematical studies demonstrate that strong anti-predator responses or high levels of fear can stabilise the predator-prey system by eliminating the possibility of periodic solutions. An analysis of a plankton-fish system with fish-induced fear and zooplankton refuge was conducted by Kaur *et al.* [31]. They demonstrated that raising fear can inhibit periodic oscillations, which stops planktonic blooms. An interested reader can find numerous publications [32, 33, 34, 35] to examine the prey-predator system involving the predator-induced fear effect.

A significant element that might affect the dynamics of prey-predator systems is the accessibility of additional food sources. Predators in many habitats can eat a variety of food sources in addition to their primary prey. The population dynamics of predator and prey can be affected by this additional food, which can also change the intensity of interactions between them. The impact of predation on the main prey can be reduced in prey-predator systems as a result of

additional food. Predators may consume less of the primary prey when they have access to additional food sources, which can result in increased prey population densities. Gosh *et al.* [36] studied additional food's impact for predator on the prey-predator dynamics with prey refuge. They show that high quantity and high quality of additional food help to sustain oscillatory coexistence of species. They noted that predator extinction in ecological systems with high prey refuge can be avoided by the supply of additional food to them. Srinivasu *et al.* [37] investigated the effects of providing additional food on the system's dynamics in terms of biological pest management. They discovered that by varying the quantity and quality of this food, they could control the prey population and eradicate it. They observed that providing additional food could alleviate oscillations in the system or create them if they are absent. Nazmul *et al.* [38] analyzed the combined effects of fear, additional food, and refuge in a prey–predator system with Crowly–Martin type functional response. They found that the existence of prey refuges and increased food for predators are known to have possible effects on maintaining prey and predator in their respective habitats. However, the fear of predators significantly impacts the densities of prey and predator populations. When increasing either the prey's growth rate or the predator's growth rate due to other food, the system first experiences a supercritical Hopf-bifurcation and, subsequently, a subcritical Hopf-bifurcation. After a certain point, increasing the quality or amount of additional food leads to the extinction of prey species and a sharp increase in predators.

The phrase "carry-over effect" was introduced due to repeated clinical studies; carry-over effects result from an individual's background and prior experiences and might affect their current performance [39]. When the previous habitat lost due to a lethal or non-lethal factor was of low quality, the carry-over effect has a positive influence on the population, but it might have the opposite effect when the lost habitat was of high quality. As a result, the change in population will rely on (i), which demographic factors generate strong carry-over effects throughout this period, and (ii) not just the quantity but also the quality of lost habitat. There is experimental proof that the carry-over effects can manifest in a single season in amphibians, insects, marine invertebrates, and other organisms [40, 41, 42]. Consequently, there is a growing trend to include carry-over effects in mathematical modeling and empirical research, as evidenced by the publications [43, 44, 45]. Hence, incorporating carry-over effects into a population model can aid in understanding the potential connection between the cost of reproduction and trade-offs in life histories.

Non-autonomous prey-predator models are mathematical models that describe the dynamics of a prey-predator system where the physical parameters involved in this model depend on time-varying factors such as seasonal changes, weather conditions, or human interventions. Non-autonomous prey-predator models are useful in understanding the complex interactions between predator and prey populations in real-world ecosystems, and in predicting the effects

of environmental changes or human interventions on these populations. A model becomes difficult when seasonality is incorporated, so we recommend reading some of the papers [46, 47] to discover the methods for investigating the permanence, presence of periodic solutions, and their global attractivity. Mandal *et al.* [48], using the methods described in [46, 47, 35], investigated how phytoplankton and zooplankton interacted with the presence of environmental contaminants and seasonality. They investigated both seasonal and non-seasonal models. With relation to various parameters, they conducted sensitivity and bifurcation analyses. Also, they looked at the related slow-fast model, which revealed the existence of bursting oscillations. Saswati *et al.* [49] worked on a eco-epidemiological model with virally infected toxic phytoplankton and zooplankton with the inclusion of a time lag for viral replication. They considered replication of free viruses as seasonally forced and observed the chaotic behavoiur of this seasonal system which reflects the arise of harmful blooms. Mondal *et al.* [50] explored the roles of refuge, fear, and hunting cooperation on a prey-predator system's dynamics, while harvesting the predator population at non-linear rate. They analyzed the non-seasonal and seasonal model analytically as well as numerically. They observed that if the non-seasonal system is unstable, then the seasonal variation of the growth rate of prey can induces higher periodic oscillations whereas when it is stable then one and two periodic solutions are induced.

1.2 Objectives of the thesis

The goal of this thesis is to address several issues involving biological populations subject to ecological stability and to investigate numerous traits that substantially impact the ecosystem's stability. With the above literature review, we identified some gaps which we state as objectives of this thesis.

(i) To study the stability switching and chaos in a multiple delayed prey-predator model with fear effect and anti-predator behavior.

(ii) To study the chaos control in a multiple delayed phytoplankton-zooplankton model with group defence and predator's interference.

(iii) To study a phytoplankton-zooplankton-fish model with chaos control: In the presence of fear effect and an additional food.

(iv) To study the chaotic dynamics of a plankton-fish system with fear and its carry over effects in the presence of a discrete delay.

(v) To study the seasonal effects of environmental toxin on nutrient-plankton system.

1.3 Biological preliminaries

1.3.1 Phytoplankton

The foundation of the marine food chain is made up of microscopic, free-floating aquatic plants called phytoplankton. Almost all bodies of water, including rivers, ponds, lakes, and oceans, contain these species. Around half of the world's oxygen is produced by phytoplankton, which also significantly affects climate change on earth [51]. Being photosynthetic organisms, phytoplankton uses light and nutrients to produce energy and expand. Although certain species can form colonies, they are mainly single-celled. From small coccolithophores to bigger diatoms and dinoflagellates, phytoplankton comes in a variety of sizes and shapes. Because they serve as the main food supply for zooplankton, which in turn feeds larger species like fish, whales, and seabirds, phytoplankton are essential to the marine food web. Marine ecosystems can be significantly impacted by the quantity and health of phytoplankton communities, and shifts in these populations can point to broader environmental changes. Despite being tiny, phytoplankton play a crucial role in maintaining the health of the earth. They assist in preserving atmospheric oxygen levels and controlling the climate on a global scale. Therefore, it is crucial for our comprehension of the earth's ecosystems and the effects of climate change that we comprehend and monitor these organisms.

1.3.2 Zooplankton

An assortment of tiny creatures known as zooplankton can be found in lakes, rivers, and oceans. These are small organisms that drift with the currents of the ocean. Since they serve as predator for phytoplnakton so they are crucial components of aquatic food webs. Zooplankton includes a wide range of organisms, from little ones like protozoa and rotifers to bigger ones like crabs and jellyfish. They are important to aquatic environments despite their modest size because they serve as the main food supply for many fish and other aquatic species. Holoplankton and meroplankton are the two primary categories of zooplankton. Meroplankton only spend a portion of their life cycle in the water column, whereas holoplankton spend their full life cycle there. An essential part of the global carbon cycle is played by zooplankton. They eat a lot of organic material and aid in moving nutrients from the surface to deeper waters, where other creatures can use them. Zooplankton, despite their diminutive size, are essential to aquatic ecosystems. They play a crucial role in preserving the health of our oceans, lakes, and rivers by sustaining the base of the food chain and assisting in the transportation of nutrients.

1.3.3 Species

A group of organisms that have similar traits and may breed with one another to create fertile offspring is referred to as a species in biology. The study of biology, ecology, and evolution all revolve around the concept of species, which is essential to understanding the variety of life on Earth. Several criteria, including as morphology, genetics, behaviour, and ecological habitat, have been employed to describe species as they have developed over time. The biological species concept, which defines a species as a collection of organisms that can interbreed and produce healthy offspring under natural conditions but are reproductively isolated from other groups, is currently the most frequently recognised definition of a species.

1.3.4 Food chain

A food chain is a sequence of living creatures that illustrates the flow of nutrients and energy as one organism consumes another. Plants are at the bottom of a conventional food chain, where they are devoured by herbivores, which in turn eaten by carnivores. By converting dead plants and animals into nutrients that can be utilised by other organisms, decomposers like fungus and bacteria play a significant part in the food chain. The term "trophic level" refers to each level of the food chain and denotes a distinct phase in the movement of nutrients and energy. Understanding food chains is crucial for comprehending the links and functions of many species in an ecosystem.

1.3.5 Ecosystem

A community of living things that interact with one another and their surroundings, such as plants, animals, and microorganisms, is referred to as an ecosystem. Abiotic and biotic elements make up an ecosystem's two main parts. The non-living components of an ecosystem are known as abiotic variables, and examples include temperature, water, air, soil, and sunlight. These elements greatly influence how the environment is shaped and which animals may coexist there. The living components of an ecosystem, such as all the plants, animals, and bacteria, are known as biotic factors. These creatures work together and with the abiotic elements to create intricate webs of interconnected communities. An ecosystem's health and efficiency depend on both biotic and abiotic components. The ecology as a whole may be significantly impacted by changes to either component.

1.4 Functional response

The relationship between a predator's rate of prey intake and the quantity of prey present in a certain environment is referred to as a functional response. The sort of functional response exhibited by a predator is influenced by a number of variables, including handling time, encounter rate, search efficiency, the predator's feeding habits, prey escape ability, prey habitat's structure and the surrounding environment. Predicting the dynamics of prey-predator systems and the effects of predation on prey populations requires an understanding of functional response.

Holling [52] discussed four types of functional responses, known as Holling type I, II, III, and IV. The Type I functional response presupposes that the intake rate increases linearly with food density. The linear rise is based on the supposition that the consumer's processing time for food items is minimal or that eating does not interfere with the food search. Mathematically, this response can be written as

$$F_1(x) = mx,$$

where, m is the maximum attack rate. This functional response is also known as the law of mass action. Holling type II (or Michaelis-Menten) response is reflected by an asymptotic curve, in which the rate of consumption (number of prey per predator) increases and approaches a maximum value asymptotically. The mathematical form for this response is

$$F_2(x) = \frac{mx}{1+hmx},$$

where, m is the maximum attack rate and h is handling time taken by predator per prey. In this response rate of consumption increases rapidly when prey quantity is abundant and finally attains its maximum saturated value, after which it becomes constant. Holling type III response is sigmoid in which the consumption rate is similar to Holling type II at high prey density but is low when the prey population size is small. Its sigmoid nature is due to the generalist nature of predator who may switch from one food to another when the first one is not abundant. The type III response can be written in the following form

$$F_3(x) = \frac{mx^2}{1+hmx^2}.$$

Andrew [53] proposed a response of the type

$$F_4(x) = \frac{mx}{x^2+\alpha x+\beta},$$

which is equivalent to Holling type *II* response at low prey population concentration and involves an inhibitory effect at high prey population. A situation in a prey-predator interaction can arise when prey species form a group against the predator species as an act of anti-predator behaviour. The phytoplankton-zooplankton interaction [54] is a particular example of this in which highly dense phytoplankton starts releasing the toxic chemicals against zooplankton, due to which zooplankton avoids the areas of these highly dense phytoplankton, reducing their consumption. Mathematically, this response can be presented as

$$F_5(x) = \frac{mx}{\frac{x^2}{j} + x + \beta},$$

where, j gives the tolerance or predator's immunity from, the prey. Here, m is the maximum attack rate, and β is half saturation constant without inhibitory effect. This response, when $j \to \infty$, gets reduced to Holling type *II* response [55]. This functional response reflects the group defence mechanism of prey against the predator, which results in a reduction in predation when prey populations are high.

All above mentioned responses are only prey dependent but Arditi and Ginzburg [56] argues that the consumption rate may decrease as the predator population rises. They proposed the ratio dependent function which depends upon both the densities of prey as well of predator, and be represented in the from of $f(\frac{x}{y})$. Beddington [57] gave functional response (known as Beddington-DeAnelis response) of the form

$$F_6(x) = \frac{mx}{1 + mhx + by},$$

where m is the maximum attack rate, h is handling time, and b can be interpreted as magnitude of interference among predators.

1.5 Definitions and mathematical preliminaries

In most of cases, the physical or ecological phenomena can be described by the ordinary differential equations of the form

$$\frac{dy}{dt} = f(y),\ y(t_0) = y_0, \tag{1.1}$$

where $y = (y_1, y_2, ...y_n),\ f = (f_1, f_2, ...f_n)$, the enough smoothness of f ensures the existence and uniqueness of solution of (1.1) whereas t belongs to an interval containing t_0 such that $y(t_0) = y_0$ and $\frac{dy(t)}{dt} = f(y(t))$.

Definition 1.5.1. *The solution $y(t, t_0, y_0)$ of (1.1) is called a stable solution if for every $\varepsilon > 0\ \exists$ a $\delta > 0$ and t_1 such that for each solution $\bar{y}(t) = y(t, t_0, \bar{y}_0)$ of (1.1), the inequality $||\bar{y}_0 - y_0|| < \delta$*

implies $||\bar{y}(t) - y(t)|| < \varepsilon \ \forall t > t_1$. *In a simple manner, we can say that a solution* $y(t, t_0, y_0)$ *is said to be locally stable if any other solution started in some* $\delta-$ *nbh. of* y_0 *continue to stay in* $\varepsilon-$ *nbh. of* $y(t)$ *after a certain amount of time.*

Definition 1.5.2. *The solution* $y(t, t_0, y_0)$ *of (1.1) is called a asymptotic stable solution if* $\exists$ *a* $\delta > 0$ *such that for each solution* $\bar{y}(t) = y(t, t_0, \bar{y}_0)$ *of (1.1), the inequality* $||\bar{y}_0 - y_0|| < \delta$ *implies* $||\bar{y}(t) - y(t)|| \to 0$ *as* $t \to \infty$. *In a simple manner, we can say that a solution* $y(t, t_0, y_0)$ *is said to be a locally asymptotic stable solution if any other solution started in some* $\delta-$ *nbh. of* y_0 *converges to* $y(t)$ *as time approaches to infinity.*

Definition 1.5.3. *The solution of (1.1) is called unstable if it not stable.*

Definition 1.5.4. *A point* $\hat{y} \in R^n$ *is called an equilibrium point or stationary point or steady state of (1.1) if* $f(\hat{y}) = 0$. *This equilibrium is known as hyperbolic equilibrium point if none of the eigenvalue of* $Df(\hat{y})$ *(Jacobian of* f *evaluated at* $\hat{y}$*) have zero real part.*

Definition 1.5.5. *A steady state* $\hat{y}$ *of (1.1) is known as source (unstable) or sink (stable) if all the corresponding eigenvalues of* $Df(\hat{y})$ *have positive or negative real parts, respectively. It is called a saddle point if it is hyperbolic and* $Df(\hat{y})$ *has at least one eigenvalue with negative and one with positive real part.*

Definition 1.5.6. *A steady state* $\hat{y}$ *of (1.1) is said to be globally asymptotically stable if any solution started from a bounded domain converges to* $\hat{y}$.

Definition 1.5.7. *A closed solution curve of (1.1) is called as a periodic orbit or cycle if it is not a steady state. The stability or asymptotic stability or instability of this periodic orbit can be employed from Definition 1.5.2.*

Definition 1.5.8. *The trajectory or orbit* $\phi(t_0)$ *of (1.1) is defined as*

$$\phi(t_0) = \{y \in R^n : y = y(t, t_0, y_0), t \in R\}$$

where $y(t, y_0)$ *is any solution of (1.1) defined* $\forall t \in R$ *such that* $y(t_0) = y_0$.

Definition 1.5.9. *[24] A point* $q \in E$ *(subset of* R^n *such that* $f \in C^1(E)$*) is called a* $\omega-$ *limit point of* ϕ *if* $\exists$ *a sequence* $\{t_n\}$, $t_n \to \infty$ *as* $n \to \infty$ *such that*

$$\lim_{n \to \infty} \phi(t_n, y_0) = q.$$

In a similar manner, a point $p \in E$ *is called an* α*-limit point of* ϕ *if* $\exists$ *a sequence* $\{t_n\}$, $t_n \to -\infty$ *as* $n \to \infty$ *such that*

$$\lim_{n \to \infty} \phi(t_n, y_0) = p.$$

The collection of all ω-limit points of a orbit Γ is known as ω-limit set of orbit Γ , and the collection of all α-limit points of a orbit Γ is known as α-limit set of orbit Γ.

Definition 1.5.10. *[24] A periodic solution Γ of (1.1) is known as limit cycle if it is either ω or α-limit set of some another orbit. If a periodic orbit Γ is ω-limit set of every orbit in some nbh. of Γ then it known as a stable limit cycle whereas if it α-limit set of every orbit in some nbh. of Γ then it is known as an unstable limit cycle. If Γ is α-limit set of one orbit other than itself and ω-limit set of another orbit other than itself then is known as a semi-stable limit cycle*

Definition 1.5.11. *The collection of all points $y_0 \in R^n$ is known as basin (or region) of attraction for an attractor $\hat{A}$ (it can be a steady state or periodic solution) of (1.1) if*

$$\lim_{t\to\infty} y(t,y_0) = \hat{A}.$$

For studying the non-autonomous model (Chapter 6) , we need some more definitions and results which are given below.

Definition 1.5.12. *A non-negative bounded solution $y(t)$ of a non-autonomous model is said to be globally attractive (or globally asymptotically stable) if any another solution $\widetilde{y}(t)$ satisfy*

$$\lim_{t\to\infty} |y(t) - \widetilde{y}(t)| = 0.$$

Definition 1.5.13. *[58] Let $D \subset \mathbb{R}^N$ be a bounded open subset and $H : \overline{D} \to \mathbb{R}^N$ be a $C^1(\overline{D})$ map, furthermore $H'(x)$ be its Jacobian, and $\det H'(x)$ be the the determinant of this Jacobian. If $z \notin H(\partial D)$, then the Brouwer degree is defined by*

$$\deg(H,D,z) := \sum_{x\in H^{-1}(z)} \text{sign } \det H'(x).$$

Definition 1.5.14. *[59] Let X, Y are two Banach spaces and an operator $H : X \to Y$ is said to be a Fredholm operator if dimension of its kernal and codimension of its image are finite. The index of this Fredholm operator is given by*

$$\text{index} H = \dim \text{Ker} H - \text{codim Im} H.$$

Lemma 1.5.1. *[60] If function h is a non-negative, uniform continuous and integrable on $[0,\infty)$, then $\lim_{t\to\infty} h(t) = 0$.*

For the existence of periodic solutions of a non-autonomous model, we use continuation theorem from coincidence degree theory by Gains and Mawhin [61]. Let U and V are two normed

vector spaces, $F : \mathrm{Dom}U \subset U \to V$ is a linear map, and $W : U \to V$ is a continuous map. If F is a Fredholm operator of index zero i.e., dim $\mathrm{Ker}F = \mathrm{codim}\ \mathrm{Im}F < \infty$ and there exist continuous projection $S : U \to U$ and $R : V \to V$ such that $\mathrm{Im}S = \mathrm{Ker}F$, $\mathrm{Im}F = \mathrm{Ker}R = \mathrm{Im}(I-R)$ then $F|\mathrm{Dom}F \cap \mathrm{Ker}S : (I-P)X \to \mathrm{Im}F$ is invertible. Let F_S^{-1} be the inverse of of F. Let Ω is an open bounded subset of U such that $RW(\overline{\Omega})$ is bounded and $F_S^{-1}(I-R)W : \overline{\Omega} \to U$ is compact then W is said to be F-compact on $\overline{\Omega}$. Let $\mathrm{Im}R$ is isomorphic to $\mathrm{Ker}F$, so there exists an isomorphism $K : \mathrm{Im}R \to \mathrm{Ker}F$.

Lemma 1.5.2. *[61] Let F be a Fredholm operator with index zero whereas W be a F-compact on $\overline{\Omega}$. If*

1. *for each $\rho \in (0,1)$, each solution y of $Fy = \rho Wy$ is such that $y \notin \partial\Omega$,*
2. *$RWy \neq 0$ for every $y \in \partial\Omega \cap \mathrm{Ker}F$,*
3. *the Brouwer degree $\deg(KRW, \Omega \cap \mathrm{Ker}F, 0) \neq 0$,*

then the equation $Fy = Wy$ has at least one solution in $\mathrm{Dom}F \cap \overline{\Omega}$.

1.6 The mathematical tools employed in the analysis

1. **Linearization of a non-linear system**
   The local nature of the system (1.1) in the nbh. of a hyperbolic equilibrium $\hat{y}$ is determined by the nature of the linear system
   $$\frac{dz}{dt} = Az,$$
   where $A = Df(\hat{y})$ (Jacobian of f evaluated at $\hat{y}$), and $z = y - \hat{y}$.

2. **Local stability**
   The local stability of of a hyperbolic equilibrium $\hat{y}$ depends upon sign of real parts of the eigenvalues of $Df(\hat{y})$, and we determine the nature of signs by using Hurwitz's Theorem [62], given below.

   Theorem 1.6.1. *A necessary and sufficient condition for all the solutions of the equation (1.2)*
   $$\lambda^n + B_1\lambda^{n-1} + B_2\lambda^{n-2} + \ldots B_n = 0, \tag{1.2}$$

with real coefficients, to have negative real parts, is the positivity of all principle diagonals of minors of the Hurwitz matrix

$$H_n = \begin{bmatrix} B_1 & 1 & 0 & 0 & 0 & 0 & \dots & 0 \\ B_3 & B_2 & B_1 & 1 & 0 & 0 & \dots & 0 \\ B_5 & B_4 & B_3 & B_2 & B_1 & 1 & \dots & 0 \\ \dots & \dots & \dots & \dots & \dots & \dots & \dots & \dots \\ 0 & 0 & 0 & 0 & 0 & 0 & 0 & B_n \end{bmatrix}.$$

We can observe that the entries in H_n on principal diagonal are the coefficients of (1.2), and the alternating columns of H_n consist either the coefficients with only even or with only odd indices. Thus, $H_n = (A_{ij})$, where $A_{ij} = B_{2i-k}$, with missing coefficients being replaced with zero.

The conditions for negative real parts of the solutions of (1.2) for some values of $n = 2,\ 3$ and 4 are given below, however the use of this theorem become impractical for large n.

$$\begin{aligned} &n = 2; B_1 > 0,\ B_2 > 0, \\ &n = 3; B_1 > 0,\ B_3 > 0,\ B_1 B_2 > B_3, \\ &n = 4; B_1 > 0,\ B_2 > 0,\ B_3 > 0,\ B_4 > 0,\ B_1 B_2 B_3 > B_3^2 + B_1^2 B_4. \end{aligned}$$

3. **Global stability**

In the last segment, we discussed about the local stability of the system around a steady state of a dynamical system. Now, we will discuss the procedure to investigate the global stability of this steady state, and establish the sufficient conditions for it by choosing a suitable Lyapunov's function which is a positive definite function. We consider a system

$$\frac{dy}{dt} = f(y), y(t_0) = y_0, \tag{1.3}$$

where $f \in C^1(R^n)$ to ensure the existence-uniqueness of solution of (1.3), $S_\mu = \{y \in R^n : ||y|| < \mu\}$, and $\hat{y}$ is the steady state.

To provide the sufficient criteria for global stability, we have some significant results.

Theorem 1.6.2. *If there is a positive definite (about $\hat{y}$) function $V(y)$ such that $\frac{dV}{dt} \leq 0$ on S_μ then $\hat{y}$ is stable.*

Theorem 1.6.3. *If there is a positive definite (about $\hat{y}$) function $V(y)$ such that $\frac{dV}{dt} < 0$ on S_μ then $\hat{y}$ is asymptotically stable.*

Theorem 1.6.4. *If there is a scalar function $V(y)$ such that $V(\hat{y}) = 0$ and $\frac{dV}{dt} > 0$ on S_μ and in every nbh. M of $\hat{y}$, $M \subset S_\mu$, there is y_0 with $V(y_0) > 0$ then $\hat{y}$ is unstable.*

4. Now, we state an important theorem which provides a sufficient condition for the non-existence of any periodic solution of a planner dynamical system

   Theorem 1.6.5. *Consider a planner dynamical system*

   $$\frac{dy_1}{dt} = F_1(y_1, y_2), \ \frac{dy_2}{dt} = F_2(y_1, y_2), \tag{1.4}$$

   where F_1 and F_2 are continuously differentiable functions on a simple connected domain $\mathfrak{D}$, and B is smooth function on $\mathfrak{D}$. If

   $$\nabla.(BF_1, BF_2) = \frac{\partial BF}{\partial y_1} + \frac{\partial BF_2}{\partial y_2}$$

   have one sign throughout $\mathfrak{D}$, then there is no periodic solution of (1.4) in $\mathfrak{D}$.

5. **Numerical simulation**
   In each chapter of this thesis, numerical simulation experiments are conducted to prove the theoretical findings in that particular chapter. We have used MALTLAB/ MATHEMATICA to perform tedious calculations and to draw different types of time-series graph, phase-portraits, basins of attraction, and bifurcation diagrams.

1.7 Bifurcation theory

Let us consider a system

$$\frac{dy}{dt} = f(y, \nu), \tag{1.5}$$

then the qualitative behaviour of system (1.5) may change on varying the value of parameter $\nu \in R$ around its critical value ν_0. This qualitative change may accompanied by number of change of steady states or stability of a steady state corresponding to (1.5) . On basis of this, there are several kinds of bifurcations given below.

(i) **Saddle-node**
In this bifurcation, on varying the critical (bifurcation) parameter, two steady states, out which one is sink and one is saddle, come together to collide and annihilate each other at $\nu = \nu_0$.
Let $y = y_0$ be the corresponding hyperbolic equilibrium at $\nu = \nu_0$ with p and q be the

eigenvectors corresponding to zero eigenvalue of $A = Df(y_0, \nu_0)$ and A^T. Then the transversality conditions from Sotomayor's theorem [24] for saddle-node bifurcation are

$$q^T f_\nu(y_0, \nu_0) \neq 0,\ q^T [D^2 f(y_0, \nu_0)(p, p)] \neq 0. \tag{1.6}$$

An example of dynamical system for this bifurcation is

$$\frac{dy}{dt} = \nu - y^2.$$

(ii) **Transcritical bifurcation**

In this bifurcation, two steady states interchange their stability as we vary the bifurcation parameter ν. At this critical value, the steady state $y = y_0$ becomes hyperbolic, and if the conditions (1.6) are replaced with

$$\begin{aligned} q^T f_\nu(y_0, \nu_0) &\neq 0, \\ q^T [Df_\nu(y_0, \nu_0)p] &\neq 0, \\ q^T [D^2 f(y_0, \nu_0)(p, p)] &\neq 0, \end{aligned} \tag{1.7}$$

then system (1.5) suffers transcritical bifurcation at the steady state $y = y_0$ at $\nu = \nu_0$. An example for this bifurcation is

$$\frac{dy}{dt} = \nu y - y^2.$$

(iii) **Pitchfork bifurcation**

In this bifurcation, system (1.5) transits from one stable (or unstable) steady state to three steady states, out of which two newly arose steady states are stable (or unstable) and the already existing steady state become unstable (or stable). If conditions (1.6) are replaced with

$$\begin{aligned} q^T f_\nu(y_0, \nu_0) &\neq 0, \\ q^T [Df_\nu(y_0, \nu_0)p] &\neq 0, \\ q^T [D^2 f(y_0, \nu_0)(p, p)] &\neq 0, \\ q^T [D^3 f(y_0, \nu_0)(p, p, p)] &\neq 0, \end{aligned} \tag{1.8}$$

then then system (1.5) suffers picthfork bifurcation at the steady state $y = y_0$ at $\nu = \nu_0$. An example for this bifurcation is

$$\frac{dy}{dt} = \nu y - y^3.$$

(iv) **Hopf bifurcation**

In last bifurcations, at the critical value $\nu = \nu_0$, one eigenvalue of $Df(y_0, \nu_0)$ become zero but in Hopf bifurcation $Df(y_0, \nu_0)$ has a pair of purely imaginary eigenvalues with no other eigenvalue have zero real part. As the eigenvalue passes through the imaginary axis on varying ν there is occurrence of supercritical or subcritical Hopf bifurcation at $\nu = \nu_0$. In supercritical case, the steady state which is going under bifurcation, is stable earlier and on varying ν, it becomes unstable at bifurcation point and there is arise of a stable limit cycle around it. In subcritical case, the steady state is unstable before going under bifurcation and after it, the steady state become stable and there is arise of unstable limit cycle around.

A general planner system

$$\frac{dY_1}{dt} = f_1(Y_1, Y_2, \nu), \ \frac{dY_2}{dt} = f_2(Y_1, Y_2, \nu) \tag{1.9}$$

which undergoes Hopf bifurcation about the steady state $S^* = (Y_1^*, Y_2^*)$ at $\nu = \nu_0$ can be written in the form of (1.10) by using the using the transformation $y_1 = Y_1 - Y_1^*$, $y_2 = Y_2 - Y_2^*$ and the Taylor's series expansion.

$$\begin{aligned} \frac{dy_1}{dt} &= a_{10}y_1 + a_{01}y_2 + \sum_{i+j\geq 2} a_{ij}y_1^i y_2^j, \\ \frac{dy_2}{dt} &= b_{10}y_1 + b_{01}y_2 + \sum_{i+j\geq 2} b_{ij}y_1^i y_2^j, \end{aligned} \tag{1.10}$$

where $a_{ij} = \frac{1}{i!j!}\frac{\partial^{i+j} f_1}{\partial Y_1^i Y_1^j}\Big|_{(S^*,\nu=\nu_0)}$, $b_{ij} = \frac{1}{i!j!}\frac{\partial^{i+j} f_2}{\partial Y_1^i Y_1^j}\Big|_{(S^*,\nu=\nu_0)}$.

The fisrt Lyapunov coefficient l_1 [24] for (1.10) is given by

$$\begin{aligned} l_1 = -\frac{3\pi}{2a_{01}\Theta^{\frac{3}{2}}}\Big\{ &\Big[a_{10}b_{10}\left(a_{11}^2 + a_{11}b_{02} + a_{02}b_{11}\right) + a_{10}a_{01}\left(b_{11}^2 + a_{20}b_{11} + a_{11}b_{02}\right) \\ &+ b_{10}^2\left(a_{11}a_{02} + 2a_{02}b_{02}\right) - 2a_{10}b_{10}\left(b_{02}^2 - a_{20}a_{02}\right) - 2a_{10}a_{01}\left(a_{20}^2 - b_{20}b_{02}\right) \\ &- a_{01}^2\left(2a_{20}b_{20} + b_{11}b_{20}\right) + \left(a_{01}b_{10} - 2a_{10}^2\right)\left(b_{11}b_{02} - a_{11}a_{20}\right)\Big] \\ &- \left(a_{10}{}^2 + a_{01}b_{10}\right)\Big[3\left(b_{10}b_{03} - a_{01}a_{30}\right) \\ &+ 2a_{10}\left(a_{21} + b_{12}\right) + \left(b_{10}a_{12} - a_{01}b_{21}\right)\Big]\Big\}\Big|_{(y_0;\nu=\nu_0)} \end{aligned} \tag{1.11}$$

with $\Theta = (a_{10}b_{01} - a_{01}b_{10})|_{(y_0;\nu=\nu_0)}$.

Theorem 1.7.1. *If $l_1 \neq 0$ then system (1.10) suffers Hopf bifurcation at S^* for $\nu = \nu_0$; if*

$l_1 < 0$ then a stable limit cycle arises from S^* as vary ν and if $l_1 > 0$ then there is arise of an unstable limit cycle. The case when we have $l_1 < 0$, there is supercritical Hopf bifurcation and when $l_1 > 0$ then we have subcritical Hopf bifurcation.

1.8 Delay differential equation

A differential equation with delays in the dependent variable is known as a delay differential equation (DDE). In other words, the dependent variable's rate of change at any given moment depends both on its current value and its values in the past. DDEs are employed in a variety of fields, including physics, ecology, and finance.

The general form of a delay differential equation [63] is given by

$$\frac{dy}{dt} = f(t, y(t), y(\tau_1(t, y(t))), y(\tau_2(t, y(t))), ..., y(\tau_m(t, y(t)))) \tag{1.12}$$

where $0 \leq \tau_i(t, y(t)) \leq t$.
There are mainly three types of delays [63] as given below.

(i) **Time dependent delay**
If the delays can be written in the from $t - \tau_i(t)$ with $\tau_i(t) > 0$, then delays are called as time dependent delay.

(ii) **State dependent delay**
If the delays can be written in the form $t - \tau_i(x(t))$ with $\tau_i(t) > 0$, then delays are called as time dependent delay.

(iii) **Generalized delays**
The form of the delays represented in (1.12) are called generalized delay

For more details related to examples of above types of delays and numerical solutions of these one can refer to [63].

1.9 Non-autonomous differential equations

Any differential equation whose coefficients or functions explicitly depend on the independent variable is said to be a non-autonomous differential equation. Thus, the solution's behaviour may change over time since the equation is not time-invariant. There are numerous uses for non-autonomous differential equations in physics, biology, and engineering. For instance, in physics, systems where the coefficients or functions depend on time, such as in the

case of a forced oscillator, can be modelled using non-autonomous differential equations. Non-autonomous differential equations can be used in biology to simulate population growth and decline when the birth and death rates are time-dependent. Non-autonomous differential equations in engineering can be used to simulate control systems where the system's input changes over time.

A system of non-autonomous differential equation [62] can be expresses as

$$\frac{dy}{dt} = f(t,y), \tag{1.13}$$

where $f \in C[I \times S_\mu, R^n]$, $I = [t_0, \infty)$, and $S_\mu = \{y \in R^n : ||y|| < \mu\}$. The theory related to non-autonomous differential equations which we have used, is discussed in chapter 6.

1.10 Basic ecological models

1. **Malthusian model**
   In this model, Malthusian [1] assumed that the rate of change in density (say X) of species is directly proportional to population's growth rate. Mathematically this model can written as

   $$\frac{dX}{dt} = aX,\ X(0) = X_0,$$

   where a is the growth rate. The solution of above differential is given by $X(t) = X_0 \exp(at)$. Thus the solution of above system grows exponentially for $a > 0$. The main limitation of this model is that it reflects the limitless growth of the population which is not possible in realistic conditions.

2. **Logistic growth model**
   The logistic growth model was given by Pierre Verhulst [2] in which he accounts the fact that the increase in population density may be limited due the interference among the members of population. Mathematically, the logistic growth model is described as

   $$\frac{dX}{dt} = aX\left(1 - \frac{X}{K}\right),\ X(0) = X_0,$$

   where K is the carrying capacity of the habitat in which population is living. The solution of this logistic growth model is given by

   $$X(t) = \frac{KX_0e^{at}}{(K - X_0) + X_0e^{at}},$$

and from this solution we can observe that as $t \to \infty$ then $X(t) \to K$.

3. **Lotka-Volterra model**

   The Lotka-Volterra model, also known as the predator-prey model, is a mathematical framework used to study the dynamics of two interacting species. Volterra [4] then expanded upon the work of Lotka in his book. Two differential equations; one for the population of the predator species and the other for the population of the prey species form the basis of the model. As a result of their interactions with one another and their environment, these equations characterise the rate of change of each species' population through time. The model assumes that the prey species has an endless supply of food and that the predator species only consumes the prey species. It also presupposes that interactions between species are only local and that each species' population growth rate is constrained by its own density.

   Let $X_1(t)$ and $X_2(t)$ denote the population densities prey and predator, respectively. Then the prey-predator model proposed by Lotka and Volterra is given by

$$\begin{aligned} \frac{dX_1}{dt} &= aX_1 - bX_1X_2, \\ \frac{dX_2}{dt} &= cbX_1X_2 - dX_2, \end{aligned} \tag{1.14}$$

   with $a,b,c,d > 0$ and $X_1(0) \geq 0, X_2(0) \geq 0$. In (1.14), a is the growth rate of prey, b is predator's attack rate on prey, c is conversion efficiency of predator on prey and d is death rate of predator.

Chapter 2

Stability switching and chaos in a multiple delayed prey-predator model with fear effect and anti-predator behavior[1]

2.1 Introduction

An essential aspect of an ecosystem is its dynamics which gives the idea about the growth of population living in that particular ecological community. The momentum of progress for these inhabitants relies on various components like the carrying capacity of supporting infrastructure, the interrelationship of one with others, age, atmospheric conditions, etc. This inspires us to study the factors which affect the complexity of the system. Firstly, it was done by Malthus [1]. He discussed the major causes and their cures about the fast-growing population of England. His theory was mainly based upon the idea that the rate of population is proportional to the present population which means the population grows exponentially. This assumption became the main element of criticism for his conjecture as each habitat has a limited potential to sustain its denizens. After that, the logistic growth model was proposed by Verhulst[2]. He incorporated the intraspecific interactions among the population's individuals and made the model more realistic. On later Lotka's *Elements of Physical Biology*[3] was a major advancement in population dynamics. He introduced the interaction of two species in the form of a system of two non-linear differential equations, known as the prey-predator model. Then Volterra extended Lotka's work in his book [4]. Brief detail about the origin and initial work on the prey-predator model is described in [5]. Prey-predator interactions can be seen in every aspect of living organisms, which provokes us to explore its various segments. This inspiration brought enormous attention to this system and made it a major area of ecological research. A lot of study has been done by several researchers [6, 7, 8, 9, 10] in this domain. In a prey-predator system,

[1] A considerable part of this chapter is published in *Mathematics and Computers in Simulation*, 188(2021) 164–192.

how predator consumes the prey is a very important factor to deal with because a change in the way of interaction between them can change the whole dynamics of the system. The term 'Functional response', which gives the predator's per capita feeding rate on prey, is a crucial component that helps us to investigate the kinetics of the model in a more realistic way. There are numerous types of functional responses and a massive amount of work has been done using them by many researchers, Holling type-II in [11], Holling type-III in [12], Holling type-IV in [13], Beddington-DeAngelis in [14], Crowley-Martin in [15, 16], Hassell-Varley in [17], Leslie–Gower in[18].

In the phase of evolution of prey-predator model our prolonged perspective was that, the prey is affected by predator only through direct hunting, but there is another significant medium of influencing the prey population, which is the fear of the predator. There is a considerable impact of this fright on the attitude of prey. Because of this worry of being killed, sometimes prey has to shift their locality to such a site that does not support them to spend their lives in a good manner. This fear does not allow prey to roam freely in their own territory, which cut down the prey population's mating rate, leading to their abatement. Pandey *et al.* [64] studied the three species food chain model in which the growth of middle predator is reduced due to fear of top predator and growth rate of prey is decreased by the fear of middle predator and the interaction between the species are dealt with Holling type II functional response. Recently Das & Samanta [65] has studied the impact of fear on prey when additional food is provided to predator with a stochastic prey-predator model and deduced the conditions for annihilation and perseverance for the system. The analysis of the impact of fear of predator on prey is done by many researchers, [66, 67, 68, 15]. Wang *et al.* [30] modeled the prey-predator interaction in which they examined the relationships between fear effect and other parameters and demonstrated that the direction of Hopf-bifurcation changes by varying the value of fear. In recent times, Pandey *et al.* [69] proposed and analyzed a prey-predator model with fear effect and delay. They found that for gradual increase of delay, the dynamics of the system switches more than once. Authors also observed node-cycle bi-stability behavior between the positive equilibrium and stable limit cycle of the delayed system.

At any place on the earth, when one species attacks another for its consumption, then the attacked one has a natural tendency to protect itself and this temperament of rescuing is called anti-predator behavior by prey against the predator. There is a great number of activities performed by prey in the anti-predator behavior like camouflage, imitation of some harmful breed, escape instead of direct encounter, use of noxious chemicals in the form of chemical defence, changing body color etc. So, the efforts of a defence vary species to species of prey. A good elaboration about anti-predator behavior possessed by prey is provided in [70]. Ives *et al.* [71] proposed a prey-predator model showing that more efficient anti-predator behavior increases the prey population density by reducing the per capita predation rate. They excluded such

anti-predator behaviors, which can affect prey population in an adverse way. A fine job on anti-predator behavior is done by Matsuda *et al.* [72]. They have formulated a model consisting of two predators sharing common prey and have investigated both the short-term and long-term effects of anti-predator behavior on predators by varying their densities. Recently, Liu & Zhang [73] have investigated the prey-predator model with anti-predator behavior with the incorporation of delay and diffusion with the help of partial differential equations.

Most of the biological proceedings come with time delays. The effects of factors involved in these processes are not visible instantly. They take some time to manifest themselves and this time is known as the time delay. The models consisting of time delays are investigated with the help of delay differential equations, which are more complex than the ordinary differential equations. Volterra [4] introduced delayed prey-predator models in form of integrodifferential equations and these delays are known as distributed delays. Discrete delays are derived from distributed delays by taking kernal as delta function. There are several types of discrete delays like maturation delay, which is time taken by the immature individual to become mature, gestation delay, which is time taken by the predator to reproduce after consuming the prey. Fear of predator has a negative impact on reproduction rate of prey in many ways but this impact in not seen instantly. The effect of this fear on growth of prey takes some time to become visible, so fear response delay is the amount of time after which the density of prey population starts getting change due to fear of the predator. Such delay in fear response has not been observed in the literature. The majority of studies show that delays are capable of destabilizing the system. Chakraborty & Haldar [74] derived conditions for global stability and bifurcation of a prey-predator model with stage structure. Chen *et al.* [18] explored the prey-predator model with prey refuge and Leslie-Gower functional response. They inferred the threshold value for the refuge parameter, before which increasing its value increases the predator's density and beyond which it decreases the predator's density. There are many studies [75, 23, 76, 77, 78, 79, 80] with more than one delays in which they have estimated the critical value of delays for the occurrence of bifurcation. Nakaoka *et al.* [81] worked on pure-delay-type systems which are prey-predator model without instantaneous intraspecific competitions and showed that this delayed system is globally asymptotically stable for small values of delays and system has chaotic behavior as the value of delay for interaspecific competition among predators is increased to a large number.

Therefore, we figure out that the interaction between prey and predator does not only results in direct killing of prey, but there is an adverse effect of the fear induced by the predator on prey, and they respond to this fear by showing certain kinds of anti-predator behaviors towards the predator.

To the best of author's knowledge, an interaction between prey and predator with (i) effect of fear in prey, (ii) anti-predator behavior by prey against predator, (iii) simplified Holling type

IV functional response, (iv) fear response delay in prey, (v) gestation delay in predator has not been studied. Hence, this encourages us to investigate the prey-predator model's kinetics by incorporating the fear effect, anti-predator behavior in response to this fear with the fear response and gestation delay. In Section 2.2, we formulate both the models, non-delayed and delayed. In Section 2.3, we perform analysis for the non-delayed model and drive conditions for stability and Hopf-bifurcation. Then local stability and Hopf-bifurcation of the delayed model is discussed in Section 2.4. In Section 2.5, we determine the direction and stability of Hopf-bifurcation using the normal form method and center manifold theory. Section 2.6 is dedicated to numerical simulations supporting our theoretical findings in previous sections. Then we end this chapter with its conclusions and significances.

In this chapter, our study is restricted to such anti-predators behaviors (or their respective extent) which do not have any negative effect on the prey population and assumes that anti-predator behavior only increases the prey population by decreasing the per capita feeding rate.

2.2 Mathematical model

We consider two-dimensional autonomous system of differential equations which gives the interaction between prey and predator. Let $x(t)$ and $y(t)$ be the population densities of prey and predator respectively at time t. The model has been developed under the following assumptions.

1. The prey population grows logistically in the absence of predation so, the per capita growth rate of the prey population is

$$\frac{dx}{dt} = rx - r_0 x - r_1 x^2. \tag{2.1}$$

2. Most of the researchers have worked on the prey-predator model on the assumption that the predator effects prey only by direct killing, but in the previous section, we saw that the fear of predator also affects the growth of prey individuals. So, this fear diminishes the reproduction rate of the prey community. Due to this reason, its legitimate to include the fear term in our model to make it sounder. so, the expression (2.1) can be modified to get

$$\frac{dx}{dt} = \frac{rx}{1+ky} - r_0 x - r_1 x^2. \tag{2.2}$$

3. Since most of the biological processes involve delay because the effect of any factor involved in that process takes some time to become visible. So, the effect of fear on the prey population is also not instantaneous, and there is a delay in effecting the growth of prey species. Hence, here we introduce a delay τ_1 known as fear response delay. Now

expression (2.2) can further be modified to

$$\frac{dx}{dt} = \frac{rx}{1+ky(t-\tau_1)} - r_0x - r_1x^2.$$

4. We consider that the interaction between prey and predator species is followed by modified Holling type IV functional response which is simpler version of Monod-Haldane functional response. This is only prey dependent functional response and it is given by

$$f(x,y) = \frac{\alpha x}{ax^2+b}.$$

5. As explained earlier, there is some delay in biological processes. So, there is a time lag between consuming the prey and reproducing the progeny by the predator. Hence it is reasonable to incorporate a delay say τ_2 known as gestation delay, which is the time gap between the consumption of the prey and reproduction of its progeny. It is assumed that the rate of change of predator species depends upon the number of prey and predators present at the time $(t-\tau_2)$ and delay τ_2 is considered only in numeric response.

6. Due to the fear of predator, prey shows different kinds of anti-predator behaviors and try to save themselves by fleeing, covering itself, etc. Sometimes prey befool the predator by the technique of diversion display in which prey divert their attention to protect their vital areas. For example, lizards are capable of twitching their tails, which have lives. So, lizards use this skill to make way for escape. But in case of an encounter, prey exhibit different type of behaviors like retaliation, chemical defence, use of morphological structures, etc., and a good detail about these behaviors is provided in [70]. So, it is important to introduce this behavior in our model.

Under all the above assumptions, the interaction between prey and predator species is modeled by the following system of DDEs:

$$\begin{aligned}
\frac{dx}{dt} &= \frac{rx}{1+ky(t-\tau_1)} - r_0x - r_1x^2 - \frac{\alpha xy}{ax^2+b}, \\
\frac{dy}{dt} &= \frac{c\alpha x(t-\tau_2)y(t-\tau_2)}{ax^2(t-\tau_2)+b} - \delta_0y - \delta_1y^2 - \eta xy,
\end{aligned} \tag{2.3}$$

subjected to non-negative conditions $x(s) = \phi_1(s) \geq 0,\ y(s) = \phi_2(s) \geq 0,\ s \in [-\tau, 0],\ \tau = max\{\tau_1, \tau_2\}$ and $\phi_i(s) \in C([-\tau,0]) \to R_+), (i = 1,2)$, where τ_1 and τ_2 denotes fear response and gestation time delay respectively.

System (2.3) takes the following form in the absence of both the delays

$$\begin{aligned}\frac{dx}{dt} &= \frac{rx}{1+ky} - r_0x - r_1x^2 - \frac{\alpha xy}{ax^2+b},\\ \frac{dy}{dt} &= \frac{c\alpha xy}{ax^2+b} - \delta_0 y - \delta_1 y^2 - \eta xy.\end{aligned} \tag{2.4}$$

The biological meaning and dimension of the variables and parameters used in system (2.3) and (2.4) are described in the Table 2.1.

Variable/Parameter	Biological meaning
x	Prey density
y	Predator density
r	Birth rate of prey population
r_0	Death rate of prey population
r_1	Coefficient of intraspecfic interference among prey individuals
α	Attack rate
k	Cost of fear
a	Inverse measure of inhibitory effect
b	Half-saturation constant
c	Conversion effeciency of y on x
δ_0	Death rate of predator population
δ_1	Coefficient of intraspecfic interference among predator individuals
η	Rate of anti-predator behavior of prey to the predator
τ_1	Fear response delay in prey
τ_2	Gestation delay in predator

Table 2.1: List of variables and parameters with their biological meaning, used in system (2.3) and (2.4) (for more details on the dimensions of parameters, one can refer to [82])

2.3 Dynamics of Non-delayed Model

Here we shall analyze the properties like positivity, persistence and boundedness for the solution of system (2.4) which is followed by the investigation of local and global behavior of the system around existing equilibrium points.

2.3.1 Positivity, permanence and boundedness of the solution

The model (2.4) can be written as

$$\frac{dx}{dt} = x\phi_1(x,y), \quad \frac{dy}{dt} = y\phi_2(x,y),$$

where

$$\phi_1(x,y) = \frac{r}{1+ky} - r_0 - r_1 x - \frac{\alpha y}{ax^2+b}, \quad \phi_2(x,y) = \frac{c\alpha x}{ax^2+b} - \delta_0 - \delta_1 y - \eta x.$$

This implies

$$x(t) = x(0)e^{\int_0^t \phi_1(x(\tau),y(\tau)d\tau} \geq 0,$$
$$y(t) = y(0)e^{\int_0^t \phi_2(x(\tau),y(\tau)d\tau} \geq 0.$$

So, the solution $(x(t),y(t))$ with positive initial condition $(x(0),y(0)) \in R^2_+$ will be positive for the whole future time.

Lemma 2.3.1. *The set* $\Omega = \{(x,y) : 0 \leq x \leq \frac{r}{r_1}, 0 \leq cx+y \leq \frac{cr^2}{\delta^* r_1}\}$ *is a region of attraction for all solutions intiating in the positive quadrant, where* $\delta^* = min\{r_0, \delta_0\}$.

Proof. The first equation of the system (2.4) signifies

$$\frac{dx}{dt} \leq (r-r_0)x - r_1 x^2,$$

which gives

$$\limsup_{t\to\infty} x(t) \leq \frac{r}{r_1}.$$

Now let $M(t) = cx(t) + y(t)$, which gives

$$\frac{dM}{dt} = c\frac{dx}{dt} + \frac{dy}{dt} = \frac{crx}{1+ky} - cr_0 x - cr_1 x^2 - \delta_0 y - \delta_1 y^2 - \eta xy \leq \frac{cr^2}{r_1} - \delta^* M,$$

where $\delta^* = min\{r_0, \delta_0\}$.
Thus,

$$\limsup_{t\to\infty} M(t) \leq \frac{cr^2}{\delta^* r_1}.$$

Hence, the solutions of (2.4) are bounded. It can be noted that if $x > \frac{r}{r_1}$ and $M > \frac{cr^2}{\delta^* r_1}$ then $\frac{dx}{dt} < 0$ and $\frac{dM}{dt} < 0$, hence Ω is an invariant set. □

Theorem 2.3.2. *Let the following inequalities hold true:*

$$r > (1+ky_a)\left(r_0 + \frac{\alpha}{b}y_a\right), \quad \eta < \frac{1}{x_a}\left(\frac{c\alpha x_b}{ax_a^2+b} - \delta_0\right).$$

Then model (2.4) is uniformly persistence, where x_a, x_b *and* y_a *are defined in the proof.*

Proof. Uniform persistence or permanence of a system signifies that all the species which are present initially, will remain for the whole future time and none of them will go for extinction. System (2.4) is said to be uniformly persistence if there exists positive constants L_1 and L_2 such that each positive solution $X(t) = (x(t), y(t))$ with positive initial conditions satisfies

$$L_1 \leq \liminf_{t\to\infty} X(t) \leq \limsup_{t\to\infty} X(t) \leq L_2.$$

Using Lemma 2.3.1, we define

$$x_a = \frac{r}{r_1}, \;\; y_a = \frac{cr^2}{\delta^* r_1}.$$

Keeping above in view, we define

$$L_2 = max\{x_a, y_a\},$$

which follows that

$$\limsup_{t\to\infty} X(t) \leq L_2.$$

Above equation shows that for any arbitrary $\varepsilon > 0 \;\; \exists$ a $T > 0$ such that $\forall\, t \geq T$, the following holds:

$$x < x_a + \varepsilon, \;\; y < y_a + \varepsilon.$$

Now from the first equation of the model (2.4), for all $t \geq T$, we can write

$$\frac{dx}{dt} \geq \frac{rx}{1+k(y_a+\varepsilon)} - r_0 x - r_1 x^2 - \frac{\alpha x(y_a+\varepsilon)}{b}$$

$$= \left[\frac{r}{1+k(y_a+\varepsilon)} - r_0 - \frac{\alpha(y_a+\varepsilon)}{b}\right] x - r_1 x^2,$$

this implies

$$\liminf_{t\to\infty} x(t) \geq \frac{1}{r_1}\left[\frac{r}{1+k(y_a+\varepsilon)} - r_0 - \frac{\alpha(y_a+\varepsilon)}{b}\right],$$

which is true for arbitrary $\varepsilon > 0$, thus

$$\liminf_{t\to\infty} x(t) \geq \frac{1}{r_1}\left[\frac{r}{1+ky_a} - r_0 - \frac{\alpha y_a}{b}\right] =: x_b,$$

so, the prey population is persistent under the condition:

$$r > (1+ky_a)\left(r_0 + \frac{\alpha}{b} y_a\right).$$

Now from the second equation of model (2.4), we can write

$$\frac{dy}{dt} \geq \frac{c\alpha x_b y}{a(x_a+\varepsilon)^2+b} - \delta_0 y - \eta(x_a+\varepsilon)y - \delta_1 y^2$$

$$= \left[\frac{c\alpha x_b}{a(x_a+\varepsilon)^2+b} - \delta_0 - \eta(x_a+\varepsilon)\right] y - \delta_1 y^2,$$

which follows that

$$\liminf_{t\to\infty} y(t) \geq \frac{1}{\delta_1}\left[\frac{c\alpha x_b}{a(x_a+\varepsilon)^2+b} - \delta_0 - \eta(x_a+\varepsilon)\right],$$

which is true for every $\varepsilon > 0$, so

$$\liminf_{t\to\infty} y(t) \geq \frac{1}{\delta_1}\left[\frac{c\alpha x_b}{ax_a^2+b} - \delta_0 - \eta x_a\right] =: y_b.$$

So, the condition for the predator population to be persistent is

$$\eta < \frac{1}{x_a}\left(\frac{c\alpha x_b}{ax_a^2+b} - \delta_0\right).$$

Let $L_1 = min\{x_b, y_b\}$, hence the theorem follows.

□

Remark 2.3.1. *Above investigation shows that the prey population will not go for extinction if the birth rate of prey population is greater then a threshold value and the predator population remains persistent if the rate of anti-predator behavior of prey to predator is less then some threshold value.*

2.3.2 Existence of equilibrium points

An equilibrium point is a steady state solution for a dynamical system. It is investigated that system (2.4) has three equilibria named as $E_0(0,0)$, $E_1(x_1,0)$ and $E^*(x^*,y^*)$. The equilibrium $E_0(0,0)$ exists trivially and $E_1(x_1,0)$ exists if $r > r_0$, where $x_1 = \frac{r-r_0}{r_1}$. Now we shall show the existence of the interior equilibrium $E^*(x^*,y^*)$.

- **Existence of interior equilibrium $E^*(x^*,y^*)$:** Here x^*, y^* are the positive solutions of the algebraic equations:

$$\frac{r}{1+ky} - r_0 - r_1 x - \frac{\alpha y}{ax^2+b} = 0, \tag{2.5}$$

$$\frac{c\alpha x}{ax^2+b} - \delta_0 - \delta_1 y - \eta x = 0. \tag{2.6}$$

For equation (2.5) we have the following outcomes:

1. Let $y = 0,$ which implies $x = \frac{1}{r_1}(r - r_0) =: x_1 > 0$ as $r > r_0$.

2. When $x = 0$, then we get

$$\alpha k y^2 + (\alpha + r_0 bk)y - b(r - r_0) = 0. \tag{2.7}$$

So, equation (2.7) has unique positive root y_1 given by

$$y_1 = \frac{-r_0 bk + \sqrt{(r_0 bk)^2 + 4\alpha k(r - r_0)}}{2\alpha k}.$$

3. Now it is easy to prove that

$$\frac{dy}{dx} = \frac{-r_1 + \frac{2\alpha axy}{(ax^2+b)^2}}{\frac{rk}{(1+ky)^2} + \frac{\alpha}{(ax^2+b)}},$$

and $\frac{dy}{dx} < 0$ if

$$\delta^* b^2 r_1^3 > 2\alpha acr^3 \text{ implies } \frac{dy}{dx} < 0 \text{ if } r < r_1 \left(\frac{\delta^* b^2}{2\alpha ac}\right)^{\frac{1}{3}}, \tag{2.8}$$

where $\delta^* = min\{r_0, \delta_0\}$.

From above investigation we conclude that equation (2.5) passes through the points $(x_1, 0), (0, y_1)$ and y is a decreasing function of x under condition (2.8).
For equation (2.6) we can figure out the following outcomes:

1. Let $x = 0,$ which implies $y = -\frac{\delta_0}{\delta_1} =: y_2 < 0$.

2. If $y = 0$, then we get

$$P_3 x^3 + P_2 x^2 + P_1 x + P_0 = 0, \tag{2.9}$$

where $P_0 = \delta_0 b,\ P_1 = \eta b - c\alpha,\ P_2 = \delta_0 a$ and $P_3 = \eta a$. Now by using Descartes' rule of sign and discriminant for a cubic equation for equation (2.9) we can easily note that equation (2.9) has exactly two positive roots named as x_2 and x_2' when both of the following conditions hold simultaneously:

$$\eta b - c\alpha < 0,\ 18P_3P_2P_1P_0 - 4P_2^3P_0 + P_2^2P_1^2 - 4P_3P_1^3 - 27P_3^2P_0^2 > 0, \tag{2.10}$$

and without loss of generality we assume that $x_2 < x_2'$.

3. Now it is easy to see that

$$\frac{dy}{dx} = \frac{c\alpha(b-ax^2)}{\delta_1(ax^2+b)^2}, \quad \frac{d^2y}{dx^2}\Big|_{x=\sqrt{\frac{b}{a}}} < 0.$$

From above analyses for equation (2.6) we conclude that equation (2.6) passes through the points $(0,y_2),(x_2,0)$ and $(x_2',0)$. At $x=\sqrt{\frac{b}{a}}$ equation (2.6) has unique global maximum in positive quadrant such that $x=\sqrt{\frac{b}{a}}$ lies between x_2 and x_2'. Assuming the following condition:

$$x_2 < \frac{1}{r_1}(r-r_0) < x_2', \tag{2.11}$$

we can conclude that the system of equations (2.5) and (2.6) has unique positive point of intersection if the conditions (2.8),(2.10) and (2.11) hold simultaneously. Thus we can state the following theorem.

Theorem 2.3.3. *The system (2.4) has a unique interior equilibrium point if conditions (2.8),(2.10) and (2.11) hold concurrently.*

Remark 2.3.2. *Ecologically, we can say that the interior equilibrium exists if the prey population's birth rate is less than some threshold value and carrying capacity for the same lies between two positive values at which y-nullcline intersects the x-axis, with the condition (2.10). To see the existence of unique interior equilibrium, we take a set of parameters;* $r=3,\ r_0=0.9,\ r_1=5,\ k=1,\ \alpha=1,\ c=0.63,\ \delta_0=0.1,\ \delta_1=0.2,\ \eta=0.2,\ a=0.5,\ b=1.2,$ *for which all the conditions in Theorem 2.3.3 hold. Therefore, for this set of parameters the non-delayed system has a unique interior equilibrium point which is depicted in Fig. 2.1.*

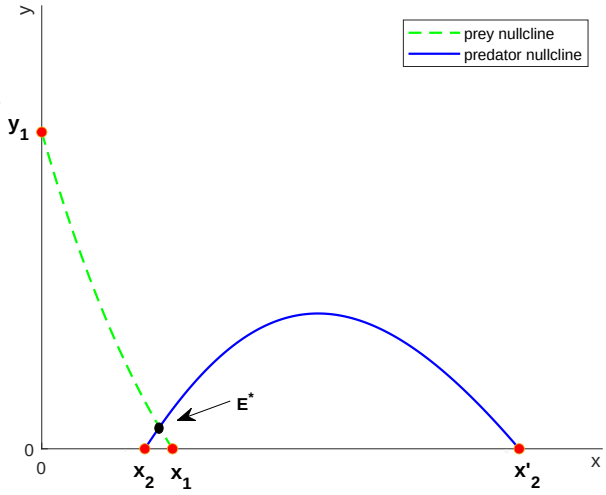

Fig. 2.1: Existence of unique interior equilibrium.

Remark 2.3.3. *Fig. 2.2 shows that how the number of interior equilibrium points changes as the rate of anti-predator behavior of prey to predator varies. In Table 2.2. we have given the number and nature for the equilibrium points shown in Fig. 2.2.*

η	Number of equilibrium points	Equilibrium point	Nature
1.458	2	(0.39724929, 0.28323503)	unstable focus
		(0.45801734, 0.29012915)	saddle point
1.46106707	1	(0.42608974, 0.28639905)	saddle point
1.462	0	-	-

Table 2.2: Number and nature of interior equilibrium points for three different values of η.

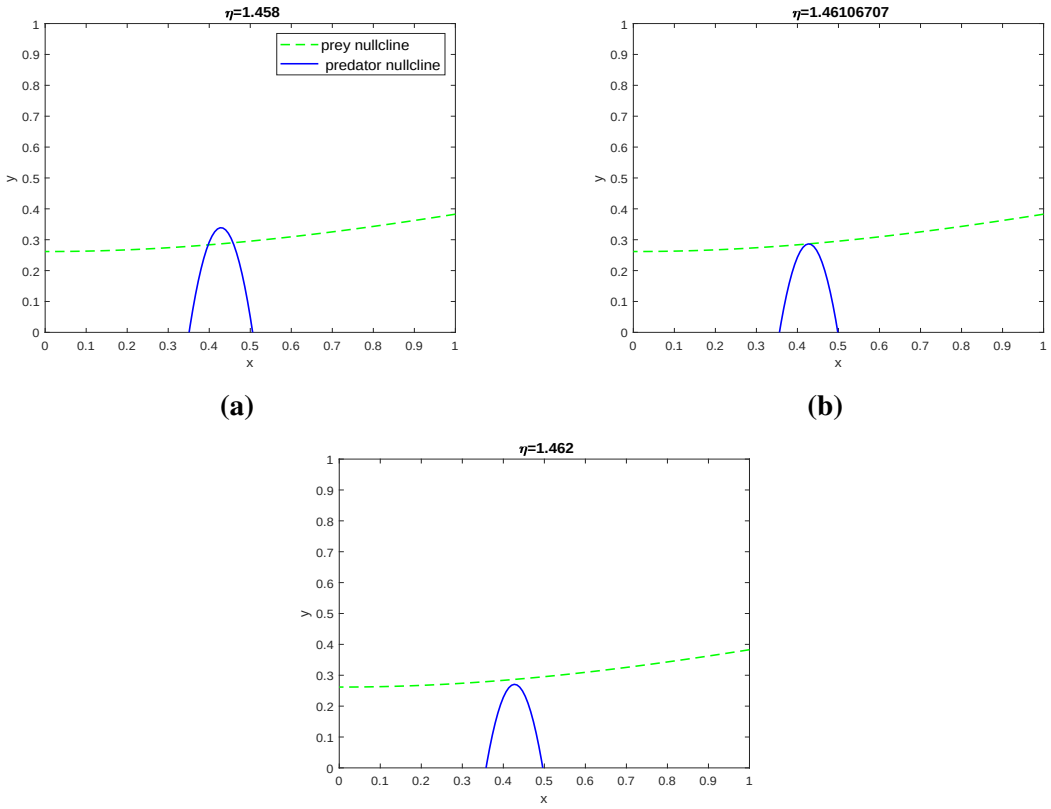

Fig. 2.2: Phase portraits depicting the change in number of interior equilibriums for r_1=0.01, k=1.5, with remaining all the parameters same as in (2.33).

2.3.3 Stability analysis

Local stability behavior of an equilibrium point corresponding to a dynamical system is determined by calculating the variational matrix corresponding to that system and further evaluating it around that point.

- It is easy to see that the equilibrium point $E_0(0,0)$ is a saddle point with stable manifold locally in the y-direction and unstable manifold in the x-direction.

- The variational matrix evaluated at $E_1(x_1,0)$ is given by

$$J|_{E_1} = \begin{bmatrix} -(r-r_0) & -rk(\frac{r-r_0}{r_1}) - \frac{\alpha(r-r_0)r_1}{a(r-r_0)^2+br_1^2} \\ 0 & \frac{c\alpha(r-r_0)r_1}{a(r-r_0)^2+br_1^2} - \delta_0 - \eta(\frac{r-r_0}{r_1}) \end{bmatrix}.$$

  Hence, it follows that

  1. $E_1(x_1,0)$ is locally asymptotically stable if $\frac{c\alpha(r-r_0)r_1}{a(r-r_0)^2+br_1^2} < \delta_0 + \eta(\frac{r-r_0}{r_1})$.
  2. $E_1(x_1,0)$is a saddle point with stable manifold locally along the x-direction and with unstable manifold along y-direction if $\frac{c\alpha(r-r_0)r_1}{a(r-r_0)^2+br_1^2} > \delta_0 + \eta(\frac{r-r_0}{r_1})$.

- The variational matrix evaluated at $E^*(x^*,y^*)$ is given by

$$J|_{E^*} = \begin{bmatrix} \frac{2\alpha a x^{*2} y^*}{(ax^{*2}+b)^2} - r_1 x^* & -\frac{rx^*k}{(1+ky^*)^2} - \frac{\alpha x^*}{(ax^{*2}+b)} \\ -\frac{c\alpha y^*(ax^{*2}-b)}{(ax^{*2}+b)^2} - \eta y^* & -\delta_1 y^* \end{bmatrix}.$$

  The characteristic equation corresponding to the above variational matrix is

$$\lambda^2 + A_1\lambda + A_2 = 0, \tag{2.12}$$

  where A_1 and A_2 are given by
  $A_1 = r_1x^* + \delta_1 y^* - \frac{2\alpha a x^{*2} y^*}{(ax^{*2}+b)^2}$,
  $A_2 = \left(r_1x^* - \frac{2\alpha a x^{*2} y^*}{(ax^{*2}+b)^2}\right)\delta_1 y^* - \left[\left(\frac{rx^*k}{(1+ky^*)^2} + \frac{\alpha x^*}{(ax^{*2}+b)}\right)\left(\frac{c\alpha y^*(ax^{*2}-b)}{(ax^{*2}+b)^2} + \eta y^*\right)\right]$.
  Now using the Routh-Hurwitz criteria we can say that both the eigenvalues of $J|_{E^*}$ have negative real part if and only if $A_1 > 0$ and $A_2 > 0$.
  Hence, we have the following theorem.

Theorem 2.3.4. *The system (2.4) is locally asymptotically stable around the interior equilibrium point $E^*(x^*,y^*)$ in the xy-plane if and only if*

$$A_1 > 0, \;\; A_2 > 0. \tag{2.13}$$

Now it is easy to see that (2.13) holds if

$$r_1 > \frac{2\alpha a x^* y^*}{(ax^{*2}+b)^2}, \quad \eta < \frac{c\alpha(b-ax^{*2})}{(ax^{*2}+b)^2}. \tag{2.14}$$

Remark 2.3.4. *The interior equilibrium point $E^*(x^*,y^*)$ is locally asymptotically stable in xy-plane if (2.14) holds.*

In the next theorem, we are able to show the occurence of Hopf-bifurcation under certain conditions.

Theorem 2.3.5. *For $k=k^*=\frac{G}{y}$ and $A_2>0$, where $G=\left(\frac{r}{r_0+2r_1x^*+\frac{\alpha y^*(b-ax^{*2})}{(ax^{*2}+b)^2}+\delta_1 y^*}-1\right)$, system (2.4) undergoes Hopf-bifurcation around the interior equilibrium point $E^*(x^*,y^*)$ provided $G>0$.*

Proof. For $k=k^*$, which is defined above, $trace(J|_{E^*})=0$, $det(J|_{E^*})>0$ which means that the Jacobian $J|_{E^*}$ has a pair of purely imaginary eigenvalues and $\left[\frac{d}{dk}(trace(J|_{E^*}))\right]_{k=k^*}=-\frac{rk^*y^*}{(1+k^*y^*)^2}<0$.
So, by Kot [55] (Theorem(Hopf) on page 129), the system (2.4) goes under Hopf-bifurcation around E^*.
Then we conclude that

- If $A_1<0$, $A_2>0$ then $k<k^*$ and E^* is unstable.
- If $A_1>0$, $A_2>0$ then $k>k^*$ and the interior equilibrium E^* is locally asymptotically stable.

□

Now we evaluate a sufficient condition for the global stability of unique interior equilibrium $E^*(x^*,y^*)$ and for this we assume a pre-condition that Theorem 2.3.3 holds.

Theorem 2.3.6. *The system (2.4) is globally asymptotically stable around the point $E^*(x^*,y^*)$ if the following inequalities hold:*

$$\begin{gathered} br_1^2(ax^{*2}+b)>\alpha ay^*(r+r_1x^*),\\ c\left[\frac{rk}{1+ky^*}+\frac{\eta}{c}+a\alpha x^*\left(\frac{r+r_1x^*}{r_1(ax^{*2}+b)}\right)\right]^2<4\delta_1\left[r_1-\frac{\alpha ay^*(r+r_1x^*)}{br_1(ax^{*2}+b)}\right]. \end{gathered} \tag{2.15}$$

Proof. Choose a Lyapunov function around the equilibrium point $E^*(x^*,y^*)$ defined as

$$V(x,y)=\left(x-x^*-x^*-ln\frac{x}{x^*}\right)+l_1\left(y-y^*-y^*-ln\frac{y}{y^*}\right),$$

where $l_1 > 0$ is a positive constant to be chosen on later stage. Now on differentiating V with respect to time along the solutions of system (2.4) we get

$$\frac{dV}{dt} = (x-x^*)\frac{dx}{dt} + l_1(y-y^*)\frac{dy}{dt}.$$

After doing some algebraic manipulations, we can get

$$\frac{dV}{dt} = -\left(r_1 - \frac{\alpha a y^*(x+x^*)}{(ax^2+b)(ax^{*2}+b)}\right)(x-x^*)^2 + \left(-\frac{rk}{(1+ky)(1+ky^*)} - \frac{\alpha}{(ax^2+b)} + \frac{cl_1\alpha}{(ax^2+b)} - \eta l_1 - \frac{acl_1\alpha x^*(x+x^*)}{(ax^2+b)(ax^{*2}+b)}\right)(x-x^*)(y-y^*) - l_1\delta_1(y-y^*)^2.$$

Now choosing $l_1 = \frac{1}{c}$, we get

$$\frac{dV}{dt} = -\left(r_1 - \frac{\alpha a y^*(x+x^*)}{(ax^2+b)(ax^{*2}+b)}\right)(x-x^*)^2 + \left(-\frac{rk}{(1+ky)(1+ky^*)} - \frac{\eta}{c} - \frac{a\alpha x^*(x+x^*)}{(ax^2+b)(ax^{*2}+b)}\right)(x-x^*)(y-y^*) - \frac{\delta_1}{c}(y-y^*)^2,$$

which implies that $\frac{dV}{dt}$ is negative definite under the stated conditions . Therefore, system (2.4) is globally asymptotically stable around E^* under the conditions given by (2.15).

□

2.3.4 Non-existence and existence of periodic orbit

Here, we shall figure out certain conditions for existence and non-existence of periodic orbit for system (2.4).

Theorem 2.3.7. *If* $\frac{\delta^* r_1^2}{cr^2} + \frac{r_1\delta_1}{r} > \frac{2\alpha a r}{r_1 b^2}$, *then the system (2.4) has no periodic solution in the interior of positive quadrant of the xy-plane.*

Proof. Let

$$h_1(x,y) = \frac{rx}{1+ky} - r_0 x - r_1 x^2 - \frac{\alpha xy}{ax^2+b},$$

$$h_2(x,y) = \frac{c\alpha xy}{ax^2+b} - \delta_0 y - \delta_1 y^2 - \eta xy.$$

In the interior of positive quadrant of xy-plane, consider a continuously differentiable function given as

$$H(x,y) = \frac{1}{xy}.$$

So,

$$\nabla = \frac{\partial(h_1 H)}{\partial x} + \frac{\partial(h_2 H)}{\partial y}$$
$$= -\frac{r_1}{y} + \frac{2\alpha a x}{(ax^2+b)^2} - \frac{\delta_1}{x}.$$

Now $\nabla < 0$, if

$$\frac{r_1}{y} + \frac{\delta_1}{x} > \frac{2\alpha a x}{(ax^2+b)^2},$$

holds, i.e. if the minimum of L.H.S. is greater than the maximum of R.H.S.. Therefore, y and x are replaced by $y = y_a = \frac{cr^2}{\delta^* r_1}$, $x = x_a = \frac{r}{r_1}$ (their respective maximum values) in L.H.S. of above inequality. As, $\frac{x}{(ax^2+b)^2} < \frac{x_a}{b^2} = \frac{r}{r_1 b^2}$. So, we replace $\frac{x}{(ax^2+b)^2}$ by $\frac{r}{r_1 b^2}$ in R.H.S. of of above inequality. Therefore, $\nabla < 0$ if $\frac{\delta^* r_1^2}{cr^2} + \frac{r_1\delta_1}{r} - \frac{2\alpha a r}{r_1 b^2} > 0$. Thus, by Dulac-Bendixson criterion, we can conclude that system (2.4) does not have periodic orbit under this assumption. □

Theorem 2.3.8. *Assume* $\frac{c\alpha(r-r_0)r_1}{a(r-r_0)^2+br_1^2} > \delta_0 + \eta(\frac{r-r_0}{r_1})$ *and in equation (2.12) if*

$$A_2 < 0. \tag{2.16}$$

or

$$A_1 < 0,\ A_2 > 0. \tag{2.17}$$

hold, then the system (2.4) has a periodic solution.

Proof. From Lemma 2.3.1, we get that int(Ω) is an invariant set and from equations (2.16) and (2.17) implies that E^* is an unstable equilibrium point and as $\frac{c\alpha(r-r_0)r_1}{a(r-r_0)^2+br_1^2} > \delta_0 + \eta(\frac{r-r_0}{r_1})$, so E_1 is a saddle point. Therefore, positive limit set does not contain any equilibrium point. Hence, by using Poincarè– Bendixson theorem it implies that system has a periodic solution. □

Remark 2.3.5. *It may be pointed out here that due to mathematical complexity, it is not easy to check the independency of the conditions obtained in Theorem 2.3.7 and Theorem 2.3.8. However, both the theorems (Dulac-Bendixson criterion and Poincarè– Bendixson theorem) assures that conditions in Theorems 2.3.7 and 2.3.8 can not hold simultaneously.*

2.4 Properties of delayed Model

2.4.1 Local stability and Hopf-bifurcation

System (2.3) can be expressed as

$$\frac{dU}{dt} = F(U(t), U(t-\tau_1), U(t-\tau_2)),$$

where $U(t) = [x(t), y(t)]^T$, $U(t-\tau_1) = [x(t-\tau_1), y(t-\tau_1)]^T$ and $U(t-\tau_2) = [x(t-\tau_2), y(t-\tau_2)]^T$.
Assume $\bar{x}(t) = x(t) - x^*$ and $\bar{y}(t) = y(t) - y^*$. After this, the linearized system (2.3) around the interior equilibrium $E^*(x^*, y^*)$ is

$$\frac{dW}{dt} = A'W(t) + B'W(t-\tau_1) + C'W(t-\tau_2),$$

where

$$A' = \left(\frac{\partial F}{\partial U}\right)_{E^*}, \quad B' = \left(\frac{\partial F}{\partial U(t-\tau_1)}\right)_{E^*}, \quad C' = \left(\frac{\partial F}{\partial U(t-\tau_2)}\right)_{E^*},$$

and $W(t) = [\bar{x}(t), \bar{y}(t)]^T$. The Jacobian matrix of the system (2.3) at E^* is given by

$$J = A' + B'e^{-\lambda\tau_1} + C'e^{-\lambda\tau_2}.$$

After a little calculation, we get

$$J = \begin{bmatrix} a_1 & a_2 + a_3 e^{-\lambda\tau_1} \\ -\eta y^* + a_4 e^{-\lambda\tau_2} & a_5 + a_6 - a_5 e^{-\lambda\tau_2} \end{bmatrix},$$

where

$$a_1 = -r_1 x^* + \frac{2\alpha a x^{*2} y^*}{(ax^{*2}+b)^2},\ a_2 = -\frac{\alpha x^*}{(ax^{*2}+b)},\ a_3 = -\frac{rx^*k}{(1+ky^*)^2},\ a_4 = -\frac{c\alpha y^*(ax^{*2}-b)}{(ax^{*2}+b)^2},$$
$$a_5 = -\frac{c\alpha x^*}{(ax^{*2}+b)},\ a_6 = -\delta_1 y^*.$$

Corresponding characteristic equation of above variational matrix is

$$\lambda^2 + b_1\lambda + b_2 + e^{-\lambda\tau_1}b_3 + e^{-\lambda\tau_2}(b_4\lambda + b_5) + e^{-\lambda(\tau_1+\tau_2)}b_6 = 0, \tag{2.18}$$

where

$b_1 = -(a_1 + a_5 + a_6),\ b_2 = a_1(a_5 + a_6) + a_2\eta y^*,\ b_3 = a_3\eta y^*,\ b_4 = a_5,\ b_5 = -a_1a_5 - a_2a_4,$
$b_6 = -a_3a_4.$

Now equation (2.18) takes different forms when we take both τ_1 and τ_2 zero, one of τ_1 and τ_2 is zero, when both τ_1 and τ_2 are non-zero.

Case 1: $\tau_1 = \tau_2 = 0$. Then (2.18) becomes

$$\lambda^2 + (b_1 + b_4)\lambda + (b_2 + b_3 + b_5 + b_6) = 0. \tag{2.19}$$

This characteristic equation (2.19) is same as that of the characteristic equation (2.12) for the non-delayed system (2.4) which we have studied before.
$(H_1):\ (b_1 + b_4) > 0,\ (b_2 + b_3 + b_5 + b_6) > 0.$
All the zeros of equation (2.19) have negative real parts if and only if (H_1) holds.
Case(2): $\tau_1 = 0,\ \tau_2 > 0$. The equation (2.18) becomes

$$\lambda^2 + b_1\lambda + (b_2 + b_3) + e^{-\lambda\tau_2}(b_4\lambda + (b_5 + b_6)) = 0. \tag{2.20}$$

Assume $i\omega(\omega > 0)$ be a zero of the equation (2.20), then we get

$$-\omega^2 + b_1 i\omega + (b_2 + b_3) + (cos(\omega\tau_2) - isin(\omega\tau_2))(b_4 i\omega + (b_5 + b_6)) = 0. \tag{2.21}$$

After equating real and imaginary parts on both sides of above equation we get

$$\begin{aligned} b_4\omega sin(\omega\tau_2) + (b_5 + b_6)cos(\omega\tau_2) &= \omega^2 - (b_2 + b_3), \\ (b_5 + b_6)sin(\omega\tau_2) - b_4\omega cos(\omega\tau_2) &= b_1\omega, \end{aligned} \tag{2.22}$$

which gives

$$z^2 + p_1 z + q_1 = 0, \tag{2.23}$$

and let $f(z) = z^2 + p_1 z + q_1$, where $z = \omega^2,\ p_1 = b_1^2 - b_4^2 - 2(b_2 + b_3),\ q_1 = (b_2 + b_3)^2 - (b_5 + b_6)^2$.
$(H_2):\ p_1 > 0,\ q_1 > 0.$

- If assumption (H_2) is true, equation (2.23) has no positive roots which means such ω does not exists. Hence, E^* is asymptotically stable for all $\tau_2 > 0$ if hypotheses (H_1) and (H_2) hold.

$(H_3):\ q_1 < 0$. Then equation (2.23) has unique positive root w_0^2. On substituting w_0^2 in equation (2.22), we get

$$b_4\omega_0 sin(\omega_0\tau_2) + (b_5+b_6)cos(\omega_0\tau_2) = \omega_0^2 - (b_2+b_3),$$

$$(b_5+b_6)sin(\omega_0\tau_2) - b_4\omega_0 cos(\omega_0\tau_2) = b_1\omega_0,$$

which gives

$$\tau_{2_j} = \frac{1}{\omega_0}cos^{-1}\left[\frac{(\omega_0^2-(b_2+b_3))(b_5+b_6)-b_1b_4\omega_0^2}{(b_5+b_6)^2+b_4^2\omega_0^2}\right] + \frac{2\pi j}{\omega_0},\ \ j=0,1,2\ldots . \tag{2.24}$$

$(H_4):\ p_1>0,\ q_1>0,\ p_1^2>4q_1$.
If (H_1) and (H_4) holds, then equation (2.23) possess two positive roots ω_+^2 and ω_-^2. Substituting $\omega_\pm^2$ in (2.22) we get

$$\tau_{2_k}^{\pm} = \frac{1}{\omega_\pm}cos^{-1}\left[\frac{(\omega_\pm^2-(b_2+b_3))(b_5+b_6)-b_1b_4\omega_\pm^2}{(b_5+b_6)^2+b_4^2\omega_\pm^2}\right] + \frac{2\pi k}{\omega_\pm},\ \ k=0,1,2\ldots .$$

Let $\lambda(\tau_{2_j}) = i\omega_0$ be a root of equation (2.20). Then a little calculation leads to

$$Re\left[\frac{d\lambda}{d\tau_2}\right]^{-1}_{\lambda=i\omega_0,\ \tau_2=\tau_{2_j}} = \frac{f'(\omega_0^2)}{b_4^2\omega_0^2+(b_5+b_6)^2}.$$

$(H_{51}):\ f'(\omega_0^2)>0$.
As sign of $\left[\frac{d}{d\tau_2}(Re(\lambda))\right]_{\lambda=i\omega_0,\ \tau_2=\tau_{2_j}}$ is same as sign of $\left[Re(\frac{d\lambda}{d\tau_2})\right]_{\lambda=i\omega_0,\ \tau_2=\tau_{2_j}}$.
Hence $\left[\frac{d}{d\tau_2}(Re(\lambda))\right]_{\lambda=i\omega_0,\ \tau_2=\tau_{2_j}} > 0$ under assumption (H_{51}).
Similarly if $\lambda(\tau_{2_k}^{\pm}) = i\omega_\pm$ are the roots of (2.20).
$(H_{52}):\ f'(\omega_+^2)>0$ (rep. $f'(\omega_-^2)<0$) holds, then

$$\left[\frac{d}{d\tau_2}(Re(\lambda))\right]_{\lambda=i\omega_+,\ \tau_2=\tau_{2_k}^+} > 0, \quad \left[\frac{d}{d\tau_2}(Re(\lambda))\right]_{\lambda=i\omega_-,\ \tau_2=\tau_{2_k}^-} < 0.$$

Now we can summarize above analysis in the following theorem.

Theorem 2.4.1. *For system (2.3), with $\tau_1=0$ and $\tau_2>0$, we can make following conclusions:*

1. *If (H_1) and (H_2) hold then the equilibrium E^* is locally asymptotically stable for all $\tau_2>0$.*

2. *If (H_1) fails and (H_2) holds then E^* is unstable for all $\tau_2>0$.*

3. *If* (H_1), (H_3) *and* (H_{51}) *hold then* E^* *is locally asymptotically stable for* $\tau_2 < \tau_{2_0}$ *and unstable for* $\tau_2 > \tau_{2_0}$ *and system (2.3) undergoes Hopf-bifurcation at* $\tau_2 = \tau_{2_0}$.

4. *If* (H_1), (H_4), (H_{52}) *hold then equilibrium point* E^* *is locally asymptotically stable when* $\tau_2 \in [0, \tau_{2_0}^+) \cup (\tau_{2_0}^-, \tau_{2_1}^+) \cup ... \cup (\tau_{2_{n-1}}^-, \infty)$ *and when* $\tau_2 \in (\tau_{2_0}^+, \tau_{2_0}^-) \cup (\tau_{2_1}^+, \tau_{2_1}^-) \cup ... \cup (\tau_{2_n}^+, \infty)$, E^* *is unstable. Moreover system (2.3) undergoes Hopf-bifurcation at* E^* *when* $\tau_2 = \tau_{2_k}^{\pm}$, $k = 0, 1, 2...$.

Case(3): $\tau_1 > 0,\ \tau_2 = 0.$

Theorem 2.4.2. *For,* $\tau_1 > 0$ *and* $\tau_2 = 0$, *the equilibrium point* $E^*(x^*, y^*)$ *is locally asymptotically stable for* $\tau_1 < \tau_{1_0}$ *and unstable when* $\tau_1 > \tau_{1_0}$. *Furthermore, system (2.3) undergoes Hopf-bifurcation at* $\tau_1 = \tau_{1_0}$ *given by*

$$\tau_{1_0} = \frac{1}{\omega_{10}} cos^{-1}\left[\frac{\omega_{10}^2 - (b_2 + b_5)}{(b_3 + b_6)}\right],$$

where ω_{10} *is the root of corresponding characteristic equation.*

Proof. It is similar as in case(2). □

Case(4): $\tau_1 > 0,\ \tau_2 > 0$. we assume that in (2.18) τ_2 is in stable interval $(0, \tau_{2_0})$ and τ_1 is considered as a parameter. Let $\lambda = i\omega_1 (\omega_1 > 0)$ is a zero of (2.18). Then substituting $\lambda = i\omega_1$ in (2.18) and after separating real and imaginary parts we get

$$\begin{aligned} -{\omega_1}^2 + b_2 + b_5 cos(\omega_1\tau_2) + b_4\omega_1 sin(\omega_1\tau_2) =& -b_3 cos(\omega_1\tau_1) - b_6 cos(\omega_1\tau_1)cos(\omega_1\tau_2) \\ &+ b_6 sin(\omega_1\tau_1)sin(\omega_1\tau_2), \\ b_1\omega_1 + b_4\omega_1 cos(\omega_1\tau_2) - b_5 sin(\omega_1\tau_2) =& b_3 sin(\omega_1\tau_1) + b_6 sin(\omega_1\tau_1)cos(\omega_1\tau_2) \\ &+ b_6 cos(\omega_1\tau_1)sin(\omega_1\tau_2). \end{aligned} \tag{2.25}$$

Now eliminating τ_1 from (2.25) leads to a transcendental equation:

$$\begin{aligned} H(\omega_1) = \omega_1^4 + \omega_1^3(-2b_4 sin(\omega_1\tau_2)) + \omega_1^2(b_4^2 + b_1^2 - 2b_2 + 2(b_1b_4 - b_5)cos(\omega_1\tau_2)) \\ + \omega_1(2(b_2b_4 - b_1b_5)sin(\omega_1\tau_2)) + b_2^2 + b_5^2 - b_3^2 - b_6^2 + 2(b_2b_5 - b_3b_6)cos(\omega_1\tau_2) = 0. \end{aligned} \tag{2.26}$$

Being a transcendental equation of (2.26) it is not easy to predict the nature of its roots. So, we assume that it has finite positive roots $\omega_1^{(1)}, \omega_1^{(2)}, \omega_1^{(3)}, ..., \omega_1^{(m)}$ and for fixed $\omega_1^{(i)} (i = 1, 2, 3, ..., m)$, there exists a sequence $\{\tau_{1_i}^{(r)} | r = 1, 2, 3, ...\}$ satisfying (2.25). So, (2.25) can be written as

$$\begin{aligned} -F_1 cos(\omega_1^i \tau_{1_i}^{(r)}) + F_2 sin(\omega_1^i \tau_{1_i}^{(r)}) = F_3, \\ F_1 sin(\omega_1^i \tau_{1_i}^{(r)}) + F_2 cos(\omega_1^i \tau_{1_i}^{(r)}) = F_4, \end{aligned} \tag{2.27}$$

where,

$$F_1 = b_3 + b_6 cos(\omega_1^{(i)}\tau_2),\ F_2 = b_6 sin(\omega_1^{(i)}\tau_2),$$
$$F_3 = -{\omega_1^{(i)}}^2 + b_2 + b_5 cos(\omega_1^{(i)}\tau_2) + b_4\omega_1^{(i)} sin(\omega_1^{(i)}\tau_2),$$
$$F_4 = b_1\omega_1^{(i)} + b_4\omega_1^{(i)} cos(\omega_1^{(i)}\tau_2) - b_5 sin(\omega_1^{(i)}\tau_2).$$

Then from (2.27), the critical value of $\tau_{1_i}^{(r)}$ for each $\omega_1^{(i)}$ is

$$\tau_{1_i}^{(r)} = \frac{1}{\omega_1^{(i)}} sin^{-1}\left[\frac{F_2F_3 + F_1F_4}{F_1^2 + F_2^2}\right] + \frac{2\pi r}{\omega_1^{(i)}},\ i = 1,2,3,...,m,\ r = 0,1,2,... . \tag{2.28}$$

Assume $\tau_1^* = min\{\tau_{1_i}^{(0)},\ i = 1,2,...,m\}$ and ω_1^* be the corresponding root of (2.18) with $\tau_2 \in [0,\tau_{2_0}]$.

For verifying the transversality condition, substitute $\lambda(\tau_1) = \xi(\tau_1) + i\omega(\tau_1)$ in (2.18) and differentiating the same with respect to τ_1. Substituting $\tau_1 = \tau_1^*,\ \omega = \omega_1^*,\ \xi = 0$ we obtain

$$\begin{aligned} P_1\left[\frac{d\xi}{d\tau_1}\right]_{\tau_1=\tau_1^*,\ \omega=\omega^*} - P_2\left[\frac{d\omega}{d\tau_1}\right]_{\tau_1=\tau_1^*,\ \omega=\omega^*} &= Q_1, \\ P_2\left[\frac{d\xi}{d\tau_1}\right]_{\tau_1=\tau_1^*,\ \omega=\omega^*} + P_1\left[\frac{d\omega}{d\tau_1}\right]_{\tau_1=\tau_1^*,\ \omega=\omega^*} &= Q_2, \end{aligned} \tag{2.29}$$

which implies

$$\left[\frac{d\xi}{d\tau_1}\right]_{\tau_1=\tau_1^*,\ \omega=\omega^*} = \frac{P_1Q_1 + P_2Q_2}{P_1^2 + P_2^2}, \tag{2.30}$$

where,

$$\begin{aligned} P_1 &= b_1 - b_3\tau_1^* cos(\omega_1^*\tau_1^*) + b_4 cos(\omega_1^*\tau_2) - b_6\tau_1^*[cos(\omega_1^*(\tau_1^* + \tau_2))], \\ P_2 &= 2\omega_1^* + b_3\tau_1^* sin(\omega_1^*\tau_1^*) - b_4 sin(\omega_1^*\tau_2) + b_6\tau_1^*[sin(\omega_1^*(\tau_1^* + \tau_2))], \\ Q_1 &= b_3\omega_1^* sin(\omega_1^*\tau_1^* + b_6\omega_1^*[sin(\omega_1^*(\tau_1^* + \tau_2))], \\ Q_2 &= b_3\omega_1^* cos(\omega_1^*\tau_1^* + b_6\omega_1^*[cos(\omega_1^*(\tau_1^* + \tau_2))]. \end{aligned}$$

$(H_6):\ P_1Q_1 + P_2Q_2 \neq 0.$

Theorem 2.4.3. *For system (2.3), let (H_1), (H_6) hold with τ_2 in the stable interval $[0,\tau_{2_0})$. Then the equilibrium E^* is locally asymptotically stable when $\tau_1 \in (0,\tau_1^*)$. Furthermore (2.3) undergoes Hopf-bifurcation at E^* when $\tau_1 = \tau_1^*$.*

Case 5: $\tau_1 > 0,\ \tau_2 > 0$ with τ_1 lies in the stable interval $(0, \tau_{1_0})$ and τ_2 is treated as parameter. Then under an analysis similar to Case 4, we can note the following theorem.

Theorem 2.4.4. *For (2.3), when τ_1 is in stable interval $[0, \tau_{1_0})$ and τ_2 is taken as parameter then same analysis can be done as in above Theorem 2.4.3 to get such τ_2^* such that E^* is locally asymptotically in the interval $(0, \tau_2^*)$. Moreover (2.3) undergoes Hopf-bifurcation when $\tau_2 = \tau_2^*$ and it is given as*

$$\tau_2^* = \frac{1}{\omega_2^*} cos^{-1}\left[\frac{E_1E_3 + E_2E_4}{E_1^2 + E_2^2}\right] + \frac{2\pi n}{\omega_2^*},\ n = 0, 1, 2, \dots,$$

where, $E_1 = b_5 + + b_6 cos(\omega_2^*\tau_1)$, $E_2 = b_4\omega_2^* - b_6 sin(\omega_2^*\tau_1)$, $E_3 = \omega_2^{*2} - b_2 - b_3 cos(\omega_2^*\tau_1)$, $E_4 = b_3 sin(\omega_2^*\tau_1) - b_1\omega_2^*$ and $i\omega_2^*$ is the root of Eq. (2.18).

2.5 Direction and Stability of Hopf-bifurcation

In previous section we have determined different conditions under which system (2.3) undergoes Hopf-bifurcation for different combinations of fear response delay τ_1 and gestation delay τ_2. Now, in this section we will determine the direction and stability of of bifurcated solutions of system (2.3) with respect to $\tau_1 = \tau_1^*$ and $\tau_2 = \tau_2{}' \in (0, \tau_{2_0})$ by using normal form method and center manifold theorem introduced by Hassard *et al.* [83].

Without loss of generality, we assume that $\tau_2{}' < \tau_1^*$ and let

$x_1(t) = x(t) - x^*,\ y_1(t) = y(t) - y^*$ and still denote $x_1(t),\ y_1(t)$ by $x(t),\ y(t)$.

Let $\tau_1 = \tau_1^* + \mu,\ \mu \in R$. Then at $\mu = 0$ system (2.3) undergoes Hopf-bifurcation. Rescaling the time delay $t \to (t/\tau_1)$, system (2.3) can be rewritten as

$$\dot{U} = (\tau_1^* + \mu)\Big(P'U(t) + R'U\big(t - \frac{\tau_2{}'}{\tau_1^*}\big) + Q'U(t-1) + f(x,y)\Big), \tag{2.31}$$

where

$$U(t) = (x(t), y(t))^T,\ P' = \begin{bmatrix} a_1 & a_2 \\ -ny^* & a_5 + a_6 \end{bmatrix},\ Q' = \begin{bmatrix} 0 & a_3 \\ 0 & 0 \end{bmatrix},\ R' = \begin{bmatrix} 0 & 0 \\ a_4 & -a_5 \end{bmatrix},$$

$$f(x,y) = \begin{bmatrix} f_1 \\ f_2 \end{bmatrix}.$$

The non-linear term f_1 and f_2 are given by

$$f_1 = e_1x^2(t) + e_2y^2(t-1) + e_3x(t)y(t) + e_4x(t)y(t-1) + p_1x^3(t) + p_2y^3(t-1) + p_3x^2(t)y(t) + p_4x(t)y^2(t-1)...,$$

$$f_2 = g_1y^2(t) + g_2x^2\big(t - \frac{\tau_2{}'}{\tau_1^*}\big) + g_3x(t)y(t) + g_4x\big(t - \frac{\tau_2{}'}{\tau_1^*}\big)y\big(t - \frac{\tau_2{}'}{\tau_1^*}\big) + h_1x^2\big(t - \frac{\tau_2{}'}{\tau_1^*}\big)y\big(t - \frac{\tau_2{}'}{\tau_1^*}\big)...,$$

where

$$e_1 = -2r_1 + \frac{2\alpha ax^*y^*(3b - ax^{*2})}{(ax^{*2}+b)^3},\ e_2 = \frac{2rk^2x^*}{(1+ky^*)^3},\ e_3 = \frac{\alpha(b-ax^{*2})}{(ax^{*2}+b)^2},\ e_4 = -\frac{rk}{(1+ky^*)^2},$$

$$p_1 = -\frac{6a\alpha y^*(a^2x^{*4} - 6abx^{*2} + b^2)}{(ax^{*2}+b)^4},\ p_2 = -\frac{brk^3x^*}{(1+ky^*)^4}, p_3 = \frac{2\alpha a(3b - ax^{*2})}{(ax^{*2}+b)^3},\ p_4 = \frac{2rk^2}{(1+ky^*)^3},$$

$$g_1 = -2\delta_1,\ g_2 = -\frac{2c\alpha ax^*y^*(3b - ax^{*2})}{(ax^{*2}+b)^3},\ g_3 = -\eta,\ g_4 = \frac{c\alpha(b-ax^{*2})}{(ax^{*2}+b)^2},$$

$$h_1 = -\frac{2c\alpha ax^*(3b - ax^{*2})}{(ax^{*2}+b)^3}.$$

The delayed system can be written in the functional form

$$L_\mu(\phi) = (\tau_1^* + \mu)\Big(P'\phi(0) + R'\phi\big(-\frac{\tau_2{}'}{\tau_1^*}\big) + Q'\phi(-1)\Big).$$

Using Riez representation theorem, $\exists$ a 2×2 matrix $\eta'(\theta,\ \mu),\ \theta \in [-1,0]$, whose elements are of bounded variation functions such that

$$L_\mu(\phi) = \int_{-1}^{0} d\eta'(\theta,\ \mu)\phi(\theta)$$

for $\phi \in C([-1,0], R^2)$. In fact, we can choose

$$\eta'(\theta,\ \mu) = \begin{cases} (\tau_1^* + \mu)(P' + R' + Q'), & \theta = 0 \\ (\tau_1^* + \mu)(Q' + R'), & \theta \in \big[-\frac{\tau_2'}{\tau_1^*}, 0\big) \\ (\tau_1^* + \mu), & \theta \in \big[-1,\ -\frac{\tau_2'}{\tau_1^*}\big) \\ 0, & \theta = -1. \end{cases}$$

For $\phi \in C^1([-1,0],R^2)$, define

$$A(\mu)\phi(\theta) = \begin{cases} \frac{d\phi(\theta)}{d\theta}, & \theta \in [-1,0] \\ \int_{-1}^{0} d\eta'(\xi,\ \mu)\phi(\xi), & \theta = 0, \end{cases}$$

and

$$R(\mu)\phi = \begin{cases} 0, & \theta \in [-1,0] \\ h(\mu,\phi), & \theta = 0, \end{cases}$$

where

$$h(\mu,\phi) = (\tau_1^* + \mu)\begin{bmatrix} h_1 \\ h_2 \end{bmatrix},\ \phi = (\phi_1,\phi_2)^T \in C([-1,0],R^2),$$

$$\begin{aligned} h_1 &= e_1{\phi_1}^2(0) + e_2{\phi_2}^2(-1) + e_3\phi_1(0)\phi_2(0) + e_4\phi_1(0)\phi_2(-1) + p_1{\phi_1}^3(0) \\ &\quad + p_2{\phi_2}^3(-1) + p_3{\phi_1}^2(0)\phi_2(0) + p_4\phi_1(0){\phi_2}^2(-1)..., \\ h_2 &= g_1{\phi_2}^2(0) + g_2{\phi_1}^2\big(-\frac{{\tau_2}'}{\tau_1^*}\big) + g_3\phi_1(0)\phi_2(0) + g_4\phi_1\big(-\frac{{\tau_2}'}{\tau_1^*}\big)\phi_2\big(-\frac{{\tau_2}'}{\tau_1^*}\big) \\ &\quad + h_1{\phi_1}^2\big(-\frac{{\tau_2}'}{\tau_1^*}\big)\phi_2\big(-\frac{{\tau_2}'}{\tau_1^*}\big)... \ . \end{aligned}$$

Then system (2.3) is equivalent to following form

$$\dot{U}_t = A(\mu)U_t + R(\mu)U_t,$$

where $\dot{U}_t = U(t+\theta)$ for $\theta \in [-1,0]$.
For $\phi \in C([-1,0],R^2),\ \psi \in C^1([-1,0],(R^2)^*)$, define

$$A^*\psi(s) = \begin{cases} \frac{d\psi(s)}{ds}, & s \in (0,1] \\ \int_{-1}^{0} \psi(-\xi)d\eta'(\xi,0), & \theta = 0, \end{cases}$$

and a bilinear form

$$\big\langle \psi(s),\ \phi(\theta)\big\rangle = \overline{\psi}(0)\phi(0)) - \int_{-1}^{0}\int_{\xi=0}^{\theta} \overline{\psi}(\xi-\theta)d\eta'(\theta)\phi(\xi)d\xi,$$

where $\eta'(\theta) = \eta'(\theta,0)$, $A = A(0)$ and A^* are adjoint operators.

We know that $\pm i\omega_1^*\tau_1^*$ are the eigenvalues of $A(0)$ and therefore they are also the eigenvalues of A^* and $q(\theta) = (1,\rho)^T e^{i\tau_1^*\omega_1^*\theta}(\theta \in [-1,0])$ and $q^*(s) = D(1,\rho^*)e^{i\tau_1^*\omega_1^* s}(s \in [-1,0])$ are the eigenvectors of $A(0)$ and A^* corresponding to eigenvalues $i\omega^*\tau_1^*$ and $-i\omega^*\tau_1^*$ and

$$\big\langle q^*(s),\ q(\theta)\big\rangle = 1,\ \big\langle q^*(s),\ q(\bar{\theta})\big\rangle = 1,$$

$$\rho = \frac{i\omega_1^* - a_1}{a_2 + a_3 e^{-i\omega_1^*\tau_1^*}}, \quad \rho^* = -\frac{i\omega_1^* + a_1}{-\eta y^* + a_4 e^{\frac{-i\omega_1^*\tau_2'}{\tau_1^*}}},$$

$$\overline{D} = \left[1 + \overline{\rho^*}\rho + a_3\rho\tau_1^* e^{-i\omega_1^*\tau_1^*} + a_4\tau_2'\overline{\rho^*}e^{-i\omega_1^*\tau_2'} - a_5\tau_2'\overline{\rho^*}\rho e^{-i\omega_1^*\tau_2'}\right]^{-1}.$$

Following the algorithms explained in [83] and using computation process similar to that in [84] , to obtain the properties of Hopf-bifurcation, we get

$$g_{20} = -\tau_1^*\overline{D}\left[2rk\rho e^{-i\omega_1^*\tau_1^*} - rW_{20}^{(1)}(0) + 2r_1 + \frac{2\rho\alpha}{b} - \frac{2\rho\overline{\rho^*}c\alpha}{b}e^{-2i\omega_1^*\tau_2'} + 2\overline{\rho^*}\rho^2\delta_1 + 2\rho\overline{\rho^*}\eta\right]$$

$$g_{11} = -\tau_1^*\overline{D}\left[rk\overline{\rho}e^{i\omega_1^*\tau_1^*} + rk\rho e^{-i\omega_1^*\tau_1^*} - rW_{11}^{(1)}(0) + 2r_1 + \frac{\alpha\overline{\rho}}{b} + \frac{\alpha\rho}{b} - \frac{\overline{\rho}\overline{\rho^*}c\alpha}{b} - \frac{\rho\overline{\rho^*}c\alpha}{b}\right.$$
$$\left. + 2\rho\overline{\rho}\overline{\rho^*}\delta_1 + \overline{\rho}\overline{\rho^*}\eta + \rho\overline{\rho^*}\eta\right],$$

$$g_{02} = \tau_1^*\overline{D}\left[2rk\overline{\rho}e^{i\omega_1^*\tau_1^*} - rW_{02}^{(1)}(0) + 2r_1 + \frac{2\alpha\overline{\rho}}{b} - \frac{2c\alpha\overline{\rho^*}\overline{\rho}e^{2i\omega_1^*\tau_2'}}{b} + 2\overline{\rho^2}\,\overline{\rho^*}\delta_1 + 2\overline{\rho}\overline{\rho^*}\eta\right]$$

$$g_{21} = -\tau_1^*\overline{D}\left[r\left\{2kW_{11}^{(2)}(-1) + kW_{20}^{(2)}(-1) + k\overline{\rho}e^{i\omega_1^*\tau_1^*} + 2W_{11}^{(1)}(0)k\rho e^{-i\omega_1^*\tau_1^*}\right\} + r_1\left\{4W_{11}^{(1)}(0)\right.\right.$$
$$\left. + 2W_{20}^{(1)}(0)\right\} + \alpha\left\{\frac{2}{b}W_{11}^{(2)}(0) + \frac{1}{b}W_{20}^{(2)}(0) + \frac{1}{b}W_{20}^{(1)}(0)\overline{\rho} + \frac{2}{b}W_{11}^{(1)}(0)\rho\right\}$$
$$+ \overline{\rho^*}c\alpha\left\{-\frac{2}{b}W_{11}^{(2)}\left(\frac{-\tau_2'}{\tau_1^*}\right)e^{-i\omega_1^*\tau_2'} - \frac{1}{b}W_{20}^{(2)}\left(\frac{-\tau_2'}{\tau_1^*}\right)e^{i\omega_1^*\tau_2'} - \frac{1}{b}W_{20}^{(1)}\left(\frac{-\tau_2'}{\tau_1^*}\right)\overline{\rho}e^{i\omega_1^*\tau_2'}\right.$$
$$\left. - \frac{2}{b}W_{11}^{(1)}\left(\frac{-\tau_2'}{\tau_1^*}\right)\rho e^{-i\omega_1^*\tau_2'}\right\} - \overline{\rho^*}\delta_1\left\{-4W_{11}^{(2)}(0)\rho - 2W_{20}^{(2)}(0)\overline{\rho}\right\} - \overline{\rho^*}\eta\left\{-2W_{11}^{(2)}(0)\right.$$
$$\left.\left. - W_{20}^{(2)}(0) - \overline{\rho}W_{20}^{(1)}(0) - 2\rho W_{11}^{(1)}(0)\right\}\right],$$

where

$$W_{20}(\theta) = \frac{ig_{20}}{\omega_1^*\tau_1^*}q(0)e^{i\omega_1^*\tau_1^*\theta} + \frac{i\bar{g}_{02}}{3\omega_1^*\tau_1^*}\bar{q}(0)e^{-i\omega_1^*\tau_1^*\theta} + M_1 e^{2i\omega_1^*\tau_1^*\theta},$$
$$W_{02}(\theta) = -\frac{ig_{02}}{3\omega_1^*\tau_1^*}q(0)e^{i\omega_1^*\tau_1^*\theta} - \frac{i\bar{g}_{20}}{\omega_1^*\tau_1^*}\bar{q}(0)e^{-i\omega_1^*\tau_1^*\theta} + M_2 e^{-2i\omega_1^*\tau_1^*\theta},$$
$$W_{11}(\theta) = -\frac{ig_{11}}{\omega_1^*\tau_1^*}q(0)e^{i\omega_1^*\tau_1^*\theta} + \frac{i\bar{g}_{11}}{\omega_1^*\tau_1^*}\bar{q}(0)e^{-i\omega_1^*\tau_1^*\theta} + M_3,$$

$M_1 = (M_1^{(1)}, M_1^{(2)})^T \in R^2$, $M_2 = (M_2^{(1)}, M_2^{(2)})^T \in R^2$, $M_3 = (M_3^{(1)}, M_3^{(2)})^T \in R^2$ are constant vectors, computed as:

$$M_1 = 2\begin{bmatrix} 2i\omega_1^* - a_1 & -a_2 - a_3 e^{-2i\omega_1^*\tau_1^*} \\ \eta y^* - a_4 e^{-2i\omega_1^*\tau_2'} & 2i\omega_1^* - a_5 - a_6 + a_5 e^{-2i\omega_1^*\tau_2'} \end{bmatrix}^{-1} \begin{bmatrix} -r + r_1 + \alpha\rho \\ -c\alpha\rho e^{-2i\omega_1^*\tau_2'} + \delta_1\rho^2 + \eta\rho \end{bmatrix},$$

$$M_2 = 2\begin{bmatrix} -2i\omega_1^* - a_1 & -a_2 - a_3 e^{2i\omega_1^*\tau_1^*} \\ \eta y^* - a_4 e^{2i\omega_1^*\tau_2'} & -2i\omega_1^* - a_5 - a_6 + a_5 e^{2i\omega_1^*\tau_2'} \end{bmatrix}^{-1} \begin{bmatrix} -r + r_1 + \alpha\bar{\rho} \\ -c\alpha\bar{\rho}e^{2i\omega_1^*\tau_2'} + \delta_1\bar{\rho}^2 + \eta\bar{\rho} \end{bmatrix},$$

$$M_3 = 2\begin{bmatrix} -a_1 & -a_2 - a_3 \\ \eta y^* - a_4 & -a_5 - a_6 + a_5 \end{bmatrix}^{-1} \begin{bmatrix} -r + r_1 + \frac{1}{2}\alpha(\rho + \bar{\rho}) \\ -\frac{1}{2}c\alpha(\rho + \bar{\rho}) + \delta_1\rho\bar{\rho} + \frac{1}{2}\eta(\rho + \bar{\rho}) \end{bmatrix}.$$

Consequently, g_{ij} can be expressed by the parameters and delay τ_1^* and τ_2'. Thus, we can get:

$$c_1(0) = \frac{i}{2\omega_1^*\tau_1^*}\left(g_{20}g_{11} - 2|g_{11}|^2 - \frac{|g_{02}|^2}{3}\right) + \frac{g_{21}}{2},\ \mu_2 = -\frac{Re(c_1(0))}{Re(\lambda'(\tau_1^*))},\ \beta_2 = 2Re(c_1(0)),$$
$$T_2 = -\frac{Im(c_1(0)) + \mu_2 Im((\lambda'(\tau_1^*)))}{\omega_1^*\tau_1^*}.$$

Above expressions give description of the bifurcating periodic solutions in the center manifold of system (2.3) at critical value $\tau_1 = \tau_1^*$ which can be stated as the following theorem:

Theorem 2.5.1.

1. μ_2 gives the direction of Hopf-bifurcation. If $\mu_2 > 0 (< 0)$, the Hopf-bifurcation is supercritical(subcritical).
2. β_2 gives the stability of bifurcated periodic solution. If $\beta_2 > 0 (\beta_2 < 0)$ then the bifurcated periodic solutions are unstable (stable).
3. T_2 gives the period of bifurcated solution, the period increases(decreases) if $T_2 > 0 (< 0)$.

2.6 Numerical Simulation

In this section we carry out numerical simulation by using MATLAB R2019a. All the calculations are done by taking eight digits after decimal. For numerical simulation, the chosen sets of parameters are given below:

$$r = 3,\ r_0 = 0.7,\ r_1 = 0.5,\ k = 3,\ \alpha = 0.5,\ c = 0.4,\ \delta_0 = 0.45,\ \delta_1 = 0.025,\ \eta = 0.01,\ a = 0.07,\ b = 0.09. \tag{2.32}$$

$$r = 3,\ r_0 = 0.7,\ r_1 = 0.5,\ k = 1,\ \alpha = 0.5,\ c = 0.4,\ \delta_0 = 0.2,\ \delta_1 = 0.025,\ \eta = 0.01,\ a = 0.07,\ b = 0.09. \tag{2.33}$$

For the parameters, we have taken in the above (2.32), the non-delayed system (2.4) has three equilibria points, the points, the eigenvalues of the variational matrix evaluated at them and their nature is described in Table 2.3.

From this table we can see that E_0 and E_1 both are saddle points and the the variational matrix at

Equilibrium point	Eigenvalues	Nature
$E_0(0,0)$	(2.300,-0.4500)	saddle point
$E_1(4.6,0)$	(-2.300,0.08953971)	saddle point
$E^*(0.21295807,0.19946731)$	-0.019263081 $\pm$ 0.86676509i	locally asmptotically stable

Table 2.3: Equilibrium points and the corresponding eigenvalues (which define the nature of these points).

E^* has complex conjugate eigenvalues with negative real parts, i.e. E^* is locally asymptotically stable equilibrium point which validates the result given by Remark 2.3.4 for the above chosen parameters.

The cost of fear k is an important parameter to study because system (2.4) undergoes Hopf-bifurcation with respect to this parameter. For the parameters chosen in (2.32) and using Theorem 2.3.5, the critical value of k is $k = k^* = 0.68660621$. For $k > k^*$, the non-delayed system is stable and undergoes Hopf-bifurcation at $k = k^*$ and is unstable for $k < k^*$. Fig. 2.3 gives an interpretation for $k = 3 > k^*$ in which E^* is asymptotically stable. Fig. 2.3(a) describes how the curves for prey and predator population initially oscillate for some time, and then the oscillations keep damping after that the curves rest to their steady states.

The same behavior can be observed in Fig. 2.3(b) in which solution starting from an initial point converge to the equilibrium point E^* after a time showing the asymptotic stable behavior of E^*. An illustration for the unstable behavior of E^* is provided in Fig. 2.4(a) with undamped oscillations in time series plot and a stable limit cycle in Fig. 2.4(b) in which any solution starting from inside (red) or outside (black) approaches to this periodic solution for a particular value of $k = 0.3$ under its critical value k^*.

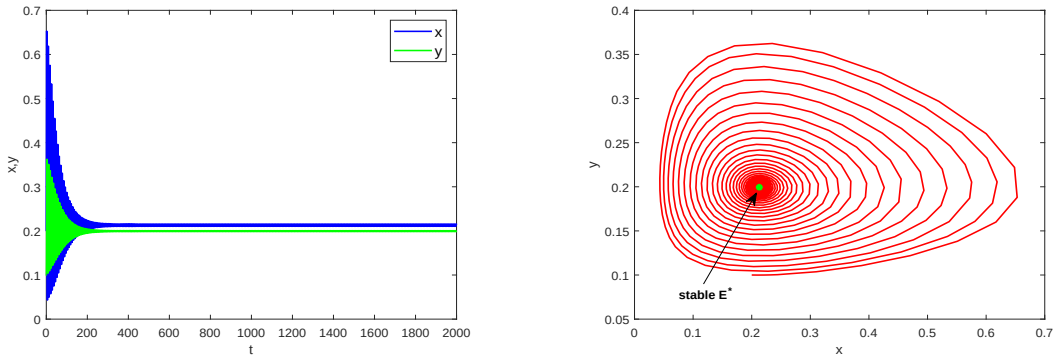

(a) **(b)**

Fig. 2.3: For $k = 3 > k^*$, (a) time series plot for x and y, (b) phase portrait in xy-plane showing the asymptotic stability of E^* with all the parameters same as in (2.32).

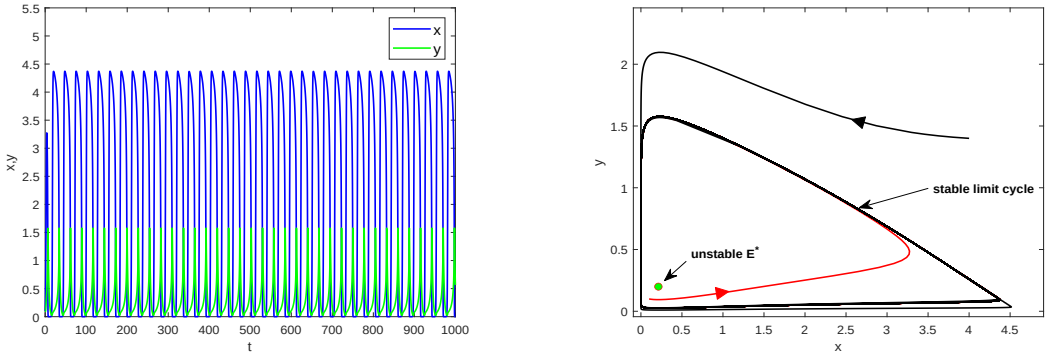

(a) **(b)**

Fig. 2.4: Existence of limit cycle and instability of E^* for $k = 0.3 < k^*$ with all the parameters same as in (2.32).

As it is very difficult to analyse the different types of anti-predator behaviors individually, exhibited by the prey in response to fear induced by the predator, so we try to evaluate the effect of k on η (which represents the cumulative effect of these behaviors). As the cost of fear increases, the prey is expected to enhance its efficiency of anti-predator behavior. That is, anti-predator behavior should be proportional to the cost of fear. The same trend has been observed in our model which is demonstrated in Fig. 2.5.

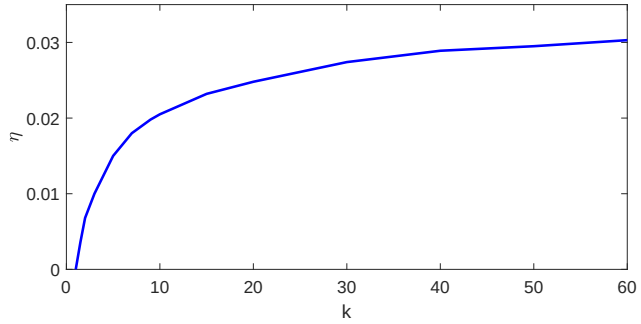

Fig. 2.5: $k\eta$-graph for $x^* = 0.21295807$.

A dynamical system exhibit the characteristic of bi-stability when the system has two locally asymptotically stable equilibrium points. Due to this property of the system, the whole set of region of attraction for all solutions gets divided into two separate regions of attraction corresponding to both equilibrium points, and these regions of attraction are separated by a curve, known as separatrix. Our system (2.4) also possesses this attribute of bi-stability and set Ω is divided into two sets separated by a closed curve, demonstrated in Fig. 2.6. The respective locally asymptotically equilibrium points are $E_1(4.6,0)$, $E^*(0.14595837,0.22291377)$ (for $k = 1,\ \alpha = 0.7,\ c = 0.8, \eta = 3$, with remaining all the parameters same as in (2.32)). The region of attraction for E^* is the portion inside the closed curve, as shown in the figure, and if we start the solution inside this closed region, the solution tends to E^*. The region of attraction for E_1 is

the part of the set Ω excluding the area covered by the closed trajectory, and solution initiated in this region will approach E_1.

Now we simulate the system (2.4) for different values of α keeping all the parameters same as in (2.32). Fig. 2.7 illustrates that as we increase the attack rate of predator on prey, x settles down to lower equilibrium value which is the actual expected behavior of prey species with an increment in attack rate by predator. With increase of α the equilibrium value for y should increase as the predator starts killing prey with a greater rate, but a different character than the conventional one is shown by the time series plot of y as we increase α, value of steady-state solution for y falls off. The fact behind this particular nature exhibited by the predator species is that as the predator starts hunting the prey with a higher value of attack rate, the population density of prey starts shrinking, due to which the availability of prey to predator reduces which also adds a competition among the predator species to access the food. Thus reduction in the accessible food and increase in the struggle among predators leads to decrement in the equilibrium value of y.

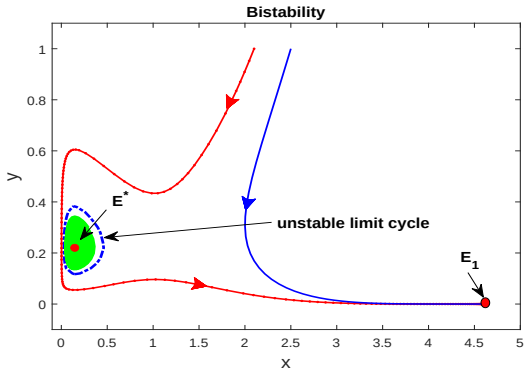

Fig. 2.6: Phase portrait diagram showing the property of bi-stabilty for $k = 1$, $\alpha = 0.7$, $c = 0.8$, $\eta = 3$, with remaining all the parameters same as in (2.32).

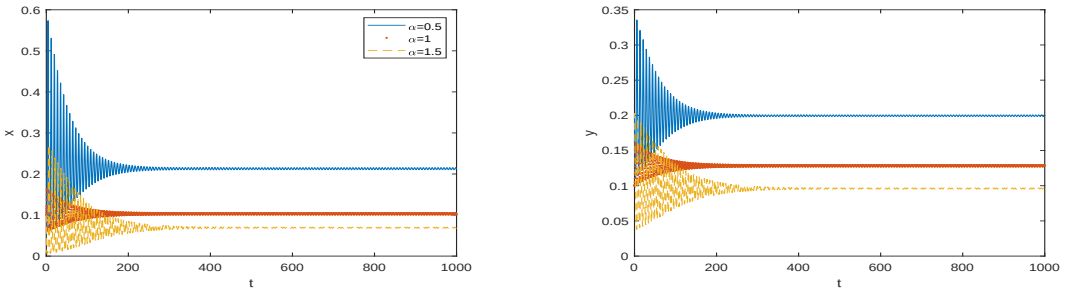

(a) **(b)**

Fig. 2.7: Behavior of x and y with time t for different values of α with all other parameters same as in (2.32)

Now we perform simulation for validating the results that we got for delayed model (2.3) in section 4. For this we will use the same set of parameters given in (2.32). The introduction of the fear response and gestation time delay does not effect the equilibrium point. Therefore $E^*(0.21295807,0.19946731)$ is the interior equilibrium point for system (2.4). The simulation examples for the different cases discussed in section 4 are given as the cases below:

Case 1 : When $\tau_1 = \tau_2 = 0$, system (2.3) reduces to system (2.4) and the simulation for this are given in Figs. 2.3 and 2.4.

In the delayed system, the stable equilibrium E^* co-exists with a stable limit cycle. This property of delayed system can be seen in all the following cases.

Case 2 : $\tau_1 = 0$ and $\tau_2 > 0$.

For the parameters in (2.32), conditions (H_1) and (H_3) are satisfied so, taking $j = 0$ in Eq.(2.24) , we get

$$\omega_0 = 0.85634590 \text{ and } \tau_{2_0} = 0.05231278.$$

For above ω_0, τ_{2_0},the condition (H_{51}) is also satisfied, so the transversality condition is also satisfied. Therefore, from Theorem 2.4.1, E^* is locally asymptotically stable for $\tau_2 < \tau_{2_0}$ which is verified by the time series plot given in Fig. 2.8 where we have taken $\tau_2 = 0.03 < \tau_{2_0}$. From phase portrait diagram in Fig. 2.8, we can see the existence of an unstable limit cycle around E^* and which is further surrounded by a stable limit cycle. For $\tau_2 > \tau_{2_0}$, E^* is an unstable equilibrium enclosed by a stable limit cycle, which is illustrated by time series graph and phase portrait diagram given in Fig. 2.9. So, we can observe that as we decrease $\tau_2 > \tau_{2_0}$ to $\tau_2 < \tau_{2_0}$, an unstable equilibrium bifurcates into a stable equilibrium and an unstable limit cycle i.e. E^* suffers subcritical Hopf-bifurcation w.r.t. delay τ_2. We also have presented this whole scenario by a bifurcation diagram for species x in Fig. 2.10.

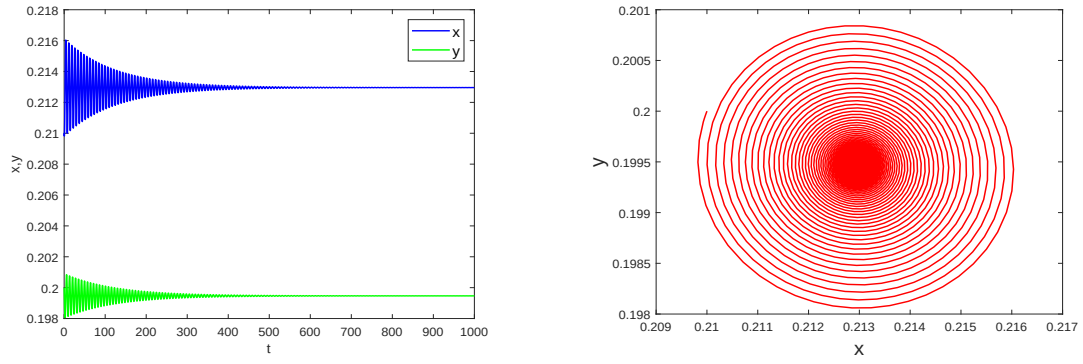

(a) **(b)**

Fig. 2.8: Local stability of E^* with multiple limit cycles for $\tau_1 = 0$ and $\tau_2 = 0.03$, with all the parameters same as in (2.32).

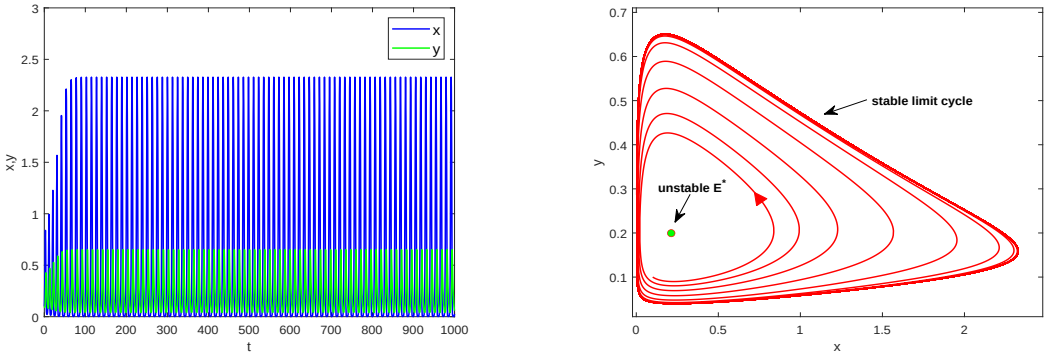

(a) **(b)**

Fig. 2.9: Time series plot of x, y and phase portrait diagram in xy-plane showing unstable nature of E^* when $\tau_1 = 0,\ \tau_2 = 0.07 > \tau_{2_0}$ with all the parameters same as in (2.32).

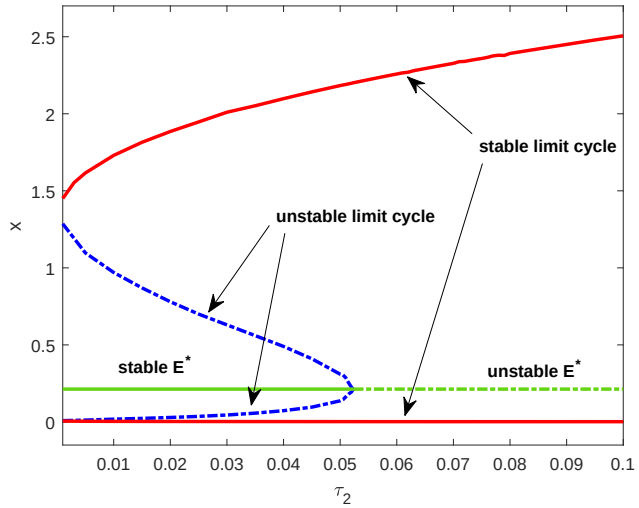

Fig. 2.10: Bifurcation diagram for x with $\tau_1 = 0,\ \tau_2 > 0$ and all the parameters from (2.32).

Case 3 : $\tau_1 > 0,\ \tau_2 = 0.$

To study the switching of stability twice for the delayed system around E^* as we vary τ_1 we perform simulation with respect to parameters given in (2.33) in this case.

With the change in value of parameters, there is change in interior equilibrium point. The new equilibrium point is $E^*(0.09430142, 0.28704906)$ which is locally asymptotically stable. Using (2.33) and $E^*(0.09430142, 0.28704906)$ in Theorem 2.4.2 we get $\omega_{10}^{(1)} = 0.65403249,\ \omega_{10}^{(2)} = 0.46755180$ and $\tau_{1_0}^{(1)} = 0.30872245,\ \tau_{1_0}^{(2)} = 6.41837400$ are the critical values of τ_1 corresponding to $\omega_{10}^{(1)},\ \omega_{10}^{(2)}$.

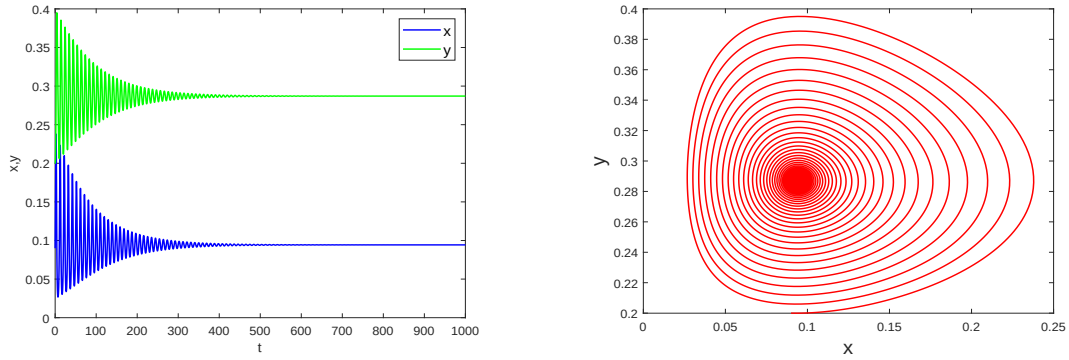

(a) **(b)**

Fig. 2.11: Time series plot and phase portrait diagram showing the local stability of E^* being enclosed by an unstable and a stable limit cycle for $\tau_2 = 0,\ \tau_1 = 0.1 < \tau_{1_0}^{(1)}$ and the parameters chosen in (2.33).

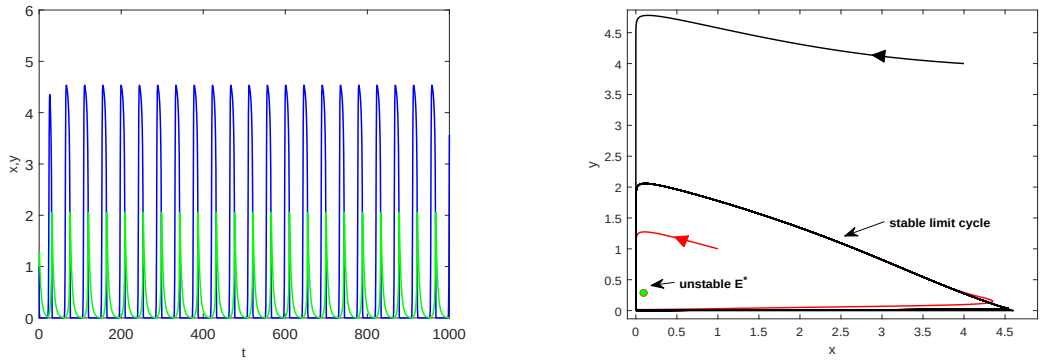

(a) **(b)**

Fig. 2.12: Unstable nature of E^* shown by the continuous oscillations in time series evolution of x, y (a) and stable limit cycle (b) for $\tau_2 = 0,\ \tau_{1_0}^{(1)} < \tau_1 = 3 < \tau_{1_0}^{(2)}$ with all the parameters same as in (2.33).

For the parameters chosen in (2.33), when $\tau_1 \in (0, \tau_{1_0}^{(1)})$, the equilibrium point E^* remains locally asymptotically stable inside an unstable limit cycle which is further wrapped by a stable limit cycle (Fig. 2.11(b). The system remains unstable for $\tau_1 \in (\tau_{1_0}^{(1)}, \tau_{1_0}^{(2)})$ (Fig. 2.12). Therefore, we can say that the delayed system undergoes subcritical Hopf-bifurcation at $\tau_1 = \tau_{1_0}^{(1)}$ as we move from right to left on τ_1 axis. Now, as we increase τ_1, E^* becomes locally asymptotically stable, and an unstable limit cycle comes into existence at $\tau_1 = \tau_{1_0}^{(2)}$ via subcritical Hopf-bifurcation. For $\tau_1 > \tau_{1_0}^{(2)}$, a stable limit cycle is also present around the unstable one (Fig. 2.13(a). The entire dynamics of the delayed system for this case is presented by a bifurcation diagram in Fig. 2.14, for prey species. From this figure, we can observe that the delayed system switches its stability twice around E^* through Hopf-bifurcation as we vary τ_1 keeping

$\tau_2 = 0$. It is interesting to point out that the two solutions trajectories with different initial conditions cannot intersect each other in the case of ODEs, while they may intersect each other in the case of DDEs [85, 86]. In Fig. 2.13, two trajectories ate plotted with different initial conditions in the presence of τ_1. Thus, both the trajectories are intersecting.

Case 4 : $\tau_1 > 0,\ \tau_2 > 0$. With $\tau_2 = 0.03 \in (0, \tau_{2_0}) = (0, 0.05231278)$ and all the parameters in (2.32), τ_1 as parameter, our simulation yields

$$\omega_1^*\text{=}0.86054924 \text{ and } \tau_1^* = 0.05542075.$$

Using all these three $\omega^*,\ \tau_1^*,\ \tau_2$ in Eq. (2.30) we get $\left[\frac{d\xi}{d\tau_1}\right]_{\tau_1=\tau_1^*,\ \omega=\omega^*} = 0.14750804 \neq 0$. So, the transversality condition is satisfied. Therefore the conditions required to hold Theorem 2.4.2 are satisfied.

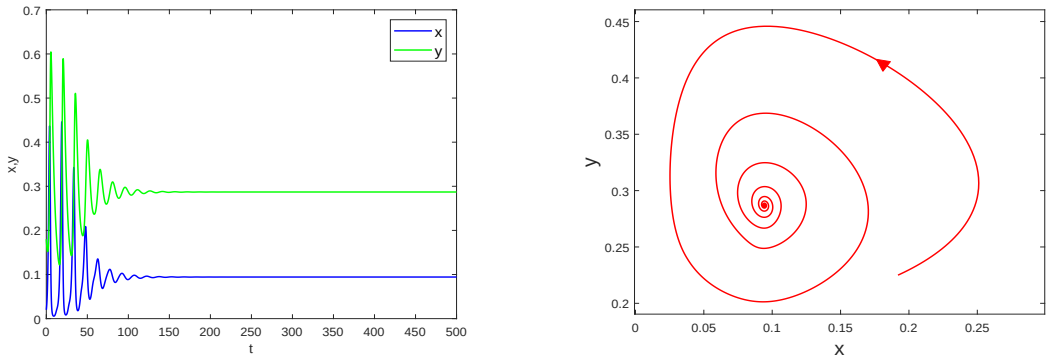

(a) **(b)**

Fig. 2.13: Time series plot (a) and phase portrait diagram (b) showing the local stability of E^* being enclosed by an unstable and a stable limit cycle for $\tau_{1_0}^{(2)} < \tau_1 = 8$, keeping parameters fixed from (2.33).

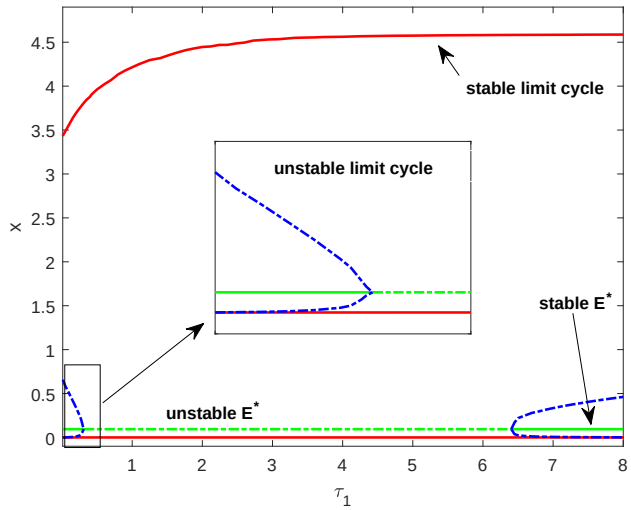

Fig. 2.14: Bifurcation diagram for $\tau_2 = 0,\ \tau_1 > 0$ and all the parameters same as in (2.33).

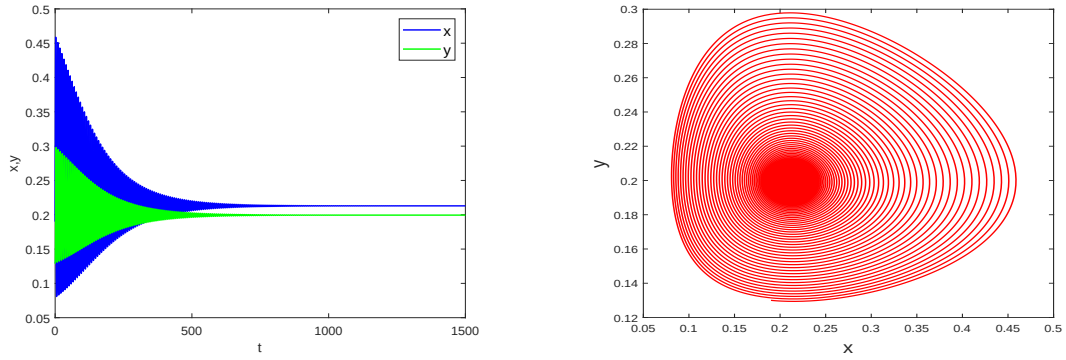

(a) **(b)**

Fig. 2.15: For all the parameters same as in (2.32) and $\tau_2 = 0.03,\ \tau_1 = 0.02 < \tau_1^*$, steady-state solution E^* is locally asymptotically stable.

The system (2.3) is locally asymptotically stable around E^* for $\tau_1 \in (0, \tau_1^*) = (0, 0.05542075)$ with $\tau_2 = 0.03$ and is unstable for $\tau_1 > \tau_1 *$. Fig. 2.15 gives a simulation example showing E^* is locally asymptotically stable when $\tau_2 = 0.03,\ \tau_1 = 0.02 < \tau_1^*$. Fig. 2.16 depicts that E^* is unstable for $\tau_2 = 0.03,\ \tau_1 = 0.06 > \tau_1^*$ with endless oscillations in Fig. 2.16(a) and a stable limit cycle in Fig. 2.16(b). Hence, we can say that system becomes locally asymptotically stable around E^* via subcritical Hopf-bifurcation at $\tau_1 = \tau_1^*$ as we decrease τ_1 keeping τ_2 constant. Numerical simulation yields

$$c_1(0) = 0.48740465 - 1.71282661i,\ \mu_2 = -3.30443830,\ \beta_2 = 0.97480930,\ T_2 = 35.28436282,$$

so, from Theorem 2.5.1, we note that the Hopf-bifurcation is subcritical in nature and the bifurcated periodic solutions are unstable, where period of bifurcated solution increases.

Delayed system (2.3) shows chaotic behavior for higher values of fear response delay. We have analysed the delayed system for $\tau_1 \in [10, 30]$ keeping $\tau_2 = 0$. The chaotic nature of the solutions can be seen from time series plots for both prey and predator in Fig. 2.17 and the chaotic attractor in Fig. 2.18 for $\tau_1 = 27$. For prey species, we have plotted the bifurcation diagram in Fig. 2.19(a), exhibiting the chaotic character of the system for large values of τ_1. From this figure (2.19(a), we can observe that as we increase delay τ_1, firstly the delayed system becomes chaotic and then enters into a periodic window. This periodic nature of the delayed system is again repeated on further increase of τ_1. Then the more increment in this delay push the system in chaotic regime again. This irregular nature of delayed system with respect to fear response delay is confirmed by the corresponding maximum Lyapunov exponent in Fig. 2.19(b). It become positive for $\tau_1 = 24$ and falls to negative values on increasing τ_1 which represent the periodic behavior of the delayed system in the course of increasing τ_1. Then it again become positive on increasing τ_1 showing the chaotic behaviour of delayed system (2.3).

Sensitivity to initial condition is basic property of chaotic system. For a chaotic system, if we perturb the initial condition by a small value, the behavior of the solution trajectory varies to a large extent. The same trend can be seen in our system when we change the initial condition for x, 0.2 to 0.201, keeping same for y, a major change in solution trajectory of both x and y is observed, shown in Fig. 2.20.

For parameters in (2.32), we have simulated a stability diagram in Fig. 2.21 in $\tau_1\tau_2$-plane in which the mustered colored area gives the stability region for delayed system where the white colored area gives the unstability region for the same. It may be noted here that Fig. 2.21 has been drawn using case (4) from the local stability and Hopf-bifurcation. Taking τ_2 from its stable interval each time, τ_1 is evaluated from $\tau_1^* = \frac{1}{\omega_1^*} sin^{-1}\left[\frac{F_2F_3+F_1F_4}{F_1^2+F_2^2}\right]$. It is observed that for equidistant points of τ_2, corresponding points of τ_1 are almost equidistant. Thus, the bifurcation curve in Fig. 2.21 appears to be almost linear.

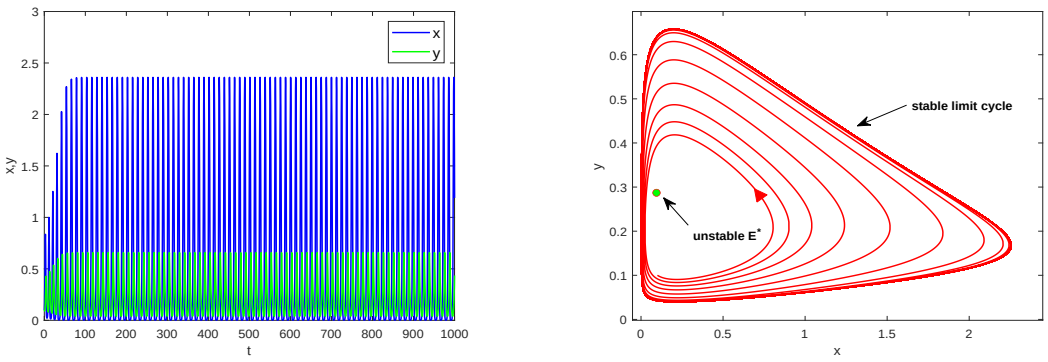

(a) **(b)**

Fig. 2.16: The interior equilibrium E^* is unstable when $\tau_2 = 0.03,\ \tau_1 = 0.06 > \tau_1^*$ with existence of stable periodic solution with all the parameters same as in (2.32).

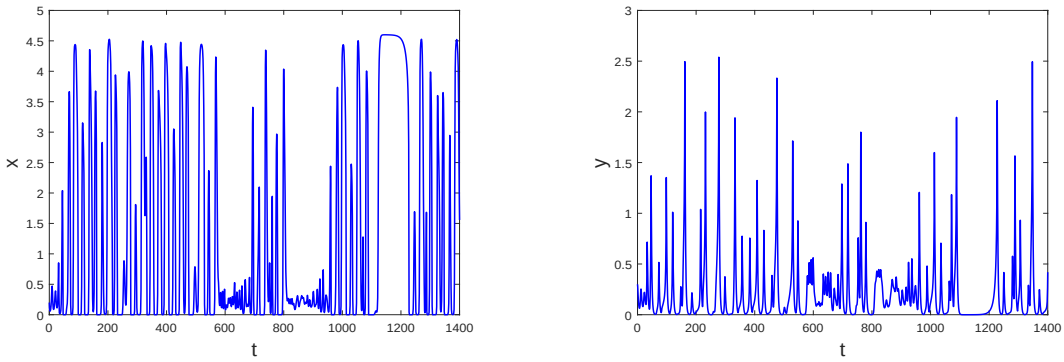

(a) **(b)**

Fig. 2.17: Time series plot for x and y when $\tau_1 = 27$ and parameters chosen in (32).

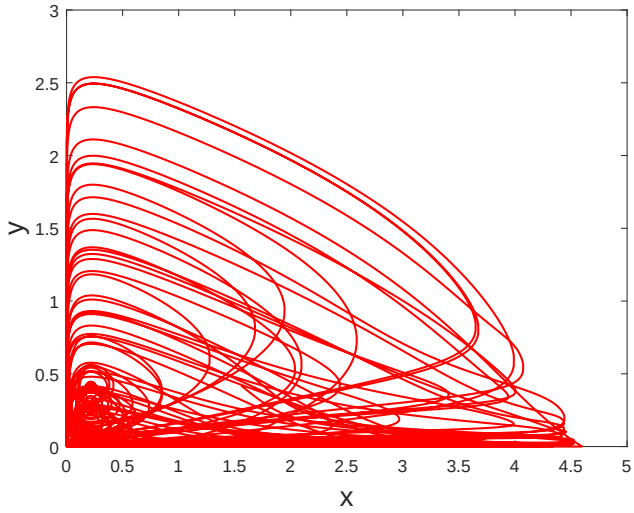

Fig. 2.18: Chaotic attractor for $\tau_1 = 27$ for parametric set (2.32).

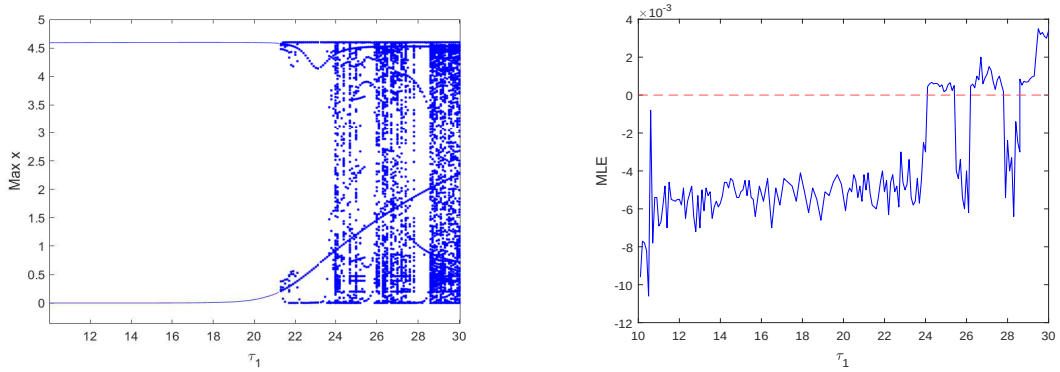

(a) **(b)**

Fig. 2.19: Bifurcation diagram (a) and corresponding Maximum Lyapunov exponent (b) for prey population for fear response delay.

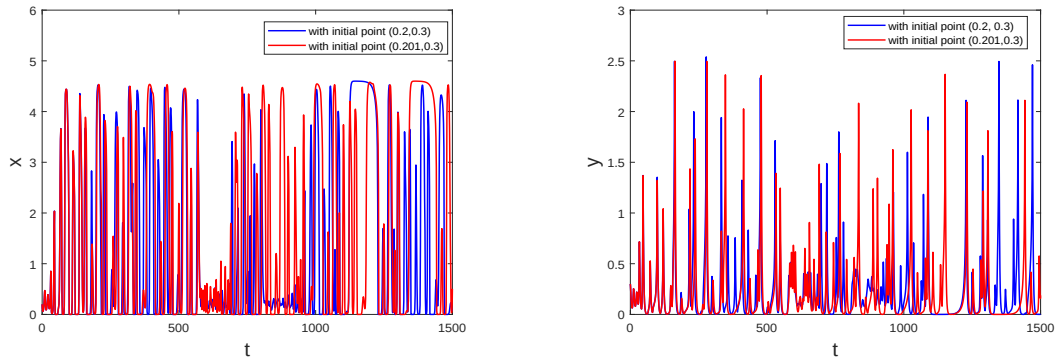

(a) **(b)**

Fig. 2.20: Sensitive solutions to initial condition for $\tau_1 = 27$ for parameters in (2.32).

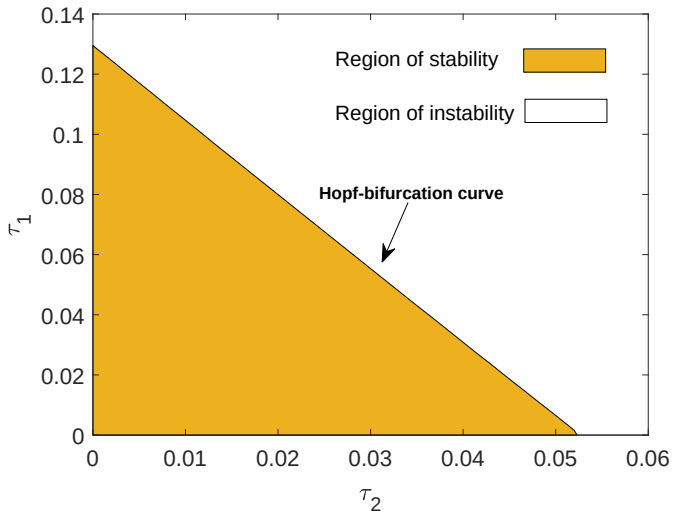

Fig. 2.21: Regions of stability and unstability in $\tau_1\tau_2$-plane for parameters in (2.32).

From this whole discussion, we can observe that our system may exhibits the properties of Hopf-bifurcation, bi-stability, multiple stability switching and chaos which manifests the dynamical richness of the system.

2.7 Conclusion

In this work, we proposed a prey-predator model with the impact of fear in prey, provoked by the predator, and to respond to this fear, the behavior known as anti-predator exhibited by prey towards the predator is also considered. Prey population grows logistically, and predator consume them with simplified Holling type IV functional response. Since the effect of fear in prey due to the predator is not instantaneous, so to make the model more precise, we incorporated the fear response delay. Further, the gestation delay is introduced for the predator in our model. Firstly, we proved the well-posedness of our model by showing the positivity, boundedness, and persistence for the non-delayed model (2.4). Population densities of both prey and predator are bounded in the compact set Ω in the non-negative plane. This fact agrees with the limited bearing capacity of the ecosystem. The system is uniformly persistence if the birth-rate of the prey population is greater than a threshold value, while the rate of anti-predator behavior is less than a threshold value. Then we noted that the system has three points of equilibria, E_0, E_1, and E^*. The positive equilibrium point E^* exists under conditions (2.8), (2.10) and (2.11). The rate of anti-predator behavior is an important parameter. In Fig. 2.2, we can see that the number of interior equilibrium points changes as the value of rate of anti-predator behavior varies. In stability analysis, we observed that E_0 is a saddle point, further the condition for asymptotic stability for E_1 is derived by evaluating the variational matrix about E_1. The interior equilibrium

E^* is stable under condition (2.14). Then we studied the conditions for occurrence of Hopf-bifurcation with respect to cost of fear. Further, we deduce the criteria for the global stability of the system by choosing a suitable Lyapunov function. Using Dulac-Bendixson criterion and Poincarè-Bendixon theorem we obtained the conditions for existence and non-existence of periodic solution. Then we studied the relationship between cost of fear and rate of anti-predator behavior which is depicted in Fig. 2.5. Further non-delayed system showed the property of bi-stability, in which both E^*, E_1 are stable equilibrium points, depicted in Fig. 2.6.

In the dynamical behavior of delayed model (2.3), we examined local stability behavior of the system and properties of Hopf-bifurcation. Using fear response delay and gestation delay as the bifurcation parameters, we discussed Hopf-bifurcation. In all the possible cases, we derived the critical values for respective bifurcation parameters. We noted that, the system suffers subcritical Hopf-bifurcation respect to both delays. In Case 3, the delayed system switches its stability twice as we vary τ_1. Further, we analyzed the direction and stability of Hopf-bifurcation using the normal form method and center manifold theory. Further, chaotic behavior of delayed system is observed for large values of fear response delay and which is supported by the bifurcation diagram and positiveness of maximum Lyapunov exponent. Moreover, we performed numerical simulation with respect to parameters in (2.32), (2.33), supporting our analytical results. In Fig. 2.21, we have drawn the regions of stability and unstability for delayed system in $\tau_1\tau_2$-plane.

We hope that this work will help to understand the dynamics of prey-predator system with effect of fear in prey due to predator and anti-predator behavior in response to this fear including fear response delay and gestation delay.

Chapter 3

Chaos control in a multiple delayed phytoplankton-zooplankton model with group defence and predator's interference[1]

3.1 Introduction

Phytoplankton-zooplankton interactions significantly contribute to the various dynamical proceedings happening in the ecosystem, which makes it a prominent topic of research. This interplay is a particular kind of prey-predator interaction which means that theories developed to deal with prey-predator relationships can be utilized to study such specific type of dynamics. Classically, Edwards and Brindley [87] studied an NPZ (nutrient-phytoplankton-zooplankton) model, which was mainly focussed on determining the parameter ranges to observe bifurcation and oscillatory behavior of the system. They also determined some parametric values for which the system has multiple attractors. Edwards [88] in the continuation of work [87], studied two plankton systems having concentrations of nutrient, phytoplankton, zooplankton, and detritus. In this extended work, he added detritus to the earlier NPZ model for simulating remineralization more realistically. In the first model, zooplankton is assumed to consume only phytoplankton whereas in second one, it can have phytoplankton and detritus both. They noticed that dynamics of NPZ system is not too much effected by addition of detritus when zooplankton is not allowed to graze on it (first model) but dynamics of the system changes substantially when zooplankton is allowed to consume detritus as well (second model). There are many more papers [89, 90, 91] in the literature in which explorers have investigated mathematical models involving phytoplankton-zooplankton species. Pal *et al.* [92] analysed an NPZ model in which the Monod–Haldane type response reflects the bloom formation by toxic phytoplankton. They observed that system also shows chaotic behavior for a set of chosen parameters.

[1] A considerable part of this chapter is published in *Chaos*, 31, 083101 (2021)

Zhang and Wang [93] considered an NPZ model in an aquatic environment in which they analytically verified classical and discontinuous Hopf-bifurcations for the proposed model. They also obtained bistability between a stable equilibrium point and a stable limit cycle (subcritical Hopf-bifurcation). The occurrence of saddle-node bifurcation is also endorsed with the help of numerical simulation in this paper. Upadhyay *et al.* [94] studied a spatial four component model (nutrient-phytoplankton-zooplankton-fish) with Holling type IV response. They established the conditions for local stability, global stability, instability for both spatial and non-spatial situations. They also investigated the effect of critical wavelength which drives system to instability and also got very much complex Turing patterns with the help of simulation.

As some of the zooplankton can identify toxic and non-toxic phytoplankton[95, 96], thus splitting phytoplankton into two categories: toxic producing phytoplankton (TPP) and non-toxic phytoplankton (NTP) can help us to analyse the dynamical behavior of plankton systems more precisely. One can see some papers [97, 98, 99] in which authors have divided phytoplankton into TPP and NTP and observed that this classification can help us to get more rich and realistic dynamical findings. Chowdhury *et al.* [100] studied a four-dimensional model with migratory consumption of zooplankton on TPP and NTP. They divided zooplankton into two groups, out of which one was consuming TPP and the other one NTP. They explored this system with different combinations of toxin inhibition and migratory parameters. They also observed that this nomadic grazing of zooplankton has a crucial impact on the system's stability and oscillatory bahavior. Banerjee and Venturino [101] extended the work of Pal *et al.* [92] and dealt with a three-dimensional PZ system by dividing phytoplankton into NTP-TPP groups to detect the poisoning effect of TPP on zooplankton explicitly. They derived stability conditions for various feasible equilibria. They also proved the persistence of the proposed model using the classical results given by Freedman and Waltman [102].

Another variable that can make dynamical systems more rational and play a vital role in their dynamics is the time delay. Incorporating a time delay in an ordinary differential equation transform it into a delay differential equation. Time delay can be added in a dynamical system in many terms like maturation time, gestation time, traveling, incubation, feedback time, etc. Inclusion of time delay may result in the generation of fluctuations around the stable equilibrium and sometimes it can also lead to chaos [103, 104, 105, 106]. Gakkhar and Singh [23] worked on prey-predator model with two discrete dalays. They noted that addition of delays lead to formation of periodic solutions and occurrence of chaos through Hopf-bifurcation. Rahim and Imran [107] dealt with a PZ model with two delays. The first delay in this paper corresponds to gestation time, whereas the second delay signifies the time required by TPP to get mature before producing noxious chemicals. They observed the multiple switching of stability around the interior equilibrium due to Hopf-bifurcatin with the increase of delay. Misra *et al.* [108] explored a 4D-model (nutrient-algae density-detritus density-applied efforts) to review

the applied efforts to control the algae and detritus from a lake to curtail the occurrence of algae blooms. Two delays: first for converting detritus into nutrients whereas second in applying the control efforts are also incorporated by them. Multiple switching of stability due to Hopf-bifurcation is too observed using both delays as control parameters. They found that that high accumulation of nutrients magnifies the occurrence of blooms, and so the applied efforts play a crucial role in reducing the concentration of algae bloom. Kumar and Dubey [15] analysed the effect of fear induced by the predator in prey with prey refuge and gestation delay. They observed that this fear effect could lead to Hopf-bifurcation in the system. Chaotic oscillations are also observed in their delayed model for high values of gestation delay via Hopf-bifurcation.

The kinetics of a dynamical system is very much dependent on the mode of interaction between interacting species. Predator's functional response to prey plays a crucial role in the prey-predator concept. Some prey species can use the approach of group formation as their defense against predators to protect themselves. This technique is one of the types of anti-predator behaviors endorsed by prey species against the predators [70]. In dynamical systems, this particular behavior of prey species is described by Holling type IV response (Monod–Haldane type response). Liu and Huang [109] investigated a prey-predator model with Monod–Haldane type response where both the species are subjected to harvesting. They examined how harvesting can affect equilibria, their stability and bifurcations related to the proposed system. Thakur and Ojha [54] studied a plankton-fish model with the assumption of phytoplankton as a prey, zooplankton the middle predator whereas fish species acting as the top predator. In this model, both planktons are assumed to exhibit defense skills against their respective predator via Monod–Haldane type response. They also incorporated time delay in middle predator and observed that increasing time delay leads to double Hopf-bifurcation. Predators can also interfere with each other for a available or favourite food. Beddington–DeAngelis response [110] is one of the responses which depends upon both the populations of prey, predator and manifest predator's interference. This response becomes free of predator's interference at high prey density as it becomes independent of predator density at this point. Upadhyay *et al.* [111] examined a reaction-diffusion model for a phytoplankton-zooplankton-fish system in which zooplankton grazes phytoplankton by Beddington–DeAngelis response and fish consumes zooplankton by Holiing type III response. They found that interference among zooplankton species, the spatial heterogeneity, and the rate of fish predation play important roles in the governance of the aquatic system's spatiotemporal kinetics. The other point observed by them is that diffusion drives instability to this marine system, whereas fish predation can behave like a regularizing factor.

This chapter extends the work of Banerjee and Venturino [101] by replacing linear and simplified Holling type IV responses by Beddington–DeAngelis and generalized Holling type IV responses, respectively. We also have incorporated two discrete delays to explore the system

more practically. The main objective of this work is to investigate the interactions of two populations of phytoplankton (NTP and TPP) on zooplankton explicitly in presence of two different kinds of delays. This chapter is organised as fellows: Section 3.2 corresponds for the formulation of mathematical model. In Section 3.3, we have analysed the dynamics of the non-delayed model, like the well-posedness of the model, the existence of various equilibria and their stability analysis, the persistence of the model, and bifurcation analysis. Assessments related to the delayed model are done in Section 3.4, which includes local stability analysis, direction and stability of Hopf-bifurcation. In Section 3.5, we have performed numerical simulations to assist our theoretical findings.

3.2 Model formulation

Classifying phytoplankton into two groups, namely, non-toxic phytoplankton (NTP) and toxic producing phytoplankton (TPP) can produce complex dynamical outcomes in a PZ system. Thus we categorize phytoplankton into two sub-populations: toxic and non-toxic, and propose a 3-dimensional dynamical model with these two phytoplankton strains and zooplankton as a generalist predator. Let $p_1,\ p_2$ are the population densities of non-toxic and toxic phytoplankton, respectively whereas z is the population density of zooplankton species, feeding on these two phytoplankton. Formulation of the model is based upon the following assumptions:

1. Both phytoplankton are assumed to grow logistically with $r_i,\ K_i$ as the intrinsic growth rates of ith species and carrying capacities of the environment for ith species, respectively, in the absence of each other and the zooplankton species. They also possess a inter-species competition for the available resources, where γ_{ij} is the rate of inter-species competition of jth species over ith species $(i \neq j = 1,2)$.
   Thus we can have
   $$\frac{dp_1}{dt} = r_1 p_1\left(1-\frac{p_1}{K_1}\right) - \gamma_{12} p_1 p_2,\quad \frac{dp_2}{dt} = r_2 p_2\left(1-\frac{p_2}{K_2}\right) - \gamma_{21} p_1 p_2.$$

2. As some of the zooplankton species have the capability of differentiating between NTP and TPP, but they can also progress toward the toxic one in the deficiency of non-toxic fee [95, 96]. Thus the NTP may act as a favourite food for zooplankton, so we assume that the zooplankton can compete with each other for this non-toxic resource. Accordingly, the interplay between NTP and zooplankton is dealt with Beddington–DeAngelis type response that has the characteristic of interference among the predator species during foraging, and which is given by, $f(p_1,z) = \frac{m_1 p_1}{\alpha+p_1+\beta z}$. Here, m_1 is the consumption rate of zooplankton over NTP, β is the coefficient of intra-specific competition among

zooplankton for this non-toxic food and α is half-saturation constant. As NTP is zooplankton's favourite food so in its absence, zooplankton die with death rate of δ_0. With all these assumptions and c_1 as the conversion efficiency of zooplankton over NTP, we have

$$\frac{dp_1}{dt} = r_1 p_1\left(1-\frac{p_1}{K_1}\right) - \gamma_{12} p_1 p_2 - \frac{m_1 p_1 z}{\alpha + p_1 + \beta z}, \quad \frac{dz}{dt} = \frac{c_1 m_1 p_1 z}{\alpha + p_1 + \beta z} - \delta_0 z.$$

3. In the deficiency of NTP, the rise in the consumption of TPP magnifies the decrement of zooplankton due to its negative (poisoning) effect. As a result, an excessive amount of zooplankton gets killed, which reduces the further consumption of toxic phytoplankton. Such lesser ingestion will decrease the further negative effect of toxic phytoplankton on zooplankton's growth. We use Holling type IV response to handle this kind of interaction which takes care of the fact that zooplankton avoids highly dense toxic phytoplankton. It is also known as a group defense mechanism by toxic phytoplankton against zooplankton, and this is given by, $g(p_2) = \frac{m_2 p_2}{a{p_2}^2 + b p_2 + c}$. Here, m_2 is the predation rate of zooplankton over TPP, a measures the inhibitory effect of TPP against zooplankton and c is half saturation constant. Thus with conversion efficiency c_2 of zooplankton over TPP, we have

$$\begin{aligned}\frac{dp_2}{dt} &= r_2 p_2\left(1-\frac{p_2}{K_2}\right) - \gamma_{21} p_1 p_2 - \frac{m_2 p_2 z}{a{p_2}^2 + b p_2 + c},\\ \frac{dz}{dt} &= \frac{c_1 m_1 p_1 z}{\alpha + p_1 + \beta z} - \frac{c_2 m_2 p_2 z}{a{p_2}^2 + b p_2 + c} - \delta_0 z.\end{aligned}$$

Thus, the proposed mathematical model is given by:

$$\begin{aligned}\frac{dp_1}{dt} &= r_1 p_1\left(1-\frac{p_1}{K_1}\right) - \gamma_{12} p_1 p_2 - \frac{m_1 p_1 z}{\alpha + p_1 + \beta z} =: F_1(p_1, p_2, z),\\ \frac{dp_2}{dt} &= r_2 p_2\left(1-\frac{p_2}{K_2}\right) - \gamma_{21} p_1 p_2 - \frac{m_2 p_2 z}{a{p_2}^2 + b p_2 + c} =: F_2(p_1, p_2, z),\\ \frac{dz}{dt} &= \frac{c_1 m_1 p_1 z}{\alpha + p_1 + \beta z} - \frac{c_2 m_2 p_2 z}{a{p_2}^2 + b p_2 + c} - \delta_0 z =: F_3(p_1, p_2, z).\end{aligned} \tag{3.1}$$

A schematic diagram for the kinetical interactions presented in model (3.1) is depicted in Fig. 3.1.

4. The effects of these functional responses are not instantaneous. So, for more realistic and rich dynamics, we use two types of delays. Here, τ_1 is the gestation period for zooplankton after the predation of non-toxic phytoplankton. The process of toxin liberation by TPP is also followed by a time lag τ_2, which is the time taken by toxic producing phytoplankton's cells to get mature and release toxins; this delay is known as toxic liberation

delay [112]. Therefore, incorporating this two delays, model (3.1) becomes:

$$\begin{aligned}
\frac{dp_1}{dt} &= r_1 p_1\left(1-\frac{p_1}{K_1}\right) - \gamma_{12} p_1 p_2 - \frac{m_1 p_1 z}{\alpha + p_1 + \beta z},\\
\frac{dp_2}{dt} &= r_2 p_2\left(1-\frac{p_2}{K_2}\right) - \gamma_{21} p_1 p_2 - \frac{m_2 p_2 z}{a p_2^2 + b p_2 + c},\\
\frac{dz}{dt} &= \frac{c_1 m_1 p_1(t-\tau_1) z(t-\tau_1)}{\alpha + p_1(t-\tau_1) + \beta z(t-\tau_1)} - \frac{c_2 m_2 p_2(t-\tau_2) z(t-\tau_2)}{a p_2(t-\tau_2)^2 + b p_2(t-\tau_2) + c} - \delta_0 z,
\end{aligned} \tag{3.2}$$

and for biological feasibility, we assume $p_1(s) = \phi_1(s) \geq 0,\ p_2(s) = \phi_2(s) \geq 0,\ y(s) = \phi_3(s) \geq 0,\ s \in [-\tau, 0],\ \tau = max\{\tau_1, \tau_2\}$ and $\phi_j(s) \in C([-\tau, 0]) \to R_+, (j = 1,2,3)$, where C denotes the Banach space of continuous functions. All the parameters in (3.1) and (3.2) are assumed to be positive.

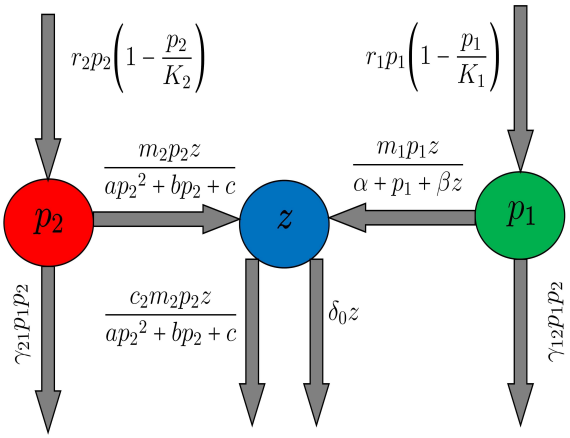

Fig. 3.1: Schematic diagram of kinetical interactions among NTP, TPP and zooplankton species, for the non-delayed model.

3.3 Dynamics of non-delayed model

In this section, we firstly prove the biological well-posedness of model (3.1) by proving the existence, uniqueness, positivity and boundedness of its solution. Then it is followed by finding its all feasible stationary points. Next, we investigate local and global stability behavior of model (3.1) around these points. Further, the theorems related to Hopf and transcritical bifurcations are presented.

3.3.1 Existence, positivity and boundedness of solution

As we can see that (F_1, F_2, F_3) is Lipschitz continuous for any bounded subset of R_+^3. Thus for any set of initial values $(p_1(0),\ p_2(0),\ z(0)) in R_+^3$, model (3.1) has a unique solution on

bounded subsets of R^3_+.

From model (3.1), we can have

$$p_1(t) = p_1(0)exp\Big[\int_0^t \Big\{r_1\Big(1-\frac{p_1(\kappa)}{K_1}\Big) - \gamma_{12}p_2(\kappa) - \frac{m_1 z(\kappa)}{\alpha+p_1(\kappa)+\beta z(\kappa)}\Big\}d\kappa\Big],$$

$$p_2(t) = p_2(0)exp\Big[\int_0^t \Big\{r_2\Big(1-\frac{p_2(\kappa)}{K_2}\Big) - \gamma_{21}p_1(\kappa) - \frac{m_2 z(\kappa)}{ap_2(\kappa)^2+bp_2(\kappa)+c}\Big\}d\kappa\Big],$$

$$z(t) = z(0)exp\Big[\int_0^t \Big\{\frac{c_1 m_1 p_1(\kappa)}{\alpha+p_1(\kappa)+\beta z(\kappa)} - \frac{c_2 m_1 p_2(\kappa)}{ap_2(\kappa)^2+bp_2(\kappa)+c} - \delta_0\Big\}d\kappa\Big].$$

Hence, any solution starting inside the positive octant of p_1p_2z-space, remains positive for the whole future time. Now, we present a theorem to determine the invariant set for solutions of the non-delayed system.

Theorem 3.3.1. *All the solutions of system (3.1) initiating in R^3_+ remain enclosed inside the region*
$\Upsilon = \Big\{(p_1,\ p_2,\ z) \in R^3_+ : 0 \le p_1 \le K_1,\ 0 \le p_2 \le K_2,\ 0 \le p_1 + \frac{1}{c_1}z \le \frac{2r_1K_1}{\delta_1}\Big\}$, *where* $\delta_1 = min\{r_1,\ \delta_0\}$.

Proof. From the first equation of model (3.1), we can easily observe

$$\frac{dp_1}{dt} \le r_1 p_1\Big(1-\frac{p_1}{K_1}\Big) \text{ which implies } \limsup_{t\to\infty} p_1(t) \le K_1.$$

Similarly,

$$\limsup_{t\to\infty} p_2(t) \le K_2.$$

Now, let $W(t) = p_1 + \frac{1}{c_1}z$, then we have

$$\begin{aligned}\frac{dW}{dt} &= \frac{dp_1}{dt} + \frac{1}{c_1}\frac{dz}{dt}\\ &= r_1p_1\Big(1-\frac{p_1}{K_1}\Big) - \gamma_{12}p_1p_2 - \frac{c_2m_2p_2z}{c_1(ap_2^2+bp_2+c)} - \frac{\delta_0 z}{c_1}\\ &\le 2r_1K_1 - \delta_1 W(t).\end{aligned}$$

Thus $\limsup_{t\to\infty} W(t) \le \frac{2r_1K_1}{\delta_1}$, where $\delta_1 = min\{r_1, \delta_0\}$. Therefore, all the solutions of model (3.1), starting inside R^3_+ are confined to the region Υ. □

3.3.2 Feasible biomass equilibria with their stability analysis

Now, we establish the existence of various equilibrium points associated with model (3.1). These steady states can be named as: $E_0(0,0,0)$, $E_1(K_1,0,0)$, $E_2(0,K_2,0)$, $E_3(\hat{p}_1,\hat{p}_2,0)$, $E_4(\bar{p}_1,0,\bar{z})$ and $E^*(p_1^*,p_2^*,z^*)$. The equilibrium points E_0, E_1, E_2 are the trivial steady states. Now, we need to drive the conditions under which the remaining equilibrium points exists.

- For the existence of $E_3(\hat{p}_1, \hat{p}_2, 0)$:
  Here, $\hat{p}_1$ and $\hat{p}_2$ are solutions of set of equations given by:

$$r_1\hat{p}_1 + \gamma_{12}K_1\hat{p}_2 = r_1K_1, \tag{3.3}$$

$$\gamma_{21}K_2\hat{p}_1 + r_2\hat{p}_2 = r_2K_2. \tag{3.4}$$

  Solving (3.3) and (3.4), we obtain $\hat{p}_1 = \frac{r_2K_1(r_1-\gamma_{12}K_2)}{\Delta}$, $\hat{p}_2 = \frac{r_1K_2(r_2-\gamma_{21}K_1)}{\Delta}$,
  where $\Delta = r_1r_2 - \gamma_{12}\gamma_{21}K_1K_2$.
  Therefore, both $\hat{p}_1, \hat{p}_2$ exist positively and so is the equilibrium $E_3(\hat{p}_1, \hat{p}_2, 0)$ if any one of the following conditions holds:

  (i) $r_1 > \gamma_{12}K_2$ and $r_2 > \gamma_{21}K_1$.

  (ii) $r_1 < \gamma_{12}K_2$ and $r_2 < \gamma_{21}K_1$

- For the existence of $E_4(\bar{p}_1, 0, \bar{z})$:
  Here, $\bar{p}_1$ and $\bar{z}$ are solutions of the eqs. (3.5) and (3.6) given by :

$$r_1\left(1 - \frac{\bar{p}_1}{K_1}\right) = \frac{m_1\bar{z}}{\alpha + \bar{p}_1 + \beta\bar{z}}, \tag{3.5}$$

$$\frac{c_1m_1\bar{p}_1}{\alpha + \bar{p}_1 + \beta\bar{z}} = \delta_0. \tag{3.6}$$

  From (3.6), we obtain

$$\bar{z} = \frac{(c_1m_1 - \delta_0)\bar{p}_1 - \delta_0\alpha}{\delta_0\beta}, \tag{3.7}$$

  which exists positively if

$$(c_1m_1 - \delta_0)\bar{p}_1 > \delta_0\alpha. \tag{3.8}$$

  Now, using this $\bar{z}$ into (3.5), we get a quadratic polynomial in $\bar{p}_1$ given by

$$\bar{p}_1^2(-r_1c_1m_1\beta) + \bar{p}_1(k_1m_1(r_1c_1\beta - (c_1m_1 - \delta_0))) + m_1K_1\alpha\delta_0 = 0. \tag{3.9}$$

  Hence, it can be seen that, (3.9) has a positive root $\bar{p}_1$. By putting this $\bar{p}_1$ in (3.7), we can get $\bar{z}$ to receive $E_4(\bar{p}_1, 0, \bar{z})$. Therefore, E_4 exists under condition (3.8).

- Existence of interior equilibrium $E^*(p_1^*, p_2^*, z^*)$:
  Interior equilibrium $E^*(p_1^*, p_2^*, z^*)$ is the solution of the set of algebraic equations given below:

$$r_1\left(1 - \frac{p_1^*}{K_1}\right) - \gamma_{12}p_2^* - \frac{m_1z^*}{\alpha + p_1^* + \beta z^*} = 0, \tag{3.10}$$

$$r_2\left(1-\frac{p_2^*}{K_2}\right)-\gamma_{21}p_1^*-\frac{m_2z^*}{ap_2^{*2}+bp_2^*+c}=0, \tag{3.11}$$

$$\frac{c_1m_1p_1^*}{\alpha+p_1^*+\beta z^*}-\frac{c_2m_1p_2^*}{ap_2^{*2}+bp_2^*+c}-\delta_0=0. \tag{3.12}$$

From (3.12), we get

$$z^*=\frac{1}{\beta}\left(\frac{c_1m_1p_1^*}{M}-\alpha-p_1^*\right)=:G, \tag{3.13}$$

which is positive when

$$\left(\frac{c_1m_1}{M}-1\right)p_1^*-\alpha>0, \tag{3.14}$$

where $M=\frac{c_2m_2p_2^*}{ap_2^{*2}+bp_2^*+c}+\delta_0$.
Using z^* from (3.13) in (3.10), we get :

$$g_1(p_1^*,p_2^*)=r_1\left(1-\frac{p_1^*}{K_1}\right)-\gamma_{12}p_2^*-\frac{m_1G}{\alpha+p_1^*+\beta G}=0. \tag{3.15}$$

In (3.15), we have the following:

1. When $p_1^*\to 0$ which gives $p_2^*\to\infty$.
2. When $p_2^*=0$, we obtain

$$p_1^{*2}\left(-\frac{r_1c_1}{\delta_0K_1}\right)+p_1^*\left(\frac{r_1c_1}{\delta_0}-\frac{c_1m_1}{\beta\delta_0}+1\right)+\frac{\alpha}{\beta}=0. \tag{3.16}$$

   So, (3.16) has a positive root $p_{1\mu}$.
3. From (3.15), $\frac{dp_1^*}{dp_2^*}=-\frac{g_{1p_2^*}}{g_{1p_1^*}}<0$, if

$$\begin{gathered} g_{1p_2^*}>0 \text{ and } g_{1p_1^*}>0 \\ \text{or} \\ g_{1p_2^*}<0 \text{ and } g_{1p_1^*}<0. \end{gathered} \tag{3.17}$$

Now using (3.13) in (3.11), we get

$$g_2(p_1^*,p_2^*)=r_2\left(1-\frac{p_2^*}{K_2}\right)-\gamma_{21}p_1^*-\frac{m_2G}{ap_2^{*2}+bp_2^*+c}=0 \tag{3.18}$$

In (3.18), we have the following:

1. When $p_1^* = 0$, then we get

$$p_2^{*3}(-\alpha\beta r_2) + p_2^{*2}(\beta(\alpha K_2 - br_2)) + p_2^*(\beta r_2(bK_2 - c)) + K_2(\beta r_2 + \alpha m_2) = 0. \tag{3.19}$$

So, (3.19) has a positive root $p_{2\mu}$.

2. When $p_2^* = 0$, then (3.18) has a positive root, $p_{1\nu} = \frac{r_2 + \frac{m_2\alpha}{c\beta}}{\gamma_{21} + \frac{m_2}{c\beta}(\frac{c_1 m_1}{\delta_0} - 1)} > 0$,if

$$c_1 m_1 > \delta_0. \tag{3.20}$$

3. From (3.18), $\frac{dp_1^*}{dp_2^*} = -\frac{g_{2p_2^*}}{g_{2p_1^*}} < 0$, if

$$\begin{gathered} g_{2p_2^*} > 0 \text{ and } g_{2p_1^*} > 0 \\ \text{or} \\ g_{2p_2^*} < 0 \text{ and } g_{2p_1^*} < 0 \end{gathered} \tag{3.21}$$

Therefore, nullclines (3.15) and (3.18) has a unique point of intersection (p_1^*, p_2^*), when (3.14), (3.17), (3.20) and (3.21) hold with the inequality $p_{1\mu} < p_{1\nu}$. Then by putting p_1^* and p_2^* in (3.13), we obtain z^* and it establishes the existence of $E^*(p_1^*, p_2^*, z^*)$.

Theorem 3.3.2. *The non-delayed system has a unique interior equilibrium if in addition to conditions: (3.14), (3.17), (3.20) and (3.21), the inequality $p_{1\mu} < p_{1\nu}$ holds.*

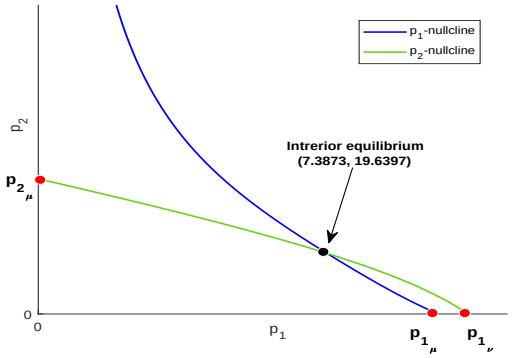

Fig. 3.2: p_1-nullcline and p_2-nullcline satisfies all conditions stated in Theorem 3.3.2, and hence intersect at a unique point for parameters given in Remark 3.3.1.

Remark 3.3.1. *To show the existence of unique interior equilibrium numerically, we take a set of parameters;* $r_1 = 3$, $K_1 = 30$, $\gamma_{12} = 0.1$, $m_1 = 0.48$, $\alpha = 10$, $\beta = 0.1$, $r_2 = 1.2$, $K_2 = 40$, $\gamma_{21} = 0.08$, $a = 0.02$, $b = 0.01$, $c = 50$, $m_2 = 0.1$, $c_1 = 0.28$, $c_2 = 0.4$, $\delta_0 = 0.04$. *For these parametric values, all conditions stated in Theorem 3.3.2 hold. For better visualization we have*

plotted interior equilibrium $(7.3873, 19.6397, 11.4803)$ *in the* p_1p_2*-plane which is depicted in Fig. 3.2.*

Now, for local stability analysis, firstly we linearise the non-linear system (3.1) around the desired equilibrium by evaluating the variational matrix at the same and then we check the sign of real part of every eigenvalue corresponding to that matrix. For an equilibrium point $E(p_1, p_2, z)$, the general variational matrix corresponding to model (3.1) is given by:

$$J|_E = \begin{bmatrix} j_{11} & j_{12} & j_{13} \\ j_{21} & j_{22} & j_{23} \\ j_{31} & j_{32} & j_{33} \end{bmatrix},$$

where,

$j_{11} = r_1 - \frac{2r_1p_1}{K_1} - \gamma_{12}p_2 + \frac{m_1z(\alpha+\beta z)}{(\alpha+p_1+\beta z)^2},\ j_{12} = -\gamma_{12}p_1,\ j_{13} = -\frac{m_1p_1(\alpha+p_1)}{(\alpha+p_1+\beta z)^2},$

$j_{21} = -\gamma_{21}p_2,\ j_{22} = r_2 - \frac{2r_2p_2}{K_2} - \gamma_{21}p_1 - \frac{m_2z(-ap_2^2+c)}{(ap_2^2+bp_2+c)^2},\ j_{23} = -\frac{m_2p_2}{ap_2^2+bp_2+c},$

$j_{31} = \frac{c_1m_1z(\alpha+\beta z)}{(\alpha+p_1+\beta z)^2},\ j_{32} = -\frac{c_2m_2z(-ap_2^2+c)}{(ap_2^2+bp_2+c)^2}, j_{33} = \frac{c_1m_1p_1(\alpha+p_1)}{(\alpha+p_1+\beta z)^2} - \frac{c_2m_2p_2}{ap_2^2+bp_2+c} - \delta_0.$

- We can be easily observe that E_0 is always a saddle point with two dimensional unstable manifold and one dimensional stable manifold.

- The Jacobian matrix evaluated about $E_1(K_1, 0, 0)$ is

$$J|_{E_1} = \begin{bmatrix} -r_1 & -\gamma_{12}K_1 & -\frac{m_1K_1}{\alpha+K_1} \\ 0 & r_2 - \gamma_{21}K_1 & 0 \\ 0 & 0 & \frac{c_1m_1K_1}{\alpha+K_1} - \delta_0 \end{bmatrix}.$$

  So, eigenvalues of above matrix are $-r_1$, $r_2 - \gamma_{21}K_1$ and $\frac{c_1m_1K_1}{\alpha+K_1} - \delta_0$. Therefore there can be the following sub-cases:

  1. E_1 is a saddle point with $\dim(W^s(E_1)) = 1$ and $\dim(W^u(E_1)) = 2$, if $r_2 > \gamma_{21}K_1$ and $\frac{c_1m_1K_1}{\alpha+K_1} > \delta_0$.
  2. E_1 is a saddle point with $\dim(W^s(E_1)) = 2$ and $\dim(W^u(E_1)) = 1$, if $r_2 < \gamma_{21}K_1$ and $\frac{c_1m_1K_1}{\alpha+K_1} > \delta_0$ or $r_2 > \gamma_{21}K_1$ and $\frac{c_1m_1K_1}{\alpha+K_1} < \delta_0$.
  3. E_1 is a locally asymptotically stable equilibrium point with $\dim(W^s(E_1)) = 3$, if $r_2 < \gamma_{21}K_1$ and $\frac{c_1m_1K_1}{\alpha+K_1} < \delta_0$.

- The Jacobian matrix corresponding to E_2 is

$$J|_{E_2} = \begin{bmatrix} r_1 - \gamma_{12}K_2 & 0 & 0 \\ -\gamma_{21}K_2 & -r_2 & -\frac{m_2K_2}{ap_2^2+bp_2+c} \\ 0 & 0 & -\frac{c_2m_2K_2}{ap_2^2+bp_2+c} - \delta_0 \end{bmatrix}.$$

Eigenvalues of above matrix, $J|_{E_2}$ are $r_1 - \gamma_{12}K_2$, $-r_2$ and $-\frac{c_2m_2K_2}{ap_2^2+bp_2+c} - \delta_0$.
So,

1. E_2 is a saddle point with $\dim(W^s(E_2)) = 2$ and $\dim(W^u(E_2)) = 1$ if $r_1 > \gamma_{12}K_2$.
2. Model (3.1) is locally asymptotically stable in the vicinity of E_2 if $r_1 < \gamma_{12}K_2$

- Assuming the existence of $E_3(\hat{p}_1, \hat{p}_2, 0)$, the corresponding variational matrix is

$$J|_{E_3} = \begin{bmatrix} -\frac{r_1\hat{p}_1}{K_1} & -\gamma_{12}\hat{p}_1 & -\frac{m_1\hat{p}_1}{\alpha+\hat{p}_1} \\ -\gamma_{21}\hat{p}_2 & -\frac{r_2\hat{p}_2}{K_2} & -\frac{m_2\hat{p}_2}{a\hat{p}_2^2+b\hat{p}_2+c} \\ 0 & 0 & \frac{c_1m_1\hat{p}_1}{\alpha+\hat{p}_1} - \frac{c_2m_2\hat{p}_2}{a\hat{p}_2^2+b\hat{p}_2+c} - \delta_0 \end{bmatrix}.$$

One of the eigenvalues of $J|_{E_3}$ is $\frac{c_1m_1\hat{p}_1}{\alpha+\hat{p}_1} - \frac{c_2m_2\hat{p}_2}{a\hat{p}_2^2+b\hat{p}_2+c} - \delta_0$ and other two are the roots of the equation

$$\Gamma^2 + B_1\Gamma + B_2 = 0, \tag{3.22}$$

where, $B_1 = \frac{r_1\hat{p}_1}{K_1} + \frac{r_1\hat{p}_2}{K_2}$ and $B_2 = \hat{p}_1\hat{p}_2\left(\frac{r_1r_2}{K_1K_2} - \gamma_{12}\gamma_{21}\right)$. Both the zeros of (3.22) have negative real parts iff $B_2 > 0$. So, we have the following theorem:

Theorem 3.3.3. *Sufficient conditions for system (3.1) to be locally asymptotically stable in the neighbourhood of E_3 are*
(i) $\frac{c_1m_1\hat{p}_1}{\alpha+\hat{p}_1} < \frac{c_2m_2K_2}{a\hat{p}_2^2+b\hat{p}_2+c} + \delta_0$,
(ii) $\frac{r_1r_2}{K_1K_2} > \gamma_{12}\gamma_{21}$.

- Variational matrix about $E_4(\bar{p}_1, 0, \bar{z})$ (assumed to be exist under condition (3.8)) is:

$$J|_{E_4} = \begin{bmatrix} -\frac{r_1\bar{p}_1}{K_1} + \frac{m_1\bar{p}_1\bar{z}}{(\alpha+\bar{p}_1+\beta\bar{z})^2} & -\gamma_{12}\bar{p}_1 & -\frac{m_1\bar{p}_1(\alpha+\bar{p}_1)}{(\alpha+\bar{p}_1+\beta\bar{z})^2} \\ 0 & r_2 - \gamma_{21}\bar{p}_1 - \frac{m_2\bar{z}}{c} & 0 \\ \frac{c_1m_1\bar{z}(\alpha+\beta\bar{z})}{(\alpha+\bar{p}_1+\beta\bar{z})^2} & -\frac{c_2m_2\bar{z}}{c} & -\frac{\beta c_1m_1\bar{p}_1\bar{z}}{(\alpha+\bar{p}_1+\beta\bar{z})^2} \end{bmatrix}.$$

It is easy to see that one eigenvalue of $J|_{E_4}$ is $r_2 - \gamma_{21}\bar{p}_1 - \frac{m_2\bar{z}}{c}$, where other are the roots of equation given below:

$$\Lambda^2 + C_1\Lambda + C_2 = 0, \tag{3.23}$$

where, $C_1 = \frac{r_1\bar{p}_1}{K_1} - \frac{m_1\bar{p}_1\bar{z}}{(\alpha+\bar{p}_1+\beta\bar{z})^2} + \frac{\beta c_1 m_1\bar{p}_1\bar{z}}{(\alpha+\bar{p}_1+\beta\bar{z})^2}$,
and $C_2 = \left(\frac{r_1\bar{p}_1}{K_1} - \frac{m_1\bar{p}_1\bar{z}}{(\alpha+\bar{p}_1+\beta\bar{z})^2}\right)\left(\frac{\beta c_1 m_1\bar{p}_1\bar{z}}{(\alpha+\bar{p}_1+\beta\bar{z})^2}\right) + \left(\frac{m_1\bar{p}_1(\alpha+\bar{p}_1)}{(\alpha+\bar{p}_1+\beta\bar{z})^2}\right)\left(\frac{c_1 m_1\bar{z}(\alpha+\beta\bar{z})}{(\alpha+\bar{p}_1+\beta\bar{z})^2}\right)$.
Roots of (3.23) have negative real parts iff $C_1 > 0,\ C_2 > 0$. Therefore, we state the following theorem

Theorem 3.3.4. *Equilibrium point $E_4(\bar{p}_1, 0, \bar{z})$ is locally asymptotically if $r_1 > \frac{m_1 K_1\bar{z}}{(\alpha+\bar{p}_1+\beta\bar{z})^2}$ and $r_2 < \gamma_{21}\bar{p}_1 + \frac{m_2\bar{z}}{c}$.*

Remark 3.3.2. *From Theorem 3.3.4, we can observe that toxic-phytoplankton free equilibrium is locally asymptotically stable if intrinsic growth rates of non-toxic and toxic producing phytoplankton are greater and lesser than some respective threshold values.*

- For investigation of local stability analysis around the coexistence equilibrium $E^*(p_1^*, p_2^*, z^*)$, the evaluated variational matrix is:

$$J|_{E^*} = \begin{bmatrix} e_{11} & e_{12} & e_{13} \\ e_{21} & e_{22} & e_{23} \\ e_{31} & e_{32} & e_{33} \end{bmatrix},$$

where,
$e_{11} = -\frac{r_1 p_1^*}{K_1} + \frac{m_1 p_1^* z^*}{(\alpha+p_1^*+\beta z^*)^2},\ e_{12} = -\gamma_{12} p_1^*,\ e_{13} = -\frac{m_1 p_1^*(\alpha+p_1^*)}{(\alpha+p_1^*+\beta z^*)^2},$
$e_{21} = -\gamma_{21} p_2^*,\ e_{22} = -\frac{r_2 p_2^*}{K_2} + \frac{m_2 z^*(2ap_2{*}^2+bp_2^*)}{(ap_2{*}^2+bp_2^*+c)^2},\ e_{23} = -\frac{m_2 p_2^*}{ap_2{*}^2+bp_2^*+c},$
$e_{31} = \frac{c_1 m_1 z^*(\alpha+\beta z^*)}{(\alpha+p_1^*+\beta z^*)^2},\ e_{32} = -\frac{c_2 m_2 z^*(-ap_2{*}^2+c)}{(ap_2{*}^2+bp_2^*+c)^2},\ e_{33} = -\frac{\beta c_1 m_1 p_1^* z^*}{(\alpha+p_1^*+\beta z^*)^2}.$

Characteristic equation for above Jacobian is given by

$$\Pi^3 + E_1\Pi^2 + E_2\Pi + E_3 = 0, \tag{3.24}$$

where,
$E_1 = -\mathrm{tr}(J|_{E^*})$,
$E_2 = (e_{22}e_{33} - e_{23}e_{32}) + (e_{11}e_{33} - e_{13}e_{31}) + (e_{11}e_{22} - e_{12}e_{21})$,
$E_3 = -\det(J|_{E^*})$. All three roots of (3.24) have negative real parts iff $E_1 > 0$,$E_3 > 0$ and $E_1E_2 > E_3$. Thus, we have the following theorem:

Theorem 3.3.5. *The non-delayed model is locally asymptotically stable in the vicinity of coexistence equilibrium $E^*(p_1^*, p_2^*, z^*)$ if $E_1 > 0$,$E_3 > 0$ and $E_1E_2 > E_3$.*

Now, we drive the conditions under which the non-delayed model is globally asymptotically stable around the interior equilibrium $E^*(p_1^*, p_2^*, z^*)$.

Theorem 3.3.6. *For non-delayed system (3.1), interior equilibrium $E^*(p_1^*, p_2^*, z^*)$, whenever it exists, is globally asymptotically stable in accordance with the conditions:*

$(i)\frac{r_1}{K_1} > \frac{m_1 z^*}{\alpha(\alpha+p_1^*+\beta z^*)}$,

$(ii)\frac{r_2}{K_2} > \frac{m_2 z^*(a(K_2+p_2^*)+b)}{c(ap_2^{*2}+bp_2^*+c)}$,

$(iii)(\gamma_{12}+\gamma_{21})^2 < 2\left(\frac{r_1}{K_1} - \frac{m_1 z^*}{\alpha(\alpha+p_1^*+\beta z^*)}\right)\left(\frac{r_2}{K_2} - \frac{m_2 z^*(a(K_2+p_2^*)+b)}{c(ap_2^{*2}+bp_2^*+c)}\right)$,

$(iv)m_2^2\left(\frac{1}{c} + \frac{l_1 c_2}{ap_2^{*2}+bp_2^*+c}\left(1 - \frac{ap_{2m}p_2^*}{aK_2^2+bK_2+c}\right)\right)^2 < 2\left(\frac{r_2}{K_2} - \frac{m_2 z^*(a(K_2+p_2^*)+b)}{c(ap_2^{*2}+bp_2^*+c)}\right)\left(\frac{\beta p_1^* l_1 c_1 m_1}{(\alpha+K_1+\beta Z_M)(\alpha+p_1^*+\beta z^*)}\right)$,

where $p_{2m} = \frac{K_2}{r_2}\left(r_2 - \left(\gamma_{21}K_1 + \frac{m_2 Z_M}{c}\right)\right)$, $Z_M = \frac{2c_1 r_1 K_1}{\delta_1}$ *and* l_1 *is defined in the proof.*

Proof. We choose a relevant Lyapunov function V about E^* defined as

$$V(p_1,p_2,z) = \left(p_1 - p_1^* - p_1^*\ln\frac{p_1}{p_1^*}\right) + \left(p_2 - p_2^* - p_2^*\ln\frac{p_2}{p_2^*}\right) + l_1\left(z - z^* - z^*\ln\frac{z}{z^*}\right),$$

where l_1 is a positive constant which we pick as per our comfort. Now, on differentiating V with respect to time along the solutions of (3.1) and with some algebraic exploitation, we get

$$\begin{aligned}\frac{dV}{dt} &= \left(-\frac{r_1}{K_1} + \frac{m_1 z^*}{(\alpha+p_1+\beta z)(\alpha+p_1^*+\beta z^*)}\right)(p_1-p_1^*)^2 \\ &+ \left(-\frac{r_2}{K_2} + \frac{m_2 z^*(a(p_2+p_2^*)+b)}{(ap_2^2+bp_2+c)(ap_2^{*2}+bp_2^*+c)}\right)(p_2-p_2^*)^2 - \frac{\beta p_1^* l_1 c_1 m_1}{(\alpha+p_1+\beta z)(\alpha+p_1^*+\beta z^*)}(z-z^*)^2 \\ &- (\gamma_{12}+\gamma_{21})(p_1-p_1^*)(p_2-p_2^*) + \frac{m_2}{ap_2^2+bp_2+c}\left(-1 + \frac{l_1 c_2(ap_2p_2^*-c)}{ap_2^{*2}+bp_2^*+c}\right)(p_2-p_2^*)(z-z^*) \\ &+ \frac{m_1}{(\alpha+p_1+\beta z)(\alpha+p_1^*+\beta z^*)}\left(-(\alpha+p_1^*) + l_1 c_1(\alpha+\beta z^*)\right)(p_1-p_1^*)(z-z^*).\end{aligned}$$

Taking $l_1 = \frac{\alpha+p_1^*}{c_1(\alpha+\beta z^*)}$, we obtain

$$\begin{aligned}\frac{dV}{dt} &= -V_{11}(p_1-p_1^*)^2 + V_{12}(p_1-p_1^*)(p_2-p_2^*) - \frac{1}{2}V_{22}(p_2-p_2^*)^2 \\ &- \frac{1}{2}V_{22}(p_2-p_2^*)^2 + V_{23}(p_2-p_2^*)(z-z^*) - V_{33}(z-z^*)^2,\end{aligned}$$

where,

$$V_{11} = \left(\frac{r_1}{K_1} - \frac{m_1 z^*}{(\alpha + p_1 + \beta z)(\alpha + p_1^* + \beta z^*)}\right), \; V_{22} = \left(\frac{r_2}{K_2} - \frac{m_2 z^*(a(p_2 + p_2^*) + b)}{(ap_2{}^2 + bp_2 + c)(ap_2^{*2} + bp_2^* + c)}\right),$$
$$V_{33} = \frac{\beta p_1^* l_1 c_1 m_1}{(\alpha + p_1 + \beta z)(\alpha + p_1^* + \beta z^*)}, \; V_{12} = -(\gamma_{12} + \gamma_{21}),$$
$$V_{23} = \frac{m_2}{ap_2{}^2 + bp_2 + c}\left(-1 + \frac{l_1 c_2 (ap_2 p_2^* - c)}{ap_2^{*2} + bp_2^* + c}\right).$$

Hence, by Sylvester's criterion, $\frac{dV}{dt}$ is a negative definite function under the assumptions given by $(i), (ii), (iii)$ and (iv). Therefore, model (3.1) is globally asymptotically stable under these hypothesis. □

3.3.3 Persistence conditions

A dynamical system is said to be persistent as long as every component of this system persists if it is present initially. In other words, a differential system is persistent from a geometric view if its every solution is bounded far from the coordinate planes. In this subsection, we determine the conditions under which the interior equilibrium $E^*(p_1^*, p_2^*, z^*)$ of system (3.1) persists. Firstly we divide system (3.1) into two subsystems and determine the conditions for the non-existence of any periodic orbit about the corresponding coexistence equilibrium for each subsystem. Then these results will be used to prove the persistence of coexistence equilibrium E^*. The two subsystems are: a competitive subsystem having toxic and non-toxic phytoplankton, and a prey-predator subsystem with non-toxic phytoplankton and zooplankton.

The competitive subsystem is given by

$$\begin{aligned} \frac{dp_1}{dt} &= r_1 p_1\left(1 - \frac{p_1}{K_1}\right) - \gamma_{12} p_1 p_2 = h_1(p_1, p_2), \\ \frac{dp_2}{dt} &= r_2 p_2\left(1 - \frac{p_2}{K_2}\right) - \gamma_{21} p_1 p_2 = h_2(p_1, p_2). \end{aligned} \tag{3.25}$$

Now, we define a continuous differentiable function $H_1 = \frac{1}{p_1 p_2}$ in the interior of positive quadrant of the $p_1 p_2$-plane. Then we have

$$\nabla_1 = \frac{\partial}{\partial p_1}(h_1 H_1) + \frac{\partial}{\partial p_2}(h_2 H_1) = -\frac{r_1}{p_2 K_1} - \frac{r_2}{p_1 K_2} < 0.$$

Thus using Bendixson's-Dulac's negative criterion [55], we deduce that competitive model (3.25) does not have any closed solution around its coexistence equilibrium.

Similarly, the prey-predator submodel is given by

$$\begin{aligned} \frac{dp_1}{dt} &= r_1 p_1\left(1-\frac{p_1}{K_1}\right)-\frac{m_1 p_1 z}{\alpha+p_1+\beta z}=h_3(p_1,z),\\ \frac{dz}{dt} &= \frac{c_1 m_1 p_1 z}{\alpha+p_1+\beta z}-\delta_0 z=h_4(p_1,z). \end{aligned} \tag{3.26}$$

Non-existence of any periodic solution around the above prey-predator subsystem's coexistence equilibrium can be proved by choosing $H_2=\frac{\alpha+p_1+\beta z}{p_1 z}$ in the interior of positive quadrant of the p_1z-plane. Indeed

$$\nabla_2=\frac{\partial}{\partial p_1}(h_3H_2)+\frac{\partial}{\partial z}(h_4H_2)=\frac{r_1}{z}-\frac{r_1}{zK_1}(\alpha+\beta z)-\frac{2r_1p_1}{zK_1}-\frac{\delta_0\beta}{p_1}.$$

Thus $\nabla_2<0$ if $K_1<\alpha$. Therefore, the coexistence equilibrium of prey-predator subsystem (3.26) is not enclosed by any periodic orbit if $K_1<\alpha$. We will use this condition to establish the persistence of E^*.

Now, the persistence of interior equilibrium E^* of model (3.1) is proved by using the method proposed by Freedman and Waltman [102]. In accordance with Theorem 2.1 [102], both $E_1(K_1,0,0)$ and $E_2(0,K_2,0)$ must be hyperbolic saddle points. Now, E_1 is a hyperbolic saddle point if one or both conditions $r_2>\gamma_{21}K_1$ and $\frac{c_1m_1K_1}{\alpha+K_1}>\delta_0$ hold. Axial equilibrium E_2 is a hyperbolic saddle point whenever $r_1>\gamma_{12}K_2$.

As per further conditions of this theorem, both planner equilibriums $E_3(\hat{p}_1,\hat{p}_2,0)$ and $E_4(\bar{p}_1,0,\bar{z})$ must be unique and unstable in the positive direction orthogonal to p_1p_2 and p_1z-planes, respectively, if they exist. From subsection 3.3.2, we can see that both of these equilibriums are unique if they are feasible. Equilibrium E_3 is unstable along z-axis if $\frac{c_1m_1\hat{p}_1}{\alpha+\hat{p}_1}>\frac{c_2m_2\hat{p}_2}{a\hat{p}_2^2+b\hat{p}_2+c}+\delta_0$ is satisfied whereas E_4 is unstable along p_2-axis if $r_2>\gamma_{21}\bar{p}_1+\frac{m_2\bar{z}}{c}$ holds. Therefore, in addition to the condition $K_1<\alpha$ if these conditions are also satisfied then the coexistence equilibrium E^* persists.

3.3.4 Bifurcation exploration

Here, we provide a theorem related to Hopf-bifurcation analysis for non-delayed model (3.1).

Theorem 3.3.7. *For occurrence of Hopf-bifurcation for system (3.1) around E^* at $\alpha=\alpha^{hf}$, the necessary and sufficient conditions are that the following inequalities hold true:*

1. $E_1(\alpha^{hf})>0,\ E_3(\alpha^{hf})>0.$
2. $E_1(\alpha^{hf})E_2(\alpha^{hf})-E_3(\alpha^{hf})=0.$

3. $\frac{d}{d\alpha}(Re(\Pi))_{\alpha=\alpha^{hf}} \neq 0$ *or* $\frac{dR}{d\alpha} \neq 0$, *where,* $R = E_1E_2 - E_3$.

Proof. At $\alpha = \alpha^{hf}$, $E_1E_2 - E_3 = 0$ and the characteristic equation (3.24) becomes

$$(\Pi + E_1)(\Pi^2 + E_2) = 0, \tag{3.27}$$

from which we get $\Pi_{1,2} = \pm i\sqrt{E_2}$, a pair of purely imaginary roots and $\Pi_3 = -E_1$, a negative real root.
On differentiating equation (3.24) w.r.t α, we obtain

$$\frac{d\Pi}{d\alpha} = -\frac{\dot{E}_1\Pi^2 + \dot{E}_2\Pi + \dot{E}_3}{3\Pi^2 + 2E_1\Pi + E_2},$$

implies

$$\begin{aligned}\left.\frac{d\Pi}{d\alpha}\right|_{\Pi=i\sqrt{E_2}} &= \frac{-\dot{E}_1E_2 + E_3 + i\dot{E}_2\sqrt{E_2}}{2\dot{E}_2 - 2iE_1\sqrt{E_2}} \\ &= \frac{1}{2}\frac{\left((\dot{E}_3 - \dot{E}_1E_2) + i\dot{E}_2\sqrt{E_2}\right)(E_2 + iE_1\sqrt{E_2})}{E_2^2 + E_1^2E_2}.\end{aligned}$$

Thus

$$\left.\frac{d\Pi}{d\alpha}\right|_{\Pi=i\sqrt{E_2}} = -\frac{1}{2}\frac{dR/d\alpha}{(E_1^2 + E_2)} + i\Big(\frac{\sqrt{E_2}\dot{E}_2}{2E_2} - \frac{E_1\sqrt{E_2}\frac{dR}{d\alpha}}{2E_2(E_1^2 + E_2)}\Big),$$

Consequently,

$$\frac{d}{d\alpha}(Re(\Pi))_{\alpha=\alpha^{hf}} = -\left.\frac{1}{2}\frac{dR/d\alpha}{(E_1^2 + E_2)}\right|_{\alpha=\alpha^{hf}} \neq 0.$$

Thus, $\frac{d}{d\alpha}(Re(\Pi))_{\alpha=\alpha^{hf}} \neq 0$ if $\frac{dR}{d\alpha} \neq 0$. This completes the theorem. □

Remark 3.3.3. *Hopf-bifurcation analysis with respect to any other parameter will be similar to as given for* α *in above Theorem (3.3.7).*

Now, we present a theorem regarding the transcritical bifurcation which involves zooplankton free equilibrium E_3 and the interior equilibrium E^*, using δ_0 as the bifurcation parameter.

Theorem 3.3.8. *Through a transcritical bifurcation, zooplankton free equilibrium* E_3 *changes its nature by becoming stable from unstable and the interior equilibrium* E^* *disappears, when* δ_0 *passes across its threshold value,* δ_0^{tc}.

Proof. For proving our assertion, we use Sotomayor's theorem [24]. At $\delta_0 = \delta_0^{tc} = \frac{c_1m_1\hat{p}_1}{\alpha+\hat{p}_1} - \frac{c_2m_2\hat{p}_2}{a\hat{p}_2^2+b\hat{p}_2+c}$, E_3 becomes a non-hyperbolic equilibrium point. Let $v = [v_1, v_2, v_3]^T$ and $w =$

$[w_1,w_2,w_3]^T$ are the eigenvectors corresponding to zero eigenvalue of $J|_{(E_3:\delta_0^{tc})}$ and $J^T|_{(E_3:\delta_0^{tc})}$, respectively. Here, $v_1=\frac{a_{12}a_{23}-a_{13}a_{22}}{a_{22}a_{11}-a_{12}a_{21}}$, $v_2=\frac{a_{13}a_{21}-a_{23}a_{11}}{a_{22}a_{11}-a_{12}a_{21}}$, $v_3=1$ and $w=[0,0,1]^T$, where a_{ij} for $i,j=1,2,3$ is an entry of $J|_{(E_3:\delta_0^{tc})}$.
Here, we define $Y(p_1,p_2,z)=[F_1,F_2,F_3]^T$. Then $Y_{\delta_0}=[0,0,-z]^T$, and by Sotomayor's theorem, the transversality conditions are:
$w^T Y_{\delta_0}(E_3:\delta_0^{tc})=0,$

$w^T[DY_{\delta_0}(E_3:\delta_0^{tc})]v=-1\neq 0,$

$w^T[D^2Y(E_3:\delta_0^{tc})(v,v)]=2\left(-\frac{\beta c_1 m_1\hat{p}_1}{(\alpha+\hat{p}_1)^2}+\frac{\alpha v_1}{(\alpha+\hat{p}_1)^2}+\frac{c_2m_2(a\hat{p}_2^2-c)v_2}{(a\hat{p}_2^2+b\hat{p}_2+c)^2}\right).$
So, if $\left(-\frac{\beta c_1 m_1\hat{p}_1}{(\alpha+\hat{p}_1)^2}+\frac{\alpha v_1}{(\alpha+\hat{p}_1)^2}+\frac{c_2m_2(a\hat{p}_2^2-c)v_2}{(a\hat{p}_2^2+b\hat{p}_2+c)^2}\right)\neq 0$, then system (3.1) goes through a transcritical bifurcation at $\delta_0=\delta_0^{tc}$. □

3.4 Dynamics of delayed model

In this section, we shall investigate the kinetics of the delayed model.

3.4.1 Local stability analysis and Hopf-bifurcation

Now, we will examine local stability behavior of delayed system (3.2) around the interior equilibrium E^* and determine the criterion for occurrence of Hopf-bifurcation, using delay terms as the control parameters. For this, let's assume $p_1(t)=\tilde{p}_1(t)+p_1^*$, $p_2(t)=\tilde{p}_2(t)+p_2^*$ and $z(t)=\tilde{z}(t)+z^*$. Therefore, the linearised form of system (3.2) is

$$\frac{dW}{dt}=AW(t)+BW(t-\tau_1)+CW(t-\tau_2), \tag{3.28}$$

where
$A=\begin{bmatrix} a_1 & -\gamma_{12}p_1^* & a_2\\ -\gamma_{21}p_2^* & a_3 & a_4\\ 0 & 0 & -\delta_0\end{bmatrix}$, $B=\begin{bmatrix}0&0&0\\0&0&0\\a_5&0&a_6\end{bmatrix}$, $C=\begin{bmatrix}0&0&0\\0&0&0\\0&a_7&a_8\end{bmatrix}$ and
$a_1=-\frac{r_1p_1^*}{K_1}+\frac{m_1p_1^*z^*}{(\alpha+p_1^*+\beta z^*)^2}$, $a_2=-\frac{m_1p_1^*(\alpha+p_1^*)}{(\alpha+p_1^*+\beta z^*)^2}$, $a_3=-\frac{r_2p_2^*}{K_2}+\frac{m_2z^*(2ap_2{}^{*2}+bp_2^*)}{(ap_2^{*2}+bp_2^*+c)^2}$, $a_4=-\frac{m_2p_2^*}{ap_2^{*2}+bp_2^*+c}$
$a_5=\frac{c_1m_1z^*(\alpha+\beta z^*)}{(\alpha+p_1^*+\beta z^*)^2}$, $a_6=\frac{c_1m_1p_1^*(\alpha+p_1^*)}{(\alpha+p_1^*+\beta z^*)^2}$, $a_7=-\frac{c_2m_2z^*(-ap_2^{*2}+c)}{(ap_2^{*2}+bp_2^*+c)^2}$, $a_8=-\frac{c_2m_2p_2^*}{ap_2^{*2}+bp_2^*+c}$,
and $W(t)=[\tilde{p}_1(t),\tilde{p}_1(t),\tilde{z}(t)]^T$.
Thus, Jacobian matrix for the delayed system at E^* is given by

$$J=A+Be^{-\lambda\tau_1}+Ce^{-\lambda\tau_2}.$$

So, the characteristic equation of above Jacobian matrix is

$$\lambda^3 + b_1\lambda^2 + b_2\lambda + b_3 + e^{-\lambda\tau_1}(b_4\lambda^2 + b_5\lambda + b_6) + e^{-\lambda\tau_2}(b_7\lambda^2 + b_8\lambda + b_9) = 0, \tag{3.29}$$

where
$b_1 = -(a_1 + a_3 - \delta_0)$, $b_2 = (a_1a_3 - \gamma_{12}\gamma_{21}p_1^*p_2^* - \delta_0(a_1 + a_3))$, $b_3 = \delta_0(a_1a_3 - \gamma_{12}\gamma_{21}p_1^*p_2^*)$, $b_4 = -a_6$,
$b_5 = a_6(a_1 + a_3) - a_2a_5$, $b_6 = a_3(a_2a_5 - a_1a_6) + \gamma_{12}p_1^*(a_6\gamma_{21}p_2^* + a_4a_5)$, $b_7 = -a_8$, $b_8 = a_8(a_1 + a_3) - a_4a_7$,
$b_9 = a_1(a_4a_7 - a_3a_8) + a_8\gamma_{12}\gamma_{21}p_1^*p_2^* + a_2a_7\gamma_{21}p_2^*$.
Now, we discuss the following cases:
Case I: $\tau_1 = \tau_2 = 0$.
In this case, (3.29) reduces to (3.24), so the stability conditions for this are provided in Theorem 3.3.5.
Case II: $\tau_1 > 0$, $\tau_2 = 0$.
Substituting $\tau_2 = 0$ in (3.29), we have

$$\lambda^3 + (b_1 + b_7)\lambda^2 + (b_2 + b_8)\lambda + (b_3 + b_9) + e^{-\lambda\tau_1}(b_4\lambda^2 + b_5\lambda + b_6) = 0. \tag{3.30}$$

For Hopf-bifurcation, let $\lambda = i\omega(\omega > 0)$ be the root of (3.30). Using this we get

$$\begin{aligned}(-b_4\omega^2 + b_6)\cos\omega\tau_1 + b_5\omega\sin\omega\tau_1 &= (b_1 + b_7)\omega^2 - (b_3 + b_9),\\ b_5\omega\cos\omega\tau_1 + (b_4\omega^2 - b_6)\sin\omega\tau_1 &= \omega^3 - (b_2 + b_8)\omega.\end{aligned} \tag{3.31}$$

Now, on squaring and adding above equations in (3.31), τ_1 gets eliminate and we get a 6th-degree equation in ω :

$$\omega^6 + q_1\omega^4 + q_2\omega^2 + q_3 = 0, \tag{3.32}$$

where $q_1 = (b_1 + b_7)^2 - 2(b_2 + b_8) - b_4^2$, $q_2 = (b_2 + b_8)^2 - 2(b_1 + b_7)(b_3 + b_9) + 2b_4b_6 - b_5^2$, $q_3 = (b_3 + b_9)^2 - b_6^2$.
Taking $\omega^2 = n_1$ in (3.32), we have a cubic equation:

$$R(n_1) = n_1^3 + q_1n_1^2 + q_2n_1 + q_3 = 0. \tag{3.33}$$

If we assume that $(b_3+b_9)^2 < b_6^2$, then $R(0) < 0$ and $R(\infty) > 0$. So, (3.33) has at least one positive root. Therefore ω_1 (say) is a root of (3.32). Substituting this ω_1 in (3.31), we get

$$\tau_{1_i} = \frac{1}{\omega_1}\arccos\left[\frac{D_1\omega_1^4 + D_2\omega_1^2 + D_3}{D_4\omega_1^4 + D_5\omega_1^2 + D_6}\right] + \frac{2i\pi}{\omega_1},\ i = 0,1,2,3..., \tag{3.34}$$

where
$D_1 = b_5 - b_4(b_1+b_7),\ D_2 = b_6(b_1+b_7) + b_4(b_3+b_9) - b_5(b_2+b_8),\ D_3 = -b_6(b_3+b_9),$
$D_4 = b_4^2,\ D_5 = b_5^2 - 2b_4b_6,\ D_6 = b_6^2.$
To establish transversality condition, put $\lambda = \xi + i\omega$ in (3.30) and on separating real and imaginary parts, we get

$$\begin{aligned}&\xi^3 - 3\xi\omega^2 + (b_1+b_7)(\xi^2-\omega^2) + \xi(b_2+b_8) + (b_3+b_9)\\ &\quad + e^{-\xi\tau_1}\cos\omega\tau_1(b_4(\xi^2-\omega^2) + b_5\xi + b_6) + e^{-\xi\tau_1}\sin\omega\tau_1(2b_4\xi\omega + b_5\omega) = 0,\end{aligned} \tag{3.35}$$

and

$$\begin{aligned}&-\omega^3 + 3\xi^2\omega + 2\xi\omega(b_1+b_7) + \omega(b_2+b_8)\\ &\quad + e^{-\xi\tau_1}\cos\omega\tau_1(2b_4\xi\omega + b_5\omega) - e^{-\xi\tau_1}\sin\omega\tau_1(b_4(\xi^2-\omega^2) + b_5\xi + b_6) = 0.\end{aligned} \tag{3.36}$$

Differentiating (3.35) and (3.36) with respect to τ_1 and replacing $\xi = 0,\ \tau_1 = \tau_{1_0}$ and $\omega = \omega_1$, yields

$$\begin{aligned}P_1\left[\frac{d[Re(\lambda(\tau_1))]}{d\tau_1}\right] + P_2\left[\frac{d[Im(\lambda(\tau_1))]}{d\tau_1}\right] &= R_1,\\ -P_2\left[\frac{d[Re(\lambda(\tau_1))]}{d\tau_1}\right] + P_1\left[\frac{d[Im(\lambda(\tau_1))]}{d\tau_1}\right] &= R_2,\end{aligned} \tag{3.37}$$

where
$P_1 = [-3\omega^2 + (b_2+b_8) + (b_5 + (b_4\omega^2 - b_6)\tau_1)\cos\omega\tau_1 + (2\omega b_4 - b_5\omega\tau_1)\sin\omega\tau_1]_{\tau_1=\tau_{1_0},\ \omega=\omega_1},$
$P_2 = [-2\omega(b_1+b_7) + (b_5 + (b_4\omega^2 - b_6)\tau_1)\sin\omega\tau_1) + (-2\omega b_4 + b_5\omega\tau_1)\cos\omega\tau_1]_{\tau_1=\tau_{1_0},\ \omega=\omega_1},$
$R_1 = [\omega(b_6 - b_4\omega^2)\sin\omega\tau_1 - b_5\omega^2\cos\omega\tau_1]_{\tau_1=\tau_{1_0},\ \omega=\omega_1},$
$R_2 = [\omega(b_6 - b_4\omega^2)\cos\omega\tau_1 + b_5\omega^2\sin\omega\tau_1]_{\tau_1=\tau_{1_0},\ \omega=\omega_1}.$
Solving system (3.37), we get $\left[\frac{d[Re(\lambda(\tau_1))]}{d\tau_1}\right] = \frac{R_1P_1 - R_2P_2}{P_1^2+P_2^2}$. Hence tranversality condition for Hopf-bifurcation is satisfied at $\tau_1 = \tau_{1_0}$ if $R_1P_1 - R_2P_2 > 0$.

Theorem 3.4.1. *For system (3.2), suppose $(b_3+b_9)^2 < b_6^2$ and $R_1P_1 - R_2P_2 > 0$ hold, then there exists a $\tau_1 = \tau_{1_0}$ such that the interior equilibrium E^* is locally asymptotically stable when $\tau_1 < \tau_{1_0}$ and is unstable for $\tau_1 > \tau_{1_0}$. Moreover, the delayed system undergoes Hopf-bifurcation around E^* at $\tau_1 = \tau_{1_0}$.*

Case III: $\tau_1 = 0,\ \tau_2 > 0.$

Under an analysis similar to case II, we get

$$\tau_{2_i} = \frac{1}{\omega_2}\arccos\left[\frac{D_1'\omega_2^4 + D_2'\omega_2^2 + D_3'}{D_4'\omega_2^4 + D_5'\omega_2^2 + D_6'}\right] + \frac{2i\pi}{\omega_2},\ i = 0,1,2,3..., \tag{3.38}$$

where

$D_1' = b_8 - b_7(b_1+b_4),\ D_2' = b_9(b_1+b_4) + b_7(b_3+b_6) - b_8(b_2+b_5),$

$D_3' = -b_9(b_3+b_6),\ D_4' = b_7^2,\ D_5' = b_8^2 - 2b_7b_9;\ D_6' = b_9^2.$

Derivation of transversality condition is similar to case II, and its given by

$\left[\frac{d[Re(\lambda(\tau_2))]}{d\tau_2}\right] = \frac{R_3P_3 - R_4P_4}{P_3^2+P_4^2} > 0,$

where

$P_3 = [-3\omega^2 + (b_2+b_5) + (b_8 + (b_7\omega^2 - b_9)\tau_2)\cos\omega\tau_2 + (2\omega b_7 - b_8\omega\tau_2)\sin\omega\tau_2]_{\tau_2=\tau_{2_0},\ \omega=\omega_2},$

$P_4 = [-2\omega(b_1+b_4) + (b_8 + (b_7\omega^2 - b_9)\tau_2)\sin\omega\tau_2) + (-2\omega b_7 + b_8\omega\tau_2)\cos\omega\tau_2]_{\tau_2=\tau_{2_0},\ \omega=\omega_2},$

$R_3 = [\omega(b_9 - b_7\omega^2)\sin\omega\tau_2 - b_8\omega^2\cos\omega\tau_2]_{\tau_2=\tau_{2_0},\ \omega=\omega_2},$

$R_4 = [\omega(b_9 - b_7\omega^2)\cos\omega\tau_2 + b_8\omega^2\sin\omega\tau_2]_{\tau_2=\tau_{2_0},\ \omega=\omega_2}.$

Hence, we have the following theorem regarding this case.

Theorem 3.4.2. *For delayed system, if* $(b_3+b_6)^2 < b_9^2$ *and* $R_3P_3 - R_4P_4 > 0$ *hold, then there exists a* $\tau_2 = \tau_{2_0}$ *such that the interior equilibrium* E^* *is locally asymptotically stable when* $\tau_2 < \tau_{2_0}$ *and is unstable for* $\tau_2 > \tau_{2_0}$. *Furthermore, system (3.2) undergoes Hopf-bifurcation around* E^* *at* $\tau_2 = \tau_{2_0}$.

Case IV: $\tau_1 > 0,\ \tau_2 \in (0, \tau_{2_0}).$

Consider (3.29), with τ_2 as fixed in its stable interval $(0, \tau_{2_0})$ and τ_1 as the varying parameter. Substituting $\lambda = i\omega(\omega > 0)$ in (3.29). Separating real and imaginary parts we get

$$\begin{aligned}(-b_4\omega^2 + b_6)\cos\omega\tau_1 + b_5\omega\sin\omega\tau_1 &= b_1\omega^2 - b_3 + (b_7\omega^2 - b_9)\cos\omega\tau_2 - b_8\omega\sin\omega\tau_2,\\ b_5\omega\cos\omega\tau_1 + (b_4\omega^2 - b_6)\sin\omega\tau_1 &= \omega^3 - b_2\omega - b_8\omega\cos\omega\tau_2 - (b_7\omega^2 - b_9)\sin\omega\tau_2.\end{aligned} \tag{3.39}$$

Squaring and adding the equations in above system gives:

$$\omega^6 + f_1\omega^5 + f_2\omega^4 + f_3\omega^3 + f_4\omega^2 + f_5\omega + f_6 = 0, \tag{3.40}$$

where

$f_1 = -2b_7\sin\omega\tau_2,$

$f_2 = b_1^2 + b_7^2 - b_4^2 - 2b_2 + 2(b_1b_7 - b_8)\cos\omega\tau_2,$

$f_3 = (-2b_1b_8 + 2b_2b_7 + 2b_9)\sin\omega\tau_2,$

$f_4 = b_2^2 + b_8^2 - b_5^2 - 2b_1b_3 - 2b_7b_9 + 2b_4b_6 - 2(b_1b_9 + b_3b_7 - b_2b_8)\cos\omega\tau_2,$

$f_5 = 2(b_3b_8 - b_2b_9)\sin\omega\tau_2,$
$f_6 = b_3^2 + b_9^2 - b_6^2 + 2b_3b_9\cos\omega\tau_2.$
If we assume, $b_3^2 + b_9^2 + 2b_3b_9 < b_6^2$ then (3.40) has at least one positive root ω_1^* (say). So from (3.39), we get

$$\tau_{1_i}^* = \frac{1}{\omega_1^*}\arcsin\left[\frac{F_4E_{12} + F_5E_{11}}{E_{11}^2 + E_{12}^2}\right] + \frac{2i\pi}{\omega_1^*},\ i = 0,1,2,3..., \tag{3.41}$$

where
$E_{11} = b_5\omega_1^*,$
$E_{12} = b_4\omega_1^{*2} - b_6,$
$F_4 = \omega_1^{*3} - b_2\omega_1^* - b_8\omega_1^*\cos(\omega_1^*\tau_2) - (b_7\omega_1^{*2} - b_9)\sin(\omega_1^*\tau_2),$
$F_5 = b_1\omega_1^{*2} - b_3 + (b_7\omega_1^{*2} - b_9)\cos(\omega_1^*\tau_2) - b_8\omega_1^*\sin(\omega_1^*\tau_2).$
To examine the transvesality condition for Hopf-bifurcation, we have to show $\left[\frac{d[Re(\lambda(\tau_1))]}{d\tau_1}\right] = \frac{R_5P_5 - R_6P_6}{P_5^2 + P_6^2} > 0,$
where

$$P_5 = \Big[-3\omega^2 + b_2 + (b_5 + (b_4\omega^2 - b_6)\tau_1)\cos\omega\tau_1 + (2\omega b_4 - b_5\omega\tau_1)\sin\omega\tau_1 + \cos\omega\tau_2[(b_7\omega^2 - b_9)\tau_2 + b_8] + \sin\omega\tau_2[2\omega b_7 - b_8\omega\tau_2]\Big]_{\tau_1=\tau_1^*,\ \tau_2=\tau_{2_0},\ \omega=\omega_1^*},$$

$$P_6 = \Big[-2\omega b_1 + (b_5 + (b_4\omega^2 - b_6)\tau_1)\sin\omega\tau_1 + (-2\omega b_4 + b_5\omega\tau_1)\cos\omega\tau_1 + \sin\omega\tau_2[(b_7\omega^2 - b_9)\tau_2 + b_8] + \cos\omega\tau_2[-2\omega b_7 + b_8\omega\tau_2]\Big]_{\tau_1=\tau_1^*,\ \tau_2=\tau_{2_0},\ \omega=\omega_1^*},$$

$R_5 = [\omega(b_6 - b_4\omega^2)\sin\omega\tau_1 - b_5\omega^2\cos\omega\tau_1]_{\tau_1=\tau_1^*,\ \omega=\omega_1^*},$
$R_6 = [\omega(b_6 - b_4\omega^2)\cos\omega\tau_1 + b_5\omega^2\sin\omega\tau_1]_{\tau_1=\tau_1^*,\ \omega=\omega_1^*}.$
Therefore, we state the following theorem:

Theorem 3.4.3. *For system (3.2), with $\tau_2 \in (0,\tau_{2_0})$ if $b_3^2 + b_9^2 + 2b_3b_9 < b_6^2$ and $R_5P_5 - R_6P_6 > 0$ hold, then then there exists a $\tau_1 = \tau_{1_0}^*$ such that the delayed system is asymptotically stable around E^* for $\tau_1 < \tau_{1_0}^*$ and is unstable for $\tau_1 > \tau_{1_0}^*$. Moreover, the delayed system experiences Hopf-bifurcation at $\tau_1 = \tau_{1_0}^*$.*

Case V: $\tau_2 > 0,\ \tau_1 \in (0,\tau_{1_0})$.
Analysis for this case is similar to the last case. So, we omit it.

3.4.2 Direction and stability of Hopf-bifurcation

In last subsection, we have determined the conditions for emergence of Hopf-bifurcation from the interior equilibrium for delayed system (3.2). Now, we identify the direction, stability and period of bifurcating periodic solutions at $\tau_1 = \tau_{1_0}^*$ and $\tau_2 = \tau_2^* \in (0,\tau_2)$. For this, propose we use normal form and centre manifold theory [83].

Let

$$x_1 = p_1 - p_1^*,\ x_2 = p_1 - p_1^*,\ x_3 = z - z^*,$$

and still denote $x_1,\ x_2,\ x_3$ by $p_1,\ p_2,\ z$, respectively. Let $\mu = \tau_1 - \tau_{1_0}^* \in R$ and on rescaling $t \to (\frac{t}{\tau_1})$, system (3.2) is written as

$$\dot{x}(t) = L_\mu + f(\mu, x_t), \tag{3.42}$$

where $x(t) = [p_1(t), p_2(t), z(t)]^T \in R^3$,

$$L_\mu(\phi) = (\tau_{1_0}^* + \mu)\left(A\phi(0) + C\phi\left(\frac{-\tau_2^*}{\tau_1}\right) + B\phi(-1)\right),\ \text{for}\ \phi \in C([-1,0], R^3),$$

and

$$f(\mu,\phi) = \begin{bmatrix} -\frac{r_1}{K_1}\phi_1^2(0) - \gamma_{12}\phi_1(0)\phi_2(0) - \frac{m_1\phi_1(0)\phi_3(0)}{\alpha+\phi_1(0)+\beta\phi_3(0)} \\ -\frac{r_2}{K_2}\phi_2^2(0) - \gamma_{21}\phi_1(0)\phi_2(0) - \frac{m_2\phi_2(0)\phi_3(0)}{a{\phi_2}^2(0)+b\phi_2(0)+c} \\ \frac{c_1 m_1\phi_1(-1)\phi_3(-1)}{\alpha+\phi_1(-1)+\beta\phi_3(-1)} - \frac{c_2 m_2\phi_2\left(\frac{-\tau_2^*}{\tau_1}\right)\phi_3\left(\frac{-\tau_2^*}{\tau_1}\right)}{a{\phi_2}^2\left(\frac{-\tau_2^*}{\tau_1}\right)+b\phi_2\left(\frac{-\tau_2^*}{\tau_1}\right)+c} \end{bmatrix}.$$

Here, without going into detailed calculations, we directly mention the results which are derived using the computational process similar as given by Song and Wei [84]. The standard results are

$$c_1(0) = \frac{i}{2\omega_1^*\tau_{1_0}^*}\left(g_{20}g_{11} - 2|g_{11}|^2 - \frac{|g_{02}|^2}{3}\right) + \frac{g_{21}}{2},\ \mu_2 = -\frac{Re(c_1(0))}{Re(\lambda'(\tau_{1_0}^*))},$$

$$\beta_2 = 2Re(c_1(0)),\ T_2 = -\frac{Im(c_1(0)) + \mu_2 Im((\lambda'(\tau_{1_0}^*)))}{\omega_1^*\tau_{1_0}^*},$$

where, the computed coefficients $g_{20},\ g_{11},\ g_{02},\ g_{21}$ are given as

$$
\begin{aligned}
g_{20} &= 2\tau_{1_0}^{*}\overline{M}\Bigg[\Big(-\frac{r_1}{K_1}-\gamma_{12}\sigma_2-\frac{m_1\sigma_3}{\alpha}\Big)+\overline{\sigma_2^{*}}\Big(-\frac{r_2}{K_2}\sigma_2^2-\gamma_{21}\sigma_2-\frac{m_2\sigma_2\sigma_3}{c}\Big)+\overline{\sigma_3^{*}}\Big(\frac{c_1m_1\sigma_3}{\alpha}e^{-2i\omega_1^{*}\tau_{1_0}^{*}}\\
&\quad-\frac{c_2m_2\sigma_2\sigma_3}{c}e^{-2i\omega_1^{*}\tau_2^{*}}\Big)\Bigg],\\
g_{11} &= 2\tau_{1_0}^{*}\overline{M}\Bigg[\Big(-\frac{r_1}{K_1}-\gamma_{12}\mathrm{Re}\{\sigma_2\}-\frac{m_1}{\alpha}\mathrm{Re}\{\sigma_3\}\Big)+\overline{\sigma_2^{*}}\Big(-\frac{r_2}{k_2}|\sigma_2|^2-\gamma_{21}\mathrm{Re}\{\sigma_2\}-\frac{m_2}{c}\mathrm{Re}\{\sigma_2\overline{\sigma_3}\}\Big)\\
&\quad+\overline{\sigma_3^{*}}\Big(\frac{c_1m_1}{\alpha}\mathrm{Re}\{\sigma_3\}-\frac{c_2m_2}{c}\mathrm{Re}\{\sigma_2\overline{\sigma_3}\}\Big)\Bigg]\\
g_{02} &= 2\tau_{1_0}^{*}\overline{M}\Bigg[\Big(-\frac{r_1}{K_1}-\gamma_{12}\overline{\sigma_2}-\frac{m_1\overline{\sigma_3}}{\alpha}\Big)+\overline{\sigma_2^{*}}\Big(-\frac{r_2}{K_2}\overline{\sigma_2}^2-\gamma_{21}\overline{\sigma_2}-\frac{m_2\overline{\sigma_2\sigma_3}}{c}\Big)\\
&\quad+\overline{\sigma_3^{*}}\Big(\frac{c_1m_1\overline{\sigma_3}}{\alpha}e^{2i\omega_1^{*}\tau_{1_0}^{*}}-\frac{c_2m_2\overline{\sigma_2\sigma_3}}{c}e^{2i\omega_1^{*}\tau_2^{*}}\Big)\Bigg],\\
g_{21} &= 2\tau_{1_0}^{*}\overline{M}\Bigg[\Big\{-\frac{r_1}{K_1}\big(W_{20}^{(1)}(0)+2W_{11}^{(1)}(0)\big)-\gamma_{12}\big(W_{11}^{(2)}(0)+W_{11}^{(1)}(0)\sigma_2+\frac{1}{2}(W_{20}^{(2)}(0)+W_{20}^{(1)}(0)\overline{\sigma_2})\big)\\
&\quad-m_1\big(\frac{1}{\alpha}(W_{11}^{(3)}(0)+W_{11}^{(1)}(0)\sigma_3)+\frac{1}{2\alpha}(W_{20}^{(3)}(0)+W_{20}^{(1)}(0)\overline{\sigma_3})\\
&\quad+\frac{1}{\alpha^2}(\sigma_3(1+\beta\overline{\sigma_3})+\sigma_3(1+\beta\sigma_3)+\overline{\sigma_3}(1+\beta\sigma_3)))\Big\}\\
&\quad+\overline{\sigma_2^{*}}\Big\{-\frac{r_2}{K_2}(\sigma_2W_{11}^{(2)}(0))+\overline{\sigma_2}W_{20}^{(2)}(0))-\gamma_{21}(W_{11}^{(2)}(0)+\sigma_2W_{11}^{(1)}(0)+\frac{1}{2}(W_{20}^{(2)}(0)+\overline{\sigma_2}W_{20}^{(1)}(0)))\\
&\quad-m_2\big(\frac{1}{c}(W_{11}^{(3)}(0)+\sigma_3W_{11}^{(2)}(0))+\frac{1}{2c}(\overline{\sigma_2}W_{20}^{(3)}(0)+\overline{\sigma_3}W_{20}^{(2)}(0))-\frac{2b}{c^2}(2|\sigma_2|^2\sigma_3+\bar{\sigma}_3\sigma_2^2)\big)\Big\}\\
&\quad+\overline{\sigma_3^{*}}\Bigg\{c_1m_1\Bigg(\frac{e^{-i\omega_1^{*}\tau_{1_0}^{*}}}{\alpha}\big(W_{11}^{(3)}(-1)+\sigma_3W_{11}^{(1)}(-1)\big)+\frac{e^{-i\omega_1^{*}\tau_{1_0}^{*}}}{2\alpha}\big(W_{20}^{(3)}(-1)+W_{20}^{(1)}(-1)\overline{\sigma_3}\big)\\
&\quad+\frac{e^{-i\omega_1^{*}\tau_{1_0}^{*}}}{\alpha^2}\big(\sigma_3(1+\beta\overline{\sigma_3})+\sigma_3(1+\beta\sigma_3)+\overline{\sigma_3}(1+\beta\sigma_3)\big)\Bigg)\\
&\quad-c_2m_2\Bigg(\frac{e^{-i\omega_1^{*}\tau_2^{*}}}{c}\Big(W_{11}^{(3)}\Big(\frac{\tau_2^{*}}{\tau_{1_0}^{*}}\Big)+W_{11}^{(2)}\Big(\frac{\tau_2^{*}}{\tau_{1_0}^{*}}\Big)\sigma_3\Big)+\frac{e^{-i\omega_1^{*}\tau_2^{*}}}{2c}\Big(\overline{\sigma_2}W_{20}^{(3)}\Big(\frac{\tau_2^{*}}{\tau_{1_0}^{*}}\Big)+\overline{\sigma_3}W_{20}^{(2)}\Big(\frac{\tau_2^{*}}{\tau_{1_0}^{*}}\Big)\Big)\\
&\quad-\frac{2be^{-i\omega_1^{*}\tau_2^{*}}}{c^2}\Big(2|\sigma_2|^2\sigma_3+\bar{\sigma}_3\sigma_2^2\Big)\Big)\Big\}\Bigg].
\end{aligned}
$$

Here

$W_{20}(\theta)=\frac{ig_{20}}{\omega_1^{*}\tau_{1_0}^{*}}q(0)e^{i\omega_1^{*}\tau_{1_0}^{*}\theta}+\frac{i\bar{g}_{02}}{3\omega_1^{*}\tau_{1_0}^{*}}\bar{q}(0)e^{-i\omega_1^{*}\tau_{1_0}^{*}\theta}+E_1e^{2i\omega_1^{*}\tau_{1_0}^{*}\theta},$

$W_{11}(\theta) = -\frac{ig_{11}}{\omega_1^*\tau_{1_0}^*}q(0)e^{i\omega_1^*\tau_{1_0}^*\theta} + \frac{i\bar{g}_{11}}{\omega_1^*\tau_{1_0}^*}\bar{q}(0)e^{-i\omega_1^*\tau_{1_0}^*\theta} + E_2,$

where the constant vectors $E_1 = [E_1^{(1)}, E_1^{(2)}, E_1^{(3)}]^T \in R^3$ and $E_2 = [E_2^{(1)}, E_2^{(2)}, E_2^{(3)}]^T \in R^3$ are computed as

$$E_1 = 2\begin{bmatrix} 2i\omega_1^* - a_1 & \gamma_{12}p_1^* & -a_2 \\ \gamma_{21}p_2^* & 2i\omega_1^* - a_3 & -a_4 \\ -a_5 e^{2i\omega_1^*\tau_{1_0}^*} & -a_7 e^{2i\omega_1^*\tau_2^*} & 2i\omega_1^* - a_6 e^{2i\omega_1^*\tau_{1_0}^*} - a_8 e^{2i\omega_1^*\tau_2^*} + \delta_0 \end{bmatrix}^{-1}$$
$$\times \begin{bmatrix} \frac{r_1}{K_1} + \gamma_{12}\sigma_2 + \frac{m_1\sigma_3}{\alpha} \\ \frac{r_2}{K_2}\sigma_2^2 + \gamma_{21}\sigma_2 + \frac{m_2\sigma_2\sigma_3}{c} \\ -\frac{c_1 m_1 \sigma_3 e^{-2i\omega_1^*\tau_{1_0}^*}}{\alpha} + \frac{c_2 m_2 \sigma_2 \sigma_3 e^{-2i\omega_1^*\tau_2^*}}{c} \end{bmatrix},$$
$$E_2 = 2\begin{bmatrix} -a_1 & \gamma_{12}p_1^* & -a_2 \\ \gamma_{21}p_2^* & -a_3 & -a_4 \\ -a_5 & -a_7 & -a_6 - a_8 + \delta_0 \end{bmatrix}^{-1} \begin{bmatrix} \frac{r_1}{K_1} + \gamma_{12}\mathrm{Re}\{\sigma_2\} + \frac{m_1}{\alpha}\mathrm{Re}\{\sigma_3\} \\ \frac{r_2}{K_2}|\sigma_2|^2 + \gamma_{21}\mathrm{Re}\{\sigma_2\} + \frac{m_2}{c}\mathrm{Re}\{\sigma_2\overline{\sigma}_3\} \\ -\frac{c_1 m_1 \mathrm{Re}\{\sigma_3\}}{\alpha} + \frac{c_2 m_2 \mathrm{Re}\{\sigma_2\overline{\sigma}_3\}}{c} \end{bmatrix}.$$

In above calculation, the components $\sigma_2,\ \sigma_3,\ \sigma_2^*,\ \sigma_3^*$ and $\overline{M}$ are given as

$$\sigma_2 = \frac{(-i\omega_1^* + a_1)a_4 + a_2\gamma_{21}p_2^*}{(-i\omega_1^* + a_3)a_2 + a_4\gamma_{12}p_1^*},\ \sigma_3 = \frac{(-i\omega_1^* + a_1)(i\omega_1^* - a_3) + \gamma_{12}\gamma_{21}p_1^*p_2^*}{-a_2(i\omega_1^* - a_3) + a_4\gamma_{12}p_1^*},$$

$$\sigma_2^* = \frac{a_7 e^{-i\omega_1^*\tau_2^*/\tau_{1_0}^*}(i\omega_1^* + a_1) + a_5\gamma_{12}p_1^* e^{i\omega_1^*\tau_{1_0}^*}}{a_7\gamma_{21}p_2^* e^{i\omega_1^*\tau_2^*/\tau_{1_0}^*} + a_5 e^{i\omega_1^*\tau_{1_0}^*}(i\omega_1^* + a_3)}, \sigma_3^* = \frac{\gamma_{12}\gamma_{21}p_1^*p_2^* - (i\omega_1^* + a_1)(i\omega_1^* + a_3)}{a_7\gamma_{21}p_2^* e^{i\omega_1^*\tau_2^*/\tau_{1_0}^*} + a_5 e^{i\omega_1^*\tau_{1_0}^*}(i\omega_1^* + a_3)},$$

$$\frac{1}{\overline{M}} = 1 + \overline{\sigma_2^*}\sigma_2 + \overline{\sigma_3^*}\sigma_3 + \tau_2^*(\sigma_3^*(a_7\sigma_2 + a_8\sigma_3)e^{-i\omega_1^*\tau_2^*}) + \tau_{1_0}^*(\sigma_3^*(a_5 + a_6\sigma_3)e^{-i\omega_1^*\tau_{1_0}^*}).$$

Above terms provides the description of bifurcating periodic solution in the center manifold of the system (3.2) at $\tau_1 = \tau_{1_0}^*$ which is stated in the following theorem.

Theorem 3.4.4. *1. μ_2 gives the direction of Hopf-bifurcation. If $\mu_2 > 0 (< 0)$, the Hopf-bifurcation is supercritical(subcritical).*

2. β_2 gives the stability of bifurcated periodic solution. If $\beta_2 > 0 (\beta_2 < 0)$ then the bifurcated periodic solutions are unstable (stable).

3. T_2 gives the period of bifurcated solution, the period increases(decreases) if $T_2 > 0 (< 0)$.

3.5 Numerical simulation

Here, we carry out numerical simulation and try to understand the dynamics of models (3.1) and (3.2) via plotting various bifurcation diagrams, time-series and phase portraits under different situations. For this intent, we chose the following set of parametric values:

$$r_1 = 2,\ K_1 = 30,\ \gamma_{12} = 0.005,\ m_1 = 0.6,\ \alpha = 10,\ \beta = 0.1,\ r_2 = 3,\ K_2 = 40,\ \gamma_{21} = 0.01,$$
$$a = 0.02,\ b = 0.1,\ c = 30,\ m_2 = 0.3,\ c_1 = 0.5,\ c_2 = 0.3,\ \delta_0 = 0.04. \tag{3.43}$$

3.5.1 For non-delayed model

For (3.43), in Table 3.1, we have given all the feasible equilibrium points. In the second and third columns of this table, we have provided the dimensions of corresponding stable and unstable manifolds for the same set of parameters, wherein the fourth column, nature of each critical point is described. For these parameters, every equilibrium point except the coexistent one, is unstable. In Fig. 3.3(a), we observe that all the species oscillate for a finite time and then settle down to their respective steady states. In fact, the interior equilibrium is globally asymptotically stable in the interior of positive octant of the p_1p_2z-space. Starting from various points (Fig. 3.3(b)), all solutions approach E^*, which shows the attribute of global stability for interior equilibrium. The intrinsic growth rate (r_1) of non-toxic phytoplankton plays a vital role in the dynamics of the system because the survival of non-toxic phytoplankton as well as zooplankton depends upon this parameter. Another important point about this parameter is that the non-delayed system switches its stability twice in the vicinity of E^* when we vary r_1. For $r_1 \in (0.3, 0.6811)$, E^* is a stable focus and system converges to it. At $r_1^{hf_1} = 0.6811$, system encounter Hopf-bifurcation to become unstable and system converges to a stable limit cycle (for $r_1 \in (0.6811, 1.5258)$). At $r_1^{hf_2} = 1.5258$ system undergoes Hopf-bifurcation to become stable again. In Fig. 3.4, we have taken three values of r_1, as indicated. For $r_1 = 0.35 < r_1^{hf_1}$, interior equilibrium E^* is stable (red trajectory in Fig. 3.4). For $r_1^{hf_1} < r_1 = 1 < r_1^{hf_2}$, solution converges to a limit cycle attractor (green trajectory in Fig. 3.4) and if we choose $r_1 = 2 > r_1^{hf_2}$, system converges again to E^* (blue trajectory in Fig. 3.4). In all three cases, solution starts from same initial point. For $r_1 > r_1^{hf_2}$, E^* remains stable.

Non-delayed system suffers Hopf-bifurcation in the neighbourhood of E^*, when we very a. For $a < a^{hf} = 0.0323$, E^* is a spiral sink and for $a > a^{hf}$, E^* acts as a spiral source. So, a stable limit cycle bifurcates from E^* (for $a > a^{hf}$). Our claim is depicted by Fig. 3.5(a) in which solutions started from same initial point with two different values of a ($a = 0.025$ and $a = 0.05$) converges to E^* and a limit cycle attractor (red and green trajectories, respectively).

Death rate of zooplankton (δ_0) is also an important parameter to deal because for $\delta_0 < \delta_0^{hf} = 0.0288$, E^* is an unstable focus with $\dim(W^s(E)) = 1$ and $\dim(W^u(E)) = 2$. At $\delta_0 = \delta_0^{hf}$, system (3.1) suffers Hopf-bifurcation to become stable. On further increase of this death rate, interior equilibrium (E^*) and zooplankton free equilibrium (E_3) go for transcritical bifurcation at $\delta_0 = \delta_0^{tc} = 0.1651$. This leads to disappearance of E^* and change in the stability of E_3. As a result of this transcritical bifurcation E_3 becomes a stable node from a saddle point. To understand this scenario, we have given a phase portrait diagram Fig. 3.5(b) in which we drew three solution with same initial conditions and three different values of δ_0. For $\delta_0 = 0.01 < \delta_0^{hf}$ (red trajectory) solution converges to a stable limit cycle and at $\delta_0 = 0.04 > \delta_0^{hf}$ solution converges to E^* (green trajectory). Then after transcritical bifurcation, for $\delta_0 = 0.3 > \delta_0^{tc}$, solution converges to E_3 (blue trajectory).

Equilibrium point (E)	$\dim(W^s(E))$	$\dim(W^u(E))$	Nature
$E_0(0,0,0)$	1	2	saddle point
$E_1(K_1,0,0)$	1	2	saddle point
$E_2(0,K_2,0)$	2	1	saddle point
$E_3(27.2727,36.3636,0)$	2	1	saddle point
$E_4(2.3818,0,54.8170)$	0	3	unstable focus
$E^*(6.8696,35.7267,49.6050)$	3	0	stable focus

Table 3.1: Equilibrium points with dimension of their stable and unstable manifolds and the corresponding nature of points.

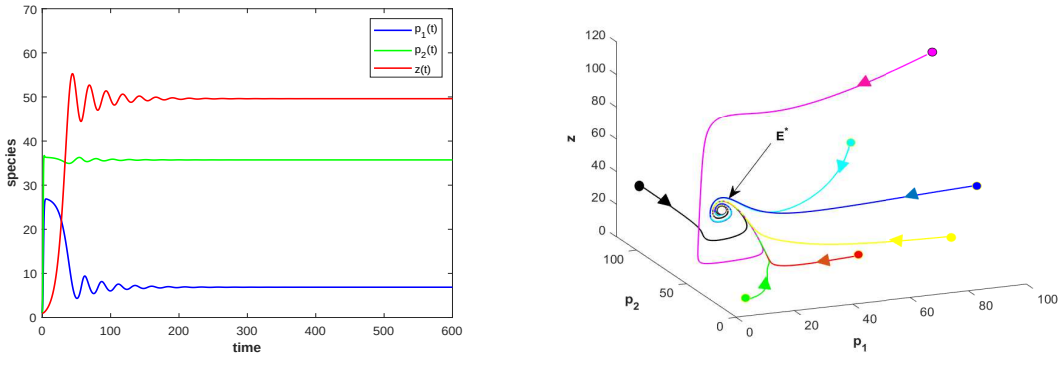

(a) **(b)**

Fig. 3.3: Global stability of E^* shown by time-series in Fig. (a) and phase portrait in Fig. (b), for all parameters from (3.43).

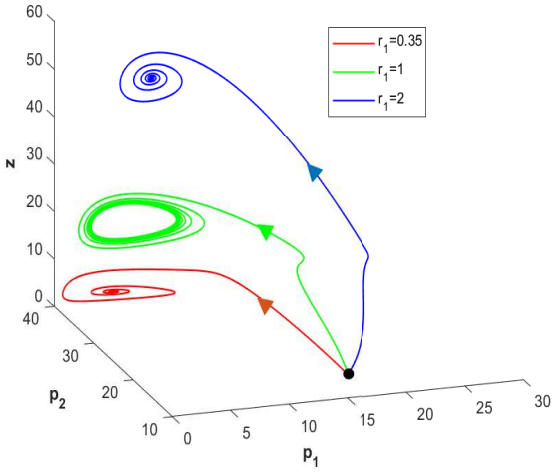

Fig. 3.4: Three solutions with different values of r_1 converging to different attractors showing the phenomena of double Hopf-bifurcation with all other parameters same as in (3.43).

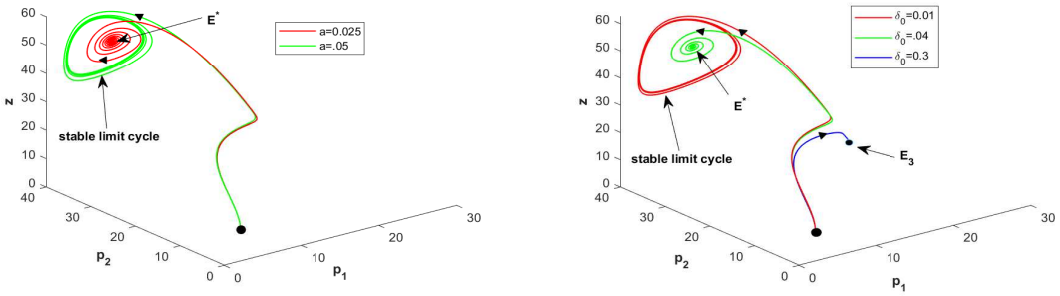

(a) **(b)**

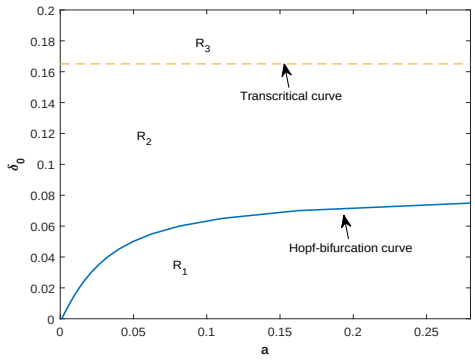

(c)

Fig. 3.5: 3D-phase portrait diagrams showing Hopf-bifurcation with respect to a and Hopf-bifurcation followed by transcritical bifurcation with respect to δ_0 in Figs. (a) and (b), respectively, and distribution of existence and stability regions for E^* and E_3 in the $a\delta_0$-plane in Fig. (c), keeping all other parameters same as in (3.43).

As we have seen that both the parameters, a and δ_0 perform a crucial role in kinetics of non-delayed system, so further, we have analyzed the system varying both these parameters simultaneously and have drawn two parametric bifurcation diagram in Fig. 3.5(c). We have divided $a\delta_0$-domain in three regions named as: R_1, R_2 and R_3. In region R_1, both equilibriums are feasible and unstable. As we crosses the Hopf-bifurcation curve (denoted by blue solid curve), E^* becomes a stable focus, where E_3 remains unstable, in region R_2. Then after crossing the transcritical curve (denoted by olive dotted curve), E^* disappears (become biologically infeasible), and E_3 becomes a stable node, in the region R_3. All these happenings are outlined in Table 3.2.

Moreover, the non-delayed system undergoes Hopf-bifurcation for β. So, as the interference among zooplankton for non-toxic phytoplankton increases, the system becomes stable in the vicinity of coexistence equilibrium. In Fig. 3.6, we have plotted two solutions with the same initial point with different levels of interference. For $\beta = 0.05 < \beta^{hf} = 0.0826$, E^* is unstable (blue coloured solution). At $\beta = \beta^{hf}$, a stable focus E^* bifurcates from the stable limit cycle. We have plotted a solution with $\beta = 0.09 > \beta^{hf}$ (black coloured) which converges to E^*.

Region	feasible equilibria	Nature (respectively)
R_1	E^* and E_3	unstable focus and unstable node
R_2	E^* and E_3	stable focus and unstable node
R_3	E_3	stable node

Table 3.2: Regions defined with reference to two-parametric bifurcation diagram given in Fig. 3.5(c).

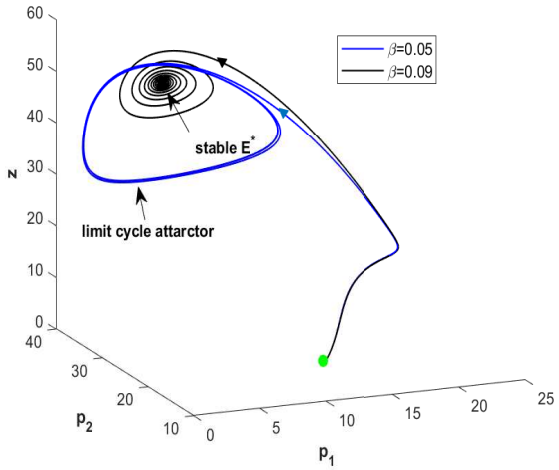

Fig. 3.6: System going under Hopf-bifurcation with respect to β, all other parameters same as in (3.43).

For more detailed behaviour of the non-delayed model with respect to variation in different physical parameters, we present various bifurcation diagrams. In Fig. 3.7(a), we have plotted a concurrent bifurcation diagram for all three species in a single frame. We can see that system (3.1) changes its stability twice in the neighbourhood E^* via Hopf-bifurcation. At $r_1 = r_1^{hf_1}$ and $r_1 = r_1^{hf_2}$, system go for Hopf-bifurcation and switch its stability multiple times. The region of $r_1 \in (r_1^{hf_1}, r_1^{hf_2})$ represents the existence of stable limit cycle. In this bifurcation diagram, we can also observe that as we increase r_1, there is a fine rise in the value of z. This rise shows how the zooplankton's growth is dependent on TPP's growth. Also, increasing r_1 enhance the rate of competition of NTP against TPP which decrease p_2. This decrement in p_2 also adds an increment to z, thus amplifying r_1 provides a boost to zooplankton population.

Now, from Table 3.3 we can observe the trend for values of interior equilibrium point when we increase the parameter a. We can observe that as initially a is increased, there is a rise in the value of p_2^* due to a decrement in consumption of TPP by zooplankton. As the consumption of this toxic producing phytoplankton is decreased, z^* increases. As zooplankton completely depends on non-toxic phytoplankton, this increasing zooplankton population enhances the grazing pressure on this non-toxic source, which reduces p_1^*. But the further rise in a ($a > 0.0206$) leads to a fall in z^* due to the continuous dropping of NTP density. Thus we can see how the initial rise in a supports zooplankton's growth, but its continuous increase leads to a decline in the zooplankton population. This whole trend also validates the modelling of proposed system. We have also drawn bifurcation diagram (Fig. 3.7(b)) for a, showing that species are going under Hopf-bifurcation when we increase a. So, we can say that increase in the inhibitory effect of TPP beyond a limit makes the system unstable.

In Fig. 3.7(c), we can see that as the interference among zooplankton for non-toxic phtoplankton decreases, non-delayed system becomes unstable via Hopf-bifurcation at $\beta = \beta^{hf}$. So, an increased interference among zooplankton makes the system stable. An interesting behavior of the non-delayed system can be seen from this bifurcation diagram for parameter β. As we increase β, z is expected to decrease, but from this bifurcation diagram, we can see that z increases as we increase β. This behavior can be explained as: on increasing β, the consumption rate of zooplankton species on NTP decreases, which increases p_1. As zooplankton is entirely dependent on NTP for its survival, this rise in p_1 finally leads to an increment in z. Also, this increased value of p_1 boosts the pressure of competition over TPP for the available resources, which results in a partial decrement in p_2 which is also evident from this Fig. 3.7(c).

Next bifurcation diagram in Fig. 3.8, presents the process of Hopf-bifurcation as well as transcritical bifurcation, when we use death rate of zooplankton (δ_0) as the control parameter. Figs. 3.8(a), 3.8(b) and 3.8(c) correspond to bifurcation diagrams for p_1, p_2 and z, respectively. For $\delta_0 < \delta_0^{hf}$ non-delayed system remains unstable and at $\delta_0 = \delta_0^{hf}$, system becomes stable in the vicinity of E^*. For $\delta_0^{hf} < \delta_0 < \delta_0^{tc}$, E^* and E_3 remain stable and unstable, respectively and

at $\delta_0 = \delta_0^{tc}$, both equilibria exchange their stability via transcritical bifurcation.

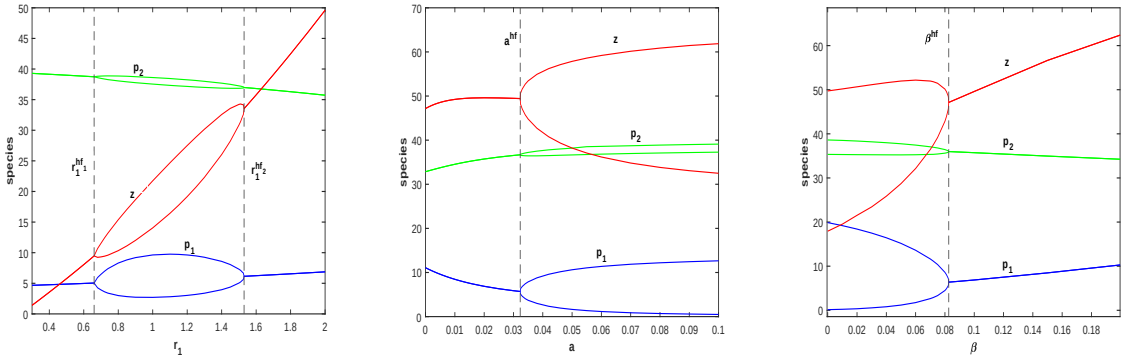

(a) **(b)** **(c)**

Fig. 3.7: Bifurcation diagrams using r_1, a and β as control parameters in Figs. (a), (b) and (c), respectively, keeping all other parameters fixed as given by (3.43).

3.5.2 For delayed model

Now we analyse the behavior of delayed system (3.2) in the neighborhood of interior equilibrium and use the set of parameters given in (3.43) to provide suitable examples for validating the results proved in Section 3.4. As E^* is independent of both delays so E^* will remain same in all the following cases as given in Table 3.1.

Case II: Using theoretical part of case II from Section 3.4 and after doing some calculations, we get: $\omega_1 = 0.2513$, $\tau_{1_0} = 0.7117$ and $\left[\frac{d[Re(\lambda(\tau_1))]}{d\tau_1}\right] = 0.0286 > 0$. Therefore from Theorem 3.4.1 it follows that system (3.2) suffers Hopf-bifurcation at $\tau_1 = \tau_{1_0} = 0.7117$. Moreover the delayed system is asymptotically stable for $\tau_1 < \tau_{1_0}$ and becomes unstable for $\tau_1 > \tau_{1_0}$, which further gives rise to a stable limit cycle. In Fig. 3.9(a), we have presented the time-series plot for all three species and from which we can observe that after oscillating for a finite time, species settle down to their corresponding stationary values for $\tau_1 = 0.3 < \tau_{1_0}$. The same behavior is reflected by the 3D-phase portrait diagram in Fig. 3.9(b). In Fig. 3.9(c), we present time-series plot in which we can see that solution curves oscillate around E^* and converge to a stable limit cycle. The 3D-phase portrait diagram (Fig. 3.9(d)) in which two solutions (red and blue) starting from outside and inside respectively tend to the limit cycle which exhibits unstable nature of delayed system around E^* and stable nature of this periodic orbit for $\tau_1 = 1 > \tau_{1_0}$. We have also plotted bifurcation diagrams (Figs. 3.9(e), 3.9(f), 3.9(g)) for p_1, p_2 and z species, taking τ_1 as the varying parameter.

a	p_1^*	p_2^*	z^*
0.001	10.7492	33.0397	47.5264
0.005	9.5972	33.7491	48.5570
0.01	8.4543	34.5324	49.2391
0.02	6.8696	35.1880	49.5288
0.0205	6.8086	35.7749	49.6053
0.03	5.8725	36.5313	49.4773
0.04	5.2089	37.0858	49.2339
0.06	4.3995	37.7801	48.7608
0.08	3.9319	38.1894	48.3972

Table 3.3: Numerical values of p_1^*, p_2^* and z^* for different values of a, with remaining parameters from (3.43).

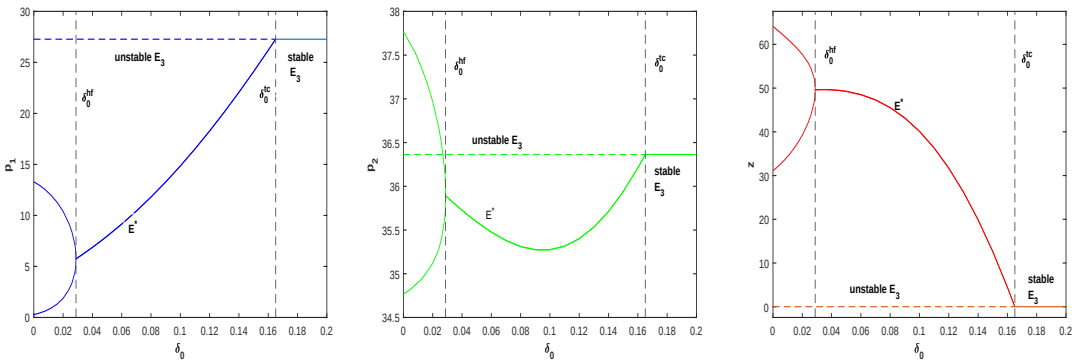

(a) **(b)** **(c)**

Fig. 3.8: Figs. (a), (b) and (c) depicts Hopf-bifurcation followed by transcritical bifurcation for NTP, TPP and zooplankton, using δ_0 as the bifurcation parameter for all parameters from (3.43).

Case III: In this case, the delayed system is stable around E^* for $\tau_2 < \tau_{2_0} = 4.6359$, which is depicted in Fig. 3.10(a) for $\tau_2 = 3$. Then the system suffers Hopf-bifurcation to become unstable at $\tau_2 = \tau_{2_0}$. This unstable nature of system (3.2) about E^* is shown by a stable limit cycle in Fig. 3.10(b) for $\tau_2 = 5$. In this figure, we have two solution trajectories, which are stared from outside (red coloured) and inside (blue coloured) the limit cycle. Both the solutions converge to limit cycle, which shows the stable nature of this periodic solution. Next, as we increase τ_2, system switches its stability at $\tau_2 = 20.6438,\ 26.6692,\ 48.2304$ and 48.7086. This whole process of switching can be seen through the bifurcation diagram for species p_1, presented in Fig. 3.11(b). When the delayed system becomes unstable at $\tau_2 = 26.6692$, on a further increase of delay, the system goes through period-doubling, and we have a stable limit cycle of period-2, which is illustrated in Fig. 3.10(c) for $\tau_2 = 35$.

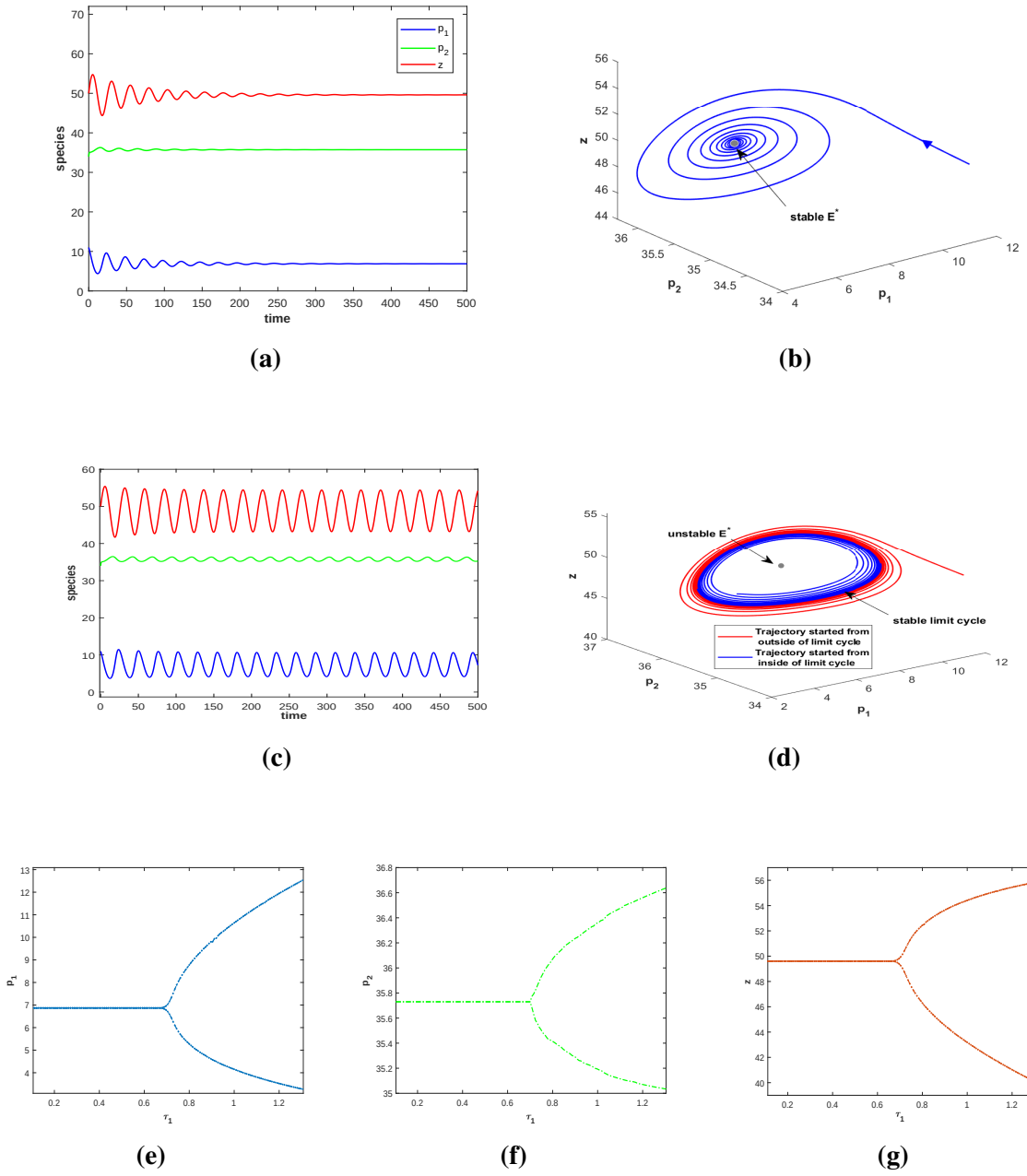

Fig. 3.9: Keeping $\tau_2 = 0$ and parameters form (3.43), for $\tau_1 = 0.3 < \tau_{1_0}$, time-series and phase portrait diagram for system (3.2) are drawn in Figs. (a) and (b), respectively. Similarly unstable nature of the delayed system is portrayed in Figs. (c) and (d) for $\tau_1 = 1 > \tau_{1_0}$. Figs. (e), (f) and (g) represent bifurcation diagrams for NTP, TPP and zooplankton, respectively, using τ_1 as the control parameter.

From the bifurcation diagram (Fig. 3.11(b)), we can see that after becoming unstable (at $\tau_2 = 48.7026$) from stable (at $\tau_2 = 48.2304$), system remains chaotic for $53.4458 < \tau_2 < 61.6255$, until it again becomes periodic with period-3. For an example of this, we have presented a stable limit cycle of period-3 in Fig. 3.10(d) for $\tau_2 = 65$. The further increase in delay pushes the system into a highly chaotic regime. To manifest the delayed system's chaotic

nature, we have given a time-series graph and a phase portrait diagram for $\tau_2 = 100$ in Figs. 3.10(e) and 3.10(f), respectively.

As sensitivity to initial conditions is an important indication of chaos in a dynamical system. Therefore for exhibiting this dependence on initial conditions, in Fig. 3.11(a), time-series plots with two different starting points (5,35,45) and (5.03,35.03,45.03) respectively are drawn for all three species. From these time-series graphs, we can observe that a small change in initial points has significantly changed the solution trajectories, illustrating the delayed system's chaotic nature. We have also drawn the maximum Lyapunov exponent for the delayed system on varying τ_2 in Fig. 3.11(c). The positiveness of maximum Lyapunov exponent confirms the chaotic nature of the delayed system. We have also sketched Poincare map in the p_1p_2-plane for the solution of delayed system corresponding to $\tau_2 = 5,\ 35,\ 65$ and 100 in Figs. 3.12(a), 3.12(b), 3.12(c) and 3.12(d), respectively. The first three diagrams in Fig. 3.12 represent stable limit cycles of period-1,2,3, whereas the last one reflects the delayed system's chaotic nature.

Remark 3.5.1. *Fig. 3.13 shows that the chaos which emerges for high values of toxic liberation delay can be controlled by increasing the value of parameter a. In Fig. 3.13(a), we have a chaotic attractor for $a = 0.02$ and when we increase a, this chaotic attractor switches to a stable limit cycle (for $a = 0.1$ in Fig. 3.13(b)). Thus increasing the inhibitory effect of toxic-phytoplankton against zooplankton can help to control the chaos.*

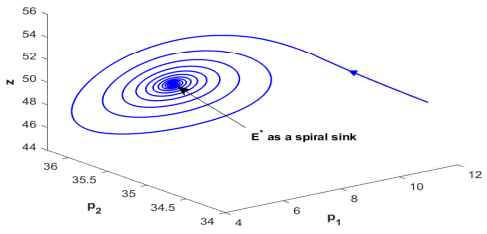

(a)

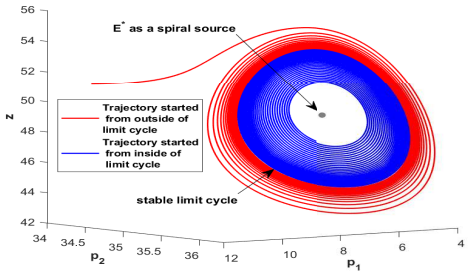

(b)

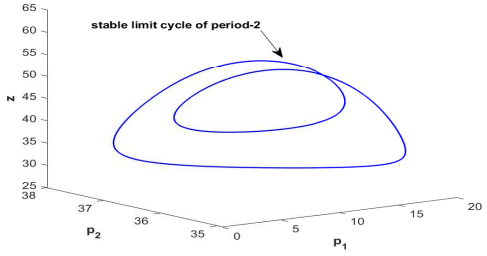

(c)

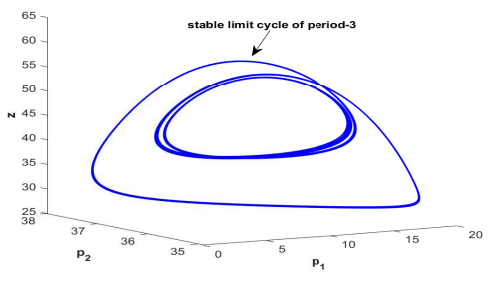

(d)

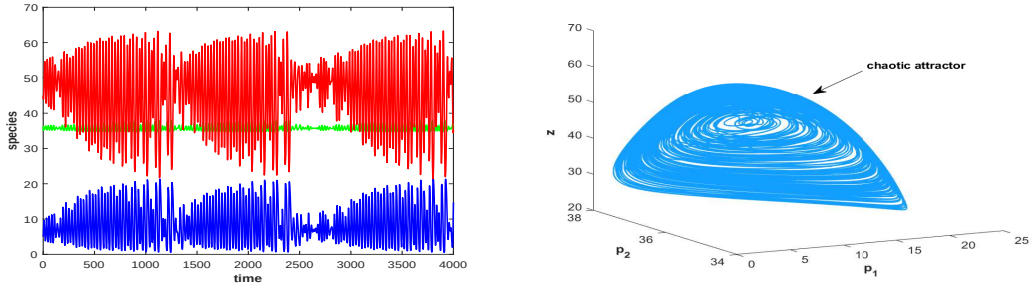

(e) **(f)**

Fig. 3.10: In Figs. (a) and (b), we have depicted stable equilibrium and a stable limit cycle for $\tau_2 = 3$ and $\tau_2 = 5$, respectively. Figs. (c) and (d) depict stable limit cycles of period-2 and period-3 for $\tau_2 = 35$ and $\tau_2 = 65$, respectively. Whereas, in Figs. (e) and (f), we have shown the chaotic nature of the delayed system for $\tau_2 = 100$ using time-series graph and phase portrait diagram. In all these sub-figures $\tau_1 = 0$, with parameters from (3.43).

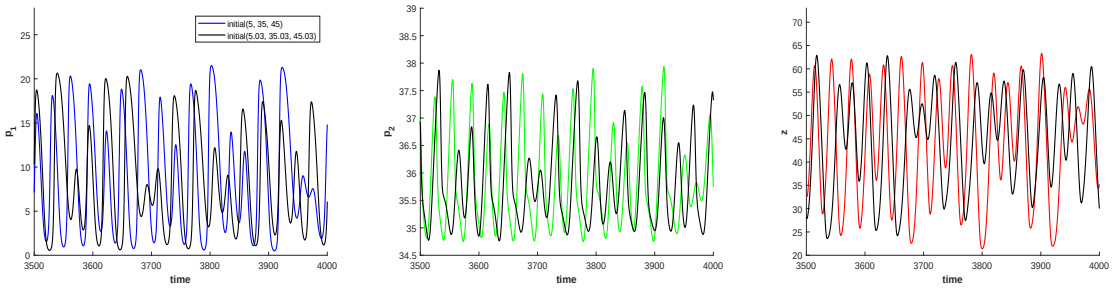

(a)

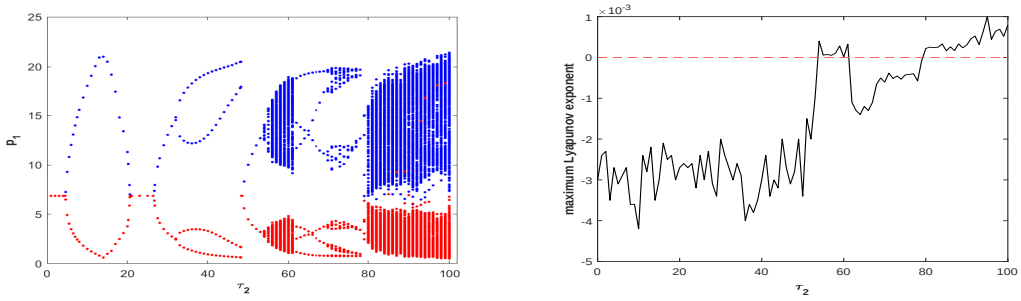

(b) **(c)**

Fig. 3.11: Fig. (a) depicts the sensitivity of solutions for two different initial conditions for $\tau_1 = 0$ and $\tau_2 = 100$. In Fig. (b), a bifurcation diagram for species p_1 is given, whereas Fig. (c) describes the evaluation of maximum Lyapunov exponent for all parameters from (3.43).

Case IV: In this case τ_1 is taken as parameter and we fix $\tau_2 = 3 \in (0, \tau_{2_0})$. From simulation we get: $\tau_1^* = 0.3553$. Therefore the delayed system undergoes Hopf-bifurcation at $\tau_1 = \tau_1^* = 0.3553$, keeping $\tau_2 = 3 \in (0, \tau_{2_0})$. For $\tau_1 = 0.1 < \tau_1^*$, stable nature of delayed system is depicted

in Fig. 3.14(a). Whereas the presence of limit cycle attractor (Fig. 3.14(b)) around E^* for $\tau_1 = 0.6 > \tau_1^*$ shows unstable nature of this system. For parametric values given in (3.43), we have $\mu_2 = 0.0997 > 0$, $\beta = -0.0067 < 0$ and $T_2 = 0.0815 > 0$. Thus from Theorem 3.4.4, the Hopf-bifurcation is supercritical, the bifurcated periodic solutions are stable, and solution's period increases as we increase τ_1.

In Fig. 3.15, we have plotted a two parameter bifurcation diagram in the $\tau_1\tau_2$ plane. Stable and unstable regions are filled with different colours as shown in the figure.

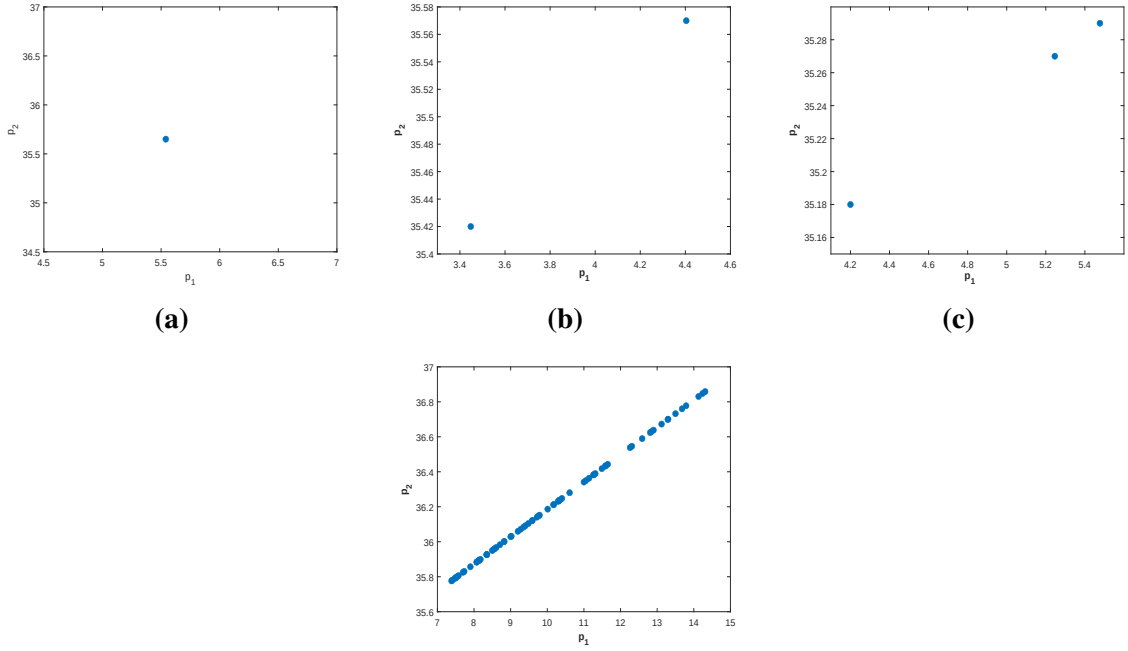

(a) **(b)** **(c)**

(d)

Fig. 3.12: Figs. (a), (b), (c) and (d) represent Poincare maps for the delayed system in the p_1p_2-plane for $\tau_2 = 5$, $\tau_2 = 35$, $\tau_2 = 65$ and $\tau_2 = 100$ respectively keeping $\tau_1 = 0$ with all other parameters from (3.43).

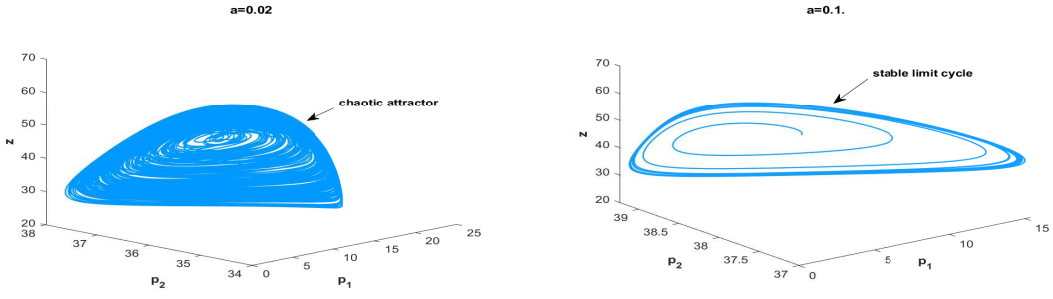

(a) **(b)**

Fig. 3.13: Phase space diagram for $\tau_1 = 0$, $\tau_2 = 100$ with $a = 0.02$ (Fig. (a)) and $a = 0.1$ (Fig. (b)) with all other parameters from (3.43).

(a) **(b)**

Fig. 3.14: Stable (Fig. (a)) and unstable (Fig. (b)) nature of delayed system (3.2) around E^* for $\tau_1 = 0.1 < \tau_1^*$ and $\tau_1 = 0.6 > \tau_1^*$ respectively, keeping $\tau_2 = 3 \in (0, \tau_{2_0})$ for all parameters from (3.43).

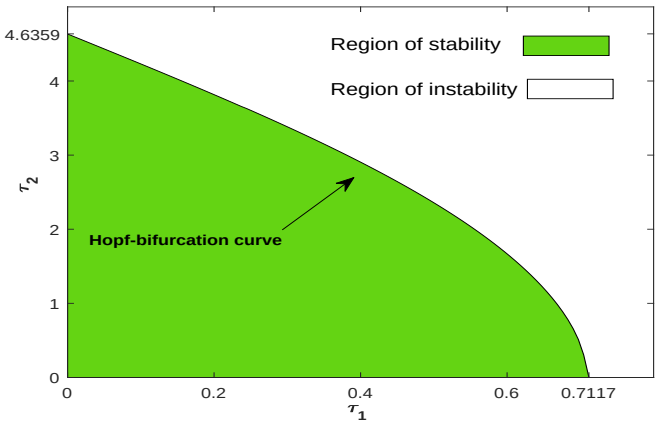

Fig. 3.15: Bifurcation diagram of interior equilibrium E^* for the delayed system in the $\tau_1\tau_2$ plane. Both the stable and unstable regions are separated by the Hopf-bifurcation curve keeping parameters from (3.43).

3.6 Discussion and conclusion

Banerjee and Venturino [101] worked on a phytoplankton-zooplankton system by splitting phytoplankton into two populations, namely, non-toxic phytoplankton (NTP) and toxic producing phytoplankton (TPP) using modified Holling type IV response. Now extending this work, we proposed a phytoplankton-zooplankton system by dividing phytoplankton into these two above-stated classes. We pick generalised Holling type IV and Beddington–DeAngelis responses to deal with zooplankton's interactions with TPP and NTP, respectively. Here, Holling type IV response is used to reflect the defense technique of TPP against zooplankton, and to outline the zooplankton's interference for its favourite food (NTP), we use Beddington–DeAngelis response. We have also incorporated two delays, accountable for time lags in reproducing

progeny and producing the toxic chemicals, correspondingly. Both the phytoplanktons are assumed to grow logistically in the absence of any inter-species competition and zooplankton. Firstly, the proposed model's well-posedness is established by proving the existence, uniqueness, positivity, and boundedness of its solution. Next, we examine the feasibility of various equilibria under certain conditions, and after that, local and global stability analysis is done around these equilibrium points. We also prove the persistence of the non-delayed model by using the standard results for persistence given by Freedman and Waltman [102].

We observe that the non-delayed system is globally stable around the interior equilibrium for a set of parameters mentioned in the text. Non-delayed model (3.1) also experiences Hopf-bifurcation and transcritical bifurcation for several parameters. The system switches its stability twice in respect of r_1 via Hopf-bifurcation. The parameter a shows a fascinating behavior when we vary it: an initial rise in its value encourages zooplankton species' growth due to less ingestion of the toxic food. This rise in zooplankton's population leads to a fall in NTP population because of its increased grazing pressure on NTP. Thus the further increase in a causes a reduction in the zooplankton population as it is completely depend upon NTP for its living. This whole trend is observable from Table 3.3. Therefore, we can say that increasing this parameter magnifies TPP population due to the expected nature of Holling type IV response but increasing it up to a limit ($a < 0.0206$) can boost zooplankton's growth as well. The death rate of zooplankton species helps to control the periodic oscillations by making the system asymptotically stable around E^*. The further increase in δ_0 causes the extinction of zooplankton species and the disappearance of E^* with changing E_3 to a stable equilibrium via a transcritical bifurcation. The effect of both a and δ_0 is depicted in a two-parametric bifurcation diagram in the $a\delta_0$-plane in Fig. 3.5(c). Predator's interference parameter β also plays a crucial role in the dynamics of the system. We observe that increment in this interference helps zooplankton species to amplify their population density instead of abating it, and this change in β also helps to control the periodic oscillations.

Further, we investigate the system's kinetics by adding two discrete delays; one is τ_1, which accounts for gestation delay, and the second one is τ_2, which measures the time lag due to time taken by TPP's cells for getting mature enough to release toxic chemicals. Our main concern is to review the effects of these delays on the system's stability around E^*. We studied all the possible cases for both these delays and noticed that both the delays are capable of destabilising the system by producing periodic solutions via Hopf-bifurcation. From the numerical simulation, we perceive that increasing the delay τ_2 can put delayed system into a chaotic region. Raising this delay also helps to control the chaos and again can make the system chaotic on further increment. In this situation, the delayed system's solutions become very sensitive to initial conditions as depicted in Fig. 3.11(a). For confirmation of chaos, we have also evaluated maximum Lyapunov exponent and drew Poincare map (or first return map) in Figs. 3.11(c) and

3.12(d) respectively. Further, we observe that this chaotic behavior can be controlled by increasing the inhibitory effect of TPP as demonstrated in Fig. 3.13. From the above discussion, we can conclude that dividing phytoplankton into groups of NTP and TPP can yield vibrant dynamics for the plankton systems. The crucial roles played by parameters a and β also represent the advantage of chosen functional responses, and incorporation of delays is also making the system's dynamics more richer. Thus, the proposed work can help ecologists to understand the progress of plankton systems more broadly and practically than the existing studies.

Chapter 4

A phytoplankton-zooplankton-fish model with chaos control: In the presence of fear effect and an additional food[1]

4.1 Introduction

The fish population in a PZF (phytoplankton-zooplankton-fish) system can potentially influence zooplankton species by causing fear of being eaten. Literature survey suggests that many planktonic rotifers, copepods, and cladocerans can notice the presence of planktivorous fish through chemical essences released by either of these fishes or by wounded or consumed prey [113, 114], and this fright can affect their lifestyle. There are many field experiments conducted by various researchers recommending the inclusion of cost of fear in a prey-predator model [27, 68, 115]. Thus, incorporating this fear factor into a model is crucial to study its kinetics more practically and realistically. Inspired by this, Wang *et al.* [30] formulated a predator-prey model involving this fear affecting the prey reproduction. They noticed that high levels of fear can help to stabilize the system by eliminating the periodic oscillations, and enhancing this fear can also alter the direction of Hopf bifurcation which means that fear can cause multi-stability in this interaction. Pandey *et al.* [64] worked on a tri-trophic food-chain system in which growth of basal prey is curtailed due to fear of middle predator and growth of intermediate predator is suppressed by the fear of the top predator. In their numerical work, they observed that the fear in primary prey can yield bistability by generating an unstable limit cycle that can further be replaced by a stable equilibrium or a stable limit cycle by introducing fear in the middle predator. They also observed that chaos in the system can also be controlled through fear. Recently, Kaur *et al.* [31] studied a PZF-system with fear of fish on zooplankton and zooplankton refuge in which they perceived that the fear of top predator does not affect prey too much but harms

[1] A considerable part of this chapter is published in *Chaos*, 32, 013114 (2022).

fish population. They also proposed different intervals of fear and zooplankton refuge for co-existence and sustainability of interior equilibrium. For more interesting results related to the fear effect, one can refer to the papers [116, 117].

Srinivasu *et al.* [37] studied the impacts of providing additional food on the system's dynamics regarding biological pest control. They found that on the variation of quantity and quality of this food, they could not only regulate the prey but also could control and wipe out predator population. They also remarked that oscillations in the system could be eliminated or produced if they are not present, by the supply of additional food. Prasad *et al.* [118] dealt with a prey-predator model, predator having additional food and mutual interference, and they integrated this predator's interference in the corresponding system with the help of Beddington–DeAngelis type response [57]. They observed that prey's extinction can be prevented through distraction caused by high mutual interference among the predators and access to high quantity and quality of secondary food. Following this, Sahoo and Poria [119] investigated a three-dimensional prey-predator system with top predator along with the availability of additional food. They showed the existence of limit point, Hopf point, and branch point for the suitable provision of supplemental food. In their model, they presented several one and two parametric bifurcation diagrams, and also controlled the chaotic dynamics of the system with the supply of additional food. We can also refer to some papers [36, 120] for more information related to this aspect of feed provided to predator population.

Bifurcation is defined as a change in the qualitative nature of a dynamical system as a result of a change in the system's parameters. Bifurcations can be classified into two types: local and global. Local type bifurcations include Hopf bifurcation, saddle-node, and transcritical, whereas global bifurcations include homoclinic, hetroclinic, and Bogdanov-Takens [55, 24]. Hopf bifurcation is a very basic and significant type of bifurcation that can occurs in both non-delayed and delayed models of biological and physical systems. A detailed introduction to Hopf bifurcation and its applications is provided by Marsden and McCracken [121]. In a dynamical system, the appearance of chaos is a very appealing event for ecologists as it gives rise to management challenges related to species because it may result in oscillations that can cause extinction or an abrupt increase of a species. Basic stuff related to chaos like the meaning of chaos, chaotic attractor, Lyapunov exponents, characteristics of chaos, approaches to detect chaos in ecological systems are well explained by Hastings *et al.* [25]. Meng *et al.* [122] examined the effect of periodicity and seasonality on a PZ-system in which complex behaviors, for example, chaos, quasi-periodic dynamics, intermittent chaos, and periodic resonance, are found. They observed that the addition of periodic forcing to the original system, which is globally stable, can make it chaotic. Jana [26] worked on a discrete prey-predator system with prey refuge, in which a combination of the intrinsic growth rate of prey species and prey refuge exhibit complex and exciting qualities. He confirmed chaos with several techniques: calculation

of Lyapunov exponent, recurrence plot and power spectral density, and fractal dimension of the map. Controlling chaos in a kinetical system is again a crucial topic of interest; several methods to control the chaos, in which a chaotic attractor is converted into a stationary point or a limit cycle, are discussed in the available literature [123, 124, 125].

The predation scheme of prey has a significant impact on the dynamics of a prey-predator relationship. There are several kinds of responses, prey-dependent: Holling type I, II, III, IV, ratio-dependent: Leslie-Gower, Beddington-Deangelis, Crowley-Martain, each of which has a different biological and mathematical implications. Holling type II response is one the basic responses, in which response reaches to a stage of saturation because of predator's handling time for prey species [55]. In marine habitats, sometimes there is a massive growth in phytoplankton species leading to the formation of harmful algal blooms, which results in the emission of toxic chemicals against zooplankton [126]. Thus zooplankton avoids this heavily grown phytoplankton, and this kind of special relationship between these two populations can be handled using Holling type IV response, which also represents the group defense technique of prey population against predator population [101, 127].

In this chapter, we intend to work on a three-dimensional PZF-system, in which PZ and ZF interactions are tackled through modified Holling type IV and Holling type II responses, respectively. We also incorporate the terms related to fear induced in zooplankton by fish, and additional food provided to fish. The structure of this chapter is given as: in Section 4.2, we have explained the complete formulation of the mathematical model. Section 4.3 is entirely devoted to the proposed model's dynamical analysis, which comprises well-posedness, equilibrium analysis, stability evaluation, and bifurcation assessment related to the model. Next, in Section 4.4, we have done an extensive numerical simulation to delineate some interesting findings associated with our system. Finally, Section 4.5 summarises the results of the proposed work.

4.2 Establishment of model

We consider an aquatic system to study the kinetical interactions of a 3D model consisting of three populations: phytoplankton, zooplankton, and planktivorous fish (i.e., PZF-system) in the presence of fear effect and additional food. Let P, Z and F be the population densities of phytoplankton, zooplankton, and planktivorous fish species, respectively at any time t. Formulation of the mathematical model, which will help us to understand the dynamics of this $PZF-$ system, is based upon the following assumptions:

1. Both the species: phytoplankton and zooplankton are assumed to be grow logistically in the absence of each other and fish population. Let r_1, r_2 be intrinsic growth rates and

k_1, k_2 are carrying capacities of the habitat for phytoplankton and zooplankton species, respectively. Here, $r_2 = r - d_1$ and $k_2 = \frac{r-d_1}{d_2}$, where r, d_1 and d_2 are birth rate, natural mortality rate and coefficient of intraspecific interference for zooplankton species. Thus we have

$$\frac{dP}{dt} = r_1 P\left(1 - \frac{P}{k_1}\right), \ \frac{dZ}{dt} = rZ - d_1 Z - d_2 Z^2.$$

2. The increasing density of phytoplankton species may lead to the formation of harmful algal blooms, which some-times liberate toxic chemicals. We assume that zooplankton species avoid these highly dense phytoplankton, so the interaction between phytoplankton and zooplankton is dealt with modified Holling type IV response [101, 55], which is given by $f_1(P) = \frac{P}{\alpha P^2 + \beta}$. Here, α gives the inhibitory effect of phytoplankton against zooplankton, and β is a half saturation constant. Such response serves the motive of this desired avoidance, and is also recognized as a group defence mechanism of prey against predator. Let a_1 be the predation rate of zooplankton over phytoplankton. As the consumed biomass cannot be converted completely into zooplankton, thus we take $b_1 = c_1 a_1$, where $c_1 \in (0,1)$ is the conversion efficiency of zooplankton over phytoplankton and b_1 is the net gain of zooplankton over phytoplankton (here $b_1 < a_1$). Therefore, the dynamics of phytoplankton-zooplankton system can be governed by the following system of ordinary differential equations

$$\frac{dP}{dt} = r_1 P\left(1 - \frac{P}{k_1}\right) - \frac{a_1 PZ}{\alpha P^2 + \beta}, \ \frac{dZ}{dt} = rZ - d_1 Z - d_2 Z^2 + \frac{b_1 PZ}{\alpha P^2 + \beta}.$$

3. Fish can induce fear in zooplankton species, due to which sometimes zooplankton have to shift their locality to such a place which may not suitably support their livelihood and can reduce the birth rate of zooplankton species [114, 128]. We assume that due to this induced fear, the birth rate of zooplankton species is diminished by the factor $g(F,k) = \frac{1}{1+kF}$ (proposed by Wang *et al.* [30]), where k denotes the level of fear in zooplankton population. This function $g(F,k)$ has the following properties [30, 129]:

   - $g(0,k) = g(F,0) = 1$,
   - $\lim_{F\to\infty} g(F,k) = \lim_{k\to\infty} g(F,k) = 0$,
   - $\frac{\partial g}{\partial F} < 0$, $\frac{\partial g}{\partial k} < 0$.

   We assume that fish predates zooplankton via Holling type II response, $f_2(F) = \frac{a_2 F}{\gamma + F}$, where a_2 and γ stands for consumption rate of fish over zooplanktoon and half saturation

constant, respectively. Therefore, we can have

$$\frac{dZ}{dt} = \frac{rZ}{1+kF} - d_1 Z - d_2 Z^2 + \frac{b_1 PZ}{\alpha P^2 + \beta} - \frac{a_2 ZF}{\gamma + Z}, \frac{dF}{dt} = \frac{b_2 ZF}{\gamma + Z} - mF,$$

where $b_2 = c_2 a_2$, is net gain of fish over zooplankton, $c_2 \in (0,1)$ is conversion efficiency of fish species over zooplankton species and m stands for mortality rate of fish population.

4. To reduce the grazing pressure of fish over zooplankton, we provide additional food to the fish population with its biomass density A. Let h_1 and h_2 are the handling time of top predator fish per unit of zooplankton and per unit quantity of additional food, respectively. Now, $\delta = \frac{h_2}{h_1}$ denotes the quality of this additional food, so if $\delta > 1$ then additional food is of superior quality as compared to zooplankton species. If e_1 and e_2 are the abilities of top predator to detect intermediate and additional food, respectively then we define $\eta = \frac{e_2}{e_1}$, and the term ηA denotes the effectual additional food biomass [37]. For more details about additional food, one can refer to different papers [118, 119]. Now, we incorporate this additional food in our model to get

$$\frac{dZ}{dt} = \frac{rZ}{1+kF} - d_1 Z - d_2 Z^2 + \frac{b_1 PZ}{\alpha P^2 + \beta} - \frac{a_2 ZF}{\gamma + \delta\eta A + Z}, \frac{dF}{dt} = \frac{b_2 (Z+\eta A)F}{\gamma + \delta\eta A + Z} - mF.$$

Thus in this food chain model, phytoplankton, zooplankton, and fish serve as prey, middle predator, and top predator, respectively. The model which we plan to study is given by:

$$\begin{aligned}
\frac{dP}{dt} &= r_1 P\left(1 - \frac{P}{k_1}\right) - \frac{a_1 PZ}{\alpha P^2 + \beta} =: G_1(P,Z,F), \\
\frac{dZ}{dt} &= \frac{rZ}{1+kF} - d_1 Z - d_2 Z^2 + \frac{b_1 PZ}{\alpha P^2 + \beta} - \frac{a_2 ZF}{\gamma + \delta\eta A + Z} =: G_2(P,Z,F) \\
\frac{dF}{dt} &= \frac{b_2 (Z+\eta A)F}{\gamma + \delta\eta A + Z} - mF =: G_3(P,Z,F),
\end{aligned} \tag{4.1}$$

for biological feasibility, all parameters in (4.1) are taken to be positive, and $P(0) > 0, Z(0) > 0, F(0) > 0$, whereas the significance and default values of parameters are provided in Table 4.1.

Remark 4.2.1. *For survivability of zooplankton, we assume that its birth rate is always greater than its death rate i.e., $r > d_1$, throughout this chapter.*

4.3 Dynamical evaluation

4.3.1 Positivity and boundedness

As we are dealing with a biological system, so solutions of our model (4.1) should be positive and bounded. The boundedness of solutions signifies that none of the populations grows indefinitely. The character of boundedness is an essential part of well behavior of the system due to confined resources.

From (4.1), (G_1, G_2, G_3) is Lipschitz continuous for any bounded domain of R^3_+, which implies that for any set of positive initial conditions, system (4.1) has a unique solution on every restricted subset of R^3_+. By the method of successive approximation, model (4.1) can be rewritten as:
$P(t) = P(0)\exp(G_{11})$, $Z(t) = Z(0)\exp(G_{22})$ and $F(t) = F(0)\exp(G_{33})$,
where

$$G_{11} = \int_0^t \left\{ r_1\left(1 - \frac{P(s)}{k_1}\right) - \frac{a_1 Z(s)}{\alpha P^2(s) + \beta} \right\} ds,$$
$$G_{22} = \int_0^t \left\{ \frac{r}{1 + kF(s)} - d_1 - d_2 Z(s) + \frac{b_1 P(s)}{\alpha P^2(s) + \beta} - \frac{a_2 F(s)}{\gamma + \delta\eta A + Z(s)} \right\} ds,$$
$$G_{33} = \int_0^t \left\{ \frac{b_2(Z(s) + \eta A)}{\gamma + \delta\eta A + Z(s)} - m \right\} ds.$$

Therefore, any solution with positive initial conditions will remain inside the positive octant of $PZF-$space hereafter.

Theorem 4.3.1. *All the solutions of model (4.1) which initiates in R^3_+ are uniformly bounded. The whole dynamics of the system proceeds in a set which is compact and invariant with respect to model (4.1), and is defined as: $\sum = \{(P,Z,F) \in R^3_+ : 0 \le P \le k_1,\ Z + \frac{a_2 F}{b_2} \le \frac{f_{max}}{\theta}\}$, where $f_{max} = \frac{1}{4d_2}(r + \frac{b_1}{2\sqrt{\alpha\beta}})^2$ and $\theta = min\{d_1, m - \frac{b_2\eta A}{\gamma+\delta\eta A}\}$, where $m > \frac{b_2\eta A}{\gamma+\delta\eta A}$.*

Proof. As $\frac{dP}{dt} = r_1 P\left(1 - \frac{P}{k_1}\right) - \frac{a_1 PZ}{\alpha P^2+\beta}$ which implies $\frac{dP}{dt} \le r_1 P\left(1 - \frac{P}{k_1}\right)$, thus $\limsup_{t\to\infty} P(t) \le k_1$.
Let $W = Z + \frac{a_2}{b_2}F$, then $\frac{dW}{dt} = \frac{dZ}{dt} + \frac{a_2}{b_2}\frac{dF}{dt}$. Using (4.1), we get
$\frac{dW}{dt} = \frac{rZ}{1+kF} - d_1 Z - d_2 Z^2 + \frac{b_1 PZ}{\alpha P^2+\beta} + \frac{a_2\eta AF}{\gamma+\delta\eta A+Z} - \frac{ma_2 F}{b_2}$.
As $f_1(P) = \frac{P}{\alpha P^2+\beta}$ has global maxima at $P = \sqrt{\frac{\beta}{\alpha}}$ such that $f_1(\sqrt{\frac{\beta}{\alpha}}) = \frac{1}{2\sqrt{\alpha\beta}}$. Using this property of f_1, we have
$\frac{dW}{dt} \le (r + \frac{b_1}{2\sqrt{\alpha\beta}})Z - d_2 Z^2 - d_1 Z - \frac{a_2}{b_2}(m - \frac{b_2\eta A}{\gamma+\delta\eta A})F$.
Now, define $f = (r + \frac{b_1}{2\sqrt{\alpha\beta}})Z - d_2 Z^2$, then f attains its maxima at $Z = \frac{1}{2d_2}(r + \frac{b_1}{2\sqrt{\alpha\beta}})$ such that

$f\left(\frac{1}{2d_2}(r+\frac{b_1}{2\sqrt{\alpha\beta}})\right) = f_{max} = \frac{1}{4d_2}(r+\frac{b_1}{2\sqrt{\alpha\beta}})^2$.
Thus, $\frac{dW}{dt} \leq f_{max} - \theta(Z+\frac{a_2}{b_2}F(t)) = f_{max} - \theta W$, where $\theta = min\{d_1, m - \frac{b_2\eta A}{\gamma+\delta\eta A}\}$.
Therefore, $\limsup_{t\to\infty} W(t) = \limsup_{t\to\infty}(Z(t)+\frac{a_2}{b_2}F(t)) \leq \frac{f_{max}}{\theta}$.
Hence, all the populations involved in the system continue to be bounded for the whole future time. □

Remark 4.3.1. *Proof of Theorem 4.3.1 shows that property of* $f_1(p) = \frac{P}{\alpha P^2+\beta}$, *to attain its global maxima i.e., group defence mechanism of phytoplankton against zooplankton helps to keep the solution of system (4.1) uniformly bounded.*

Parameters	Significance	Values	References
r_1	Intrinsic growth rate of phytoplankton	1.5	[130]–[131]
k_1	Carrying capacity of habitat for phytoplankton	40	[130]–[132]
a_1	Predation rate of zooplankton over phytoplankton	0.9	[34]
α	Inhibitory effect of phytoplankton against zooplankton	0.03	[130]
β	Half-saturation constant during the intake of phytoplankton by zooplankton	11.5	[130]
r	Birth rate of zooplankton	1.1	assumed
k	Level of fear induced in zooplankton by fish	1	[117]
d_1	Natural mortality rate of zooplankton	0.05	[130]
d_2	Measure of intraspecific interference in zooplankton species	0.02	[133]
b_1	Net gain of zooplankton over phytoplankton	0.8	[34]
a_2	Predation rate of fish over zooplankton	0.5	[130]
A	Additional food biomass density	0.7	assumed
η	Ratio of abilities of fish to detect additional food and zooplankton	0.3	assumed
δ	Additional food's quality	1	[119]
b_2	Net gain of fish over zooplankton	0.4	[130]
m	Natural mortality rate of fish	0.08	[130]
γ	Half-saturation constant during the intake of zooplankton by fish	25	[130]–[54]

Table 4.1: Biological descriptions and default values of the parameters involved in model (4.1).

4.3.2 Equilibrium analysis

Model (4.1) has six nonnegative equilibria, written below:

1. The three equilibria: zero equilibrium $E_0(0,0,0)$, zooplankton-fish free equilibrium $E_1(k_1,0,0)$, and phytoplankton-fish free equilibrium $E_2(0,\frac{r-d_1}{d_2},0)$ exist trivially.

2. The fish free equilibrium $E_3(P_1,Z_1,0)$ is the solution of the set of equations given below:

$$r_1\left(1-\frac{P_1}{k_1}\right)-\frac{a_1Z_1}{\alpha P_1^2+\beta}=0, \tag{4.2}$$

$$r-d_1-d_2Z_1+\frac{b_1P_1}{\alpha P_1^2+\beta}=0. \tag{4.3}$$

From, (4.2), we have

$$Z_1=\frac{r_1}{a_1k_1}(k_1-P_1)(\alpha P_1^2+\beta)>0. \tag{4.4}$$

Using (4.4) in (4.3), we get a five degree equation:

$$q_{15}P_1^5+q_{14}P_1^4+q_{13}P_1^3+q_{12}P_1^2+q_{11}P_1+q_{10}=0, \tag{4.5}$$

where

$$\begin{aligned}
q_{15}&=d_2r_1\alpha^2 \ \ (>0),\\
q_{14}&=-d_2r_1\alpha^2k_1 \ \ (<0),\\
q_{13}&=2\alpha\beta d_2r_1 \ \ (>0),\\
q_{12}&=k_1\alpha(a_1(r-d_1)-2d_2r_1\beta),\\
q_{11}&=d_2r_1\beta^2+a_1b_1k_1 \ \ (>0),\\
q_{10}&=\beta k_1(a_1(r-d_1)-d_2r_1\beta).
\end{aligned}$$

Thus using Descartes' rule of signs, we have the following possibilities for fish free equilibrium:

- At most two or zero equilibria if $r-d_1>\frac{2d_2r_1\beta}{a_1}$.
- At most four, two or zero equilibria if $\frac{d_2r_1\beta}{a_1}<r-d_1<\frac{2d_2r_1\beta}{a_1}$.
- At most five, three or unique equilibria if $r-d_1<\frac{d_2r_1\beta}{a_1}$.

3. The phytoplankton free equilibrium $E_4(0,Z_2,F_2)$ is the solution of the set of algebraic equations given below:

$$\frac{r}{1+kF_2}-d_1-d_2Z_2-\frac{a_2F_2}{\gamma+\delta\eta A+Z_2}=0, \tag{4.6}$$

$$\frac{b_2(Z_2+\eta A)}{\gamma+\delta\eta A+Z_2}-m=0. \tag{4.7}$$

From (4.7), we get

$$Z_2 = \frac{m\gamma + \eta A(m\delta - b_2)}{b_2 - m}, \tag{4.8}$$

which is positive if $1 < \frac{b_2}{m} < \left(\frac{\gamma}{\eta A} + \delta\right)$ or $0 < \left(\frac{\gamma}{\eta A} + \delta\right) < \frac{b_2}{m} < 1$ holds.
Using (4.8) in (4.6), we have

$$q_{22}F_2^2 + q_{21}F_2 + q_{20} = 0, \tag{4.9}$$

where

$$\begin{aligned} q_{22} &= a_2 k \ \ (>0), \\ q_{21} &= [a_2 + k[d_1 + d_2 Z_2][\gamma + \delta\eta A + Z_2]] \ \ (>0), \\ q_{20} &= -[\gamma + \delta\eta A + Z_2][r - [d_1 + d_2 Z_2]] \ \ (<0). \end{aligned}$$

As $\frac{r-d_1}{d_2}$ (carrying capacity for zooplankton species) $> Z_2$ which means $q_{20} < 0$, thus using Descartes' rule of signs, we can observe (4.9) has a unique positive root. Thus phytoplankton free equilibrium exists (infact uniquely) if the condition $1 < \frac{b_2}{m} < \left(\frac{\gamma}{\eta A} + \delta\right)$ or $0 < \left(\frac{\gamma}{\eta A} + \delta\right) < \frac{b_2}{m} < 1$ holds.

4. The interior equilibrium $E^*(P^*, Z^*, F^*)$ is the solution of set of equations:

$$r_1\left(1 - \frac{P^*}{k_1}\right) - \frac{a_1 Z^*}{\alpha P^{*2} + \beta} = 0, \tag{4.10}$$

$$\frac{r}{1 + kF^*} - d_1 - d_2 Z^* + \frac{b_1 P^*}{\alpha P^{*2} + \beta} - \frac{a_2 F^*}{\gamma + \delta\eta A + Z^*} = 0, \tag{4.11}$$

$$\frac{b_2(Z^* + \eta A)}{\gamma + \delta\eta A + Z^*} - m = 0. \tag{4.12}$$

From (4.12), we get

$$Z^* = \frac{m\gamma + \eta A(m\delta - b_2)}{b_2 - m}, \tag{4.13}$$

which exists positively if

$$1 < \frac{b_2}{m} < \left(\frac{\gamma}{\eta A} + \delta\right) \text{ or } 0 < \left(\frac{\gamma}{\eta A} + \delta\right) < \frac{b_2}{m} < 1 \text{ holds.} \tag{4.14}$$

Now, from (4.10), we get a cubic equation in P^*:

$$f(P^*) = A_3 P^{*3} + A_2 P^{*2} + A_1 P^* + A_0 = 0, \tag{4.15}$$

where

$$\begin{aligned} A_3 &= -r_1\alpha \ \ (<0),\\ A_2 &= r_1k_1\alpha \ \ (>0),\\ A_1 &= -r_1\beta \ \ (<0),\\ A_0 &= k_1[r_1\beta - a_1Z^*]. \end{aligned}$$

In (4.15), $f(P^*)$ can have none, one, two or three positive roots depending upon the following conditions:

- no positive root if $A_0 < 0$ and $\Delta < 0$,
- unique positive root if $A_0 > 0$ and $\Delta < 0$,
- two distinct positive root if $A_0 < 0$ and $\Delta > 0$,
- three distinct positive root if $A_0 > 0$ and $\Delta > 0$,

with $\Delta = 18A_3A_2A_1A_0 - 4A_2^3A_0 + A_2^2A_1^2 - 4A_3A_1^3 - 27A_3^2A_0^2$.
Using these P^* and Z^* in (4.11), we have:

$$B_2F^{*2} + B_1F^* + B_0 = 0, \tag{4.16}$$

where

$$\begin{aligned} B_2 &= a_2k \ \ (>0),\\ B_1 &= (a_2 + k(d_1 + d_2Z^* - C)(\gamma + \delta\eta A + Z^*)),\\ B_0 &= -(\gamma + \delta\eta A + Z^*)(r - d_1 - d_2Z^* + C) \ \ (<0),\\ C &= \frac{b_1P^*}{\alpha P^{*2} + \beta}. \end{aligned}$$

As $\frac{r-d_1}{d_2} > Z^*$ which implies $B_0 < 0$, thus (4.16) has a unique positive root.

Theorem 4.3.2. *System (4.1) has none, one, two or three interior equilibrium(s) accordingly with the following conditions:*

(a) No interior equilibrium if $A_0 < 0$ and $\Delta < 0$.

(b) A unique interior equilibrium if conditions $A_0 > 0$ and $\Delta < 0$ hold with (4.14).

(c) Two distinct interior equilibria if conditions $A_0 < 0$ and $\Delta > 0$ hold with (4.14).

(d) Three distinct interior equilibria if conditions $A_0 > 0$ and $\Delta > 0$ hold with (4.14).

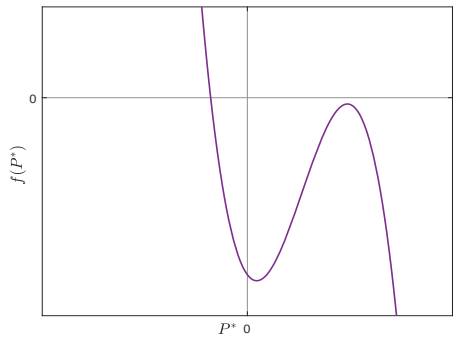

(a) $r_1 = 0.6, A_0 < 0, \Delta < 0$.

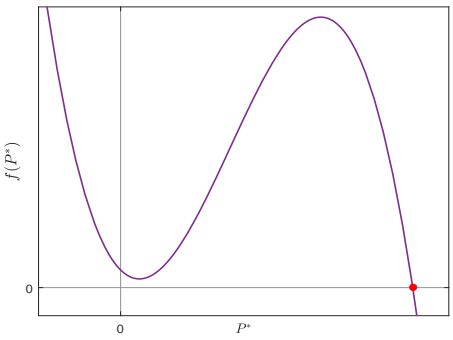

(b) $r_1 = 1.15, A_0 < 0, \Delta < 0$.

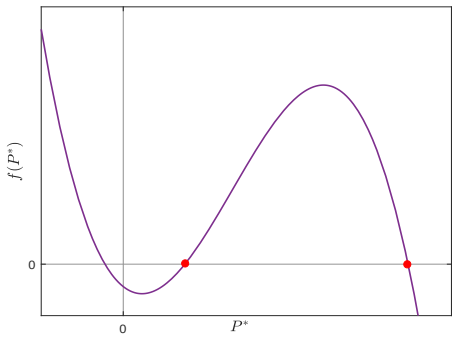

(c) $r_1 = 1, A_0 < 0, \Delta > 0$.

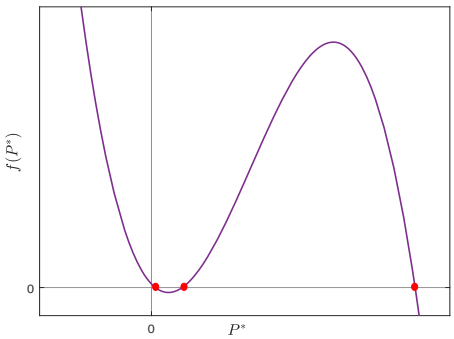

(d) $r_1 = 1.1, A_0 > 0, \Delta > 0$

Fig. 4.1: Different number of roots of $f(P^*)$ given by (4.15), on changing r_1, with $b_1 = 0.4$, $\beta = 5$, and remaining parameters from Table 4.1.

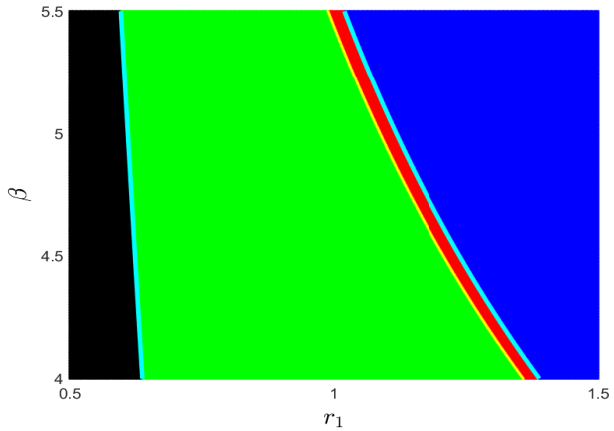

Fig. 4.2: For $b_1 = 0.4$, $r_1 \in [0.5, 1.5]$, $\beta \in [4, 5.5]$ and the other parameters from Table 4.1, black: no interior equilibrium, blue: unique interior equilibrium, green: two distinct interior equilibria, red: three distinct interior equilibria. In this figure, cyan colour represents the curve $\Delta = 0$ whereas yellow colour represents the curve $A_0 = 0$, both these curves demonstrate the transition from one region to another region.

Remark 4.3.2. *Here we draw $P^* - vs - f(P^*)$ graphs (Fig. 4.1), in which we observe that on varying $r_1 = 0.6,\ 1.15,\ 1$ or 1.1, $f(P^*)$ has no, one, two or three positive roots, respectively. These roots are indicated by red dots in these figures, and for the chosen parameters, condition (4.14) is also satisfied. Using Theorem 4.3.2, we have also drawn a bi-parametric existence diagram in $r_1\beta$-plane in Fig. 4.2 representing different number of interior equilibrium point(s) for different combinations of r_1 and β values.*

4.3.3 Stability assessment

Here, we analyse the local and global stability behavior of the system around the desired equilibrium. For local stability analysis around an equilibrium, we determine the conditions under which signs of real parts of the eigenvalues of the Jacobian matrix corresponding to same equilibrium are negative. From Theorem 4.3.1, we have $m > \frac{b_2\eta A}{\gamma+\delta\eta A}$, keeping these, we present the nature of system (4.1) around each equilibrium as follows:

1. The zero equilibrium E_0 is always a saddle point.

2. The equilibrium $E_1(k_1,0,0)$ is always a saddle point with two dimensional stable manifold and one dimensional unstable manifold.

3. The Jacobian matrix for axial equilibrium $E_2(0,\frac{r-d_1}{d_2},0)$ is

$$J|_{E_2} = \begin{bmatrix} e_{211} & 0 & 0 \\ e_{221} & e_{222} & e_{223} \\ 0 & 0 & e_{233} \end{bmatrix},$$

where

$$e_{211} = r_1 - \frac{a_1(r-d_1)}{d_2\beta},\ e_{221} = \frac{b_1(r-d_1)}{d_2\beta},\ e_{222} = -(r-d_1),$$
$$e_{223} = -\frac{rk(r-d_1)}{d_2} - \frac{a_2(r-d_1)}{(r-d_1)+d_2(\gamma+\delta\eta A)}, e_{233} = b_2\left(\frac{(r-d_1)+d_2\eta A}{(r-d_1)+d_2(\gamma+\delta\eta A)}\right) - m.$$

Thus, the eigenvalues of $J|_{E_2}$ are $e_{211} = r_1 - \frac{a_1(r-d_1)}{d_2\beta}$, $e_{222} = -(r-d_1)$ and $e_{233} = b_2\left(\frac{(r-d_1)+d_2\eta A}{(r-d_1)+d_2(\gamma+\delta\eta A)}\right) - m$. The equilibrium $E_2(0,\frac{r-d_1}{d_2},0)$ is locally asymptotically stable if $\frac{r-d_1}{d_2} > \frac{r_1\beta}{a_1}$ and $m > b_2\left(\frac{(r-d_1)+d_2\eta A}{(r-d_1)+d_2(\gamma+\delta\eta A)}\right)$ otherwise a saddle point. This means E_2 is stable if the carrying capacity of zooplankton species and death rate of fish species are greater than some respective threshold values

4. The Jacobian matrix for the fish free equilibrium $E_3(P_1, Z_1, 0)$ is

$$J|_{E_3} = \begin{bmatrix} e_{311} & e_{312} & 0 \\ e_{321} & e_{322} & e_{323} \\ 0 & 0 & e_{333} \end{bmatrix},$$

where

$$e_{311} = -\frac{r_1 P_1}{k_1} + \frac{2\alpha a_1 {P_1}^2 Z_1}{(\alpha {P_1}^2 + \beta)^2},\ e_{312} = -\frac{a_1 P_1}{\alpha {P_1}^2 + \beta},\ e_{321} = \frac{b_1 Z_1(\beta - \alpha {P_1}^2)}{(\alpha {P_1}^2 + \beta)^2},$$
$$e_{322} = -d_1 Z_1, e_{323} = -rkZ_1 - \frac{a_2 Z_1}{\gamma + \delta\eta A + Z_1}, e_{333} = \frac{b_2(Z_1 + \eta A)}{\gamma + \delta\eta A + Z_1} - m.$$

One of three eigenvalues of $J|_{E_3}$ is $e_{333} = \frac{b_2(Z_1+\eta A)}{\gamma+\delta\eta A+Z_1} - m$ and rest two are the roots of equation given by

$$\Pi^2 + C_1\Pi + C_2 = 0,$$

where $C_1 = -(e_{311} + e_{322}) = \left(\frac{r_1 P_1}{k_1} + d_1 Z_1 - \frac{2\alpha a P_1^2 Z_1}{(\alpha P_1^2+\beta)^2}\right)$ and $C_2 = e_{311}e_{322} - e_{312}e_{321} = d_1 Z_1\left(\frac{r_1 P_1}{k_1} - \frac{2\alpha a P_1^2 Z_1}{(\alpha P_1^2+\beta)^2}\right) + \frac{a_1 b_1 P_1 Z_1(\beta - \alpha P_1^2)}{(\alpha P_1^2+\beta)^3}$. Thus we have the following theorem.

Theorem 4.3.3. *The fish free equilibrium $E_3(P_1, Z_1, 0)$ is locally asymptotically stable if conditions $C_1 > 0$, $C_2 > 0$ and $m > \frac{b_2(Z_1+\eta A)}{Z_1+\gamma+\delta\eta A}$ hold together.*

To study the existence of fish free equilibrium points, we draw a curve in rP^*-plane in Fig. 4.3. From this figure, we can notice that, for a chosen set of parameters we can get zero, one or three fish free equilibrium points depending on the value of r. In this figure, a green dot indicate the sink whereas a black dot indicate the saddle point, thus the characteristic of multistability between two fish free equilibria is also illustrated by the same figure.

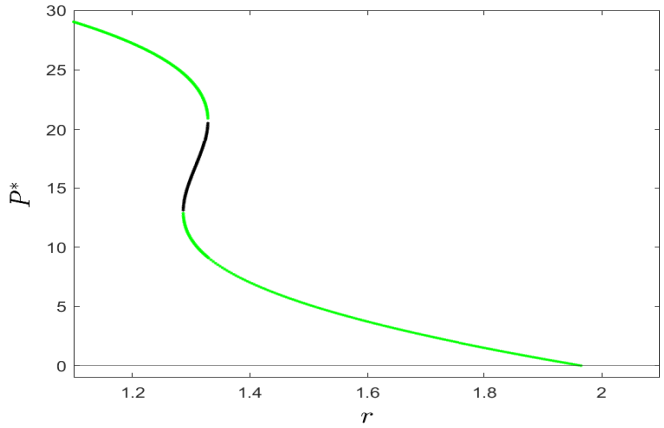

Fig. 4.3: This figure depicts the non-existence and existence of one or three positive roots of (4.5) and their stability; green dot as a sink and black dot as a saddle point with $r \in [1.1, 2.1]$, $d_2 = 0.1$, $m = 0.18$ and remaining parameters from Table 4.1.

5. The Jacobian matrix for the phytoplankton free equilibrium $E_4(0, Z_2, F_2)$ is

$$J|_{E_4} = \begin{bmatrix} e_{411} & 0 & 0 \\ e_{421} & e_{422} & e_{423} \\ 0 & e_{432} & 0 \end{bmatrix},$$

where

$$e_{411} = r_1 - \frac{a_1 Z_2}{\beta},\ e_{421} = \frac{b_1 Z_2}{\beta},\ e_{422} = -d_1 Z_2 + \frac{a_2 Z_2 F_2}{(\gamma + \delta\eta A + Z_2)^2},$$
$$e_{423} = -\frac{rkZ_2}{(1+kF_2)^2} - \frac{a_2 Z_2}{\gamma + \delta\eta A + Z_2}, e_{432} = \frac{b_2 F_2(\gamma + \eta A(\delta - 1))}{(\gamma + \delta\eta A + Z_2)^2}.$$

Again, it is easy to observe that one of the eigenvalues of $J|_{E_4}$ is $e_{411} = r_1 - \frac{a_1 Z_2}{\beta}$ whereas other two are roots of equation:

$$\Theta^2 + D_1\Theta + D_2 = 0,$$

where $D_1 = -e_{422} = d_1 Z_2 - \frac{a_2 Z_2 F_2}{(\gamma+\delta\eta A+Z_2)^2}$ and $D_2 = -e_{432}e_{423} = \left(\frac{b_2 F_2(\gamma+\eta A(\delta-1))}{(\gamma+\delta\eta A+Z_2)^2}\right)\left(\frac{rkZ_2}{(1+kF_2)^2} + \frac{a_2 Z_2 F_2}{\gamma+\delta\eta A+Z_2}\right)$. Next, we present the theorem establishing stability criterion for E_4.

Theorem 4.3.4. *The Phytoplankton free equilibrium $E_4(0, Z_2, F_2)$ is locally asymptotically stable if the conditions $r_1 < \frac{a_1 Z_2}{\beta}$, $d_1 > \frac{a_2 F_2}{(\gamma+\delta\eta A+Z_2)^2}$ and $\eta A > \frac{\gamma}{1-\delta}$ hold simultaneously.*

6. The Jacobian matrix evaluated at $E^*(P^*,Z^*,F^*)$ is given as:

$$J|_{E^*} = \begin{bmatrix} e_{11} & e_{12} & 0 \\ e_{21} & e_{22} & e_{23} \\ 0 & e_{32} & 0 \end{bmatrix},$$

where
$e_{11} = -\frac{r_1 P^*}{k_1} + \frac{2\alpha a_1 P^{*2} Z^*}{(\alpha P^{*2}+\beta)^2}$, $e_{12} = -\frac{a_1 P^*}{\alpha P^{*2}+\beta}$, $e_{21} = \frac{b_1 Z^*(\beta-\alpha P^{*2})}{(\alpha P^{*2}+\beta)^2}$, $e_{22} = -d_1 Z^* + \frac{a_2 Z^* F^*}{(\gamma+\delta\eta A+Z^*)^2}$,
$e_{23} = -\frac{rkZ^*}{(1+kF^*)^2} - \frac{a_2 Z^*}{\gamma+\delta\eta A+Z^*}$, $e_{32} = \frac{b_2 F^*(\gamma+\eta A(\delta-1))}{(\gamma+\delta\eta A+Z^*)^2}$. The characteristic equation of $J|_{E^*}$ is (where $\mathscr{O}$ is an eigenvalue of the Jacobian matrix):

$$\mathscr{O}^3 + U_1\mathscr{O}^2 + U_2\mathscr{O} + U_3 = 0, \tag{4.17}$$

where
$U_1 = -(e_{11}+e_{22})$, $U_2 = e_{11}e_{22} - e_{23}e_{32} - e_{12}e_{21}$, $U_3 = e_{11}e_{23}e_{32}$.
Now, from Routh-Hurwitz criterion [134], we can state the following theorem.

Theorem 4.3.5. *The interior equilibrium $E^*(P^*,Z^*,F^*)$ is locally asymptotically stable if the inequalities $U_1 > 0$, $U_3 > 0$ and $U_1U_2 > U_3$. hold.*

To study the global stability behavior of E^*, we first assume the existence of unique positive equilibrium $E^*(P^*,Z^*,F^*)$. Thus we assume that hypothesis (b) of Theorem 4.3.2 holds. In the next theorem, we are able to find sufficient condition for the global stability of E^*.

Theorem 4.3.6. *The interior equilibrium $E^*(P^*,Z^*,F^*)$ is globally asymptotically stable if*

$$M\left[\frac{b_1P^*}{\beta} + \frac{a_2}{\gamma+\delta\eta A}\left(Z^*+\eta A\right)\right] + \frac{ma_2F^*}{b_2} + \frac{r_1b_1}{a_1k_1}\left(\frac{k_1+P^*}{2}\right)^2 + \frac{r_2}{k_2}\left(\frac{k_2+Z^*}{2}\right)^2 < \frac{r_1b_1P^*}{a_1} + r_2Z^* + \frac{b_1NZ^*}{\alpha^2M+\beta} + \frac{a_2F^*(N+\eta A)}{\gamma+\delta\eta A+M}, \tag{4.18}$$

where M and N are defined the in proof.

Proof. We proof this theorem by constructing an appropriate Lyapunov function. We take a function $L(P,Z,F)$ which is positive definite about $E^*(P^*,Z^*,F^*)$ and is defined as:

$$L = \frac{b_1}{a_1}\left(P - P^* - P^*\ln\left(\frac{P}{P^*}\right)\right) + \left(Z - Z^* - Z^*\ln\left(\frac{Z}{Z^*}\right)\right) + \frac{a_2}{b_2}\left(F - F^* - F^*\ln\left(\frac{P}{P^*}\right)\right).$$

Thus,

$$\frac{dL}{dt} = \frac{b_1}{a_1}\left[r_1(P-P^*)\left(1-\frac{P}{k_1}\right) - \frac{a_1(P-P^*)Z}{\alpha P^2+\beta}\right] + \left[\frac{r(Z-Z^*)}{1+kF} - d_1(Z-Z^*) - d_2Z(Z-Z^*) + \frac{b_1P(Z-Z^*)}{\alpha P^2+\beta} - \frac{a_2F(Z-Z^*)}{\gamma+\delta\eta A+Z}\right] + \frac{a_2}{b_2}\left[\frac{b_2(Z+\eta A)(F-F^*)}{\gamma+\delta\eta A+Z} - m(F-F^*)\right]$$

$$\frac{dL}{dt} \leq \frac{b_1}{a_1}\left[r_1(P-P^*)\left(1-\frac{P}{k_1}\right) - \frac{a_1(P-P^*)Z}{\alpha P^2+\beta}\right] + \left[\frac{r_2}{k_2}(Z-Z^*)(k_2-Z^*) + \frac{b_1P(Z-Z^*)}{\alpha P^2+\beta} - \frac{a_2F(Z-Z^*)}{\gamma+\delta\eta A+Z}\right] + \frac{a_2}{b_2}\left[\frac{b_2(Z+\eta A)(F-F^*)}{\gamma+\delta\eta A+Z} - m(F-F^*)\right]$$

$$= \frac{r_1b_1}{a_1k_1}(Pk_1 - P^2 - k_1P^* + PP^*) + \frac{b_1P^*}{\alpha P^2+\beta} + \frac{r_2}{k_2}(Zk_2 - Z^2 - k_2Z^* + ZZ^*) - \frac{b_1Z^*P}{\alpha P^2+\beta} + \frac{a_2Z^*F}{\gamma+\delta\eta A+Z} - \frac{a_2F^*(Z+\eta A)}{\gamma+\delta\eta A+Z} + \frac{a_2\eta AF}{\gamma+\delta\eta A+Z} - \frac{ma_2F,}{b_2} + \frac{ma_2F^*}{b_2}.$$

where $r_2 = r - d_1$ and $k_2 = \frac{r-d_1}{d_2}$. From Theorem 4.3.1, we define $Z_M = \frac{f_{max}}{\theta}$, $F_M = \frac{b_2}{a_2}\frac{f_{max}}{\theta}$ and using these we get, $P_m := \frac{k_1}{r_1}\left(r_1 - \frac{a_1Z_M}{\beta}\right)$,

$Z_m := \frac{1}{d_2}\left(\frac{r}{1+kF_M} - d_1 - \frac{a_2F_M}{\gamma+\delta\eta A}\right)$.

Now, with some algebraic calculation, we have

$$\frac{dL}{dt} \leq -\frac{r_1b_1}{a_1k_1}\left(P - \frac{k_1+P^*}{2}\right)^2 + \frac{r_1b_1}{a_1k_1}\left(\frac{k_1+P^*}{2}\right)^2 - \frac{r_1b_1P^*}{a_1} + \frac{b_1P^*M}{\beta} - \frac{r_2}{k_2}\left(Z - \frac{k_2+Z^*}{2}\right)^2 + \frac{r_2}{k_2}\left(\frac{k_2+Z^*}{2}\right)^2 - r_2Z^* - \frac{b_1Z^*N}{\alpha M^2+\beta} + \frac{a_2Z^*M}{\gamma+\delta\eta A} - \frac{a_2F^*(N+\eta A)}{\gamma+\delta\eta A+M} + \frac{a_2\eta AM}{\gamma+\delta\eta A} - \frac{ma_2F}{b_2} + \frac{ma_2F^*}{b_2}$$

where $M = \max\{k_1, Z_M, F_M\}$ and $N = \min\{P_m, Z_m\}$.

Therefore, $\frac{dL}{dt} < 0$ if condition (4.18) is satisfied. Thus L is a suitable Lyapunov function inside the positive octant of PZF-space. Hence, E^* is globally asymptotically stable under condition (4.18). □

4.3.4 Bifurcation analysis

(A) Hopf bifurcation

Here, we study the analytical existence of Hopf bifurcation with respect to level of fear k, induced in zooplankton by fish as the possible bifurcation parameter, keeping other parameters fixed.

The critical value of k, let k^*, is defined by

$$U_1(k^*)U_2(k^*) - U_3(k^*) = 0. \tag{4.19}$$

Using (4.19), (4.17) becomes $(\mathscr{O} + U_1)(\mathscr{O}^2 + U_2) = 0$ at $k = k^*$. This equation has three roots, a pair of two purely imaginary roots $\mathscr{O}_{1,2} = \pm i\sqrt{U_2}$ and a negative root $\mathscr{O}_3 = -U_1$, which assures the existence of Hopf bifurcation.

For transversality condition, let k be a point in an open interval $(k-\varepsilon, k+\varepsilon)$ such that these roots become function of k, say $\mathscr{O}_{1,2} = \nu(k) \pm i\xi(k)$. As $\nu(k) + i\xi(k)$ is root of (4.17), and substituting this in (4.17) and on separating real and imaginary parts, we can have

$$\nu^3 - 3\nu\xi^2 + U_1(\nu^2 - \xi^2) + U_2\nu + U_3 = 0, \tag{4.20}$$

$$3\nu^2\xi - \xi^3 + 2U_1\nu\xi + U_2\xi = 0. \tag{4.21}$$

For Hopf bifurcation, $\xi(k) \neq 0$, so from (4.21), we have $\xi^2 = 3\nu^2 + 2U_1\nu + U_2$. Substituting this in (4.20), we get

$$8\nu^3 + 8U_1\nu^2 + 2\nu(U_1^2 + U_2) + U_1U_2 - U_3 = 0. \tag{4.22}$$

On differentiating (4.22) with respect to k and recalling that $\nu(k^*) = 0$, we have

$$\left[\frac{d\nu}{dk}\right]_{k=k^*} = -\frac{1}{2(U_1^2 + U_2)}\left[U_2\frac{dU_1}{dk} + U_1\frac{dU_2}{dk} - \frac{dU_3}{dk}\right]_{k=k^*}.$$

Thus the transversality condition for occurrence of Hopf bifurcation with respect to parameter k at its critical value $k = k^*$ is

$$\left(U_2\frac{dU_1}{dk} + U_1\frac{dU_2}{dk} - \frac{dU_3}{dk}\right)_{k=k^*} \neq 0. \tag{4.23}$$

Therefore, the following result states the existence of Hopf bifurcation.

Theorem 4.3.7. *For the occurrence of Hopf bifurcation around E^* at $k = k^*$, the necessary and sufficient conditions are:*

1. $U_1(k^*)U_2(k^*) - U_3(k^*) = 0$,
2. $\left(U_2\frac{dU_1}{dk} + U_1\frac{dU_2}{dk} - \frac{dU_3}{dk}\right)_{k=k^*} \neq 0.$

(B) Transcritical bifurcation

Theorem 4.3.8. *The transcritical bifurcation at* $r_1 = r_1^{[c]} = \frac{a_1 Z_2}{\beta}$ *produces a stable coexistence equilibrium* $E^*(P^*, Z^*, F^*)$ *from the phytoplankton free equilibrium* $E_4(0, Z_2, F_2)$*, and this bifurcation causes* E_4 *to lose its stability at this critical value of* r_1*.*

Proof. For proving the above statement, we will use the transversality conditions of Sotomayer's theorem [24]. For $r_1 = r_1^{[c]} = \frac{a_1 Z_2}{\beta}$, E_4 turns into a non-hyperbolic equilibrium point. Let $v_1 = \left[-\frac{e_1}{e_2}, 0, 1\right]^T$ and $v_2 = [1,0,0]^T$ serves as the eigenvectors for zero eigenvalue of $J|_{(E_4 : r_1^{[c]})}$ and $J^T|_{(E_4 : r_1^{[c]})}$, respectively, where $e_1 = -\frac{rkZ_2}{(1+kF_2)^2} - \frac{a_2 Z_2 F_2}{\gamma + \delta\eta A + Z_2}$, $e_2 = \frac{b_1 Z_2}{\beta}$, and $J|_{E_4}$ stands for Jacobian evaluated at E_4.

Now, we define $Y(P,Z,F) = [G_1, G_2, G_3]^T$, so $Y_{r_1} = \left[P(1 - \frac{P}{k_1}), 0, 0\right]^T$. The transversality conditions for transcritical bifurcation are:

$v_2^T Y_{r_1}(E_4 : r_1^{[c]}) = 0,$

$v_2^T [DY_{r_1}(E_4 : r_1^{[c]})] v_1 = 1 \neq 0,$

$$v_2^T [D^2 Y(E_4 : r_1^{[c]})(v_1, v_1)] = -\frac{2r_1\beta^2}{k_1 b_1^2 Z_2^2}\left(\frac{rkZ_2}{(1+kF_2)^2} + \frac{a_2 Z_2 F_2}{\gamma + \delta\eta A + Z_2}\right)^2 \neq 0.$$

Thus all the sufficient conditions of Sotomayer's theorem are satisfied, hence system (4.1) undergoes transcritical bifurcation at $r_1 = r_1^{[c]} = \frac{a_1 Z_2}{\beta}$. □

4.4 Numerical simulation

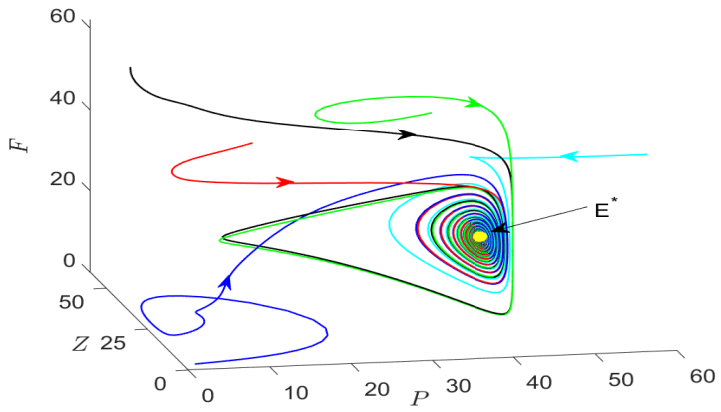

Fig. 4.4: Global stability of E^* depicted through a 3D-phase portrait, with parameters fixed from Table 4.1.

In this section, we perform the numerical simulation to support our theoretical findings and to observe different kinds of dynamical perspectives associated with model (4.1). We use MATLAB 2019b to draw all the figures in this manuscript, and solver ode45 to solve our system

numerically. Our main goal is to analyse the kinetics of this phytoplankton- zooplankton-fish system in the presence of fear-induced in zooplankton due to fish population with additional food to fish. With this aim, we choose a set of parametric values given in Table 4.1. For these values of parameters, all the possible equilibria and the further details related to them are provided in Table 4.2. From this table, we can observe that all the equilibrium points except the interior one are saddle points for the chosen parametric values. Infact E^* is globally asymptotically stable which is illustrated in Fig.4.4.

Equilibrium	Eigenvalues	Stability behavior
$E_0(0,0,0)$	(1.5000,1.0500,-0.0767)	saddle point
$E_1(40,0,0)$	(-1.5000,1.5878,-0.0767)	saddle point
$E_2(0,52.5000,0)$	(-2.6087,-1.0500,0.1913)	saddle point
$E_4(0,6.0400,3.7621)$	$(1.0273,-0.0546\pm 0.1097i)$	saddle point
$E^*(37.2742,6.0400,26.8392)$	$(-1.2636,-0.0059\pm 0.1682i)$	stable spiral

Table 4.2: Feasible Equilibria for model (4.1) with there eigenvalues and stability behavior for parameters from Table 4.1.

Fear's role in the system's dynamics and the maintenance of population coexistence

The level of fear, i.e., k, is a vital parameter to study. There are two important aspects related to k which we want to study. First, up to what extent it affects the densities of species in the interior equilibrium, and secondly, how it can affect the stability behavior of the system.

Talking about the impact on equilibrium point, from (4.13) and (4.15) we can observe that phytoplankton and zooplankton coordinates of E^* are independent of k. Thus they do not vary on increasing or decreasing the level of fear, whereas from (4.16), we can see that fish coordinate of E^* is dependent on the value of k. To observe this variation in F^* with respect to k, from (4.16), we have

$$F^* = \frac{-(a_2+k(d_1+d_2Z^*-C)(\gamma+\delta\eta A+Z^*))+\sqrt{(a_2+k(d_1+d_2Z^*-C)(\gamma+\delta\eta A+Z^*))^2+4a_2k(\gamma+\delta\eta A+Z^*)(r-d_1-d_2Z^*+C)}}{2a_2k}. \tag{4.24}$$

Now on differentiating F^* with respect k, we get

$$\frac{dF^*}{dk} = \frac{1}{2a_2k^2}\left(a_2+k(d_1+d_2Z^*-C)(\gamma+\delta\eta A+Z^*)-\sqrt{(a_2+k(d_1+d_2Z^*-C)(\gamma+\delta\eta A+Z^*))^2+4a_2k(\gamma+\delta\eta A+Z^*)(r-d_1-d_2Z^*+C)}\right)$$

$$+\frac{1}{2a_2k}\left(-(d_1+d_2Z^*-C)(\gamma+\delta\eta A+Z^*)+\frac{(a_2+k(d_1+d_2Z^*-C)(\gamma+\delta\eta A+Z^*))(d_1+d_2Z^*-C)(\gamma+\delta\eta A+Z^*)+2a_2(\gamma+\delta\eta A+Z^*)(r-d_1-d_2Z^*+C)}{\sqrt{(a_2+k(d_1+d_2Z^*-C)(\gamma+\delta\eta A+Z^*))^2+4a_2k(\gamma+\delta\eta A+Z^*)(r-d_1-d_2Z^*+C)}}\right)$$

From above expression it is easy to see that

$$\lim_{k\to\infty}\frac{dF^*}{dk}=0.$$

Now, again from (4.24), we can get

$$\lim_{k\to\infty}F^*=F_s=-\frac{(d_1+d_2Z^*-C)(\gamma+\delta\eta A+Z^*)}{a_2},$$

thus we can say that as $k\to\infty$, fish population decreases to a saturated value F_s. For the chosen set of parameters in Table 4.1, $\frac{dF^*}{dk}<0$ and $F_s=24.3697$, the decreasing slope and this saturation can be observed from Fig. 4.5. So we can say that increasing the level of fear has a negative effect on the fear-inducing fish population upto a certain extent. This observation also agrees with the existing studies [135, 120], in which fear induced by predator species does not affect prey coordinate of the coexistence equilibrium but harms the fear-inducing predator itself. From a biological point of view, we can say that rise in fear can curtail the foraging ability of the zooplankton population, which decreases its predation, leading to a reduction in the fish population's density making it to reach F_s. Thus after this saturation, coexistence equilibrium remains stable and constant.

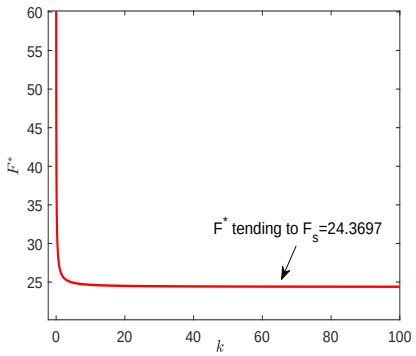

Fig. 4.5: Variation in F^* with k, with remaining parameters fixed from Table 4.1.

Now, we discuss the effect of change in fear on the stability behavior of the system. For lower levels of fear, system (4.1) has periodic and even chaotic solution. On increasing k, the system encounters a periodic window, after which it again becomes chaotic. This type of attitude is again repeated on a further increment of the fear parameter until it becomes stable via period-4,2,1 solutions. To demonstrate this route from chaos to stability, we have portrayed some time-series and phase-portrait diagrams in Fig. 4.6. The chaotic nature of the system is depicted by a time-series graph and a 3D-chaotic attractor in Fig. 4.6(a) for $k=0.05$, from which we can note that solution of the system is unpredictable, and we can not forecast its future behavior. On increasing k, this chaotic solution becomes a solution of period-4 and

then of period-2, the solutions of period-4, period-2 for $k = 0.135$, $k = 0.145$ are illustrated in Figs. 4.6(b) and 4.6(c), respectively. On continue rise in k, the solution becomes of period-1, and finally, for $k = k^* > 0.3175$, the interior equilibrium E^* becomes a stable focus via Hopf bifurcation. At $k = k^* = 0.3175$, $U_1(k^*)U_2(k^*) - U_3(k^*) = 0$ and $\left(U_2\frac{dU_1}{dk} + U_1\frac{dU_2}{dk} - \frac{dU_3}{dk}\right) = 0.4664 \neq 0$, thus both conditions of Hopf bifurcation stated in Theorem 4.3.7 hold. Both kinds of behaviors are pictured for $k = 0.25$ and 0.6 in Figs. 4.6(d) and 4.6(e), respectively. Thus we can say that raising the fear level can helps to control the chaos in system (4.1). System's whole dynamics on varying k is evident from the bifurcation diagrams given in Figs. 4.7(a), 4.7(b) and 4.7(c). From these figures it may be noted that when solution tends to stable equilibrium point asymptotically, in this case P_{max} and P_{min} are same, in-fact $P_{max} = P_{min}$ =stady state value of P. When system is unstable and we have a stable limit cycle of period-1, then P_{max} is the highest peak of the solution after removal of transient part whereas P_{min} is the lowest peak of the solution. In similar manner, we can define P_{max} and P_{min} for period-2 and so on. As we know, the solution of a chaotic system is very sensitive to the initial condition, so to check this sensitivity for our model, we have drawn two solutions with initial conditions (2,1,1) and (2.0001,1,1) for $k = 0.01$ in Fig. 4.8(a). From this figure, we can observe that these nearly started solutions diverge from each other as time progresses. We have also calculated largest Lyapunov exponent to confirm the choatic nature of the system, depicted in Fig. 4.8(b) whose positive values validate the chaotic nature of the system. With $k = 0.01$, a Poincar'e map (see, Fig 4.8(c)) for model (4.1) has also been drawn in ZF–plane ($P = 20$), in which the scattered points endorse its chaotic attitude.

Impact of additional food on the system's kinetics

To begin, we show that raising the quality of additional food can manage chaotic behavior of model (4.1). Then we look at how the increase in quality affects the densities of the populations participating in this interaction.

(A) Role of quality of additional food

The quality of additional food is another important factor to consider. Because our system exhibited chaotic behavior at low levels of fear, we will now discover that we can manage this chaos by raising additional food's quality δ. This chaos control is demonstrated for a specific value of k, which is $k = 0.01$, with $A = 5$ and other parameters are fixed as given in Table 4.1. The transformation from a chaotic system to stable one on increasing δ is depicted by the bifurcation diagrams provided in Fig. 4.9. This figure shows that as we improve the additional food quality δ, the chaotic solution transforms into a solution of finite period due to which the size of the attractor decreases and the height of oscillations declines and finally solution becomes stable. From these figures, we can observe that this control of chaos also follows a very interesting route via periodic solutions of periods-8,4,2,1.

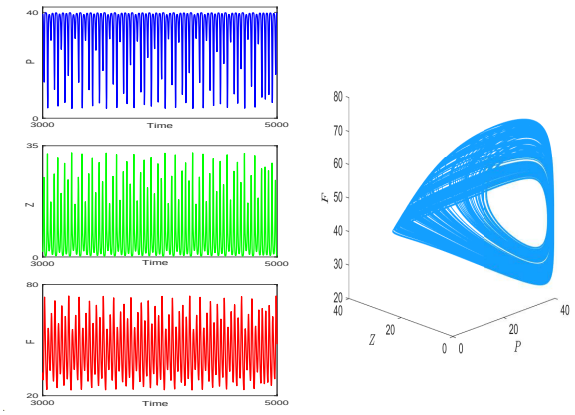

(a) $k = 0.05$

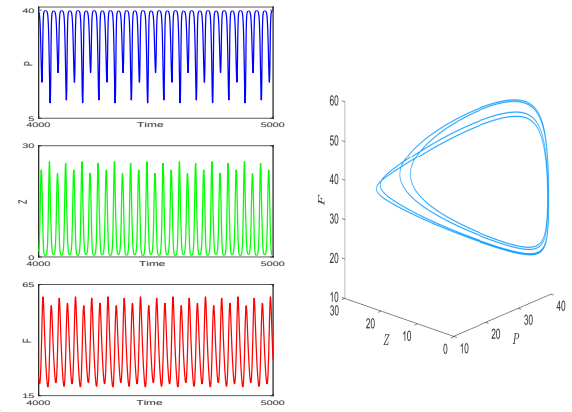

(b) $k = 0.135$

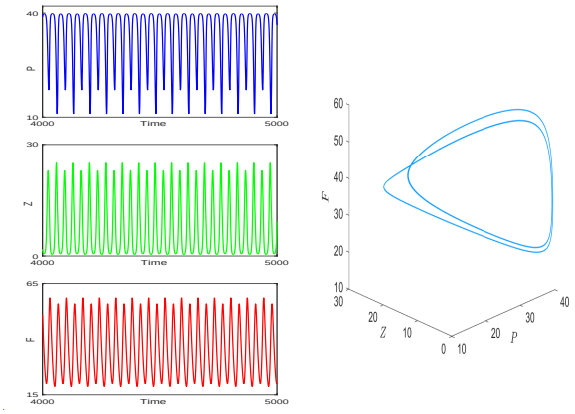

(c) $k = 0.145$

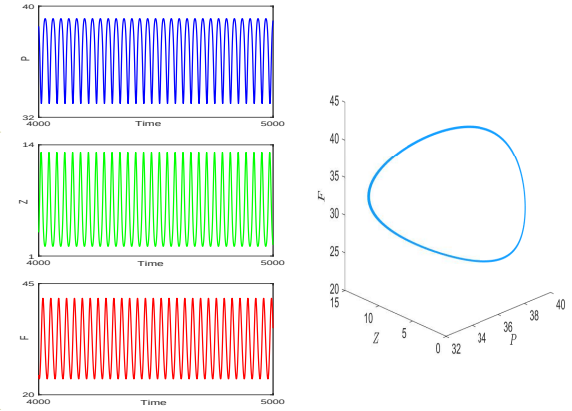

(d) $k = 0.25$

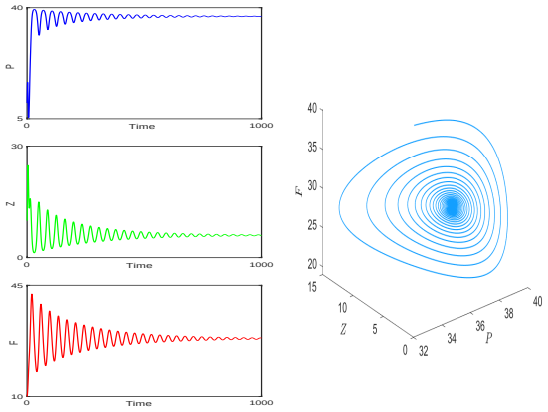

(e) $k = 0.6$

Fig. 4.6: Stability temperament of the system for various values of k, with remaining parameters from Table 4.1.

After getting into a stable position, we try to understand how the population densities are affected by varying the quality of food provided from outside. From (4.13), we know that

$$Z^* = \frac{m\gamma + \eta A(m\delta - b_2)}{b_2 - m} \text{ which implies } \frac{dZ^*}{d\delta} = \frac{m\eta A\delta}{b_2 - m} > 0 \text{ if } b_2 > m.$$

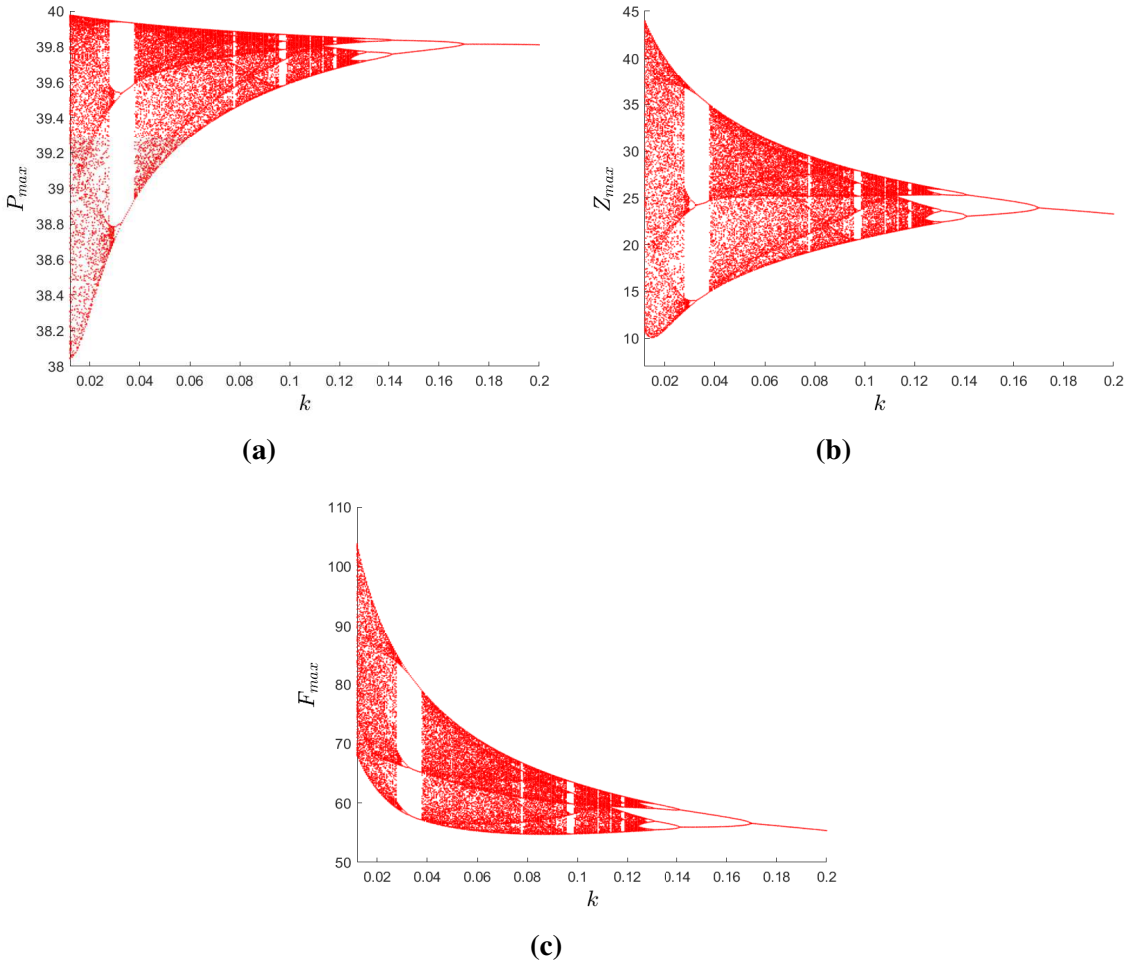

Fig. 4.7: Figs. (a), (b) and (c) show the bifurcation diagram for P_{max}, Z_{max} and F_{max}, respectively for $k \in [0.01, 0.2]$, remaining parameters same as in Table 4.1.

Due to complexity of (4.15) and (4.16), it is not easy to obtain analytical conditions, describing the shift in P^* and F^* on the variation of δ, so we examine this change numerically, which is evident from Table 4.3. Biologically speaking, as we increase δ, fish population density intensifies correspondingly, and from Section 4.2, we know that the handling time of fish for additional food is directly proportional to the quality of this food. Thus improving δ, increases the amount of time which fish population spends in handling this supplementary food, because of which the stress on the zooplankton population decreases, and their density also

gets a boost. As middle predator's density magnifies, there is a decline in prey's (phytoplankton) density due to the increased pressure of grazing on them. Parameters A and η has similar effects on the dynamics of system (4.1) as of δ, thus we omit the simulation results related to them.

δ	P^*	Z^*	F^*
19	34.0318	11.5000	108.6650
20	33.7636	11.8750	110.4952
21	33.4872	12.2500	112.2862
26	31.9537	14.1250	120.7209
30	30.4714	15.6250	126.9861

Table 4.3: Trend of species on increasing δ with $k = 0.01$, $A = 5$, and rest of the parameters from Table 4.1.

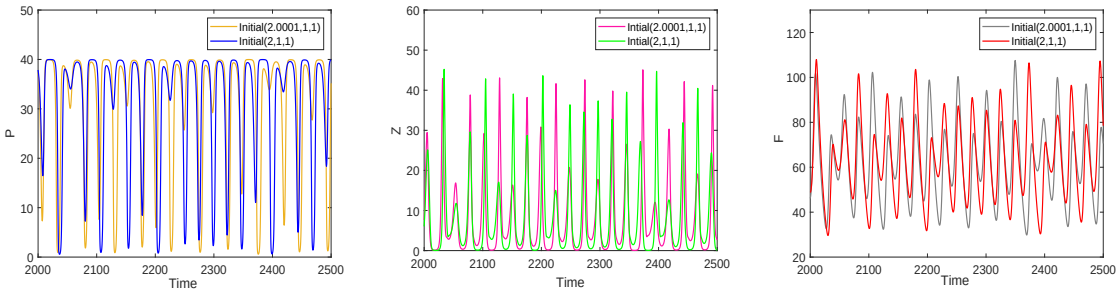

(a)

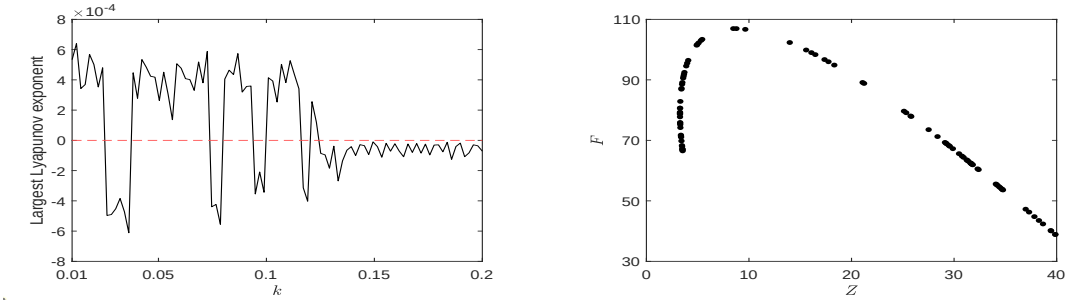

(b) **(c)**

Fig. 4.8: For $k = 0.01$, Fig. (a) depicts the sensitivity of solutions with respect to two different sets of initial conditions. Fig. (b) represents the evaluation of largest Lyapunov exponent whereas Fig. (c) portrays Poincar'e map in ZF–plane ($P = 20$) with $k = 0.01$, remaining parameters same as in Table 4.1.

Role of intrinsic growth rate of phytoplankton in the dynamics of system (4.1)

From Theorem 4.3.4, phytoplankton free equilibrium E_4 becomes stable, i.e., phytoplankton

goes to extinction if inequalities $r_1 < \frac{a_1 Z_2}{\beta}$, $d_1 > \frac{a_2 F_2}{(\gamma+\delta\eta A+Z_2)^2}$ and $\eta A > \frac{\gamma}{1-\delta}$ hold. For parameters fixed from Table 4.1, the critical value of r_1 for extinction of phytoplankton species is $r_1 = r_1^{[c]} = \frac{a_1 Z_2}{\beta} = 0.4726$ whereas other two conditions are already satisfied. We have plotted a time evolution graph for $r_1 = 0.3$ in Fig. 4.10(a) from which we can notice that phytoplankton species go to annihilation for $r_1 < r_1^{[c]}$. For $0 < r_1 < r_1^{[c]}$, E_4 is a stable focus and as we increase r_1, at $r_1 = r_1^{[c]}$, E_4 becomes a non-hyperbolic equilibrium, and a stable interior equilibrium E^* is generated via a transcritical bifurcation. At this critical value of r_1, both the equilibria E_4 and E^* exchange their stability. To depict this transcritical bifurcation, we have portrayed two solutions with same initial point (denoted with green circle) and different values of r_1 in Fig. 4.10(b). From this figure, we can observe that for $r_1 = 0.3 < r_1^{[c]}$, solution tends to E_4 and for $r_1 = 0.5 > r_1^{[c]}$, trajectory goes to E^*. A bifurcation diagram for phytoplankton species, depicting this transcritical bifurcation is also presented in Fig. 4.10(c). From this figure, we can see that a stable coexistence equilibrium E^* is generated via this bifurcation.

Bistability

From Subsection 4.3.2, we know that for $r_1 = 1$, $b_1 = 0.4$ and $\beta = 5$, keeping other parameters fixed from Table 4.1, our system has two interior equilibrium points $E_1^*(34.7169, 6.0400, 14.7717)$ and $E_2^*(7.5121, 6.0400, 20.5718)$ with $(-0.6885 + 0.0000i, -0.0112 \pm 0.1307i,)$ and $(0.0278 + 0.0000i, 0.0690 \pm 0.4268i,)$ as eigenvalues of their respective Jacobians. For the same set of parameters, phytoplankton free equilibrium $E_4(0, 6.040, 3.7621)$ with $(-0.0872 + 0.0000i, -0.0545 \pm 0.1096i,)$ as eigenvalues of the corresponding Jacobian is also a locally asymptotically stable equilibrium. Thus E_1^* and E_4 are two locally asymptotically stable equilibria in PFZ-space, which implies that our system has the characteristic of bistability which is depicted in Fig. 4.11(a). We have also drawn basins of attraction for E_1^* and E_4 in Fig. 4.11(b), red dots and blue dots are the initial conditions from which the started solution converge to E_1^* and E_4, respectively.

For $r_1 = 1.1$, the system has three interior equilibria, $E_1^*(35.3469, 6.0400, 14.5479)$, $E_2^*(4.1204, 6.0400, 12.9506)$ and $E_3^*(0.5326, 6.0400, 4.4950)$ with $(-0.7904 + 0.0000i, -0.0158 \pm 0.1312i)$, $(0.0047 + 0.0000i, -0.0082 \pm 0.5024i)$ and $(-0.0026 + 0.0000i, -0.0576 \pm 0.2411i)$ as the eigenvalues of their respective Jacobian matrices. Thus E_1^* and E_3^* are two stable focus in PZF-space having their corresponding basins of attractions. This quality of multistability for the system is portrayed in Fig. 4.12(a), and their associated regions of attraction are outlined in Fig. 4.12(b).

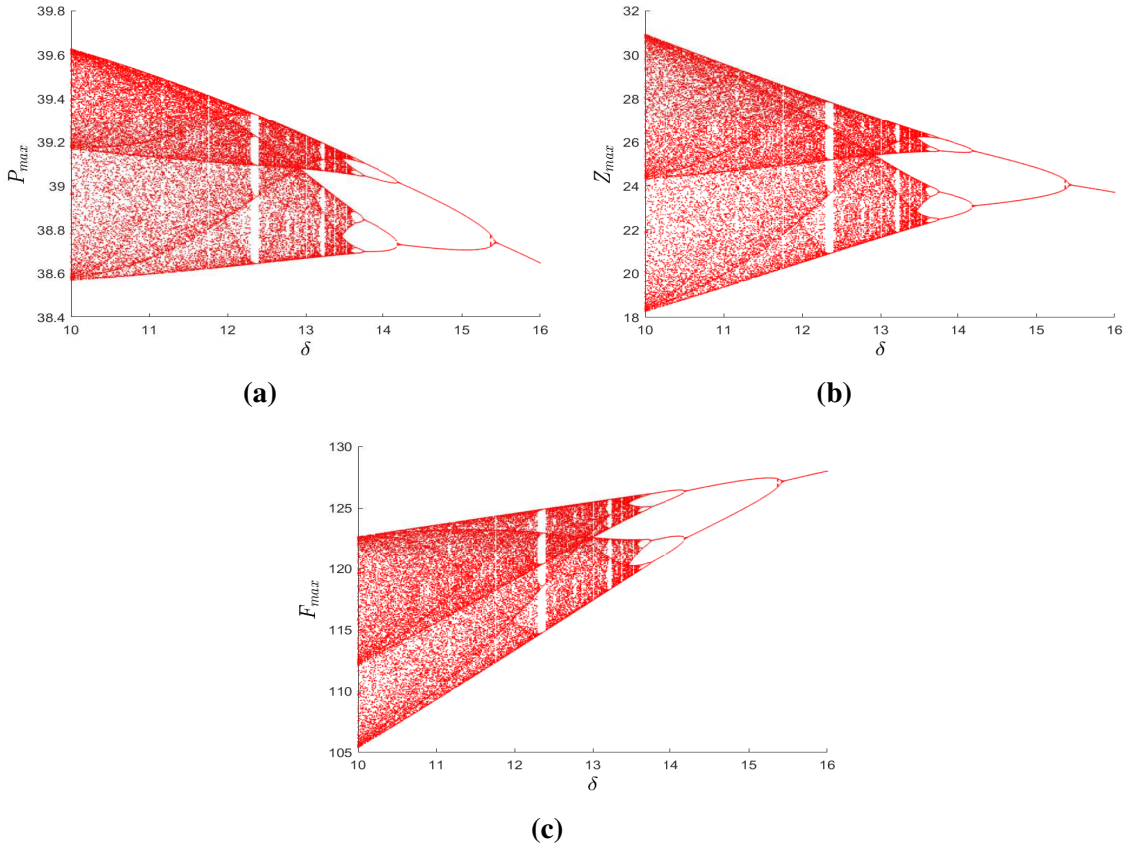

Fig. 4.9: Figs. (a), (b) and (c) represent P_{max}, Z_{max} and F_{max}, depicting the control of chaos and reducing the system into a stable one on a low level of fear, i.e., $k = 0.01$ by increasing the quality of additional food (δ) with $A = 5$, and rest of the parameters fixed from Table 4.1.

Paradox of enrichment

The term “Paradox of enrichment" was firstly given by Michael Rosenzweig [136], which means that increasing the amount of available food to prey can destabilize the system. The term “Paradox” is used because increase in the input food is unbalancing the system’s dynamics instead of making it more stable, and one can look some studies related to this here [137, 138, 139]. In our model, as we enhance the carrying capacity (k_1) of phytoplankton species, system is becoming chaotic, thus k_1 is the parameter which we use in terms of enrichment. We can visualize this paradox through bifurcation diagrams presented in Figs. 4.13(a), 4.13(b) and 4.13(c) for species P, Z and F, respectively. Here, in our model this phenomenon has been observed due to system complexity. There are several evidences of this paradox in the literature [55] where increasing the carrying capacity of the system makes it chaotic. There are several factors in ecology to explain/resolve this issue, like, prey toxicity, prey defense, unpalatability of prey, etc. In our model, we can resolve this phenomenon (system becomes stable from chaotic behavior) by increasing some model parameters, like, level of fear in zooplankton by

fish (k), additional food quality (δ), etc.

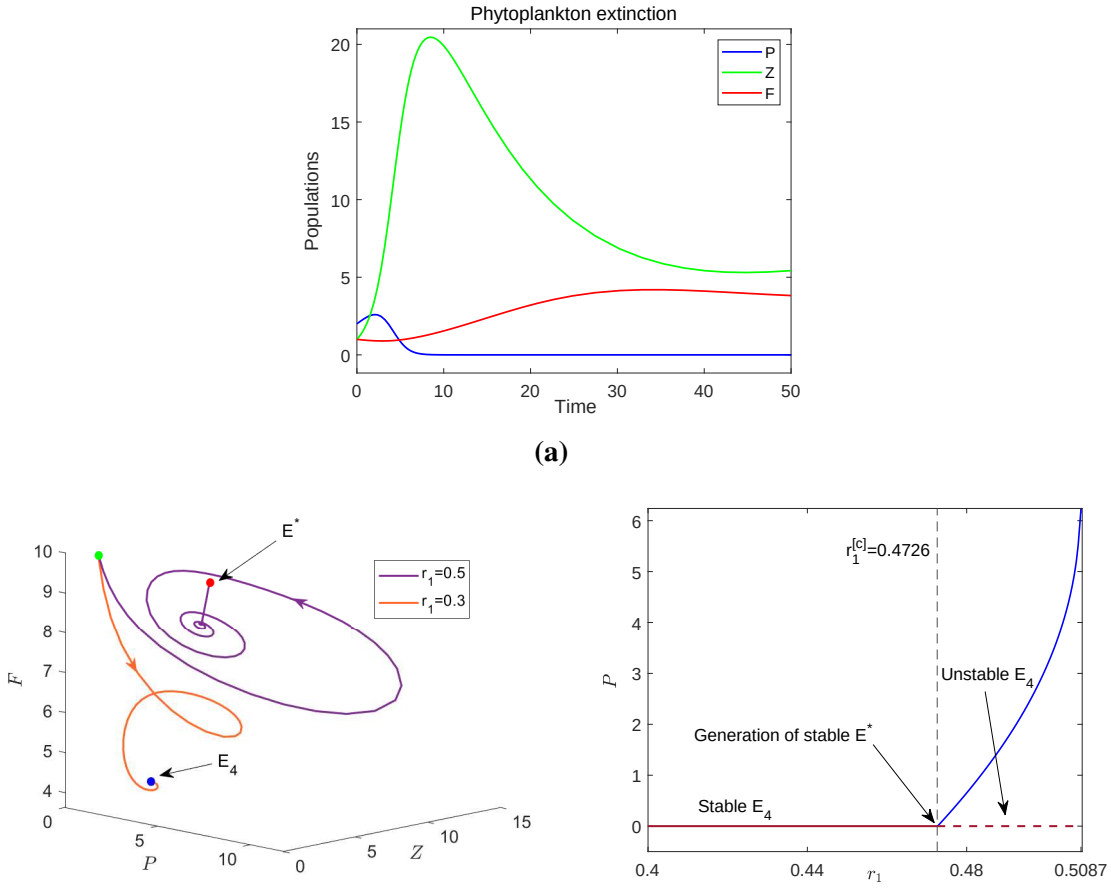

Fig. 4.10: Fig. (a) depicts extinction of phytoplankton population for $r_1 = 0.3$, Figs. (b) and (c) illustrate the occurrence of transcritical bifurcation with respect to r_1 through a phase portrait diagram and a bifurcation diagram, respectively, with others parameters from Table 4.1

.

Two-parametric analysis

Two-parametric study for a system gives better insights of its dynamics as compared to one-parametric, and as fear level k, additional food's biomass density A, and quality δ are important parameters associated with the proposed model. Thus to study the behavior of model (4.1) in more depth, we draw two-parametric bifurcation diagrams (Fig. 4.14) by varying two of these each time and keeping other parameters fixed. In this analysis, we divide the system's nature into four categories: other periodic and chaotic solutions, period-4 solution, period-2 solution and locally asymptotically stable, which depicts the shifting of system's nature from chaotic to stable one via period halving. In Fig. 4.14(a), we drew the bifurcation diagram for $k \in [0.03, 0.034]$, $\delta \in [6, 10.5]$ with $A = 5$. The dual-parametric diagram for $k \in [0.12, 0.23]$, $A \in$

$[4,5.5]$, keeping $\delta = 12$, is presented in Fig. 4.14(b), whereas for $k = 0.01$, δA-bifurcation diagram for $\delta \in [5,9]$, $A \in [7,14]$, is given in Fig. 4.14(c), in all these combinations remaining parameters are kept fixed from Table 4.1.

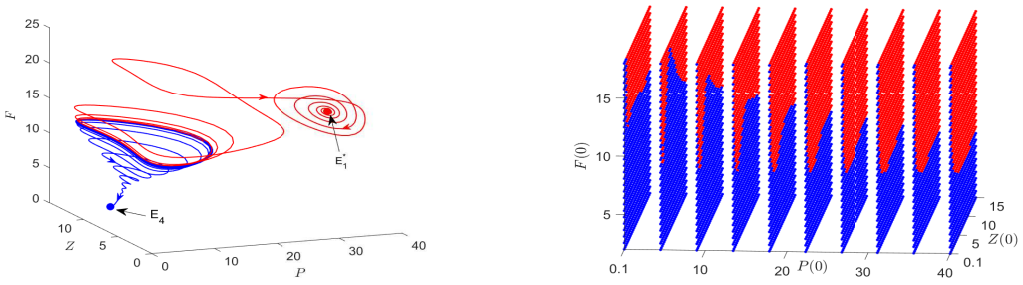

(a) **(b)** Basins of attraction for E_1^* and E_4.

Fig. 4.11: (a) Solution in blue color with initial conditions $(17.83, 9.168, 10.42)$, and solution in red color with initial conditions $(17.83, 8.726, 10.42)$ tend to E_4 and E_1^*, respectively. (b) This figure represents the basins of attraction (red region for E_1^* and blue region for E_4) for $P(0) = [0.1, 40]$, $Z(0) = [0.1, 15]$, $F(0) = [2, 18]$, with $r = 1$, $b_1 = 0.4$ and $\beta = 5$, and remaining parameters from Table 4.1.

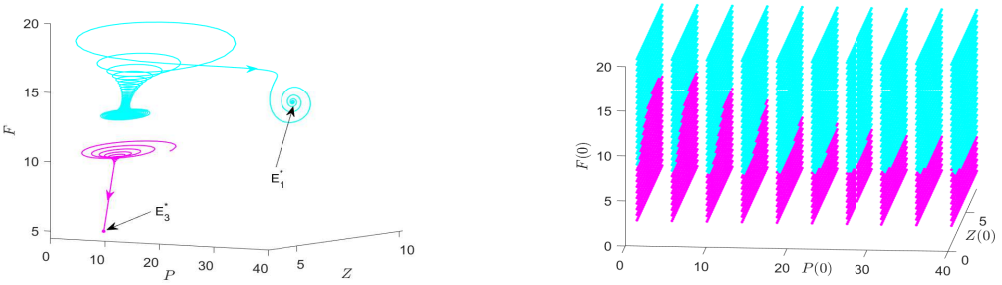

(a) **(b)** Basins of attraction for E_1^* and E_3^*.

Fig. 4.12: (a) This phase portrait illustrates bistability between two stable focus, E_1^* and E_3^*, whereas Fig. (b) manifests basins of attraction for these two equilibria (cyan region for E_1^* and magenta region for E_3^*) for $P(0) = [1, 40]$, $Z(0) = [1, 8]$, $F(0) = [2, 20]$, with $r = 1.1$, $b_1 = 0.4$ and $\beta = 5$, and other parameters from Table 4.1.

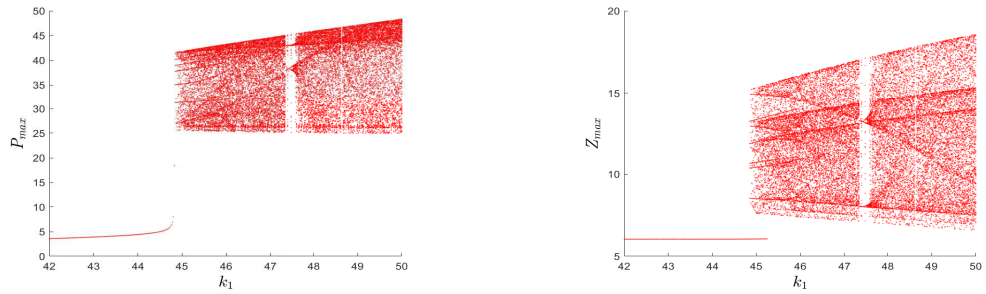

(a) **(b)**

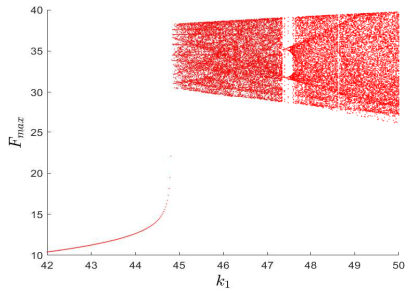

(c)

Fig. 4.13: For $r_1 = 0.5$ and remaining parameters from Table 4.1, Figs. (a), (b) and (c) represent P_{max}, Z_{max} and F_{max} which depict the phenomenon of paradox of enrichment for $k_1 \in [42, 50]$.

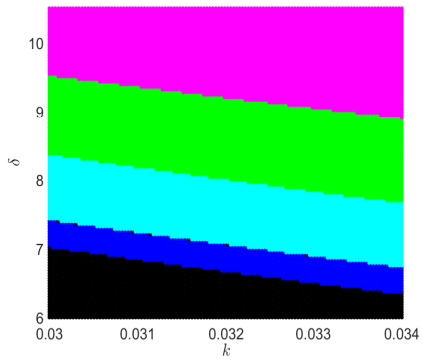

(a)

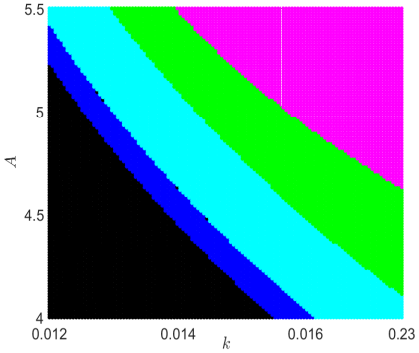

(b)

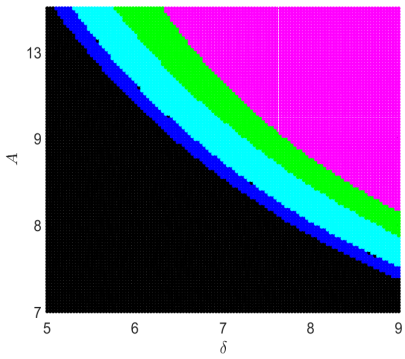

(c)

Fig. 4.14: Fig. (a) represents two-parametric bifurcation diagram in $k\delta$-plane,with $A = 5$, Fig. (b) represents two-parametric bifurcation diagram in kA-plane, with $\delta = 12$ and Fig. (c) portrays two-parametric bifurcation diagram in δA-plane, with $k = 0.01$. In all three subfigures remaining parameters are from Table 4.1. Here magenta: locally asymptotically stable, green: period-1 limit cycle, cyan: period-2 limit cycle, blue: period-4 limit cycle, and black: other periodic and chaotic solutions.

4.5 Concluding remarks

There are many articles [132, 130, 131] in the literature in which authors have dealt with PZF systems and have obtained exciting results, but a less attention is paid to PZF models in which fish induces fear in zooplankton. In recent times, Kaur *et al.* [31] have analysed a PZF model with inclusion of fear effect and prey refuge. They handled the PZ and ZF interaction through Holling type II response. Extending this work, we proposed to work on a Phytoplankton-zooplankton-fish system with fear in zooplankton due to fish and additional food to fish. The respective interactions are addressed through Holling type IV and II responses, where Holling type IV response presents zooplankton's avoidance towards highly grown phytoplankton population. This property of Holling type IV response (in form of attaining its global maxima), helps to prove the boundedness of our system, which is an essential component of well-posedness for any dynamical model.

Further, we establish the conditions under which the possible equilibrium points exist; requisites for the existence of multiple interior equilibria are also discussed in this subsection 4.3.2. Moreover, for a chosen set of parameters, we draw a bi-parametric existence diagram that depicts different regions corresponding to a different number of positive equilibria in a $r_1\beta$-plane (Fig. 4.2). Next, the local and global stability are investigated for these feasible equilibrium points. After this, the transversality conditions for the occurrence of Hopf bifurcation and transcritical bifurcation are determined in subsection 4.3.4.

In the numerical simulation, for a set of parameters, we depict the global stability of a unique coexistence equilibrium (Fig. 4.4) by starting several solutions with distinct initial points, converging to the aforementioned equilibrium. Next, we drive an expression for saturation value of F^* (fish coordinate of E^*) when $k \to \infty$, which represent that as fear increases to infinity, fish population decrease and eventually reach a value after which the coexistence equilibrium remains constant and stable. Regarding the change in behavior as we very the level of fear k, we present various time-series, phase portraits, and bifurcation diagrams in the order of increasing k (Figs. 4.6–4.7), delineating transformation from chaotic to stable through periodic dichotomy. For low values of k, the system is unstable (chaotic or periodic), chaotic nature of the system is evident from Figs. 4.8(a), 4.8(b),4.8(c). Chaos at low levels of fear can also be controlled through increasing the additional food quality δ, illustrated via bifurcation diagrams in Fig. 4.9. An interesting change in species density is observed (Table 4.3); when we raise δ, the handling time of fish for this additional source increases, which boosts zooplankton's density. This growing middle predator population intensifies its grazing pressure on the primary prey (phytoplankton), decreasing its population density. Therefore, increasing

δ has positive effects on the zooplankton and fish population but negatively impacts the phytoplankton population. The extinction of phytoplankton for its intrinsic growth rate less than a threshold value, and emergence of E^* through E_4 by virtue of transcritical bifurcation are sketched in Figs. 4.10(a), and 4.10(b)– 4.10(c), respectively.

The attribute of multistability in dynamical systems is a significant character as it provides better understanding about the coexistence of multiple stable equilibria and critical combinations of initial conditions of the solutions converging to them. In Fig. 4.11, our system shows this character between a planner and a positive steady state, and Fig. 4.12, depicts bistability between two positive steady states. In both cases, we have drawn phase portraits to manifest bistability and their respective basins of attractions. Using the carrying capacity of phytoplankton k_1 as the control parameter, the proposed model also exhibits the paradox of enrichment. When k_1 increases while the other parameters remain constant, the system becomes chaotic rather than turning more stable. We've also created bi-parametric bifurcation diagrams to investigate the system's dynamics in more better way.

On comparing our work with the study done by Kaur *et al.* [31], we can notice that for lower values of the fear parameter, their system has a periodic-1 solution. In contrast, our system behaves chaotically, and when we increase this parameter, our system becomes stable through period-halving, making the system's dynamics more elegant. The incorporation of additional food also has interesting impacts on the kinetics of the proposed model, like it can control the chaos and help to maintain the system's coexistence. The present study also shows the attribute of multistability, which is not present in their research. The presence of different number of interior equilibria under different analytical conditions also depicts the vigorous nature of the proposed model. This whole discourse outlines the vibrant dynamics of the proposed model; thus, we expect that the submitted work can assist ecologists in examining the interplay of the plankton-fish system with an inclusive and practical approach.

Chapter 5

Chaotic dynamics of a plankton-fish system with fear and its carry over effects in the presence of a discrete delay[1]

5.1 Introduction

The main goal of theoretical ecology and population biology is to know the various underlying dynamical mechanisms that govern prey-predator relationships. Plankton can be categorized mainly into two groups; phytoplankton and zooplankton. Phytoplankton plays a vital role in maintaining global climate by producing and absorbing large amounts of oxygen and carbon dioxide, respectively [140]. Zooplankton is heterotrophic plankton that predate on phytoplankton. Phytoplankton-zooplankton (PZ) interactions act as the base for most food chains operating in the marine ecosystem. In this tri-trophic PZF(Phytoplankton-zooplankton-fish) food chain, fish acts as the top predator, and zooplankton behaves as the middle predator, whereas phytoplankton serves as the basal prey.

Predator-prey relation is not only affected by the means of direct consumption but the fright of being killed modifies prey's conventional lifestyle [141]. In response to this fear, many anti-predator behaviors like, a dropped feeding rate [142], shifting to a suboptimal quality habitat [143], reduced mating rate [144] are shown by prey. For an example; due to some danger of predation, sometimes birds leave their nests as an antipredator behavior, which curtail their reproduction rate and affect the whole population [145]. Recent experiments [68] on song sparrows *Melospiza Melodia*, shows that their reproduction can be reduced by 40% due to fright of predation instead of direct killing. Inspired form this Wang *et al.* [30] modeled a prey-predator system with the inclusion of fear-caused birth rate contraction. They investigated the relationship between fear parameter and other biological parameters. Kaur *et al.* [31] analysed a plankton-fish system with fish induced fear and zooplankton refuge. They showed

[1] A considerable part of this chapter is published in *Chaos, Solitions & Fractals*, 160, 112245 (2022)

that increasing fear can eliminate periodic oscillations, ceasing planktonic blooms. There are many papers [117, 32, 33, 34, 35], to which an interested reader can refer to study the prey-predator system involving predator-induced fear effect.

The terminology "carry-over effect" emerged from the frequent clinical investigations; carry-over effects come from individual's past experiences, history, and can decide their present performance [39]. According to Norris [43], carry-over effect has positive impacts on population when the previous habitat lost due to some lethal or non-lethal factor is of low quality, and it can be opposite when the lost habitat is of good quality. Thus the change in population will depends upon (i) which demographic components in which period cause stiff carry-over effects, (ii) not only the amount, but also the quality of habitat which is lost. There are experimental evidences [40, 41, 42] that the carry-over effects can occur in a single seasons in amphibians, insects, marine invertebrates, etc. Thus there is an increasing trend of incorporating carry-over effects in mathematical modeling and empirical research [43, 44, 45]. Therefore, integration of carry-over effects in a population model can help to understand the potential link between cost of reproduction and life-history trade-offs.

The kinetics of a prey-predator population model is significantly dependent upon the mode of interaction between them, i.e., the predator's functional response over its prey. Holling type I, II, III, and IV functional responses rely only on prey's density, whereas Beddington–DeAngelis, Leslie–Gower, and Crowley-Martain responses depend upon the densities of both prey and predator populations. Holling type II functional response [55] is most widely used functional response in studying the prey-predator interrelationship. In this response, the predation rate becomes constant at high prey density because of satiation in the predator population. At high prey density, phytoplankton species start emitting toxic chemicals as their defense against the zooplankton population. Hence, we use Holling type IV functional response to deal with this type of interaction between these two populations [101, 127].

Bifurcation theory explains the qualitative as well as quantitative changes in the steady states of a dynamical systems. Hopf, transcritical, saddle-node are the main types of local bifurcations whereas Bogdanov–Takens, homoclinic and heteroclinic are global bifurcations [24]. Chaos theory discloses many new aspects of a chaotic system and explains its various strange behaviours, for an example, the solutions of chaotic system are very sensitive to initial population densities. Due to chaos in a dynamical model, sometimes there are abrupt changes in the population densities of participating species which are the main challenges in handling a chaotic system. Due to this, forecasting the behaviour of the chaotic model becomes very tough. A fine detail about chaos theory and its components like a strange attractor, Poincar'e map, Lyapunov exponents, etc., are provided by Hastings *et al.* [25]. We can confirm the occurrence of chaos in a system by using various techniques: calculation of Lyapunov exponent, power spectral density, fractal dimension of the map and recurrence plot [26].

As biological processes are associated with time lag, thus time delay has a vital role in the formulation and dynamics of their mathematical models. Adding the time delay in a differential equation makes it delay differential equation. A comprehensive detail about delay differential equations is present in the literature [22]. There are several kinds of delay like; gestation time, maturation time, traveling, feedback time, incubation, fear response delay etc. Most of the time existence of a delay in a dynamical model can destablize it and can even make chaotic [126, 117]. But sometimes addition of delay in an unstable system can suppress the oscillations and can make its stable. Sasmal and Gosh [146] investigated the impact of dispersal in a two patch prey-predator system in which prey disperse between patches with constant dispersing rate. They observed that delay induced dispersal can eliminate the oscillations by amplitude death. There are more evidences [147, 148] present in the literature in which delay can stabilize the system through amplitude death.

In this chapter, we utilize the work of Sasmal and Takeuchi [149] to introduce the fear of predation and its carry-over effects in a three-dimensional PZF-population model. To deal with PZ and ZF interactions, we choose simplified Holling type IV with Holling type II as mode of interactions, respectively. A discrete delay, carry-over delay (COE delay), corresponding to carry-over effects, is also incorporated in the model to make it more pragmatic. The main objectives of our investigation are to respond to the following question:

1. How the parameters related to these non-lethal effects will affect the stability nature of the system ?

2. What will be the impact of variation of these parameters on the population densities of the species involved in these interactions ?

3. In what manner the COE delay will change the dynamics of the system ?

The Rest of the chapter is organized as follows: In Section 5.2, we described the complete formulation of the population model with all the significant parameters involved. In Section 5.3, we gave a thorough study of the equilibrium existence and stability analysis, and we also outlined the bifurcation analysis at the end of this section. In Section 5.4, we analysed the delayed system and developed its theoretical results. Next, in Section 5.5, we did extensive simulation work to manifest the main findings of our work. In Section 5.6, we discuss the central results of our work and provide some possible future directions.

5.2 Model development

We study a three-dimensional aquatic system with three species: phytoplankton as prey, zooplankton as middle predator, and planktivorous fish as top predator. The densities of these

species are denoted by P, Z, and F, respectively, in the order mentioned above. The establishment of the proposed model is based upon the following presumptions:

1. Phytoplankton population is assumed to grow logistically with r and k as its intrinsic growth rate and carrying capacity. Zooplankton population is assumed as specialist predator which wholly depends upon phytoplankton population for its survival. As the density of phytoplankton population increases then it takes the form of harmful algal blooms (HAB), and start to liberate noxious chemicals. Thus zooplankton population reduce the intake of phytoplankton on their dense increment, and we handle this kind of interplay between these two species by using modified Holling type IV functional response, $H_1(P) = \frac{P}{\gamma P^2+\alpha}$ [101]. Thus the PZ-interaction is given by

$$\begin{aligned}\frac{dP}{dt} &= rP\left(1-\frac{P}{k}\right) - \frac{c_1 PZ}{\gamma P^2+\alpha},\\ \frac{dZ}{dt} &= \frac{c_2 PZ}{\gamma P^2+\alpha} - d_1 Z.\end{aligned}$$

2. Predator induces fear in prey which impacts prey's growth rate due to shift of locality or increment in cost of vigilance and high anti-predator attitude [68, 30]. The fear of predators also has some carry-over effects (COEs), affecting the birth rate of prey species [42]. Planktivorous fish also induce fear in zooplankton population with its carry-over effects impacting zooplankton's growth rate [114, 128, 150, 31]. Thus we use a function in our model to describe the role of both fear and its COEs in zooplankton-fish interaction which is given by $f(c,w,Z,F) = \frac{1+cZ}{1+cZ+wF}$ [149], where c is COE parameter due to fear, denoted by the parameter w. Here, f has following properties related to fear [30].

   - $f(c,0,Z,F) = f(c,w,Z,0) = 1$,
   - $\lim_{w\to\infty} f(c,w,Z,F) = \lim_{F\to\infty} f(c,w,Z,F) = 0$,
   - $\frac{\partial f}{\partial w} < 0,\ \frac{\partial f}{\partial F} < 0$.

   The properties related to COEs are listed below [149].

   - $\frac{\partial}{\partial c} f(c,w,Z,F) = \frac{wZF}{(1+cZ+wF)^2} > 0$, which shows the positive impact of COEs due to learnings from previous seasons or experiences.
   - $\frac{\partial}{\partial Z} f(c,w,Z,F) = \frac{cwF}{(1+cZ+wF)^2} > 0$, as density of zooplankton population increases, their cost of vigilance decreases, increasing their reproduction.
   - $\lim_{c\to\infty} f(c,w,Z,F) = \lim_{Z\to\infty} f(c,w,Z,F) = 1$, which implies if COE or zooplankton's density is very large then there is no decrement in reproduction.

Thus the ZF-interaction is given by

$$\frac{dZ}{dt} = \frac{c_2PZ}{\gamma P^2+\alpha}.\frac{1+cZ}{1+cZ+wF} - \frac{c_3ZF}{Z+\beta} - d_1Z,$$
$$\frac{dF}{dt} = \frac{c_4ZF}{Z+\beta} - d_2F,$$

whereas interplay between zooplankton and fish population is dealt using Holling type II functional response.

Therefore the complete non-delayed PZF-model on which we intend to work is:

$$\begin{aligned}
\frac{dP}{dt} &= rP\left(1-\frac{P}{k}\right) - \frac{c_1PZ}{\gamma P^2+\alpha} =: M_1(P,Z,F),\\
\frac{dZ}{dt} &= \frac{c_2PZ}{\gamma P^2+\alpha}.\frac{1+cZ}{1+cZ+wF} - \frac{c_3ZF}{Z+\beta} - d_1Z =: M_2(P,Z,F),\\
\frac{dF}{dt} &= \frac{c_4ZF}{Z+\beta} - d_2F =: M_3(P,Z,F),
\end{aligned} \tag{5.1}$$

with $P(0)\geq 0,\ Z(0)\geq 0,\ F(0)\geq 0.$

3. Carry over effects are those events which take place in one season and their impacts become visible in the following season or generations [43]. The COEs, due to fear, are also not immediate, and these effects of the induced fear on the prey population will surely involve some delay. Thus. in our system, using a carry over effect delay (COE delay) is biologically very significant and realistic. Now we incorporate a delay τ (COE delay) in system (5.1) to get

$$\begin{aligned}
\frac{dP}{dt} &= rP\left(1-\frac{P}{k}\right) - \frac{c_1PZ}{\gamma P^2+\alpha},\\
\frac{dZ}{dt} &= \frac{c_2PZ}{\gamma P^2+\alpha}.\frac{1+cZ(t-\tau)}{1+cZ(t-\tau)+wF} - \frac{c_3ZF}{Z+\beta} - d_1Z,\\
\frac{dF}{dt} &= \frac{c_4ZF}{Z+\beta} - d_2F,
\end{aligned} \tag{5.2}$$

and for biological reasons, we assume $P(s)=\Psi_1(s)\geq 0,\ Z(s)=\Psi_2(s)\geq 0,\ F(s)=\Psi_3(s)\geq 0,\ s\in[-\tau,0]$, and $\Psi_j(s)\in C([-\tau,0])\to R_+, (j=1,2,3)$, where C is the Banach space consisting of continuous functions. All the parameters used in systems (5.1) and (5.2) are positive and their meanings are given in Table 5.1.

Remark 5.2.1. *The per-capita growth rate of zooplankton species can be written as:*

$$PGR := \frac{c_2P}{\gamma P^2+\alpha}.\frac{1+cZ}{1+cZ+wF} - \frac{c_3F}{Z+\beta} - d_1.$$

Using the above expression for PGR of zooplankton, we depicts the simultaneous effects of fear and its carry-over effects on PGR in Fig. 5.1. From this figure, we can observe that increment in w decrease the PGR whereas increment in c increase it. Thus we can say that in the present chapter, the carry-over effect of induced fear is modeled in a way that it has only a positive influence on the prey population's per capita growth rate. This positive impact signifies the learnings and evolution through which the prey population passes while living in challenging conditions due to the fear of predation.

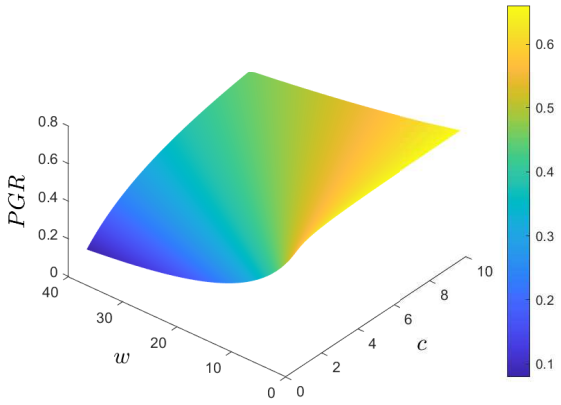

Fig. 5.1: This figure depicts the effect of fear and its carry-over effects on zooplankton's per-capita growth rate.

Parameters	Meaning	Default values	References
r	Maximum intrinsic growth rate of phytoplankton	1.5	[149]
k	Carrying capacity of supporting environment for phytoplankton	30	[127]
c_1	Rate at which zooplankton attack phytoplankton	0.9	[34]
γ	Phytoplankton's inhibitory effect against zooplankton	0.007	Selected
α	Constant of half-saturation when zooplankton consume phytoplankton	10	[130]
$c_2\ (\leq c_1)$	Zooplankton's net gain over phytoplankton	0.8	[151]
c	COE parameter	0.01	[149]
w	Fear parameter	1	[149]
c_3	Rate at which fish attacks zooplankton	0.7	[151]
β	Constant of half-saturation when fish consume zooplankton	51	Selected
d_1	Natural mortality rate of zooplankton	0.07	[131]
$c_4\ (\leq c_3)$	Fish's net gain over zooplankton	0.6	[152]
d_2	Natural mortality rate of Fish	0.08	[131]

Table 5.1: Biological significance and values for parameters which are used in system (5.1) and (5.2)

.

5.3 Dynamics of non-delayed model

5.3.1 Preliminaries

In this subsection, we provide the preliminaries like uniform boundedness and persistence of the non-delayed model to prove its well-posedness.

5.3.1.1 Uniform boundedness

Theorem 5.3.1. *All the solutions $(P(t),Z(t),F(t))$ of the model (5.1) starting in R^3_+ remain uniformly bounded in the set $\Sigma = \{(P,Z,F) \in R^3_+ : 0 \leq P+Z+F \leq \frac{(r+\nu)^2 k}{4r\nu}\}$, where $\nu = min\{d_1,d_2\}$.*

Proof. For any $P \geq 0,\ Z \geq 0$ and $F \geq 0$, we have

$$\left.\frac{dP}{dt}\right|_{P=0} = 0,\ \left.\frac{dZ}{dt}\right|_{Z=0} = 0 \text{ and } \left.\frac{dF}{dt}\right|_{F=0} = 0,$$

which means that $P = 0,\ Z = 0$ and $F = 0$ are invariant manifolds, correspondingly. Thus we can conclude that the population model (5.1) is positively invariant in R^3_+.
Now we find the invariant set in which our system remains bounded, and for this, we define a function

$$W(t) = P(t)+Z(t)+F(t).$$

Then the derivative of this equation along solutions of (5.1) gives

$$\begin{aligned}
\frac{dW}{dt} &= \frac{dP}{dt}+\frac{dZ}{dt}+\frac{dF}{dt} \\
&= rP\left(1-\frac{P}{k}\right) - \frac{c_1PZ}{\gamma P^2+\alpha} + \frac{c_2PZ}{\gamma P^2+\alpha}\cdot\frac{1+cZ}{1+cZ+wF} - \frac{c_3ZF}{Z+\beta} - d_1Z + \frac{c_4ZF}{Z+\beta} - d_2F \\
&\leq rP\left(1-\frac{P}{k}\right) + \frac{PZ}{\gamma P^2+\alpha}(-c_1+c_2) + \frac{ZF}{Z+\beta}(-c_3+c_4) - d_1Z - d_2F \\
&\leq rP\left(1-\frac{P}{k}\right) - d_1Z - d_2F.
\end{aligned}$$

Now
$\frac{dW}{dt} + \nu W \leq rP\left(1-\frac{P}{k}\right) + \nu P.$
This implies $\frac{dW}{dt} + \nu W \leq \frac{(r+\nu)^2 k}{4r}$, where $\nu = min\{d_1,d_2\}$.
Thus $\limsup_{t\to\infty} W(t) \leq \frac{(r+\nu)^2 k}{4r\nu} = M$(say), therefore all solutions of (5.1), initiating inside the

positive octant of R^3_+ are confined within the region $\Sigma = \{(P,Z,F) \in R^3_+ : 0 \leq P+Z+F \leq \frac{(r+v)^2 k}{4rv}\}$. □

5.3.1.2 Persistence

A biological system's persistence means that any species involved in its dynamics and with positive starting population density will survive and will not extinct for an extended period of time. In terms of mathematics, this means that solutions to this system that starts inside the positive octant are limited away from the coordinate planes.

Theorem 5.3.2. *System (5.1) is persistent if* $r > \frac{c_1 M}{\alpha}$, $P_m > \frac{(\gamma M^2+\alpha)(1+(c+w)M)}{c_2}(\frac{c_3 M}{\beta}+d_1)$ *and* $Z_m > \frac{d_2(M+\beta)}{c_4}$, *where* P_m, Z_m *are defined in the proof.*

Proof. From Theorem 5.3.1, we know that $\limsup_{t\to\infty}(P(t)+Z(t)+F(t)) \leq M$, thus for some $\varepsilon_1 > 0$ $\exists\, t_1 > 0$ such that $\forall\, t > t_1$, we have $P(t) < M+\varepsilon_1$, $Z(t) < M+\varepsilon_1$, $F(t) < M+\varepsilon_1$.
Now from system (5.1) we have

$$\begin{aligned}\frac{dP}{dt} &= rP\left(1-\frac{P}{k}\right) - \frac{c_1 PZ}{\gamma P^2+\alpha} \\ &\geq P\left(\left(r - \frac{c_1(M+\varepsilon_1)}{\alpha}\right) - \frac{rP}{k}\right),\end{aligned}$$

this implies $\liminf_{t\to\infty} P(t) \geq \frac{k}{r}\left(r - \frac{c_1(M+\varepsilon_1)}{\alpha}\right)$, which is true for some arbitrary $\varepsilon_1 > 0$.
So, $\liminf_{t\to\infty} P(t) \geq \frac{k}{r}\left(r - \frac{c_1 M}{\alpha}\right) =: P_m$. Thus phytoplankton species is persistent if $r > \frac{c_1 M}{\alpha}$.
Again, from (5.1)

$$\begin{aligned}\frac{dZ}{dt} &= \frac{c_2 PZ}{\gamma P^2+\alpha}.\frac{1+cZ}{1+cZ+wF} - \frac{c_3 ZF}{Z+\beta} - d_1 Z \\ &\geq Z\left(\frac{c_2 P_m}{\gamma(M+\varepsilon_1)^2+\alpha}.\frac{1+cZ}{1+(c+w)(M+\varepsilon_1)} - \frac{c_3(M+\varepsilon_1)}{\beta} - d_1\right) \\ &\geq Z\left(\frac{c_2 P_m}{(\gamma(M+\varepsilon_1)^2+\alpha)(1+(c+w)(M+\varepsilon_1))} - \frac{c_3(M+\varepsilon_1)}{\beta} - d_1 - Z\right).\end{aligned}$$

This implies $\liminf_{t\to\infty} Z(t) \geq \frac{c_2 P_m}{(\gamma(M+\varepsilon_1)^2+\alpha)(1+(c+w)(M+\varepsilon_1))} - \frac{c_3(M+\varepsilon_1)}{\beta} - d_1$, which is true for any arbitrary $\varepsilon_1 > 0$.
Thus $\liminf_{t\to\infty} Z(t) \geq \frac{c_2 P_m}{(\gamma M^2+\alpha)(1+(c+w)M)} - \frac{c_3 M}{\beta} - d_1 =: Z_m$. Hence, zooplankton population is persistent under the condition: $P_m > \frac{(\gamma M^2+\alpha)(1+(c+w)M)}{c_2}(\frac{c_3 M}{\beta}+d_1)$.

In similar manner, $\liminf_{t\to\infty} F(t) \geq \frac{c_4 Z_m}{M+\beta} - d_2 =: F_m$, which is positive if $Z_m > \frac{d_2(M+\beta)}{c_4}$. Hence, the theorem is proved.

□

Remark 5.3.1. *From the above Theorem 5.3.2, we can notice that the phytoplankton population persists if r is greater than some critical value. Persistence of zooplankton and fish population depends on the minimum values of phytoplankton and zooplankton, respectively (i.e., their respective prey). Thus we can say that the established conditions for the persistence of the population model are ecologically well behaved.*

5.3.2 Feasible equilibria and their stability analysis

5.3.2.1 Equilibrium feasibility

Model (5.1) can have at most four types of non-negative equilibrium points, which are stated below.

(i) The zero equilibrium $E_0(0,0,0)$ and zooplankton-fish free equilibrium $E_1(k,0,0)$ both exist trivially.

(ii) There can be two fish free equilibrium points $E_{21} = (P_{21}, Z_{21}, 0)$ and $E_{22} = (P_{22}, Z_{22}, 0)$ where $P_{21} = \frac{c_2+\sqrt{c_2^2-4\alpha\gamma d_1^2}}{2\gamma d_1}$, $Z_{21} = r\left(1-\frac{P_{21}}{k}\right)\frac{\gamma P_{21}^2+\alpha}{c_1}$ and $P_{22} = \frac{c_2-\sqrt{c_2^2-4\alpha\gamma d_1^2}}{2\gamma d_1}$, $Z_{22} = r\left(1-\frac{P_{22}}{k}\right)\frac{\gamma P_{22}^2+\alpha}{c_1}$. Thus fish free equilibrium exists if $P_{21} < k$, $P_{22} < k$ and $\frac{c_2}{d_1} > 2\sqrt{\alpha\gamma}$.

(iii) For coexistence equilibrium $E^*(P^*, Z^*, F^*)$, we note the following:
Z^* is given by

$$Z^* = \frac{d_2\beta}{c_4 - d_2},$$

which is positive if

$$c_4 > d_2. \tag{5.3}$$

Phytoplankton coordinate P^* of E^* is the positive root of the cubic equation

$$g(P) = \Omega_3 P^3 + \Omega_2 P^2 + \Omega_1 P + \Omega_0 = 0, \tag{5.4}$$

where

$$\Omega_3 = r\gamma \ (>0),$$
$$\Omega_2 = -r\gamma k \ (<0),$$
$$\Omega_1 = r\alpha \ (>0),$$
$$\Omega_0 = k(c_1 Z^* - r\alpha).$$

Thus (5.4) can have no, unique or multiple positive roots depending on the signs of Ω_0 and Φ, where
$\Phi = 18\Omega_3\Omega_2\Omega_1\Omega_0 - 4\Omega_2^3\Omega_0 + \Omega_2^2\Omega_1^2 - 4\Omega_3\Omega_1^3 - 27\Omega_3^2\Omega_0^2$.
Fish coordinate F^* of E^* is the positive root of quadratic equation given by

$$\Lambda_2 F^2 + \Lambda_1 F + \Lambda_0 = 0, \tag{5.5}$$

where

$$\Lambda_2 = c_3 w \ (>0),$$
$$\Lambda_1 = c_3(1+cZ^*) + d_1 w(Z^*+\beta) \ (>0),$$
$$\Lambda_0 = (1+cZ^*)(Z^*+\beta)(d_1 - \frac{c_2 P^*}{\gamma {P^*}^2+\alpha}).$$

So, (5.5) has a unique positive root if $\Lambda_0 < 0$, i.e., $d_1 < \frac{c_2 P^*}{\gamma {P^*}^2+\alpha}$ which implies that for the survival of fish population, the mortality rate of zooplankton population must be less than its numeric response over phytoplankton population. This shows the dependence of top predator over basal prey through the middle predator.

We note that for each P^*, there will be a corresponding unique F^* (for $\Lambda_0 < 0$). Using this fact, we present a theorem for existence of interior equilibrium.

Theorem 5.3.3. *The non-delayed system (5.1) can have various coexistence equilibria depending upon following conditions:*

(a) No coexistence equilibrium if $\Omega_0 > 0$ *and* $\Phi < 0$.

(b) Unique coexistence equilibrium $(P_{11}^*, Z^*, F_{11}^*)$ *if* $\Omega_0 < 0$, $\Phi < 0$ *and* $d_1 < \frac{c_2 P_{11}^*}{\gamma {P_{11}^*}^2+\alpha}$.

(c) Two coexistence equilibrium $(P_{21}^*, Z^*, F_{21}^*)$ *and* $(P_{22}^*, Z^*, F_{22}^*)$ *if* $\Omega_0 > 0$, $\Phi > 0$ *and* $d_1 < min\{\frac{c_2 P_{21}^*}{\gamma {P_{21}^*}^2+\alpha}, \frac{c_2 P_{22}^*}{\gamma {P_{22}^*}^2+\alpha}\}$.

(d) Three coexistence equilibrium $(P_{31}^*, Z^*, F_{31}^*), (P_{32}^*, Z^*, F_{32}^*)$ *and* $(P_{33}^*, Z^*, F_{33}^*)$ *if* $\Omega_0 < 0$, $\Phi > 0$ *and* $d_1 < min\{\frac{c_2 P_{31}^*}{\gamma {P_{31}^*}^2+\alpha}, \frac{c_2 P_{32}^*}{\gamma {P_{32}^*}^2+\alpha}, \frac{c_2 P_{33}^*}{\gamma {P_{33}^*}^2+\alpha}\}$.

5.3.2.2 Local stability assessment

In local stability analysis around a particular equilibrium point of a system, we evaluate the Jacobian at that point and determine the stability by checking the signs of real part of eigenvalues of this matrix. For system (5.1), local stability investigation is given below.

1. Eigenvalues of $J|_{E_0}$ (Jacobian evaluated at E_0) are r, $-d_1$ and $-d_2$, thus E_0 is a saddle point.

2. Eigenvalues of $J|_{E_1}$ are $-r$, $\frac{c_2 k}{\gamma k^2+\alpha} - d_1$ and $-d_2$, so E_1 is locally asymptotically stable $d_1 > \frac{c_2 k}{\gamma k^2+\alpha}$ otherwise a saddle point. Thus if E_1 is locally asymptotically stable, then E^* can not exist.

3. Here, we present a theorem which describes the local asymptotic stability behavior of fish free equilibrium points.

   Theorem 5.3.4. *The fish free equilibrium $E_{22} = (P_{22}, Z_{22}, 0)$ is locally asymptotically stable if the conditions $d_2 > \frac{c_4 Z_{22}}{Z_{22}+\beta}$, $\frac{r}{k} > \frac{2c_1\gamma P_{22} Z_{22}}{(\gamma P_{22}^2+\alpha)^2}$ and $P_{22} < \sqrt{\frac{\alpha}{\gamma}}$ hold whereas $E_{21} = (P_{21}, Z_{21}, 0)$ is always a saddle point whenever it exists.*

   Proof. The Jacobian matrix evaluated at fish free equilibrium E_{2i}, $i = 1, 2$, is given by:

$$J|_{E_{2i}} = \begin{bmatrix} -\frac{rP_{2i}}{k} + \frac{2c_1\gamma P_{2i}^2 Z_{2i}}{(\gamma P_{2i}^2+\alpha)^2} & \frac{-c_1 P_{2i}}{\gamma P_{2i}^2+\alpha} & 0 \\ \frac{c_2 Z_{2i}(-\gamma P_{2i}^2+\alpha)}{(\gamma P_{2i}^2+\alpha)^2} & 0 & -\frac{c_2 w P_{2i} Z_{2i}}{\gamma P_{2i}^2+\alpha} - \frac{c_3 Z^*}{Z_{2i}+\beta} \\ 0 & 0 & \frac{c_4 Z_{2i}}{Z_{2i}+\beta} - d_2 \end{bmatrix}.$$

   One eigenvalue of $J|_{E_{2i}}$ is $\frac{c_4 Z_{2i}}{Z_{2i}+\beta} - d_2$ and other two are the roots of equation

$$\Gamma^2 + A_1\Gamma + A_2 = 0, \tag{5.6}$$

   where $A_1 = \frac{rP_{2i}}{k} - \frac{2c_1\gamma P_{2i}^2 Z_{2i}}{(\gamma P_{2i}^2+\alpha)^2}$, $A_2 = \frac{c_1 c_2 P_{2i} Z_{2i}(-\gamma P_{2i}^2+\alpha)}{(\gamma P_{2i}^2+\alpha)^3}$. Using Routh-Hurwitz criterion [134], (5.6) has roots with negative real parts if $A_1 > 0$ and $A_2 > 0$. However, $A_2 > 0$ is not possible in case of E_{21}. Because in this case, $A_2 > 0$ implies $P_{21}^2 < \frac{\alpha}{\gamma}$ which means that $(c_2^2 - 4\alpha\gamma d_1^2) + c_2\sqrt{c_2^2 - 4\alpha\gamma d_1^2} < 0$, which is not true. Hence, E_{21} is always a saddle point (A_2 is negative in this case) whenever it exists while E_{22} is locally asymptotically stable if $d_2 > \frac{c_4 Z_{22}}{Z_{22}+\beta}$, $\frac{r}{k} > \frac{2c_1\gamma P_{22} Z_{22}}{(\gamma P_{22}^2+\alpha)^2}$ and $P_{22} < \sqrt{\frac{\alpha}{\gamma}}$. This completes the proof of this theorem. □

4. Now we present the conditions for asymptotic stability of interior equilibrium points. As we do not have the explicit expressions for different interior equilibria thus, we deduce the stability conditions for a general interior equilibrium point $E^*(P^*,Z^*,F^*)$.

Theorem 5.3.5. *Coexistence equilibrium E^* is locally asymptotically stable if the conditions $\sigma_2>0,\ \sigma_0>0$ and $\sigma_2\sigma_1>\sigma_0$ hold, where $\sigma_0,\ \sigma_1$ and σ_2 are defined in the proof.*

Proof. Jacobian matrix corresponding to $E^*(P^*,Z^*,F^*)$ is given by

$$J_{E^*}=\begin{bmatrix} a_{11} & a_{12} & 0\\ a_{21} & a_{22} & a_{23}\\ 0 & a_{32} & 0\end{bmatrix},$$

where $a_{11}=-\frac{rP^*}{k}+\frac{2c_1\gamma P^{*2}Z^*}{(\gamma P^{*2}+\alpha)^2},\ a_{12}=\frac{-c_1P^*}{\gamma P^{*2}+\alpha},\ a_{21}=\frac{c_2Z^*(-\gamma P^{*2}+\alpha)}{(\gamma P^{*2}+\alpha)^2}\cdot\frac{1+cZ^*}{1+cZ^*+wF^*},$
$a_{22}=\frac{c_2P^*}{\gamma P^{*2}+\alpha}\cdot\frac{wcZ^*F^*}{(1+cZ^*+wF^*)^2}+\frac{c_3Z^*F^*}{(Z^*+\beta)^2},\ a_{23}=-\frac{c_2wP^*Z^*}{\gamma P^{*2}+\alpha}\cdot\frac{1+cZ^*}{1+cZ^*+wF^*}-\frac{c_3Z^*}{Z^*+\beta},\ a_{32}=\frac{c_4\beta F^*}{(Z^*+\beta)^2}.$
The characteristic equation for J_{E^*} is

$$\Upsilon^3+\sigma_2\Upsilon^2+\sigma_1\Upsilon+\sigma_0=0, \tag{5.7}$$

where $\sigma_2=-(a_{11}+a_{22}),\ \sigma_1=a_{11}a_{22}-a_{23}a_{32}-a_{12}a_{21}$ and $\sigma_0=a_{11}a_{23}a_{32}$.

From Routh-Hurwitz criterion, roots of (5.7) have negative real parts iff $\sigma_2>0,\ \sigma_0>0$ and $\sigma_2\sigma_1>\sigma_0$. Thus, E^* is locally asymptotically stable if the conditions mentioned in the statement of this theorem hold. □

5.3.2.3 Global stability analysis

For global stability of coexistence equilibrium, first we suppose that condition in Theorem 5.3.3 (b) is satisfied so that model (5.1) has a unique positive equilibrium $E^*(P^*,Z^*,F^*)$. Thus we state the following theorem.

Theorem 5.3.6. *The unique coexistence equilibrium $E^*(P^*,Z^*,F^*)$ is globally asymptotically stable if the condition:*

$$M\left(\frac{c_1P^*}{\alpha}+\frac{c_3Z^*}{\beta}\right)+\frac{r(k+P^*)^2}{4k}+d_1Z^*+d_2F^*<$$
$$\frac{(c_1-c_2)Z_mP_m}{\gamma M^2+\alpha}+\frac{(c_3-c_4)ZmF_m}{M+\beta}+\frac{c_2P_mZ^*}{(\gamma M^2+\alpha)(1+(c+w)M)}+\frac{c_4Z_mF^*}{M+\beta}$$

holds.

Proof. For proving above theorem, we choose a Lyapunov function:

$$U = \left(P - P^* - P^* \ln\left(\frac{P}{P^*}\right)\right) + \left(Z - Z^* - Z^* \ln\left(\frac{Z}{Z^*}\right)\right) + \left(F - F^* - F^* \ln\left(\frac{F}{F^*}\right)\right).$$

Now on differentiating U with respect to solution of (5.1), we get

$$\begin{aligned}
\frac{dU}{dt} &= \frac{r}{k}(P-P^*)(k-P) - \frac{c_1 Z(P-P^*)}{\gamma P^2+\alpha} + \frac{c_2 P(Z-Z^*)}{\gamma P^2+\alpha}.\frac{1+cZ}{1+cZ+wF} - \frac{c_3 F(Z-Z^*)}{Z+\beta} - d_1(Z-Z^*) \\
&+ \frac{c_4 Z(F-F^*)}{Z+\beta} - d_2(F-F^*) \\
&\leq \frac{r}{k}(kP - P^2 - kP^* - PP^*) - \frac{c_1 ZP}{\gamma P^2+\alpha} + \frac{c_1 ZP^*}{\gamma P^2+\alpha} + \frac{c_2 PZ}{\gamma P^2+\alpha} - \frac{c_2 PZ^*}{(\gamma P^2+\alpha)(1+cZ+wF)} \\
&- \frac{c_3 FZ}{Z+\beta} + \frac{c_3 FZ^*}{Z+\beta} + d_1 Z^* + \frac{c_4 ZF}{Z+\beta} - \frac{c_4 ZF^*}{Z+\beta} + d_2 F^* \\
&\leq -\frac{r}{k}\left(P - \frac{k+P^*}{2}\right)^2 + \frac{r(k+P^*)^2}{4k} + \frac{c_1 MP^*}{\alpha} + \frac{c_3 MZ^*}{\beta} - \frac{(c_1-c_2)Z_m P_m}{\gamma M^2+\alpha} - \frac{(c_3-c_4)ZmF_m}{M+\beta} \\
&- \frac{c_2 P_m Z^*}{(\gamma M^2+\alpha)(1+(c+w)M)} - \frac{c_4 Z_m F^*}{M+\beta} - d_1 Z_m - d_2 F_m + d_1 Z^* + d_2 F^*.
\end{aligned}$$

Thus $\frac{dU}{dt} < 0$ if the condition:

$$\begin{aligned}
&M\left(\frac{c_1 P^*}{\alpha} + \frac{c_3 Z^*}{\beta}\right) + \frac{r(k+P^*)^2}{4k} + d_1 Z^* + d_2 F^* < \\
&\frac{(c_1-c_2)Z_m P_m}{\gamma M^2+\alpha} + \frac{(c_3-c_4)ZmF_m}{M+\beta} + \frac{c_2 P_m Z^*}{(\gamma M^2+\alpha)(1+(c+w)M)} + \frac{c_4 Z_m F^*}{M+\beta}
\end{aligned}$$

holds. Therefore, the non-delayed system is globally asymptotically stable if the claimed condition is true. □

5.3.3 Bifurcation analysis

5.3.3.1 Hopf bifurcation

Theorem 5.3.7. *Non-delayed model (5.1) undergoes Hopf bifurcation around E^* at $c = c^H$ if the following conditions are fulfilled:*

1. $\sigma_2(c^H)\sigma_1(c^H) - \sigma_0(c^H) = 0$,
2. $\left(\sigma_2 \frac{d\sigma_1}{dc} + \sigma_1 \frac{d\sigma_2}{dc} - \frac{d\sigma_0}{dc}\right)_{c=c^H} \neq 0.$

Proof. Here, we discuss about the Hopf-bifurcation of non-delayed model (5.1), with respect to COEs parameter c by keeping rest of the parameters fixed.

At critical value of $c = c^H$, we have

$$\sigma_2(c^H)\sigma_1(c^H) - \sigma_0(c^H) = 0. \tag{5.8}$$

At this critical value, the characteristic equation of J_{E^*}, (5.7) can be written as $(\Upsilon^2 + \sigma_1)(\Upsilon + \sigma_2) = 0$. For occurrence of Hopf bifurcation at this critical value, this equation must has a pair of purely imaginary complex roots for which we assume that $\sigma_1 > 0$ at $c = c^H$ [121]. Using Routh-Hurwitz conditions, we know that $\sigma_2 > 0$ thus (5.7) has two purely imaginary complex roots $\Upsilon_{1,2} = \pm i\sqrt{\sigma_1}$ and a negative real root $\Upsilon_3 = -\sigma_2$ at $c = c^H$. For evaluating transversality condition, we assume that the roots $\Upsilon_{1,2}$ becomes the function of c such that $\Upsilon_{1,2} = \eta_1(c) \pm i\eta_2(c)$. On substituting $\eta_1 + i\eta_2$ in (5.7), and separating real, imaginary parts, we get

$$\eta_1^3 - 3\eta_1\eta_2^2 + \sigma_2(\eta_1^2 - \eta_2^2) + \sigma_1\eta_1 + \sigma_0 = 0, \tag{5.9}$$

$$3\eta_1^2\eta_2 - \eta_2^3 + 2\sigma_2\eta_1\eta_2 + \sigma_1\eta_2 = 0. \tag{5.10}$$

As $\eta_2(c) \neq 0$ for Hopf bifurcation, thus using (5.10), we have $\eta_2^2 = 3\eta_1^2 + 2\sigma_2\eta_1 + \sigma_1$ and using this value of η_2^2 in (5.9), we get

$$8\eta_1^3 + 8\sigma_2\eta_1^2 + 2\eta_1(\sigma_2^2 + \sigma_1) + \sigma_2\sigma_1 - \sigma_0 = 0. \tag{5.11}$$

On differentiating (5.11), and using $\eta_1 = 0$, we get

$$\left[\frac{d\eta_1}{dc}\right]_{c=c^H} = -\frac{1}{2(\sigma_2^2 + \sigma_1)}\left[\sigma_1\frac{d\sigma_2}{dc} + \sigma_2\frac{d\sigma_1}{dc} - \frac{d\sigma_0}{dc}\right]_{c=c^H}.$$

So, the transversality condition is

$$\left[\sigma_1\frac{d\sigma_2}{dc} + \sigma_2\frac{d\sigma_1}{dc} - \frac{d\sigma_0}{dc}\right]_{c=c^H} \neq 0, \tag{5.12}$$

which completes the proof. □

5.3.3.2 Transcritical bifurcation

Theorem 5.3.8. *Fish free equilibrium E_{22} becomes stable through transcritical bifurcation at $d_2 = d_2^{tc} = \frac{c_4 Z_{22}}{Z_{22}+\beta}$. After this critical value of d_2, fish species goes to extinct because of which the interior equilibrium vanishes.*

Proof. At $d_2 = d_2^{tc} = \frac{c_4 Z_{22}}{Z_{22}+\beta}$, one of the eigenvalue of $J|_{E_{22}}$ becomes zero. Let $w_1 = \Big[-$

$\left[\frac{e_{23}}{e_{21}}, \frac{e_{23}e_{11}}{e_{12}e_{21}}, 1\right]^T$ and $w_2 = [0,0,1]^T$ are the eigenvectors corresponding to zero eigenvalue of $J|_{(E_{22}:d_2^{tc})}$ and $J^T|_{(E_{22}:d_2^{tc})}$, respectively, where $e_{ij}, i,j = 1,2,3$ are the entries of $J|_{(E_{22}:d_2^{tc})}$. Now let $Q(P,Z,F) = [M_1,M_2,M_3]^T$, and using Sotomayer's theorem [24], the transversality conditions for transcritical bifurcation are:

- $w_2^T Q_{d_2}(E_{22} : d_2^{tc}) = 0$,
- $w_2^T [DQ_{d_2}(E_{22} : d_2^{tc})]w_1 = -1 \neq 0$,
- $w_2^T [D^2 Q(E_{22} : d_2^{tc})(w_1,w_1)] = \frac{2e_{11}e_{23}}{e_{12}e_{21}} \cdot \frac{c_4}{(Z_{22}+\beta)^2} \neq 0$.

Therefor, all the conditions of Sotomayer's theorem are satisfied, hence system (5.1) will undergo transcritical bifurcation at $d_2 = d_2^{tc} = \frac{c_4 Z_{22}}{Z_{22}+\beta}$. □

5.4 Dynamics of delayed model

5.4.1 Local stability investigation and Hopf bifurcation

Here we discuss about local stability behavior of delayed model (5.2) about the coexistence equilibrium $E^*(P^*,Z^*,F^*)$ and evaluate the critical value of bifurcation parameter, COE delay, τ. Now let us define $P(t) = \bar{P}(t) + P^*$, $Z(t) = \bar{Z}(t) + Z^*$ and $F(t) = \bar{F}(t) + F^*$. Thus the linear form of the delayed system is

$$\frac{dW}{dt} = R_1 W(t) + R_2 W(t-\tau), \tag{5.13}$$

where

$$R_1 = \begin{bmatrix} j_{11} & j_{12} & 0 \\ j_{14} & j_{15} & j_{16} \\ 0 & j_{18} & j_{19} \end{bmatrix}, \; R_2 = \begin{bmatrix} 0 & 0 & 0 \\ 0 & j_{25} & 0 \\ 0 & 0 & 0 \end{bmatrix},$$

where

$j_{11} = -\frac{rP^*}{k} + \frac{2c_1\gamma P^{*2}Z^*}{(\gamma P^{*2}+\alpha)^2}$, $j_{12} = \frac{-c_1 P^*}{\gamma P^{*2}+\alpha}$, $j_{14} = \frac{c_2 Z^*(-\gamma P^{*2}+\alpha)}{(\gamma P^{*2}+\alpha)^2} \cdot \frac{1+cZ^*}{1+cZ^*+wF^*}$, $j_{15} = \frac{c_2 P^*}{\gamma P^{*2}+\alpha} \cdot \frac{1+cZ^*}{1+cZ^*+wF^*} - \frac{c_3\beta F^*}{(Z^*+\beta)^2} - d_1$,

$j_{16} = -\frac{c_2 w P^* Z^*}{\gamma P^{*2}+\alpha} \cdot \frac{1+cZ^*}{(1+cZ^*+wF^*)^2} - \frac{c_3 Z^*}{Z^*+\beta}$, $j_{18} = \frac{c_4\beta F^*}{(Z^*+\beta)^2}$, $j_{19} = \frac{c_4 Z^*}{Z^*+\beta} - d_2$, $j_{25} = \frac{c_2 P^* Z^*}{\gamma P^{*2}+\alpha} \cdot \frac{wcF^*}{(1+cZ^*+wF^*)^2}$,

and $W(t) = (\bar{P}(t), \bar{Z}(t), \bar{F}(t))^T$.

The variational matrix for model (5.2) at E^* is

$$J = R_1 + R_2 e^{-\lambda\tau}.$$

Thus the characteristic equation for J is

$$\lambda^3 + q_1\lambda^2 + q_2\lambda + q_3 + e^{-\lambda\tau}(q_4\lambda^2 + q_5\lambda + q_6) = 0, \tag{5.14}$$

where
$q_1 = -(j_{11} + j_{15} + j_{19})$, $q_2 = j_{15}j_{19} + j_{11}j_{19} + j_{11}j_{15} - j_{12}j_{14} - j_{16}j_{18}$, $q_3 = -j_{11}j_{15}j_{19} + j_{12}j_{14}j_{19} + j_{11}j_{16}j_{18}$, $q_4 = -j_{25}$, $q_5 = j_{25}(j_{19} + j_{11})$, $q_6 = -j_{11}j_{25}j_{19}$.
Now we can have the following cases:
Case I: When $\tau = 0$, system (5.2) reduces to system (5.1), whose stability conditions are given in subsection 5.3.2.
Case II: When $\tau \neq 0$, on substituting $\lambda = i\omega$ in (5.14), we get

$$\begin{aligned} q_5\omega\cos\omega\tau + (q_4\omega^2 - q_6)\sin\omega\tau &= \omega^3 - q_2\omega \\ (-q_4\omega^2 + q_6)\cos\omega\tau + q_5\omega\sin\omega\tau &= q_1\omega^2 - q_3, \end{aligned} \tag{5.15}$$

After squaring and adding the equations in (5.15), we have:

$$\omega^6 + (q_1^2 - 2q_2 - q_4^2)\omega^4 + (q_2^2 - 2q_1q_3 + 2q_4q_6 - q_5^2)\omega^2 + q_3^2 - q_6^2 = 0. \tag{5.16}$$

It is easy to observe that (5.16) is having at least one positive root ω if $q_3^2 - q_6^2 < 0$, substituting this ω in (5.15), we get

$$\tau_n = \frac{1}{\omega}.\arccos\left[\frac{F_1E_{11} - F_2E_{12}}{E_{11}^2 + E_{12}^2}\right] + \frac{2n\pi}{\omega},\ n = 0,1,2,3..., \tag{5.17}$$

where
$E_{11} = q_5\omega$, $E_{12} = q_4\omega^2 - q_6$, $F_1 = \omega^3 - q_2\omega$, $F_2 = q_1\omega^2 - q_3$.
For transversality condition, put $\lambda = \xi + i\omega$ in (5.14) and after separating real and imaginary parts, we get

$$\begin{aligned} &\xi^3 - 3\xi\omega^2 + q_1(\xi^2 - \omega^2) + q_2\xi + q_3 + e^{-\xi\tau_0}\cos\omega\tau_0(q_4(\xi^2 - \omega^2) + q_5\xi + q_6) \\ &+ e^{-\xi\tau_0}\sin\omega\tau_0(2q_4\xi\omega + q_5\omega) = 0, \end{aligned} \tag{5.18}$$

and

$$\begin{aligned} &-\omega^3 + 3\xi^2\omega + 2q_1\xi\omega + q_2\omega + e^{-\xi\tau_0}\cos\omega\tau_0(2q_4\xi\omega + q_5\omega) \\ &- e^{-\xi\tau_0}\sin\omega\tau_0(q_4(\xi^2 - \omega^2) + q_5\xi + q_6) = 0. \end{aligned} \tag{5.19}$$

Differentiating (5.18) and (5.19) with respect to τ and putting $\xi = 0$ provides

$$\begin{aligned} Q_1\left[\frac{d[Re(\lambda(\tau_0))]}{d\tau_0}\right] + Q_2\left[\frac{d[Im(\lambda(\tau_0))]}{d\tau_0}\right] &= R_1, \\ -Q_2\left[\frac{d[Re(\lambda(\tau_0))]}{d\tau_0}\right] + Q_1\left[\frac{d[Im(\lambda(\tau_0))]}{d\tau_0}\right] &= R_2, \end{aligned} \tag{5.20}$$

where

$Q_1 = [-3\omega^2 + q_2 + (q_5 + (q_4\omega^2 - q_6)\tau_0)\cos\omega\tau_0 + (2\omega q_4 - q_5\omega\tau_0)\sin\omega\tau_0]$,
$Q_2 = [-2\omega q_1 + (q_5 + (q_4\omega^2 - q_6)\tau_0)\sin\omega\tau_0) + (-2\omega q_4 + b_5\omega\tau_0)\cos\omega\tau_0]$,
$R_1 = [\omega(q_6 - q_4\omega^2)\sin\omega\tau_0 - q_5\omega^2\cos\omega\tau_0]$,
$R_2 = [\omega(q_6 - q_4\omega^2)\cos\omega\tau_0 + q_5\omega^2\sin\omega\tau_0]$.

From equation (5.20), we get $\left[\frac{d[Re(\lambda(\tau_0))]}{d\tau_0}\right] = \frac{R_1Q_1 - R_2Q_2}{Q_1^2 + Q_2^2}$. Thus the tranversality condition for occurrence of Hopf-bifurcation holds if $R_1Q_1 - R_2Q_2 \neq 0$. Thus, we can state the following theorem.

Theorem 5.4.1. *The delayed system is unstable (or stable) for $\tau < \tau_0$ and becomes stable (or unstable) through Hopf bifurcation at $\tau = \tau_0$ if the conditions $q_3^2 < q_6^2$ and $R_1Q_1 - R_2Q_2 < 0$ (or $R_1Q_1 - R_2Q_2 > 0$) hold simultaneously.*

5.5 Numerical work

For the purpose of numerical simulation, we have used MATLAB R2019b to draw all the figures in this manuscript. We perform the simulation experiments with the values of parameters which are provided in Table 5.1. With this set of values, the possible equilibrium points and their nature, are described in Table 5.2. From this table we can notice that for this set of parameters E_0, E_1 both are saddle points, the fish free equilibrium E_{22} is saddle point whereas a unique interior equilibrium E^* is locally asymptotically stable.

Equilibrium	Eigenvalues of corresponding Jacobian	Nature of equilibrium
$E_0(0,0,0)$	(1.5000,-0.0700,-0.0800)	Saddle point
$E_1(30,0,0)$	(-1.5000,1.4024,-0.0800)	Saddle point
$E_{22}(0.8755, 16.1890, 0)$	$(0.0646, -0.0211 \pm 0.3184i)$	Saddle point
$E^*(18.6398, 7.8462, 7.2199)$	$(-0.6300, -0.0292 \pm 0.1283i)$	LAS

Table 5.2: Possible equilibria, eigenvalues of corresponding Jacobians and nature of these equilibria for parameters from Table 5.1, where LAS stands for locally asymptotically stable.

Now we discuss the existence of multiple interior equilibria of the non-delayed system. For a set of parameters (values are given in the figure for this specific demonstration), (5.4) can have a different number of positive roots. From Fig. 5.2(a) we can see that for a particular pair of r and γ, $g(P)$ does not have a positive root, while on the variation of these two parameters, it can have one, two, or three positive roots which are evident from Figs. 5.2(b), 5.2(c) and 5.2(d), respectively. We also draw the bi-parametric existence diagram for interior equilibria in $r\gamma$-plane using Theorem 5.3.3 in Fig. 5.2(e). This Theorem divides the above plane into four different regions represented by; yellow, blue, magenta, and cyan colors accordingly with no coexistence equilibrium, one coexistence equilibrium, two coexistence equilibria, and three coexistence equilibria. The Fig. 5.2(f) portrays the number of interior equilibrium (particularly P coordinate of E^*) with their stability: green colored equilibrium is sink; red colored equilibrium is source whereas black colored equilibrium is saddle point. This attribute of change in the number of interior equilibrium points on variation of r and γ demonstrates their significance in the dynamics of the model. We also portrait the global stability for the unique coexistence equilibrium in Fig. 5.3 for the set of parameters given in Table 5.1, in which many solutions with different initial set of conditions (marked with black dots) approaches it (marked with red dot) as time passes.

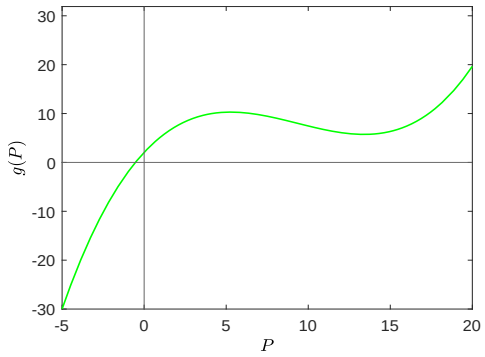

(a) $r = 0.93,\ \gamma = 0.015$.

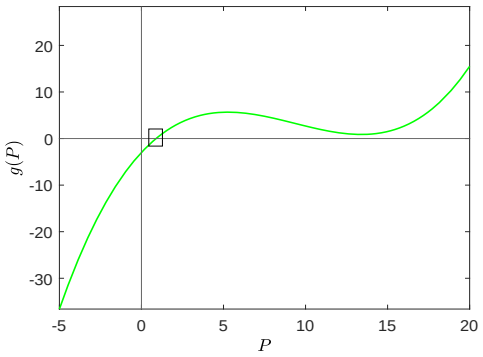

(b) $r = 1,\ \gamma = 0.015$.

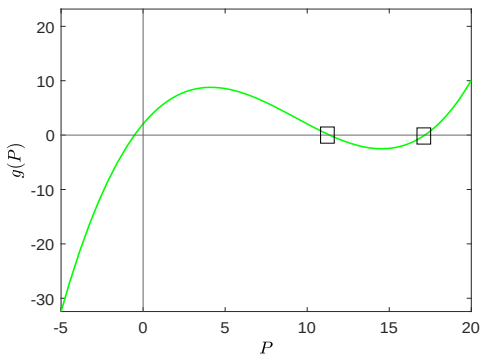

(c) $r = 0.93,\ \gamma = 0.02$.

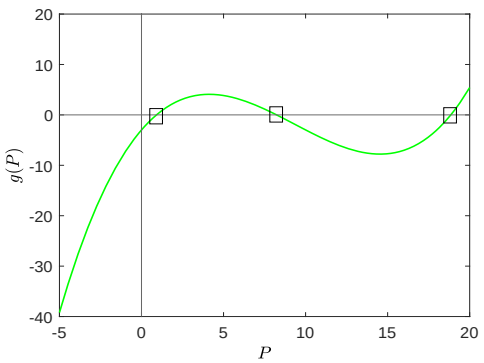

(d) $r = 1,\ \gamma = 0.02$.

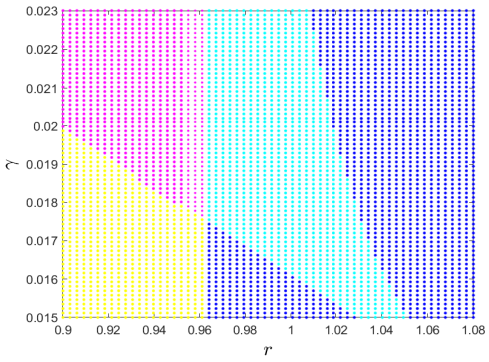

(e) Bi-parametric existence diagram for no or multiple interior equilibrium points, where yellow, blue, magenta and cyan depicts no, one, two or three interior equilibrium points, respectively.

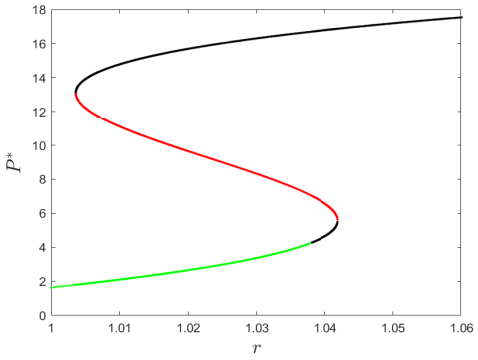

(f) r vs P^* for $\gamma = 0.016$.

Fig. 5.2: Figs. (a), (b), (c) and (d) show the non-existence and existence of multiple positive roots of $g(P)$, Fig. (e) depicts various regions in $r\gamma$-plane for different number of interior equilibrium points whereas Fig. (f) shows number of interior equilibrium with their stability; green denotes sink; red denotes source; black denotes saddle, for $\gamma = 0.016$, $k = 28$, $\alpha = 3.5$, $\beta = 22.7$, $c_4 = 0.57$ and values of remaining parameters from Table 5.1.

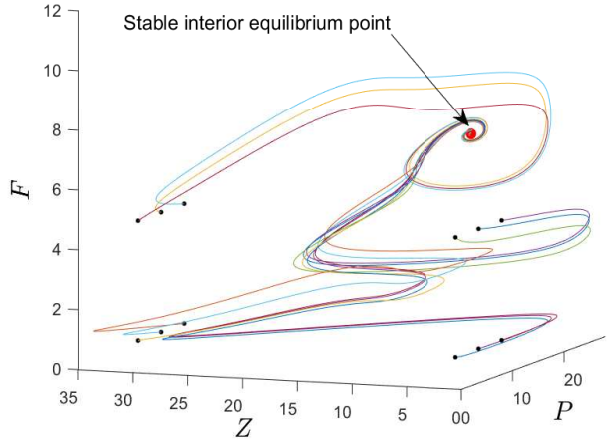

Fig. 5.3: Global stability of unique coexistence equilibrium E^* for the parameters given in Table 5.1.

From subsection 5.3.2, it is clear that phytoplankton and zooplankton coordinates (P^* and Z^*) at interior equilibrium are independent from COE parameter c whereas fish population density varies as we change c. Thus from (5.5), we get

$$F^* = \frac{-(c_3(1+cZ^*)+d_1w(Z^*+\beta))+\sqrt{(c_3(1+cZ^*)+d_1w(Z^*+\beta))^2-4c_3w(1+cZ^*)(Z^*+\beta)(d_1-\frac{c_2P^*}{\gamma P^{*2}+\alpha})}}{2c_3w}, \tag{5.21}$$

and from (5.21) we can easily get

$$\frac{dF^*}{dc} = \frac{1}{2c_3w}\left(-c_3Z^* + \frac{2(c_3(1+cZ^*)+d_1w(Z^*+\beta))c_3Z^*-4c_3wZ^*(Z^*+\beta)(d_1-\frac{c_2P^*}{\gamma P^{*2}+\alpha})}{2\sqrt{(c_3(1+cZ^*)+d_1w(Z^*+\beta))^2-4c_3w(1+cZ^*)(Z^*+\beta)(d_1-\frac{c_2P^*}{\gamma P^{*2}+\alpha})}}\right), \tag{5.22}$$

which implies

$$\lim_{c\to\infty}\frac{dF^*}{dc} = 0.$$

This implies that when parameter c tends to infinity, F^* saturates and this saturated value is given by the equation given below (obtained from (5.5))

$$\lim_{c\to\infty} F^* = -\frac{-Z^*(Z^*+\beta)(d_1-\frac{c_2P^*}{\gamma P^{*2}+\alpha})}{c_3Z^*} > 0. \tag{5.23}$$

For the set of parameters mentioned in Table 5.1, we have presented the above remark related to c in Fig. 5.4(a). This growth in fish population on the increasing parameter c can be explained; we have noticed from the formulation of our model in Section 5.2 that the carry-over effects have positive impacts on the zooplankton's PGR. Thus rising c, the per-capita growth rate of zooplankton species increases correspondingly (Fig. 5.1). As zooplankton's PGR grows, its predator fish density also amplifies in its response which is exhibited in Fig. 5.4(a).

In case of fear effect, again both phytoplankton and zooplankton coordinates of E^* are independent of fear parameter w. From equation (5.5), we have

$$\lim_{w\to\infty}\left(c_3wF^{*2}+[c_3(1+cZ^*)+(d_1w(Z^*+\beta)]F^*+(1+cZ^*)(Z^*+\beta)(d_1-\frac{c_2P^*}{\gamma P^{*2}+\alpha})\right) = 0,$$

which implies

$$\lim_{w\to\infty}\left(c_3F^{*2}+(d_1(Z^*+\beta))F^*\right) = 0,$$

thus we get

$$\lim_{w\to\infty} F^* = 0.$$

This extinction of fish species on increasing fear parameter is manifested in Fig. 5.4(b). Speaking biologically, due to increased fear of fish population, zooplankton species restrict their foraging space, which can be seen as their antipredator behavior in response to this non-lethal

effect of fish. This reduction in foraging also decreases zooplankton's predation, which correspondingly curtails fish population density. As the fish population is a specialist predator in the proposed model, thus increasing fear up to a high value leads to their extinction. The behavior of fish population on variation of both c and w simultaneously is depicted in Fig. 5.4(c). From the surface in this figure, we can observe that on increasing c, F^* increases and on increasing w, F^* decreases. These trends in fear inducing population on increasing COE parameter and fear parameters which we have observed in our investigation agree with the results presented in studie [149, 153].

About the change in stability nature of the non-delayed system as we vary c, we have presented several phase portraits in Fig. 5.5. From these figures, we can notice that the system is stable for small and large values of c, whereas we have periodic or chaotic oscillations for its intermediate values. The whole dynamics on the variation of c is also illustrated by plotting the bifurcation diagram for phytoplankton population in Fig. 5.6(a). For a better view, we have drawn the bifurcation diagrams for $c \in [0.08, 11]$, and the stable nature of the model for lower and higher values of c are depicted by the phase portraits in Figs. 5.5(a) and 5.5(f), respectively. At $c = c^H \approx 0.1064$, $\left(\sigma_2 \frac{d\sigma_1}{dc} + \sigma_1 \frac{d\sigma_2}{dc} - \frac{d\sigma_0}{dc}\right)_{c=c^H} \approx 0.0032 \neq 0$. This implies that the conditions for Hopf bifurcation (Theorem 5.3.7) are fulfilled, thus system (5.1) undergoes Hopf-bifurcation at $c = c^H \approx 0.1064$. From the bifurcation diagram, we can observe that for intermediate values of c, non-delayed system is chaotic which implies that its dynamics is very sensitive to initial conditions. These chaotic as well as periodic oscillations can be eradicated for lower and higher values of c. This implies that, for these values of c the population densities are not sensitive to their respective initial conditions and their asymptotic nature can be predicted. The amplitude of oscillations decreases as we move from chaotic regime to periodic regime, and it further decreases as we shift from a higher periodic solution to a lower periodic solution. For confirmation of the chaotic nature of the non-delayed system, we have plotted maximum Lyapunov exponent vs c graph in Fig. 5.6(b). The positive values of maximum Lyapunov exponent in this graph validates the bifurcation diagram presented in Fig. 5.6(a). We have also done the sensitivity analysis by starting two solutions (Fig. 5.7(a)) closely to each other. We observe that as time passes, these two solutions deviate from each other, showing the system's chaotic behavior. A Poincar'e map having scattered sampling points in Fig. 5.7(b), also confirms the non-delayed system's chaotic nature for $c = 4.5$.

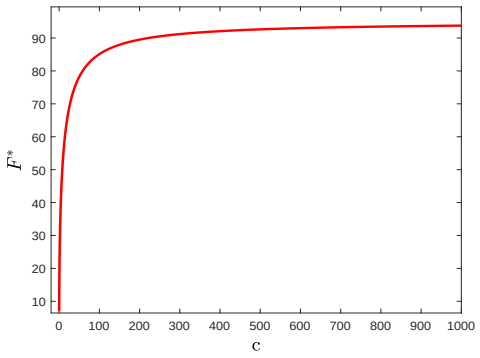

(a) ,

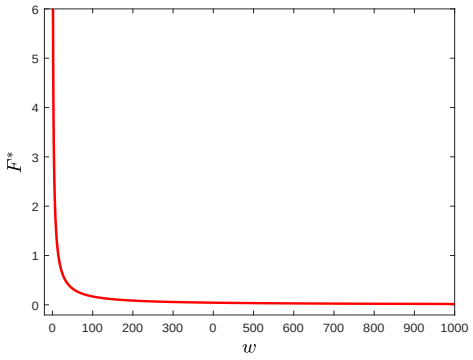

(b)

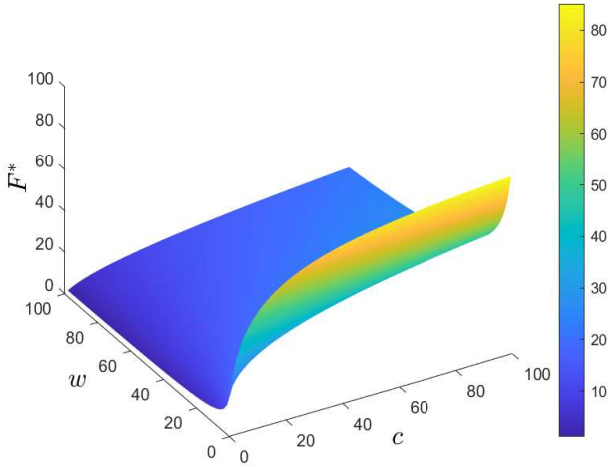

(c)

Fig. 5.4: Figs. (a) shows that F^* increases on increasing c and saturates when c is large i.e., $F^* \to 94.9495$ as $c \to \infty$, and in Fig. (b), fish species goes to extinction when $w \to \infty$, whereas Fig. (c) gives the trend of F^* in cwF^*-space, with other parameters from Table 5.1.

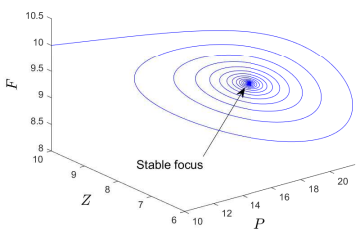

(a) $c = 0.08$

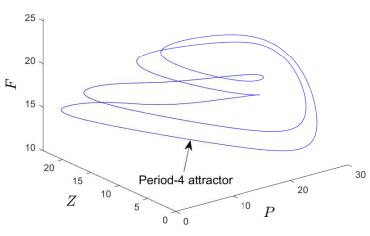

(b) $c = 1$

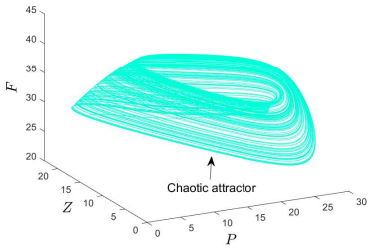

(c) $c = 4.5$

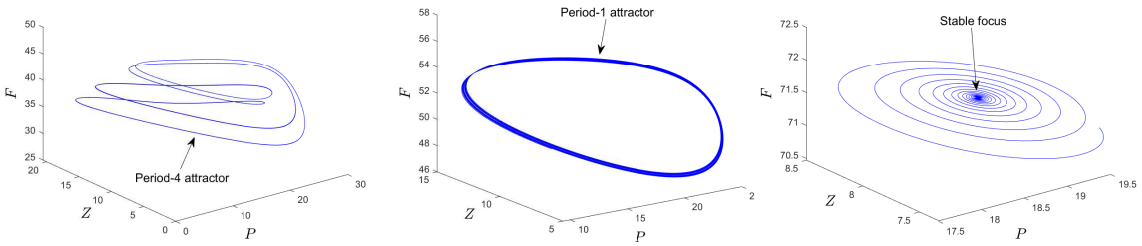

(d) $c = 6$ **(e)** $c = 11$ **(f)** $c = 30$

Fig. 5.5: Different phase portraits depicting the dynamics of the non-delayed system from stable to chaotic and again to stable on increasing the parameter c, with remaining parameters from Table 5.1.

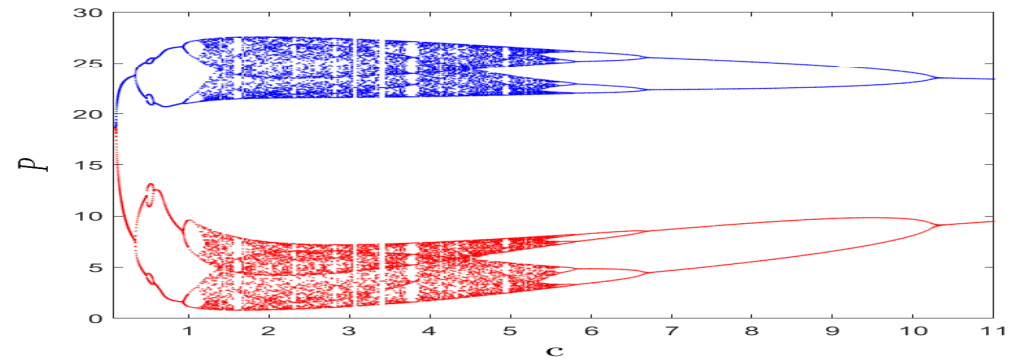

(a)

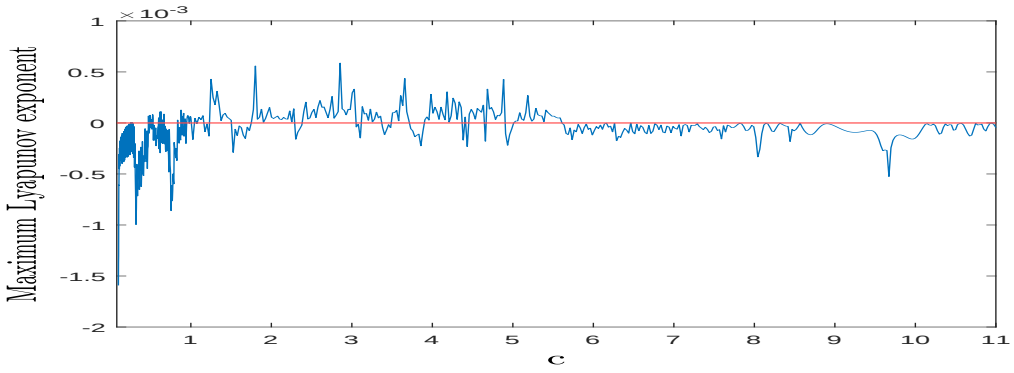

(b)

Fig. 5.6: Fig. (a) outlines the behavior of the non-delayed system by plotting P *vs* c graph whereas Fig. (b) gives maximum Lyapunov exponent on variation of c, with other parameters from Table 5.1.

The phase portrait given in Fig. 5.5(c) represents the chaotic behavior of the non-delayed system for $c = 4.5$. This chaotic behavior of the model can be controlled by decreasing the

fear parameter w, which is evident from the bifurcation diagrams given in Fig. 5.8. From these bifurcation figures, we can observe that on abating w, the chaotic oscillations are reduced to the period-8 solution, which further reduces to period-4, period-2, period-1 and finally converge to interior equilibrium.

In an ecological system, increasing the amount of available food for prey population, i.e., carrying capacity, sometimes can give rise to periodic oscillations, and this phenomenon of making the system unstable on increasing the carrying capacity is known as the paradox of enrichment [136]. There are many evidences for the occurrence of this phenomenon in the literature [55, 137]. Due to complexity, our current system also have this behavior, which is apparent from Fig. 5.9. From this figure, we can observe that the model is stable for initial values of k, but after a threshold value, it becomes unstable with a rise of period-1 solutions. In our system, we try to fix this issue by adjusting the parameter γ, which denotes phytoplankton's inhibitory effect against zooplankton due to its toxic effect (Fig.5.10(a)). From this figure, we can note that non-delayed population model (5.1) will be stable with a combination of values of k and γ from the cyan region and unstable from the black area. Thus, we can resolve this paradox in our system by decreasing γ. In a similar manner, we can eliminate the periodic oscillations by decreasing the parameter r (Fig. 5.10(b)).

Non-delayed model (5.1), undergoes transcritical bifurcation with respect to d_2. At $d_2 = d_2^{tc} = 0.1447$, $\gamma = 0.2525$ and remaining parameters from Table 5.1, fish free equilibrium E_{22} becomes stable through transcritical bifurcation. For showing this character, we have presented a phase portrait diagram (Fig. 5.11(a)) in which system is unstable for $d_2 = 0.11$ then it become stable around interior equilibrium at $d_2 = 0.13$ and on its further increase fish free equilibrium becomes stable ($d_2 = 0.145 > d_2^{tc}$). These three solutions with three different values of d_2 have same initial point. A bi-parametric bifurcation diagram in γd_2-plane is also drawn to observe this transition in Fig. 5.11(b).

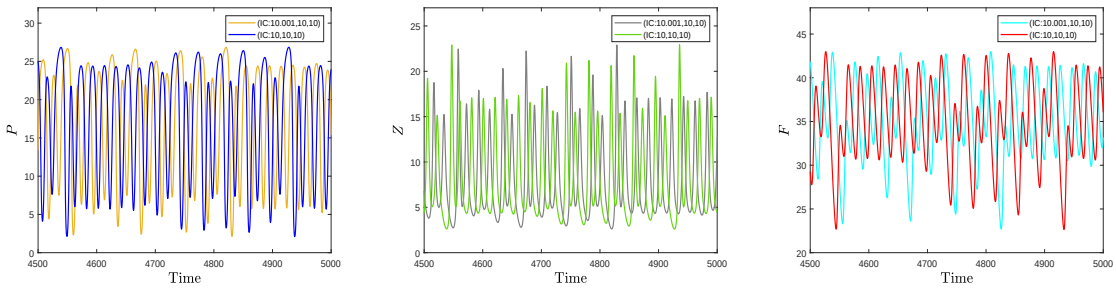

(a)

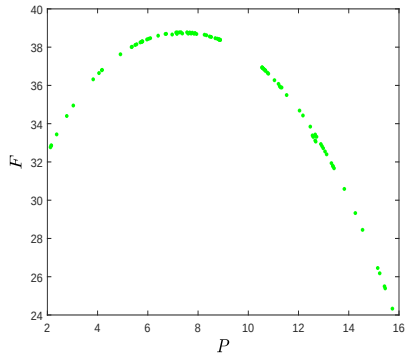

(b)

Fig. 5.7: Sensitivity of two different solutions corresponding to two different initial conditions is shown by Fig. (a) whereas Fig. (b) depicts Poincar'e map at $c = 4.5$ in PF-plane with $Z = 15$, and remaining parameters from Table 5.1.

Multistability is an attractive attribute of non-linear systems, in which it can have a number of coexisting stable attractors with the same set of parameters. The character of multistablity increases the flexibility of the corresponding model. Our non-delayed model (5.1) also shows this character, with a set of parameters (provided with figure), the system manifests bistability between a stable limit cycle and an interior equilibrium which is portrayed in Fig. 5.12(a). Both of the attractors have their respective regions of attraction; we have drawn these regions which are also known as basins of attraction, in Fig. 5.12(b). In this figure (Fig. 5.12(b)), red dots denote the initial conditions from where the solution will tend to the stable limit cycle, whereas green dots represent those initial conditions from which the solution will converge to stable interior equilibrium.

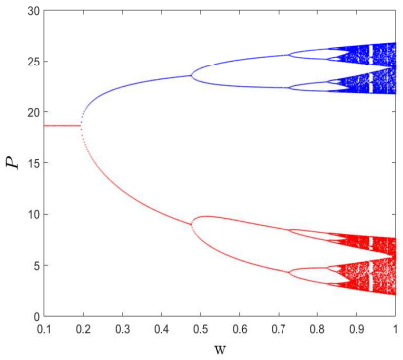

(a)

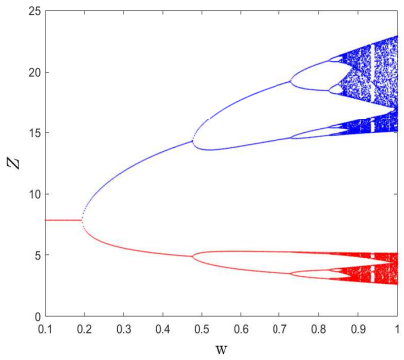

(b)

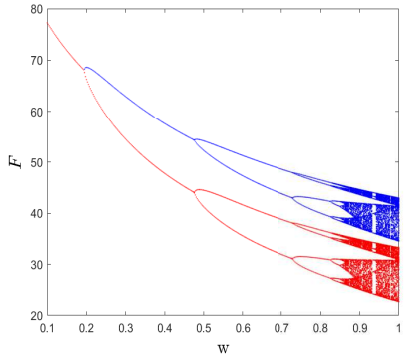

(c)

Fig. 5.8: Figs. (a), (b) and (c) show the bifurcation diagram for P, Z and F, respectively for $w \in [0.1, 1]$, $c = 4.5$, and values of remaining parameters from Table 5.1.

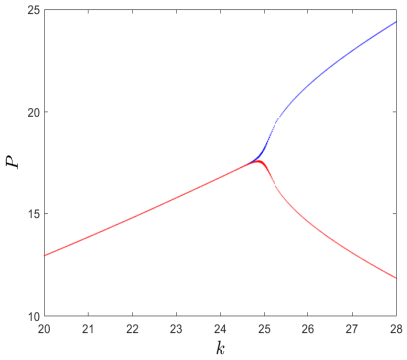

(a)

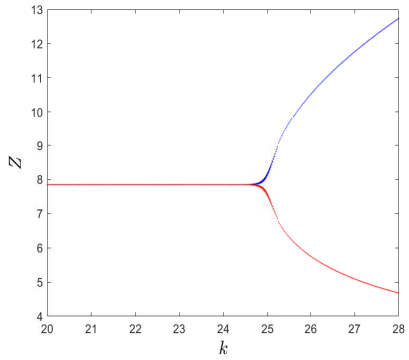

(b)

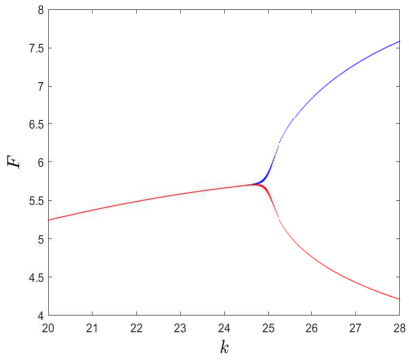

(c)

Fig. 5.9: Figs. (a), (b) and (c) demonstrate the phenomena of enrichment of paradox for system (5.1), with $\gamma = 0.02$ and values of remaining parameters from Table 5.1

.

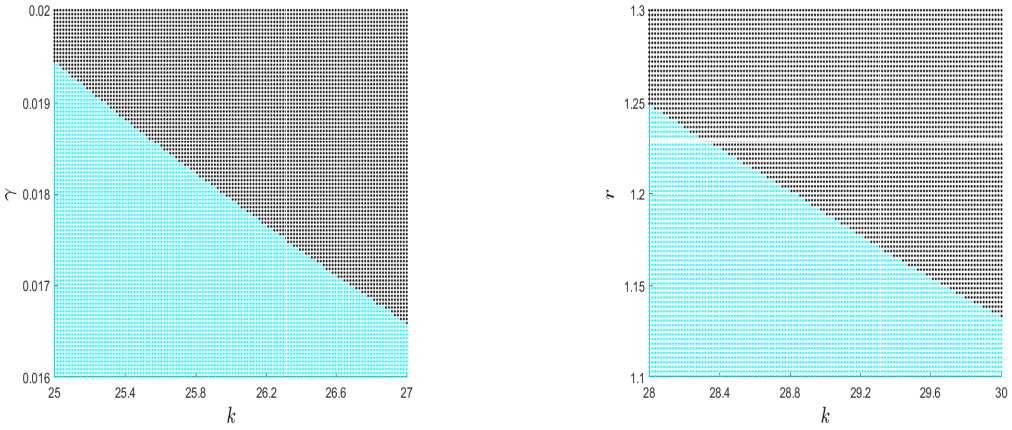

(a) **(b)**

Fig. 5.10: This figure gives biparametric bifurcation diagrams in $k\gamma-$plane (Fig. (a)), and $kr-$plane (Fig. (b)). In both the figures, the cyan-colored dot represents the combination for the stable interior equilibrium, and black for period-1 oscillations, with other parameters same as in Table 5.1.

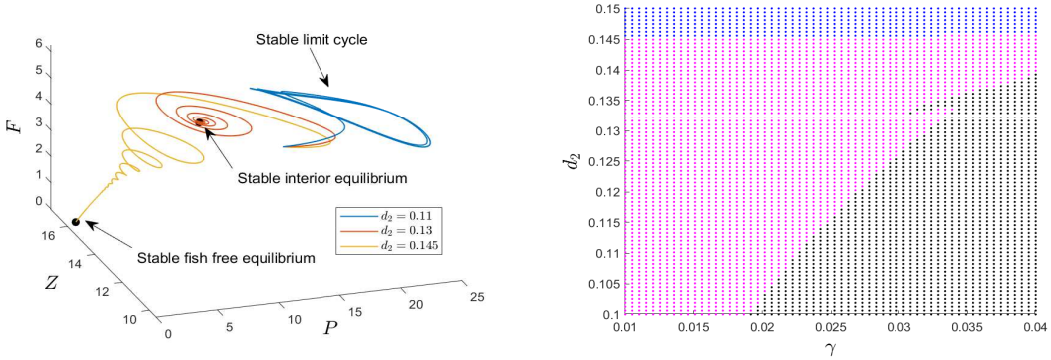

(a) **(b)**

Fig. 5.11: With $\gamma = 0.02525$ and values of remaining parameters from Table 5.1, Fig. (a) shows stable limit cycle, stable interior equilibrium point, and stable fish free equilibrium for $d_2 = 0.11, 0.13$, and 0.145, respectively. In Fig. (b) black, magenta, and blue dots represent the combinations of γ and d_2 parameters for stable limit cycle, stable interior equilibrium, and stable fish free equilibrium, respectively.

In the analysis related to delayed model, our main concern is to investigate the change in system's attitude when we introduce COE delay, τ, in the non-delayed system. For this objective we use $c = 4.5$ and the remaining parameters from Table 5.1. For these set of parameters, the non-delayed system is chaotic in nature which is illustrated in Fig. 5.5(c). Now we introduce the delay in the non-delayed model, and for a starting range of τ, system remains chaotic and on further increase of τ system's solution turn into periodic one after which it becomes chaotic once again. Now as we further increase τ, delayed system's solution becomes of finite period from infinite and finally becomes stable through period halving bifurcation (Figs. 5.13(a),

5.13(b), 5.13(c)). This happening of Hopf bifurcation and the change of system's behavior from unstable to stable with respect to delay τ is due to amplitude death (AD) phenomenon. Here, amplitude death is a situation when oscillations are eliminated when individual oscillators are coupled and return to the steady state of the system [148]. This whole event can also be verified from the analysis done in subsection 5.4.1. For the delayed model, using $c = 4.5$ and the other parameters from Table 5.1 in (5.16) and (5.17), we have the followings:

$$\omega = 0.1689,\ \tau_0 = 4.9880,\ \text{and}\ R_1Q_1 - R_2Q_2 = -0.0180 < 0.$$

As $R_1Q_1 - R_2Q_2 < 0$ which implies $\left[\frac{d[Re(\lambda(\tau_0))]}{d\tau_0}\right] < 0$, so at the critical value of $\tau = \tau_0$, the sign of real part of λ becomes negative from positive, i.e, system becomes stable after Hopf bifurcation when τ crosses its critical value. Therefore, delay induced carry-over effect can stablize our plankton-fish population model for the parameters in Table 5.1.

Like of c, the fear parameter w can also play an important role in the dynamics of the delayed model. Thus to see the combined effect of w and c on $\tau = \tau_0$, we draw a Hopf surface in $cw\tau_0$-space (Fig. 5.14). It is clear from this figure that the critical value of τ is high for combinations of greater and lower values of w and c, respectively, whereas it is low in the opposite situation.

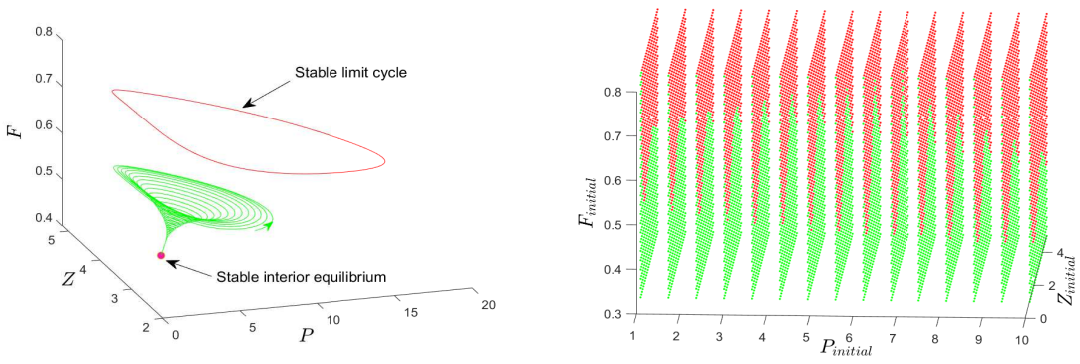

(a) **(b)**

Fig. 5.12: The phase portrait in Fig. (a) exhibits bistability whereas Fig. (b) represent their respective basins of attraction for the interior equilibrium and the stable limit cycle (red region for stable limit cycle; green region for interior equilibrium) with $P(0) \in [1,10]$, $Z(0) \in [1,5]$, $F(0) \in [0.3,0.8]$, for $r = 1.03$, $k = 28$, $\gamma = 0.016$, $\alpha = 3.5$, $w = 20$, $\beta = 22.7$, $c_4 = 0.57$ and remaining parametric values from Table 5.1.

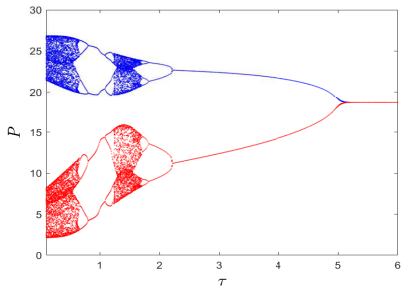

(a)

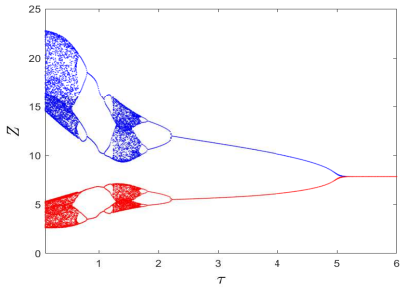

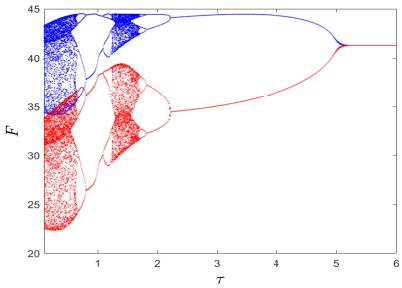

(b) **(c)**

Fig. 5.13: Figs. (a), (b) and (c) show the bifurcation diagram for P, Z and F, respectively w.r.t COE time delay τ which demonstrate transformation of chaotic system into a stable one by increasing delay τ, with $c = 4.5$ and keeping other parameters same as in Table 5.1.

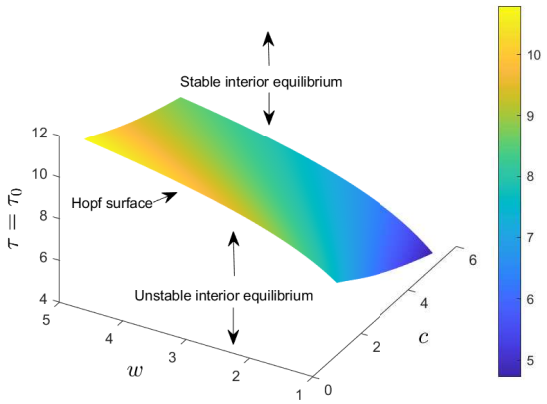

Fig. 5.14: Hopf surface in $cw\tau_0$-space, with other parameters same as in Table 5.1.

5.6 Conclusion

One of the fundamental goals of evolutionary biology is to understand the factors that influence or determine the survival and evolution of ecological species. In the literature, scientists have

mostly focused on the direct effects of predator species on prey populations in a prey-predator relationship. However, several recent studies [30, 117] have contributed to the inclusion of the predator's non-lethal influence, the induction of fear in prey-species. These non-lethal impacts are also carried over to subsequent seasons or generations [39]. In the marine ecosystem, fish generate fear in the zooplankton population in a PZF-system [114], but little attention has been paid to this form of interaction. Thus in the present chapter, we attempted to investigate the effects of fear and their carry-over effects in a PZF-system with a discrete delay.

Firstly we introduced the non-delayed and delayed PZF-population model by incorporating both the parameters related to fear and its carry-over effects with all the required assumptions. The respective PZ and ZF interplay are assumed to follow simplified Holling type IV and II functional responses. Next, in dynamical analysis, we first established the well-posedness of the non-delayed model by determining an invariant set in which the system's solution remains bounded. We also specified the conditions under which the system is persistent. Then we determined the analytical prerequisites under which the fish-free equilibrium point and a different number of coexistence equilibria exist. The presence of various interior equilibrium points is portrayed in Figs. 5.2(a), 5.2(b), 5.2(c) and 5.2(d). A bi-parametric existence diagram is also presented for these equilibrium points in Fig. 5.2(e) in $r\gamma$-plane. In stability analysis, we obtained the conditions under which the respective equilibrium points are locally asymptotically stable; this is followed by the global stability analysis of unique interior equilibrium. Further, we determine the conditions of Hopf and transcritical bifurcation with respect to c and d_2 parameters, respectively, for the non-delayed population model. Here our main objective is to investigate the individual and simultaneous effects of carry-over effect (c) and fear (w) parameters on the dynamics of the system. The phytoplankton and zooplankton coordinates of interior equilibrium are are independent of c and w parameters. For parameter c, we have proved theoretically that the fish species saturates to a finite positive value. The rise of F^* to this saturation is depicted in Fig. 5.4(a), and this growth in F^* is because of the boost in zooplankton's PGR. Unlikely c, increasing w declines F^* and causes its extinction, when we intensify w to a large value (Fig. 5.4(b)). The coexistent impact of both c and w is outlined in Fig. 5.4(c) through a three-dimension surface in cwF^*-space. For observing the change in the non-delayed population model's stability nature on the variation of c, we have presented several phase portrait diagrams in Fig. 5.5. From these phase portraits and the bifurcation diagram given in Figs. 5.5 and 5.6(a), respectively, we can notice that the non-delayed model switches its stability twice and goes through several periodic and chaotic windows before becoming stable. For confirmation of this chaos, we plotted the maximum Lyapunov exponent, did the sensitivity analysis concerning two different initial conditions, and also drew a Poincar'e map in Figs. 5.6(b), 5.7(a) and 5.7(b), respectively. The chaos in model (5.1), for intermediate values of c can be controlled by decreasing the fear parameter w, an example of this is demonstrated in

Fig. 5.8 for $c = 4.5$.

Our non-delayed system exhibits the character of enrichment of paradox (Fig. 5.9) which can be further resolved by adjusting the parameter γ or r (Fig. 5.10). Population model (5.1) suffered transcritical bifurcation with respect to parameter d_2. For demonstrating this quality of the system, we drew a phase portrait diagram and a bi-parameteric bifurcation diagram in Fig. 5.11. For a given set of parameters, our non-delayed population model showed multistability between a periodic attractor and a fixed point attractor (Fig. 5.12). Because multistability makes our model more flexible, this feature makes the dynamics of our model more interesting. As the carry-over effects are not immediate and are associated with a lag. Thus we added a COE delay τ in the non-delayed model to make it more practical and reasonable. In most of the studies [20, 130, 117], addition of delay in a model makes it unstable (periodic or chaotic) but sometimes existence of delay in an oscillatory system can make it stable by AD (amplitude death) [148]. In our model , delay τ helps to control the chaos by making it stable through AD phenomenon (Fig. 5.13). We have calculated the value of τ analytically at which the delayed system would become stable from unstable through Hopf bifurcation when it crosses this critical value. Both the parameters w and c are important parameters related to critical value of τ, thus for showing their combined impact on τ_0, we drew a Hopf surface in $cw\tau_0$-space in Fig. 5.14.

In the present chapter, we modeled the fear of fish in zooplankton species and its carry-over effects with a discrete delay in a PZF-population system. Although these non-lethal effects can also affect the death rate of prey (zooplankton) species but as the experimental evidence is not available yet for this assertion, we have not considered it. In our study, the carry-over effect parameter is modeled in such a way ($f(c,w,Z,F)$) that it always benefits the prey species, but it is not always accurate in real life. Thus, in future work, it will be exciting to formulate $f(c,w,Z,F)$ in such a way that can have negative or both positive and negative impacts on prey species' growth rate. The AD (amplitude death) phenomenon has not been studied in previous plankton-fish systems, thus we can say that this finding can also have useful implication in biological systems. Therefore, this whole discussion pictures the vigorous and noteworthy kinetics of the presented PZF-system, and we anticipate that this research will assist ecologists and biologists in formulating and investigating PZF-models in a more detailed and practical manner.

Chapter 6

A non-autonomous approach to study the impact of environmental toxins on nutrient-plankton system[1]

The study of population biology unfolds various mechanisms which operate behind the interactions among the participating species. Research areas related to population biology assist us in a significant manner to understand the biological world and various processes related to it. Plankton interplay resides at the bottom of marine food webs. These plankton's interrelationships are the particular types of predator-prey interactions. Planktons are basically of two types; one is phytoplankton which is responsible for generating a massive segment of oxygen present on earth [51], second is zooplankton which acts as a predator for the former plankton. The concentration level of nutrients (phosphorous, nitrogen, zinc, etc.) in an aquatic habitat has a crucial impact on phytoplankton's growth [154]. External supply and the decomposition of dead phytoplankton are the primary sources of these nutrients. Thus we can notice that nutrient-plankton kinetics is one of the basic dynamical processes in an aquatic medium which impacts the whole marine ecosystem.

These oceanic sources also influence the human beings as they harvests various things from these for their benefits. But as the human population is growing, they have started contaminating these aquatic habitats by dumping waste from different sources which may consist of industrial as well as household waste. Tchounwou et al. [155] studied the stage-wise movement of heavy metals (Arsenic, Cadmium, etc.) means; their environmental occurrence, generation and use, possibility to human exposure which is followed by the ways through which their toxicity affects on humen beings at molecular level. Dubey and Hussain [156] studied the impact of environmental pollution on two species models (namely, cooperation, competition, and prey-predator) in which both the populations have distinct organismal toxic concentrations. For all three models, they evaluated the criteria for local stability, instability, and global stability. They also examined the stability of system in presence of diffusion. Rana et al.[157] examined

[1] A considerable part of this chapter is published in *Applied Mathematics and Computation*, 458, 128236 (2023)

the impact of nanoparticles on a phytoplankton-zooplankton system. They assumed that when the nanoparticles of heavy metal come into the contact with cells of phytoplankton, they attach to their cells and enter into them which curtails phytoplankton's growth rate. They obtained threshold values for important parameters related to their model to get a stable kinetics. Seasonality in a biological system makes it a non-autonomous model as the seasonal parameters involved in its kinetics become the function of time. Inclusion of seasonality in a model makes it complex, and we suggest some papers [46, 47] for learning the techniques to study the permanence, periodic solution's existence, and its global attractivity. Following [157], Mandal et al. [48] studied phyroplankton-zooplankton interplay in the presence of environmental toxins and seasonality. They studied both the non-seasonal and seasonal models using the procedures given in [46, 47, 35]. They did the sensitivity and bifurcation analysis in respect to various parameters. They also studied the corresponding slow-fast model, which showed the presence of bursting oscillations.

Now, we explain the assumptions using which we formulate our system. Let's consider an aquatic ecosystem in which N is the concentration of nutrients whereas P, Z and T be the densities of phytoplankton, zooplankton and environmental toxins, respectively.

1. We consider that nutrients are continuously supplied to our system from outside at a constant rate and are also leached at the same time at a rate that is proportional to the nutrient's concentration. The dead biomass of phytoplankton also contributes to increasing nutrient concentration [158]. Nutrient concentration decreases due to their uptake by phytoplankton through Holling type II response [159], $H_1(N) = \frac{N}{l_1+N}$. The phytoplankton population is assumed to have additional food sources like bacteria and detritus, due to which it grows logistically. Thus we have the following equations.

$$\frac{dN}{dt} = N_0 - aN - \frac{mNP}{l_1+N} + \delta P, \ \frac{dP}{dt} = uP\left(1-\frac{P}{K}\right) + \frac{m_1NP}{l_1+N}.$$

2. We suppose that the zooplankton population depends on phytoplankton wholly, making zooplankton a specialist predator. The increasing density of the phytoplankton population leads to the formation of harmful algal blooms, which emit toxic chemicals, harming the zooplankton population. We assume that the zooplankton population can decrease the consumption of highly toxic phytoplankton following the modified Holling type IV interaction, $H_2(P) = \frac{P}{\alpha P^2+l_2}$ [151]. The density of the zooplankton population is assumed to be reduced by their natural mortality and crowding effect. Using these assumption, the rate of change in P and Z are given by following equations.

$$\frac{dP}{dt} = uP\left(1-\frac{P}{K}\right) + \frac{m_1NP}{l_1+N} - \frac{cPZ}{\alpha P^2+l_2}, \ \frac{dZ}{dt} = \frac{c_1PZ}{\alpha P^2+l_2} - d_1Z - d_2Z^2.$$

3. The environmental toxins (T) are added to the system with a constant supply rate, and are supposed to deplete naturally [160]. The particles of these toxins come in the touch of phytoplankton's cell membrane and reduces their growth and their capability of photosynthesis. To reflect this reduction in growth rate of phytoplankton, we use a function, $g(T,P) = \frac{u}{1+ff_1PT}$, as the phytoplankton's intrinsic growth rate [157]. Incorporating this affect of toxins on phytoplankton population, their interaction is represented by the equations given below.

$$\frac{dP}{dt} = \frac{uP}{1+ff_1PT}\left(1-\frac{P}{K}\right) + \frac{m_1NP}{l_1+N} - \frac{cPZ}{\alpha P^2+l_2}, \ \frac{dT}{dt} = A - fPT - dT.$$

Therefore, the autonomous model which we want to study is given by:

$$\begin{aligned}
\frac{dN}{dt} &= N_0 - aN - \frac{mNP}{l_1+N} + \delta P =: M_1(N,P,Z,T),\\
\frac{dP}{dt} &= \frac{uP}{1+ff_1PT}\left(1-\frac{P}{K}\right) + \frac{m_1NP}{l_1+N} - \frac{cPZ}{\alpha P^2+l_2} =: M_2(N,P,Z,T),\\
\frac{dZ}{dt} &= \frac{c_1PZ}{\alpha P^2+l_2} - d_1Z - d_2Z^2 =: M_3(N,P,Z,T),\\
\frac{dT}{dt} &= A - fPT - dT =: M_4(N,P,Z,T),
\end{aligned} \tag{6.1}$$

with $N(0)\geq 0, P(0)\geq 0, Z(0)\geq 0, T(0)\geq 0$.

In literature, most prey-predator models deal with the deterministic and unvarying environment. But most of the biological interactions proceed in highly unsteady conditions due to which physical variables like; birth rate, death rate, habitat's carrying capacity, coefficient of competition, etc., which are associated with these interactions, change significantly. Considering environmental fluctuations, our model becomes a non-autonomous model, in which physical parameters are periodic due to seasonal reasons. So taking seasonality into account, model (6.1) becomes the following model.

$$\begin{aligned}
\frac{dN(t)}{dt} &= N_0(t) - a(t)N(t) - \frac{m(t)N(t)P(t)}{l_1(t)+N(t)} + \delta(t)P(t),\\
\frac{dP(t)}{dt} &= \frac{u(t)P(t)}{1+f(t)f_1(t)P(t)T(t)}\left(1-\frac{P(t)}{K(t)}\right) + \frac{m_1(t)N(t)P(t)}{l_1(t)+N(t)} - \frac{c(t)P(t)Z(t)}{\alpha(t)P^2(t)+l_2(t)},\\
\frac{dZ(t)}{dt} &= \frac{c_1(t)P(t)Z(t)}{\alpha(t)P^2(t)+l_2(t)} - d_1(t)Z(t) - d_2(t)Z^2(t),\\
\frac{dT(t)}{dt} &= A(t) - f(t)P(t)T(t) - d(t)T(t).
\end{aligned} \tag{6.2}$$

Parameters	Meaning	Default values	References
N_0	Supply rate of nutrients to the system	0.3	[161]
a	Leaching rate of nutrients	0.03	[161, 162]
m	Rate at which nutrients are absorbed by phytoplankton	0.8	[162]
$m_1(\leq m)$	Net gain of phytoplankton over nutrients intake	0.4	[162]
l_1	Half-saturation constant for phytoplankton-nutrients interaction	15	Assumed
f	Contact rate between environmental toxin and phytoplankton	4	Assumed
f_1	Rate at which phytoplankton's growth is suppressed by environmental toxin	1	[157]
c	Rate which phytoplankton is attacked by zooplankton	0.4	Assumed
$c_1(\leq c)$	Maximum gain of zooplankton over phytoplankton	0.3	[163]
α	Phytoplankton's inhibitory effect against zooplankton	0.1	Assumed
l_2	Half-saturation constant for phytoplankton-zooplankton interaction	1	[164]
u	Maximum intrinsic growth rate for phytoplankton	2.5	[131]
K	Environmental carrying capacity for phytoplankton	20	[47]
A	Rate at which environmental toxin is added to system	7	[165]
d	Natural depletion rate of environmental toxin	0.05	[165]
δ	Rate at which phytoplankton's dead biomass gets recycled into nutrients	0.01	Assumed
d_1	Death rate of zooplankton	0.12	[162, 166]
d_2	Rate of intraspecific interference among zooplankton individuals	0.0015	[166]

Table 6.1: Biological signification and parameters' values which are employed in systems (6.1) and (6.2).

In the present chapter, we attempt to extend the model proposed by Mandal et al. [48] in which they investigated the impact of environmental toxins on phytoplankton-zooplankton interrelationship with seasonal effects. As nutrients are one of the significant feeds used by phytoplankton, and as in the modeling part, we have considered that the dead biomass of phytoplankton also contributes to nutrients back. Thus, we incorporate nutrient-phytoplankton interaction into our model to apprehend the system's dynamics in more depth. Including group defence of phytoplankton against its predator zooplankton in the form of Holling type IV response is the second main advancement in our model formulation. Therefore, this study investigates a 4-dimensional $NPZT$-model in both modes: non-seasonal as well as seasonal. We examine the dynamics of a non-seasonal system by varying some crucial parameters like f_1 and A. Both non-seasonal and seasonal models show the attribute of multistability. We also observe that including seasonality makes our system chaotic, and we provide some parametric adjustments to control it. All these features are well explained and depicted with the help of numerical simulations in the respective sections of this text.

This chapter is mainly organized in the following scheme: Section 6.1 provides the main results of autonomous model (6.1), which comprises equilibrium existence and their stability behavior and bifurcation assessment. In Section 6.2, we drive the conditions for permanence, existence, and global stability of periodic solutions for the non-autonomous model. Section 6.3 gives an extensive numerical simulation to support our theoretical results of the last sections. Lastly, Section 6.4 discusses the principal findings of our present work.

6.1 Main results for autonomous model (6.1)

Here, we discuss the dynamical features of model (6.1). It is easy to note that the RHS of (6.1) is Lipschitz continuous on a bounded subset of $\mathbb{R}^4_+$. Thus for every $(N(0),P(0),Z(0),T(0)) \in \mathbb{R}^4_+$, the current model has a unique solution.
Next, we shall determine a sub-domain of $\mathbb{R}^4_+$ in which the solutions of system (6.1) will be uniformly bounded.

Theorem 6.1.1. *Each solution $(N(t),P(t),Z(t),T(t))$ of system (6.1) with a non-negative initial condition is uniformly bounded within a set given by*

$$\mathscr{M} = \left\{(N,P,Z,T) : 0 \leq N+P+Z \leq R_1, 0 \leq T \leq R_2\right\},$$

where R_1 and R_2 are defined in the proof of this theorem.

Proof. From (6.1), it is easy to get

$$\left.\frac{dN(t)}{dt}\right|_{N=0} = N_0 > 0, \left.\frac{dP(t)}{dt}\right|_{P=0} = 0, \left.\frac{dZ(t)}{dt}\right|_{Z=0} = 0, \left.\frac{dT(t)}{dt}\right|_{T=0} = A > 0,$$

which means that $N = 0, P = 0, Z = 0, T = 0$ are positive invariant manifolds. So, any solution initiating inside the positive orthant of $NPZT$-space will not leave it.
For determining the set in which solution of (6.1) remains bounded, firstly, we define a variable $L = N+P+Z$, and for a random $\sigma > 0$, on using first three equations of system (6.1), we get

$$\frac{dL}{dt} + \sigma L \leq N_0 - (a-\sigma)N + (\delta+\sigma)P + uP\left(1-\frac{P}{K}\right) - (d_1-\sigma)Z.$$

Now, the function $F(P) = (\delta+\sigma)P + uP\left(1-\frac{P}{K}\right)$ has its global maximum $F_{max} = \frac{(u+\delta+\sigma)^2K}{4u}$ at $P = \frac{(u+\delta+\sigma)K}{2u}$. Using this property of F and choosing $\sigma \leq min\{a,d_1\}$, we obtain

$$\frac{dL}{dt} + \sigma L \leq N_0 + \frac{(u+\delta+\sigma)^2K}{4u} = M.$$

Then by using standard differential inequalities, we get

$$L(t) \leq \frac{M}{\sigma} + e^{-\sigma t}\left(L(0) - \frac{M}{\sigma}\right) \leq max\left\{\frac{M}{\sigma}, L(0)\right\} = R_1.$$

In a similar way, from the fourth equation of model (6.1), we have

$$T(t) \leq \frac{A}{d} + e^{-dt}\left(T(0) - \frac{A}{d}\right) \leq max\left\{\frac{A}{d}, T(0)\right\} = R_2.$$

Hence, we can say that all the solutions of system (6.1) are bounded above. □

6.1.1 Equilibrium assessment

System (6.1) have the following three feasible equilibria.

1. The phytoplankton-zooplankton free equilibrium is $E_1(\frac{N_0}{a},0,0,\frac{A}{d})$ and it exists trivially.

2. The zooplankton free equilibrium is $E_2(\bar{N},\bar{P},0,\bar{T})$, where $\bar{N}$ is the positive root of

$$a\bar{N}^2+(al_1+m\bar{P}-N_0-\delta\bar{P})\bar{N}-l_1(\delta\bar{P}+N_0)=0, \tag{6.3}$$

$$\bar{T}=\frac{A}{d+f\bar{P}},$$

and $\bar{P}$ is the positive root of the equation

$$Q(\bar{P})=\frac{u}{1+ff_1\bar{T}\bar{P}}\left(1-\frac{\bar{P}}{K}\right)+\frac{m_1\bar{N}}{l_1+\bar{N}}=0. \tag{6.4}$$

Now, $Q(K)=\frac{m_1\bar{N}}{l_1+\bar{N}}>0$, where $\bar{N}$ is the positive root of (6.3) for $\bar{P}=K$, and we can note that $\bar{P}\to\infty \implies Q(\bar{P})\to-\infty$. Thus we can say that $Q(\bar{P})$ will have at least one zero in (K,∞), which establishes the existence of E_2.

3. For the coexistence equilibrium $E^*(N^*,P^*,Z^*,T^*)$, we have

$$N^*=\frac{(N_0+\delta P^*-mP^*-al_1)+\sqrt{(N_0+\delta P^*-mP^*-al_1)^2+4al_1(N_0+\delta P^*)}}{2a}=U_1(P^*),$$
$$T^*=\frac{A}{d+fP^*}=U_2(P^*),$$
$$Z^*=\left(\frac{u}{1+ff_1P^*U_2(P^*)}\left(1-\frac{P^*}{K}\right)+\frac{m_1U_1(P^*)}{l_1+U_1(P^*)}\right)\frac{(l_2+\alpha P^{*2})}{c}=U_3(P^*),$$

and P^* is the positive root of equation

$$U(P)=\frac{c_1P}{\alpha P^2+l_2}-d_1-d_2U_3(P)=0. \tag{6.5}$$

As it is not easy to check the behaviour of (6.5) analytically, thus we plot $U(p)$ in Fig. 6.1 with the set of parameters given in Table 6.1. From this figure, it can be noticed that (6.5) has a unique root for these parameters.

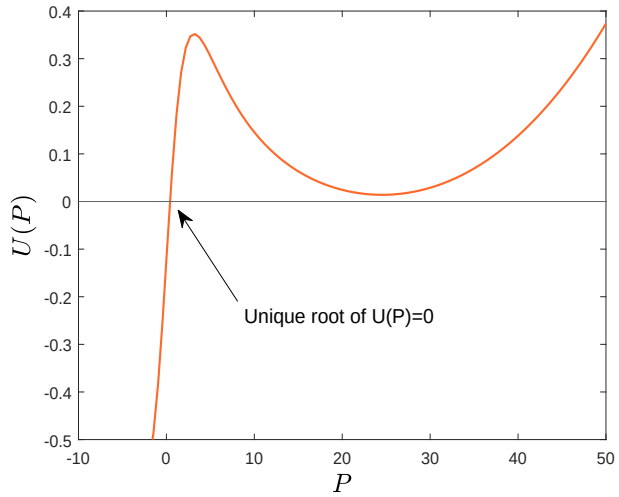

Fig. 6.1: Existence of unique root of $U(P) = 0$ with parameters from Table 6.1.

6.1.2 Stability analysis

For local stability analysis of model (6.1) about the possible equilibria, we present the following theorem.

Theorem 6.1.2.

1. *The phytoplankton-zooplankton free equilibrium,* $E_1(\frac{N_0}{a}, 0, 0, \frac{A}{d})$ *is always a saddle point.*

2. *The zooplankton free equilibrium,* $E_2(\bar{N}, \bar{P}, 0, \bar{T})$ *is stable if*

$$\frac{c_1 \bar{P}}{\alpha \bar{P}^2 + l_2} < d_1, A_1 > 0, A_3 > 0, A_1 A_2 - A_3 > 0, \tag{6.6}$$

   where $A_i (i = 1,2,3)$ *are specified in proof.*

3. *The coexistence equilibrium,* $E^*(N^*, P^*, Z^*, T^*)$ *(if exists) is locally asymptotically stable iff*

$$B_1 > 0, B_2 > 0, B_3 > 0, B_4 > 0, B_3(B_1 B_2 - B_3) - B_1^2 B_4 > 0, \tag{6.7}$$

   where $B_i (i = 1,2,3)$ *are specified in proof.*

Proof. The variational matrix for system (6.1) is given as $J = [J_{pq}]_{4\times4}$, where

$$J_{11} = -a - \frac{mPl_1}{(l_1+N)^2}, J_{12} = -\frac{mN}{l_1+N} + \delta, J_{13} = 0, J_{14} = 0, J_{21} = \frac{m_1Pl_1}{(l_1+N)^2}$$
$$J_{22} = \frac{u}{1+ff_1PT}\Big(1-\frac{P}{K}\Big) - \frac{uP}{K(1+ff_1PT)} - uP\Big(1-\frac{P}{K}\Big)\frac{ff_1T}{(1+ff_1PT)^2} + \frac{m_1N}{l_1+N} + \frac{cZ(\alpha P^2-l_2)}{(\alpha P^2+l_2)^2}$$
$$J_{23} = -\frac{cP}{\alpha P^2+l_2}, J_{24} = -uP\Big(1-\frac{P}{K}\Big)\frac{ff_1P}{(1+ff_1PT)^2}, J_{31} = 0, J_{32} = \frac{c_1Z(l_2-\alpha P^2)}{(\alpha P^2+l_2)^2}$$
$$J_{33} = \frac{c_1P}{\alpha P^2+l_2} - d_1 - 2d_2Z, J_{34} = 0,$$
$$J_{41} = 0, J_{42} = -fT, J_{43} = 0, J_{44} = -fP - d.$$

1. Eigenvalues of variational matrix J_{E_1} are $-a, u+\frac{m_1N_0}{al_1+N_0}, -d_1$ and $-d$. Thus the presence of a positive eigenvalue of J_{E_1} makes E_1 as a saddle point.

2. The characteristic equation of $J_{E_2} = [c_{pq}]_{4\times4}$ is

$$(\lambda - c_{33})(\lambda^3 + A_1\lambda^2 + A_2\lambda + A_3) = 0, \tag{6.8}$$

where

$$A_1 = -(c_{11}+c_{22}+c_{44}), A_2 = c_{11}c_{22} - c_{12}c_{21} + c_{11}c_{44} + c_{22}c_{44} - c_{24}c_{42},$$
$$A_3 = c_{11}c_{24}c_{42} - c_{11}c_{22}c_{44} + c_{12}c_{21}c_{44}$$

with the entries c_{pq} given by

$$c_{11} = -a - \frac{m\bar{P}l_1}{(l_1+\bar{N})^2}, c_{12} = -\frac{m\bar{N}}{l_1+\bar{N}} + \delta, c_{13} = c_{14} = 0, c_{21} = \frac{m_1\bar{P}l_1}{(l_1+\bar{N})^2},$$
$$c_{22} = -\frac{u\bar{P}}{K(1+ff_1\bar{P}\bar{T})} - u\bar{P}\Big(1-\frac{\bar{P}}{K}\Big)\frac{ff_1\bar{T}}{(1+ff_1\bar{P}\bar{T})^2}, c_{23} = -\frac{c\bar{P}}{\alpha\bar{P}^2+l_2},$$
$$c_{24} = -u\bar{P}\Big(1-\frac{\bar{P}}{K}\Big)\frac{ff_1\bar{P}}{(1+ff_1\bar{P}\bar{T})^2}, c_{31} = c_{32} = 0, c_{33} = \frac{c_1\bar{P}}{\alpha\bar{P}^2+l_2} - d_1,$$
$$c_{34} = c_{41} = 0, c_{42} = -f\bar{T}, c_{43} = 0, c_{44} = -f\bar{P} - d.$$

Using Routh-Hurwitz criterion on (6.8), E_2 is stable iff conditions given in (6.6) holds.

3. For interior equilibrium E^*, the entries of the variation matrix $J_{E^*} = [a_{pq}]_{4\times 4}$ are given as

$$a_{11} = -a - \frac{mP^*l_1}{(l_1+N^*)^2}, a_{12} = -\frac{mN^*}{l_1+N^*} + \delta, a_{13} = a_{14} = 0, a_{21} = \frac{m_1P^*l_1}{(l_1+N^*)^2},$$
$$a_{22} = -\frac{uP^*}{K(1+ff_1P^*T^*)} - uP^*\left(1-\frac{P^*}{K}\right)\frac{ff_1T^*}{(1+ff_1P^*T^*)^2} + \frac{2\alpha cZ^*P^{*2}}{(\alpha P^{*2}+l_2)^2},$$
$$a_{23} = -\frac{cP^*}{\alpha P^{*2}+l_2}, a_{24} = -uP^*\left(1-\frac{P^*}{K}\right)\frac{ff_1P^*}{(1+ff_1P^*T^*)^2}, a_{31} = 0, a_{32} = \frac{c_1Z^*(l_2-\alpha P^{*2})}{(\alpha P^{*2}+l_2)^2},$$
$$a_{33} = -d_2Z^*, a_{34} = a_{41} = 0, a_{42} = -fT^*, a_{43} = 0, a_{44} = -fP^* - d.$$

The characteristic equation for $[a_{pq}]_{4\times 4}$ is

$$\lambda^4 + B_1\lambda^3 + B_2\lambda^2 + B_3\lambda + B_4 = 0, \tag{6.9}$$

where

$$B_1 = -(a_{11}+a_{22}+a_{33}+a_{44}),$$
$$B_2 = a_{11}(a_{33}+a_{44}) + a_{22}(a_{11}+a_{33}) + a_{44}(a_{22}+a_{33}) - a_{12}a_{21} - a_{23}a_{32} - a_{24}a_{42},$$
$$B_3 = (a_{23}a_{32} - a_{22}a_{33})(a_{11}+a_{44}) + a_{24}a_{42}(a_{11}+a_{33}) + a_{12}a_{21}(a_{33}+a_{44}) - a_{11}a_{44}(a_{22}+a_{33}),$$
$$B_4 = -a_{44}(a_{11}a_{23}a_{32} + a_{12}a_{21}a_{33}) + a_{11}a_{33}(a_{22}a_{44} - a_{24}a_{42}).$$

Thus using Routh-Hurwitz criterion, E^* is stable if conditions given in (6.7) are satisfied.

□

6.1.3 Occurrence of Hopf bifurcation

Here, we prove the existence of Hopf bifurcation about the interior equilibrium E^*, choosing the rate at which environmental toxin is added to system, A, as the bifurcation parameter with keeping all other parameters fixed. For this, we have the following theorem.

Theorem 6.1.3.
The interior equilibrium $E^*(N^*,P^*,Z^*,T^*)$ goes through Hopf bifurcation as the parameter A passes its critical value A^h. Let $\Gamma : (0,\infty) \to R$ be the following continuously differentiable function of A

$$\Gamma(A) = B_1(A)B_2(A)B_3(A) - B_3^2(A) - B_4(A)B_1^2(A).$$

The system (6.1) suffers Hopf bifurcation if the following conditions are satisfied

1. $\Gamma(A^h) = 0$,

2. $B_1(A^h) > 0, B_2(A^h) > 0, B_3(A^h) > 0, B_4(A^h) > 0$,

3. $[B_1^2(B_1B_4 - B_2'B_3) - (B_1B_2 - 2B_3)(B_1B_3' - B_1'B_3)]|_{(A^h)} \neq 0$.

Proof. From $\Gamma(A^h) = 0$, (6.9) can be reduced to

$$\left(\lambda^2 + \frac{B_3(A^h)}{B_1(A^h)}\right)\left(\lambda^2 + B_1(A^h)\lambda + \frac{B_1(A^h)B_4(A^h)}{B_3(A^h)}\right) = 0. \tag{6.10}$$

Let $\lambda_i's, i = 1-4$ are the roots of above equation, and λ_1, λ_2 are its purely imaginary roots for $A = A^h$. Then we have

$$\lambda_3 + \lambda_4 = -B_1(A^h), \tag{6.11}$$

$$\chi_0^2 + \lambda_3\lambda_4 = B_2(A^h), \tag{6.12}$$

$$\chi_0^2(\lambda_3 + \lambda_4) = -B_3(A^h), \tag{6.13}$$

$$\chi_0^2\lambda_3\lambda_4 = B_4(A^h), \tag{6.14}$$

where $\chi_0 = img(\lambda_1(A^h)) = \sqrt{\frac{B_3(A^h)}{B_1(A^h)}}$ (using (6.11) and (6.13)). Now, there are two cases for the nature of λ_3 and λ_4. In first case, if both are complex conjugate, then from (6.11), we have $2Re(\lambda_3) = -B_1(A^h)$; in second case, if both are real, then from (6.14), both must be of same sign, and using this fact in (6.11), we infer that both should be negative. Thus in both the cases, we get $Re(\lambda_3) < 0$ and $Re(\lambda_4) < 0$.

To conclude the proof, we discuss the transversality condition. let $\lambda_{1,2} = \xi(A) \pm i\eta(A)$ is the general form of of λ_1 and λ_2 in an $\varepsilon-$ neighborhood of A^h. Substitution of $\lambda = \xi(A) \pm i\eta(A)$ into (6.9) and calculation of derivative with respect to A give us

$$L_1(A)\xi'(A) - L_2(A)\eta'(A) + L_3(A) = 0, \tag{6.15}$$

$$L_2(A)\xi'(A) + L_1(A)\eta'(A) + L_4(A) = 0, \tag{6.16}$$

where

$$\begin{aligned}
L_1(A) &= 4\xi^3 - 12\xi\eta^2 + 3(\xi^2 - \eta^2)B_1(A) + 2\xi B_2(A) + B_3(A),\\
L_2(A) &= 12\xi^2\eta - 4\eta^3 + 6\xi\eta B_1(A) + 2\eta B_2(A),\\
L_3(A) &= \xi^3 B_1'(A) - 3\xi\eta^2 B_1'(A) + (\xi^2 - \eta^2)B_2'(A) + \xi B_3'(A) + B_4'(A),\\
L_4(A) &= 3\xi^2\eta B_1'(A) - \eta^3 B_1'(A) + 2\xi\eta B_2'(A) + \eta B_3'(A).
\end{aligned}$$

At $A = A^h$, we get

$$L_1(A^h) = -2B_3(A^h), L_2(A^h) = 2\sqrt{\frac{B_3(A^h)}{B_1(A^h)}}\left(B_2(A^h) - \frac{2B_3(A^h)}{B_1(A^h)}\right),$$

$$L_3(A^h) = B_4'(A^h) - \frac{B_2'(A^h)B_3(A^h)}{B_1(A^h)}, L_4(A^h) = \sqrt{\frac{B_3(A^h)}{B_1(A^h)}}\left(B_3'(A^h) - \frac{B_1'(A^h)B_3(A^h)}{B_1(A^h)}\right).$$

Solving (6.15) and (6.16) for ξ', we get

$$\begin{aligned}\frac{d}{dA}(Re\lambda_i(A))|_{A=A^h} &= -\frac{L_2(A^h)L_4(A^h) + L_1(A^h)L_3(A^h)}{L_1^2(A^h) + L_2^2(A^h)}, \\ &= \frac{B_1^2(B_1B_4' - B_2'B_3) - (B_1B_2 - 2B_3)(B_1B_3' - B_1'B_3)}{2B_1^3B_3 + 2(B_1B_2 - 2B_3)^2}\Big|_{A=A^h} \neq 0,\end{aligned}$$

which defines the transversality condition for Hopf bifurcation for system (6.1). Thus if the conditions provided in the statement of theorem hold, then the non-seasonal model undergoes Hopf bifurcation, hence the proof. □

6.2 Main results for non-autonomous model

For the study of seasonal model (6.2), all the parameters in this model are assumed to be positive, continuous and bounded. If $f(t)$ is a continuous function of period ω, then we denote

$$f^g = \sup_{t\in\mathbb{R}} f(t), \; f^l = \inf_{t\in\mathbb{R}} f(t).$$

6.2.1 Permanence of non-autonomous system

Here, we determine an invariant set for system (6.2) and the positivity of infimums of all four populations of our model directly promotes its permanence.

Theorem 6.2.1. *Both the positive and non-negative cones of $\mathbb{R}^4$ are positively invariant for system (6.2). Let $m_j^0 > 0, \; j = 1,2,3,4$. Then*

$$\Theta_\varepsilon = \left\{(N,P,Z,T) \in \mathbb{R}^4 | m_1^\varepsilon < N(t) < M_1^\varepsilon, m_2^\varepsilon < P(t) < M_2^\varepsilon, m_3^\varepsilon < Z(t) < M_3^\varepsilon, m_4^\varepsilon < T(t) < M_4^\varepsilon\right\}$$

is an eventually bounded region for system (6.2), where $\varepsilon > 0$ is enough small with

$$M_1^\varepsilon = \frac{N_0^g + \delta^g M_2^\varepsilon}{a^l}, \; M_2^\varepsilon = \frac{K^g}{u^l}(u^g + m_1^g) + \varepsilon, \; M_3^\varepsilon = \frac{c_1^g M_2^\varepsilon}{d_2^l l_2^l}, \; M_4^\varepsilon = \frac{A^g}{d^l} + \varepsilon,$$

$$m_1^\varepsilon = \frac{N_0^l}{\alpha^g + \frac{m^u M_2^\varepsilon}{l_1^l}},\ m_2^\varepsilon = \frac{K^l}{u^g}\left(\frac{u^l}{(1+f^g f_1^g M_2^\varepsilon M_4^\varepsilon)} - \frac{c^g M_3^\varepsilon}{l_2^l}\right) - \varepsilon,$$

$$m_3^\varepsilon = \frac{1}{d_2^g}\left(\frac{c_1^l m_2^\varepsilon}{\alpha^g M_2^{\varepsilon 2} + l_2^g} - d_1^g\right),\ m_4^\varepsilon = \frac{A^l}{f^g M_2^\varepsilon + d^g}.$$

Proof. It is easy to prove the positivity of system (6.2) thus we omit it. Now, the solution for the equation

$$x'(t) = g(t,s)x(t)(b-x(t)),\ b \neq 0 \text{ is } x(t) = \frac{bx(0)\exp\left\{\int_0^t bg(s,x(s))ds\right\}}{x(0)\left[\exp\left\{\int_0^t bg(s,x(s))ds\right\} - 1\right] + b}.$$

From the second equation of (6.2), we get

$$\frac{dP}{dt} \leq u(t)P(t)\left(1 - \frac{P(t)}{K(t)}\right) + m_1 P(t),$$

which implies

$$\frac{dP}{dt} \leq \frac{u^l}{K^g}P(t)\left(\frac{K^g}{u^l}(u^g + m_1^g) - P(t)\right).$$

Thus

$$P(t) \leq \frac{M_2^0 P(0)\exp((u^g + m_1^g)t)}{P(0)[\exp((u^g + m_1^g)t) - 1] + M_2^0} \leq \frac{M_2^\varepsilon P(0)\exp((u^g + m_1^g)t)}{P(0)[\exp((u^g + m_1^g)t) - 1] + M_2^\varepsilon} \leq M_2^\varepsilon.$$

From the first equation of (6.2)

$$\frac{dN}{dt} \leq N_0(t) - a(t)N(t) + \delta(t)M_2^\varepsilon,$$

$$\leq N_0^g + \delta^g M_2^\varepsilon - a^l N(t).$$

Thus

$$N(t) \leq \frac{N_0^g + \delta^g M_2^\varepsilon}{a^l} = M_1^\varepsilon.$$

From the third equation of (6.2), we get

$$\frac{dZ}{dt} \leq \frac{c_1(t)P(t)Z(t)}{l_2(t)} - d_2(t)Z^2(t),$$

which implies

$$\frac{dZ}{dt} \leq d_2^l Z(t)\left[\frac{c_1^g M_2^\varepsilon}{d_2^l l_2^l} - Z(t)\right].$$

Therefore, it follows

$$Z(t) \leq \frac{M_3^{\varepsilon} Z(0) \exp\left(\frac{c_1^g M_2^{\varepsilon}}{l_2^l}\right) t}{Z_0\left[\exp\left(\frac{c_1^g M_2^{\varepsilon}}{l_2^l}\right) t - 1\right] + M_3^{\varepsilon}} \leq M_3^{\varepsilon}.$$

Now, from fourth equation of (6.2), we get

$$\frac{dT}{dt} \leq A^g - d^l T(t).$$

Hence, it gives

$$T(t) \leq \frac{A^g}{d^l} \leq \frac{A^g}{d^l} + \varepsilon = M_4^{\varepsilon}.$$

In the similar manner, from the first equation of (6.2)

$$\frac{dN}{dt} \geq N_0^l - \left(\alpha^g + \frac{m^g M_2^{\varepsilon}}{l_1^l}\right) N(t).$$

Hence, it gives

$$N(t) \geq \frac{N_0^l}{\alpha^g + \frac{m^g M_2^{\varepsilon}}{l_1^l}} = m_1^{\varepsilon}.$$

Now, again from the second equation of (6.2)

$$\frac{dP}{dt} \geq \left(\frac{u^l}{1 + f^g f_1^g M_2^{\varepsilon} M_4^{\varepsilon}} - \frac{c^g M_3^{\varepsilon}}{l_2^l}\right) P(t) - \frac{u^g P(t)^2}{K^l},$$

which yields

$$\frac{dP}{dt} \geq \frac{u^g}{K^l} P(t) \left(\frac{u^l K^l}{u^g (1 + f^g f_1^g M_2^{\varepsilon} M_4^{\varepsilon})} - \frac{K^l c^g M_3^{\varepsilon}}{u^g l_2^l} - P(t)\right).$$

Thus

$$P(t) \geq \frac{m_2^0 P(0) \exp\left(\frac{u^g m_1^0 t}{K^l}\right)}{P_0\left[\exp\left(\frac{u^g m_2^0 t}{K^l}\right) - 1\right] + m_2^0} \geq m_2^0 \geq m_2^{\varepsilon}.$$

Now, from the third equation

$$\frac{dZ}{dt} \geq d_2^g Z(t) \left(\left(\frac{c_1^l m_2^{\varepsilon} Z(t)}{\alpha^g M_2^{\varepsilon 2} + l_2^g} - d_1^g\right) \frac{1}{d_2^g} - Z(t)\right),$$

which gives

$$Z(t) \geq \frac{m_3^{\varepsilon} Z(0) \exp(d_2^g m_3^{\varepsilon} t)}{Z(0)[\exp(d_2^g m_3^{\varepsilon} t) - 1] + m_3^{\varepsilon}} \geq m_3^{\varepsilon}.$$

Lastly, doing the same type of calculation, we can get

$$T(t) \geq \frac{A^l}{f^g M_2^{\varepsilon g} + d^g} = m_4^{\varepsilon}.$$

Hence, Θ_ε is a positively invariant for system (6.2) and the theorem follows. □

6.2.2 Periodic solution's existence

In this subsection, we establish the existence of a periodic solution for our system (6.2) using Lemma (1.5.2).

Theorem 6.2.2. *Model (6.2) has at least one positive ω-periodic solution if the operator equation*

$$RWy = 0 \tag{6.17}$$

has finite real valued solutions $(y_{1_r}^*, y_{2_r}^*, y_{3_r}^*, y_{4_r}^*)$, $r = 1,2,...,n$ such that

$$\sum_{r=1}^{n} \text{sign det}(RW)'(y_{1_r}^*, y_{2_r}^*, y_{3_r}^*, y_{4_r}^*) \neq 0,$$

where the operators R and W are provided in proof.

Proof. Let $N(t) = e^{y_1(t)}$, $P(t) = e^{y_2(t)}$, $Z(t) = e^{y_3(t)}$, $T(t) = e^{y_4(t)}$, then from (6.2), we get

$$\begin{aligned}
\frac{dy_1(t)}{dt} &= N_0(t)e^{-y_1(t)} - a(t) - \frac{m(t)e^{y_2(t)}}{l_1(t) + e^{y_1(t)}} + \delta(t)e^{-y_1(t)+y_2(t)}, \\
\frac{dy_2(t)}{dt} &= \frac{u(t)}{1 + f(t)f_1(t)e^{y_2(t)+y_4(t)}}\left(1 - \frac{e^{y_2(t)}}{K(t)}\right) + \frac{m_1(t)e^{y_1(t)}}{l_1(t) + e^{y_1(t)}} - \frac{c(t)e^{y_3(t)}}{\alpha e^{2y_2(t)} + l_2(t)}, \\
\frac{dy_3(t)}{dt} &= \frac{c_1(t)e^{y_2(t)}}{\alpha(t)e^{2y_2(t)} + l_2(t)} - d_1(t) - d_2(t)e^{y_3(t)}, \\
\frac{dy_4(t)}{dt} &= A(t)e^{-y_4(t)} - f(t)e^{y_2(t)} - d(t).
\end{aligned} \tag{6.18}$$

Now, if system (6.18) possess a ω-periodic solution $(y_1(t), y_2(t), y_3(t), y_4(t))$, then (6.2) will have $(e^{y_1(t)}, e^{y_2(t)}, e^{y_3(t)}, e^{y_4(t)})$ as its positive ω-periodic solution. We take $U = V$ in Lemma 1.5.2 and define

$$U = V = \left\{(y_1, y_2, y_3, y_4) \in C(\mathbb{R}, \mathbb{R}^4) |\ y_j(t+\omega) = y_j(t), j = 1,2,3,4, t \in \mathbb{R}\right\},$$

with $\|(y_1,y_2,y_3,y_4)\| = \sum_{j=1}^{4} \max_{t\in[0,\omega]} |y_j(t)|$. Thus U and V are Banach space with $\|.\|$.
Let

$$F\begin{bmatrix} y_1 \\ y_2 \\ y_3 \\ y_4 \end{bmatrix} = \begin{bmatrix} y_1' \\ y_2' \\ y_3' \\ y_4' \end{bmatrix}, \qquad S\begin{bmatrix} y_1 \\ y_2 \\ y_3 \\ y_4 \end{bmatrix} = R\begin{bmatrix} y_1 \\ y_2 \\ y_3 \\ y_4 \end{bmatrix} = \begin{bmatrix} \frac{1}{\omega}\int_0^\omega y_1(t)dt \\ \frac{1}{\omega}\int_0^\omega y_2(t)dt \\ \frac{1}{\omega}\int_0^\omega y_3(t)dt \\ \frac{1}{\omega}\int_0^\omega y_4(t)dt \end{bmatrix},$$

$$W\begin{bmatrix} y_1 \\ y_2 \\ y_3 \\ y_4 \end{bmatrix} = \begin{bmatrix} N_0(t)e^{-y_1(t)} - a(t) - \frac{m(t)e^{y_2(t)}}{l_1(t)+e^{y_1(t)}} + \delta(t)e^{-y_1(t)+y_2(t)} \\ \frac{u(t)}{1+f(t)f_1(t)e^{y_2(t)+y_4(t)}}\left(1-\frac{e^{y_2(t)}}{K(t)}\right) + \frac{m_1(t)e^{y_1(t)}}{l_1(t)+e^{y_1(t)}} - \frac{c(t)e^{y_3(t)}}{\alpha e^{2y_2(t)}+l_2(t)} \\ \frac{c_1(t)e^{y_2(t)}}{\alpha(t)e^{2y_2(t)}+l_2(t)} - d_1(t) - d_2(t)e^{y_3(t)} \\ A(t)e^{-y_4(t)} - f(t)e^{y_2(t)} - d(t) \end{bmatrix}, \quad \begin{bmatrix} y_1 \\ y_2 \\ y_3 \\ y_4 \end{bmatrix} \in U.$$

Thus system (6.18) is equivalent to the equation $Fy = Wy,\ y \in \mathbb{R}^4$. Then we require to verify the conditions mentioned in Lemma 1.5.2 for the equation $Fy = Wy$ to get the existence of a ω-periodic solution for system (6.18). Next, it is easy note that

$$\mathrm{Ker}F = \left\{(y_1,y_2,y_3,y_4) \in U |\ (y_1,y_2,y_3,y_4) = (c_1,c_2,c_3,c_4) \in \mathbb{R}^4\right\},$$

$$\mathrm{Im}F = \left\{(y_1,y_2,y_3,y_4) \in U |\ \int_0^\omega y_j(t)dt = 0,\ j = 1,2,3,4\right\},$$

and $\dim \mathrm{Ker}F = \mathrm{codim}\,\mathrm{Im}F = 4$. Therefore, F is a Fredholm mapping of index zero. Mappings S and R are such projections with $\mathrm{Im}S = \mathrm{Ker}F,\ \mathrm{Im}F = \mathrm{Ker}R = \mathrm{Im}(I-R)$. The inverse F_S^{-1} of F is of the form $F_S^{-1} : \mathrm{Im}F \to \mathrm{Dom}F \cap \mathrm{Ker}S$, and is given by

$$F_S^{-1}\begin{bmatrix} y_1 \\ y_2 \\ y_3 \\ y_4 \end{bmatrix} = \begin{bmatrix} \int_0^t y_1(s)ds - \frac{1}{\omega}\int_0^\omega \int_0^t y_1(s)dsdt \\ \int_0^t y_2(s)ds - \frac{1}{\omega}\int_0^\omega \int_0^t y_2(s)dsdt \\ \int_0^t y_3(s)ds - \frac{1}{\omega}\int_0^\omega \int_0^t y_3(s)dsdt \\ \int_0^t y_4(s)ds - \frac{1}{\omega}\int_0^\omega \int_0^t y_4(s)dsdt \end{bmatrix}.$$

As RW and $F_S^{-1}(I-R)W$ are continuous thus we can easily check that $RW(\overline{\Omega})$ is bounded and $\overline{F_S^{-1}(I-R)W(\overline{\Omega})}$ is compact, i.e., W is F-compact on $\overline{\Omega}$.
From Theorem 6.2.1, we have

$$m_1^\varepsilon < N(t) < M_1^\varepsilon,\ m_2^\varepsilon < P(t) < M_2^\varepsilon,\ m_3^\varepsilon < Z(t) < M_3^\varepsilon,\ m_4^\varepsilon < T(t) < M_4^\varepsilon,$$

then for the operator equation $Fy = \rho Wy$ where $\rho \in (0,1)$, we have

$$\max_{t\in[0,\omega]} |y_1(t)| \le \max\{|\ln(m_1^{\varepsilon})|, |\ln(M_1^{\varepsilon})|\} = D_1, \max_{t\in[0,\omega]} |y_2(t)| \le \max\{|\ln(m_2^{\varepsilon})|, |\ln(M_2^{\varepsilon})|\} = D_2,$$

$$\max_{t\in[0,\omega]} |y_3(t)| \le \max\{|\ln(m_3^{\varepsilon})|, |\ln(M_3^{\varepsilon})|\} = D_3, \max_{t\in[0,\omega]} |y_4(t)| \le \max\{|\ln(m_4^{\varepsilon})|, |\ln(M_4^{\varepsilon})|\} = D_4.$$

Now, let $D = D_1 + D_2 + D_3 + D_4 + D_5$, where $D_5 > 0$ is enough large in such a way that each solution $(y_1^*, y_2^*, y_3^*, y_4^*)$ of the following equations

$$\begin{aligned}
\frac{1}{\omega}\int_0^{\omega}\left(N_0(t)e^{-y_1} - a(t) - \frac{m(t)e^{y_2}}{l_1(t)+e^{y_1}} + \delta(t)e^{-y_1+y_2}\right)dt = 0,\\
\frac{1}{\omega}\int_0^{\omega}\left(\frac{u(t)}{1+f(t)f_1(t)e^{y_2+y_4}}\left(1-\frac{e^{y_2}}{K(t)}\right) + \frac{m_1(t)e^{y_1}}{l_1(t)+e^{y_1}} - \frac{c(t)e^{y_3}}{\alpha e^{2y_2}+l_2(t)}\right)dt = 0,\\
\frac{1}{\omega}\int_0^{\omega}\left(\frac{c_1(t)e^{y_2}}{\alpha(t)e^{2y_2}+l_2(t)} - d_1(t) - d_2(t)e^{y_3}\right)dt = 0,\\
\frac{1}{\omega}\int_0^{\omega}\left(A(t)e^{-y_4} - f(t)e^{y_2} - d(t)\right)dt = 0,
\end{aligned} \tag{6.19}$$

satisfies $\|(y_1,y_2,y_3,y_4)\| < D$.

Define $\Omega = \{(y_1,y_2,y_3,y_4)^T \in U |\ \|(y_1,y_2,y_3,y_4)\| < D\}$. Then for this defined Ω, the first condition of Lemma 1.5.2 is satisfied.

Let $(y_1,y_2,y_3,y_4)^T \in \Omega \cap \mathrm{Ker}F = \partial\Omega \cap \mathbb{R}^4$, a constant vector with $\|(y_1,y_2,y_3,y_4)\| = D$, then

$$RW\begin{bmatrix} y_1\\ y_2\\ y_3\\ y_4\end{bmatrix} = \begin{bmatrix} \frac{1}{\omega}\int_0^{\omega}\left(N_0(t)e^{-y_1} - a(t) - \frac{m(t)e^{y_2}}{l_1(t)+e^{y_1}} + \delta(t)e^{-y_1+y_2}\right)dt\\ \frac{1}{\omega}\int_0^{\omega}\left(\frac{u(t)}{1+f(t)f_1(t)e^{y_2+y_4}}\left(1-\frac{e^{y_2}}{K(t)}\right) + \frac{m_1(t)e^{y_1}}{l_1(t)+e^{y_1}} - \frac{c(t)e^{y_3}}{\alpha e^{2y_2}+l_2(t)}\right)dt\\ \frac{1}{\omega}\int_0^{\omega}\left(\frac{c_1(t)e^{y_2}}{\alpha(t)e^{2y_2}+l_2(t)} - d_1(t) - d_2(t)e^{y_3}\right)dt\\ \frac{1}{\omega}\int_0^{\omega}\left(A(t)e^{-y_4} - f(t)e^{y_2} - d(t)\right)dt\end{bmatrix} \neq \begin{bmatrix}0\\0\\0\\0\end{bmatrix}.$$

Hence, the second condition of Lemma 1.5.2 is fulfilled.

Defining a homomorphism

$$K : \mathrm{Im}R \to \mathrm{Ker}F,\ (y_1,y_2,y_3,y_4)^T \to (y_1,y_2,y_3,y_4)^T,$$

we get

$$\deg(KRW, \partial\Omega \cap \mathrm{Ker}F, 0) = \deg(RW, \partial\Omega \cap \mathrm{Ker}F, 0).$$

Here, we assume that $RWy = 0$ has finite real valued solutions $(y^*_{1_r}, y^*_{2_r}, y^*_{3_r}, y^*_{4_r})$, $r = 1, 2, ..., n$ such that

$$\sum_{r=1}^{n} \mathrm{sign}\ \det(RW)'(y^*_{1_r}, y^*_{2_r}, y^*_{3_r}, y^*_{4_r}) \neq 0, \tag{6.20}$$

so under the assumption in (6.20), we have

$$\deg(KRW, \partial\Omega \cap \mathrm{Ker}F, 0) \neq 0.$$

Hence, all the conditions of Lemma (1.5.2) are verified. Thus $Fy = Wy$ possess at least one solution in $\mathrm{Dom}F \cap \overline{\Omega}$ i.e., system (6.18) has at least one ω-periodic solution $(y^*_1, y^*_2, y^*_3, y^*_4) \in \mathrm{Dom}F \cap \overline{\Omega}$. Therefore, $(x^*_1, x^*_2, x^*_3, x^*_4) = (e^{y^*_1}, e^{y^*_2}, e^{y^*_3}, e^{y^*_4})$ is a strictly positive ω-periodic solution of model (6.2). □

6.2.3 Solution's global attractivity

Now we evaluate the conditions under which the periodic solution of system (6.2) is globally attractive.

Theorem 6.2.3. *Let $(N(t), P(t), Z(t), T(t))$ be a positive ω-periodic solution for system (6.2). Then this solution is globally stable if*

$$\mathscr{J}_i > 0, i = 1, 2, 3, 4 \tag{6.21}$$

where $\mathscr{J}_i's$ are defined in proof.

Proof. Let $(N(t), P(t), Z(t), T(t))$ and $(N^*(t), P^*(t), Z^*(t), T^*(t))$ are two positive ω-periodic solutions with positive initial conditions for the non-autonomous system. Define

$$V_1(t) = |\ln N(t) - \ln N^*(t)|, V_2(t) = |\ln P(t) - \ln P^*(t)|,$$

$$V_3(t) = |\ln Z(t) - \ln Z^*(t)|, V_4(t) = |\ln T(t) - \ln T^*(t)|.$$

After calculating the right (Dini's) derivatives of $V_i(t)$ along system (6.2), we obtain

$$\begin{aligned} D^+V_1(t) &= \mathrm{sign}(N(t) - N^*(t)) \left(\frac{\dot{N(t)}}{N(t)} - \frac{\dot{N^*}(t)}{N^*(t)} \right) \\ &\leq \left\{ -\frac{N_0(t)}{N(t)N^*(t)} - \frac{\delta(t)P(t)}{N(t)N^*(t)} + \frac{m(t)P(t)}{(l_1(t)+N(t))(l_1(t)+N^*(t))} \right\} |N(t) - N^*(t)| \end{aligned} \tag{6.22}$$

$$+\left\{\frac{\delta(t)}{N^*(t)}+\frac{m(t)}{l_1(t)+N^*(t)}\right\}|P(t)-P^*(t)|;$$

$$D^+V_2(t)=\text{sign}(P(t)-P^*(t))\left(\frac{\dot{P}}{P}-\frac{\dot{P}^*(t)}{P^*(t)}\right)$$

$$\leq\frac{m_1(t)l_1(t)}{(l_1(t)+N(t))(l_1(t)+N^*(t))}|N(t)-N^*(t)|$$

$$+\left\{-\frac{u(t)f(t)f_1(t)T(t)}{(1+f(t)f_1(t)P(t)T(t))(1+f(t)f_1(t)P^*(t)T^*(t))}-\frac{u(t)}{K(t)(1+f(t)f_1(t)P^*(t)T^*(t))}\right.$$

$$\left.+\frac{u(t)f(t)f_1(t)P(t)T(t)}{K(t)(1+f(t)f_1(t)P(t)T(t))(1+f(t)f_1(t)P^*(t)T^*(t))}+\frac{c(t)\alpha(t)Z(t)(P(t)+P^*(t))}{(\alpha(t)P^2(t)+l_2(t))(\alpha(t)P^{*2}(t)+l_2(t))}\right\}$$

$$|P(t)-P^*(t)|$$

$$+\frac{c(t)}{\alpha(t)P^{*2}(t)+l_2(t))}|Z(t)-Z^*(t)|$$

$$+\left\{\frac{u(t)f(t)f_1(t)P^*(t)}{(1+f(t)f_1(t)P(t)T(t)(1+f^*(t)f_1^*(t)P^*(t)T^*(t))}\left(1+\frac{P(t)}{K(t)}\right)\right\}|T(t)-T^*(t)|;$$

$$D^+V_3(t)=\text{sign}(Z(t)-Z^*(t))\left(\frac{\dot{Z}}{Z}-\frac{\dot{Z}^*(t)}{Z^*(t)}\right)$$

$$\leq\frac{c_1(t)(\alpha(t)P(t)P^*(t)-l_2(t))}{(\alpha(t)P^2(t)+l_2(t))(\alpha(t)P^{*2}(t)+l_2(t))}|P(t)-P^*(t)|-d_2(t)|Z(t)-Z^*(t)|;$$

$$D^+V_4(t)=\text{sign}(T(t)-T^*(t))\left(\frac{\dot{T}}{T}-\frac{\dot{T}^*(t)}{T^*(t)}\right)$$

$$\leq f(t)|P(t)-P^*(t)|-\frac{A(t)}{T(t)}|T(t)-T^*(t)|.$$

Let

$$V(t)=V_1(t)+V_2(t)+V_3(t)+V_4(t).$$

The using the above inequalities involving $V_1(t),V_2(t),V_2(t),V_2(t)$, the Dini derivative of $V(t)$ is evaluated as,

$$D^+V(t)\leq-\left\{\frac{N_0(t)}{N(t)N^*(t)}+\frac{\delta(t)P(t)}{N(t)N^*(t)}-\frac{m(t)P(t)}{(l_1(t)+N(t))(l_1(t)+N^*(t))}\right.$$

$$\left.-\frac{m_1(t)l_1(t)}{(l_1(t)+N(t))(l_1(t)+N^*(t))}\right\}|N(t)-N^*(t)|$$

$$-\left\{-\frac{\delta(t)}{N^*(t)}-\frac{m(t)}{l_1(t)+N^*(t)}+\frac{u(t)f(t)f_1(t)T(t)}{(1+f(t)f_1(t)P(t)T(t))(1+f(t)f_1(t)P^*(t)T^*(t))}\right.$$

$$+\frac{u(t)}{K(t)(1+f(t)f_1(t)P^*(t)T^*(t))}$$

$$-\frac{u(t)f(t)f_1(t)P(t)T(t)}{K(t)(1+f(t)f_1(t)P(t)T(t))(1+f(t)f_1(t)P^*(t)T^*(t))}-\frac{c(t)\alpha(t)Z(t)(P(t)+P^*(t))}{(\alpha(t)P^2(t)+l_2(t))(\alpha(t)P^{*2}(t)+l_2(t))}$$

$$\left.-\frac{c_1(t)(\alpha(t)P(t)P^*(t)-l_2(t))}{(\alpha(t)P^2(t)+l_2(t))(\alpha(t)P^{*2}(t)+l_2(t))}-f(t)\right\}|P(t)-P^*(t)|$$

$$-\left\{-\frac{c(t)}{\alpha(t)P^{*2}(t)+l_2(t))}+d_2(t)\right\}|Z(t)-Z^*(t)|$$
$$-\left\{-\frac{u(t)f(t)f_1(t)P^*(t)}{(1+f(t)f_1(t)P(t)T(t)(1+f^*(t)f_1^*(t)P^*(t)T^*(t))}\left(1+\frac{P(t)}{K(t)}\right)+\frac{A(t)}{T(t)}\right\}|T(t)-T^*(t)|.$$

Then using Theorem 6.2.1, we get

$$\begin{aligned}D^+V(t)\leq&-\left\{\frac{N_0(t)}{(M_1^\varepsilon)^2}+\frac{\delta(t)P(t)}{(M_1^\varepsilon)^2}-\frac{m(t)M_2^\varepsilon}{(l_1(t)+m_1^\varepsilon)^2}-\frac{m_1(t)l_1(t)}{(l_1(t)+M_1^\varepsilon)^2}\right\}|N(t)-N^*(t)|\\&-\left\{-\frac{\delta(t)}{m_1^\varepsilon}-\frac{m(t)}{l_1(t)+m_1^\varepsilon}+\frac{u(t)f(t)f_1(t)m_4^\varepsilon}{(1+f(t)f_1(t)M_2^\varepsilon M_4^\varepsilon)^2}+\frac{u(t)}{K(t)(1+f(t)f_1(t)M_2^\varepsilon M_4^\varepsilon)}\right.\\&\left.-\frac{u(t)f(t)f_1(t)M_2^\varepsilon M_4^\varepsilon}{K(t)(1+f(t)f_1(t)m_2^\varepsilon m_4^\varepsilon)^2}-\frac{2c(t)\alpha(t)M_3^\varepsilon M_2^\varepsilon}{(\alpha(t)m_2^{\varepsilon 2}+l_2(t))^2}-\frac{c_1(t)(\alpha(t)M_2^{\varepsilon 2}-l_2(t))}{(\alpha(t)m_2^\varepsilon+l_2(t))^2}-f(t)\right\}|P(t)-P^*(t)|\\&-\left\{-\frac{c(t)}{\alpha(t)M_2^{\varepsilon 2}(t)+l_2(t))}+d_2(t)\right\}|Z(t)-Z^*(t)|\\&-\left\{-\frac{u(t)f(t)f_1(t)M_2^\varepsilon}{(1+f(t)f_1(t)m_2^\varepsilon m_4^\varepsilon)^2}\left(1+\frac{M_2^\varepsilon}{K(t)}\right)+\frac{A(t)}{M_4^\varepsilon}\right\}|T(t)-T^*(t)|.\end{aligned}$$

Thus

$$D^+V(t)\leq-\mathscr{J}_1|N(t)-N^*(t)|-\mathscr{J}_2|P(t)-P^*(t)|-\mathscr{J}_3|Z(t)-Z^*(t)|-\mathscr{J}_4|T(t)-T^*(t)|, \tag{6.23}$$

where

$$\begin{aligned}\mathscr{J}_1&=\frac{N_0(t)}{(M_1^\varepsilon)^2}+\frac{\delta(t)P(t)}{(M_1^\varepsilon)^2}-\frac{m(t)M_2^\varepsilon}{(l_1(t)+m_1^\varepsilon)^2}-\frac{m_1(t)l_1(t)}{(l_1(t)+M_1^\varepsilon)^2},\\\mathscr{J}_2&=-\frac{\delta(t)}{m_1^\varepsilon}-\frac{m(t)}{l_1(t)+m_1^\varepsilon}+\frac{u(t)f(t)f_1(t)m_4^\varepsilon}{(1+f(t)f_1(t)M_2^\varepsilon M_4^\varepsilon)^2}+\frac{u(t)}{K(t)(1+f(t)f_1(t)M_2^\varepsilon M_4^\varepsilon)}-\frac{u(t)f(t)f_1(t)M_2^\varepsilon M_4^\varepsilon}{K(t)(1+f(t)f_1(t)m_2^\varepsilon m_4^\varepsilon)^2},\\&\quad-\frac{2c(t)\alpha(t)M_3^\varepsilon M_2^\varepsilon}{(\alpha(t)m_2^{\varepsilon 2}+l_2(t))^2}-\frac{c_1(t)(\alpha(t)M_2^{\varepsilon 2}-l_2(t))}{(\alpha(t)m_2^\varepsilon+l_2(t))^2}-f(t),\\\mathscr{J}_3&=-\frac{c(t)}{\alpha(t)M_2^{\varepsilon 2}(t)+l_2(t))}+d_2(t),\\\mathscr{J}_4&=-\frac{u(t)f(t)f_1(t)M_2^\varepsilon}{(1+f(t)f_1(t)m_2^\varepsilon m_4^\varepsilon)^2}\left(1+\frac{M_2^\varepsilon}{K(t)}\right)+\frac{A(t)}{M_4^\varepsilon}.\end{aligned}$$

So under the conditions given in (6.21), $V(t)$ is non-increasing on the interval $[0,\infty)$, integrating (6.23), we get

$$V(t)+\mathscr{J}_1\int_0^t|N(s)-N^*(s)|ds+\mathscr{J}_2\int_0^t|P(s)-P^*(s)|ds+\mathscr{J}_3\int_0^t|Z(s)-Z^*(s)|ds+\mathscr{J}_4\int_0^t|T(s)-T^*(s)|ds<\infty. \tag{6.24}$$

Using lemma 1.5.1, we have

$$\lim_{t\to\infty}|N(t)-N^*(t)|=0,\ \lim_{t\to\infty}|P(t)-P^*(t)|=0,$$

$$\lim_{t\to\infty}|Z(t)-Z^*(t)|=0,\ \lim_{t\to\infty}|T(t)-T^*(t)|=0.$$

Hence, the positive ω-periodic solution of the seasonal system (6.2) is globally stable (attractive). □

6.3 Numerical simulation

In this section, we review the dynamical behaviour of systems (6.1) and (6.2) with help of numerical simulations. For this, we use the parameters' values from various literature sources, mentioned in Table 6.1.

Non-seasonal model

For the parameters given in Table 6.1, the unique interior equilibrium (shown in Fig. 6.1) is globally asymptotically stable which is evident from the Fig. 6.2 in which a number of solutions in NPZ-space starting from different initial conditions converge to it (violet coloured dot).

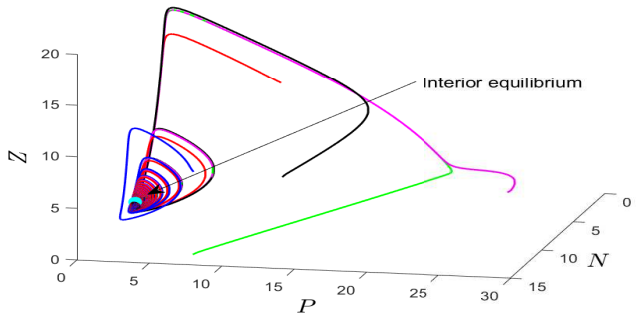

Fig. 6.2: Global Stability of interior equilibrium with parameters from Table 6.1.

Now we see the effect of the rate at which phytoplankton's growth is suppressed by environmental toxin f_1 on the kinetics of the system (6.1). For this we vary f_1 in the interval $[2.5,4]$ with $u=2$ and other parameters same as in Table 6.1. Based on the bifurcation diagrams specified in Fig. 6.3, we can notice that the system exhibits steady-state kinetics for lower values of f_1 in the taken interval. As we increase f_1 beyond its critical value, namely $f_1^h=3.2525$, our system's solution becomes periodic through Hopf bifurcation and yields a stable limit cycle. Along with the change in the system's dynamical behavior on changing f_1, observing the variation in population densities is also important. For this purpose, we have given the trend of N,P,Z and T on varying f_1 in Table 6.2, keeping it in its stable range. From this table, we can note that phytoplankton population density decreases as we increase parameter f_1. As zooplankton is the specialist predator of phytoplankton, its density also decreases but at a rapid

rate. Due to the reducing density of phytoplankton, the intake of nutrients decreases, due to which their concentration increases, and similarly, increment in T can also be explained.

To study the change in the dynamical behavior of the system with respect to parameter A, we have plotted the bifurcation diagrams for all four participants (N,P,Z,T) in Fig. 6.4 for $A \in [6,8]$. From these diagrams, we perceive that the system tends to coexistence equilibrium for the lower addition rate of environmental toxins. As A crosses $A = A^h = 6.8525$, there is a rise of the stable limit cycle attractor. The trend of change in the N,P,Z,T on varying A is reflected in Table 6.3. From these table, it is easy to notice that as the supply rate of toxins increases, T increases due to which there is depletion in phytoplankton population density. Due to which there is corresponding increment and decrement in N and Z, respectively.

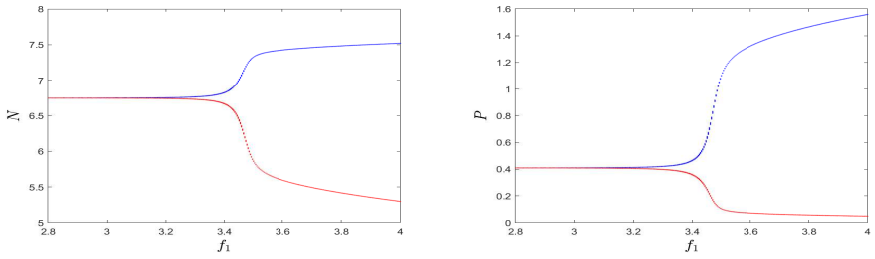

(a) **(b)**

(c) **(d)**

Fig. 6.3: Bifurcation diagrams for model (6.1) using f_1 as the bifurcation parameter for $u = 2$ and other parameters as in Table 6.1.

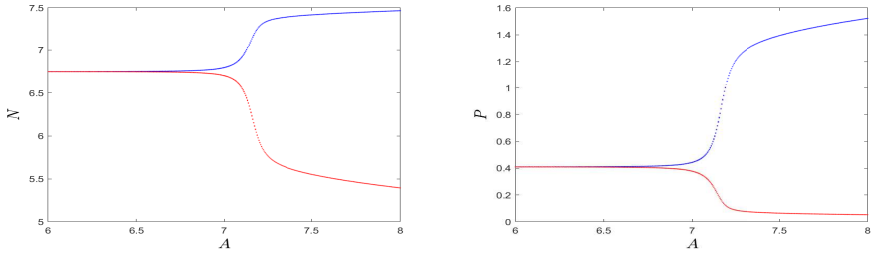

(a) **(b)**

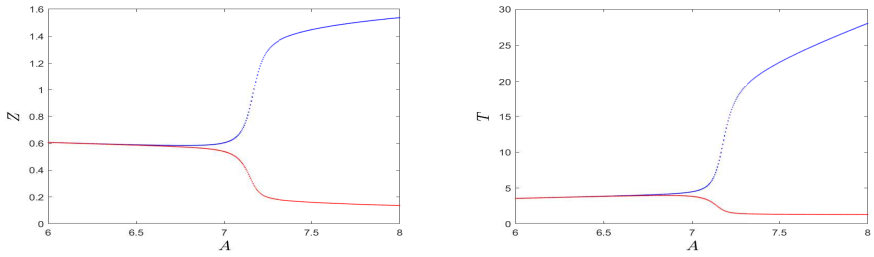

(c) **(d)**

Fig. 6.4: Bifurcation diagrams for model (6.1) using A as the bifurcation parameter for $u = 0.8$ and other parameters as in Table 6.1.

f_1	N	P	Z	T
2.5	6.7468	0.4097	0.5924	4.1447
2.7	6.7474	0.4096	0.5730	4.1457
2.9	6.7480	0.4095	0.5561	4.1466
3.1	6.7484	0.4094	0.5413	4.1473

Table 6.2: Trend of N, P, Z, T on variation of f_1 with $u = 2$ and other parameters as in Table 6.1.

A	N	P	Z	T
6	6.7464	0.4098	0.6074	3.5519
6.2	6.7466	0.4097	0.5993	3.6707
6.4	6.7469	0.4096	0.5917	3.7895
6.6	6.7471	0.4095	0.5845	3.9082

Table 6.3: Trend of N, P, Z, T on variation of A with $u = 0.8$ and other parameters as in Table 6.1.

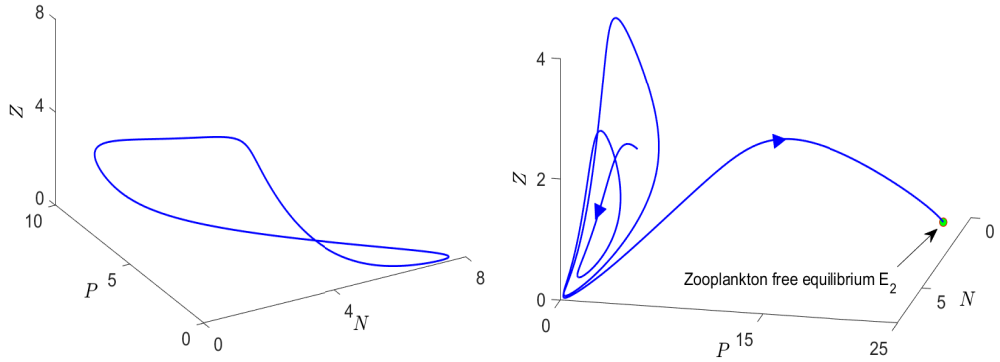

(a) Stable limit cycle for $\alpha = 0.18$. **(b)** Stable E_2 for $\alpha = 0.2$.

Fig. 6.5: This figure depicts the eradication of oscillation and attaing stability by equilibrium E_2 on increasing α, with $f_1 = 4,\ u = 2$ and other parameters as in Table 6.1.

Phytoplankton's inhibitory effect (α) against zooplankton is also one of the important parameters to be studied. The periodic oscillations for higher values of f_1 (Fig. 6.3) are eliminated and zooplankton free equilibrium E_2 becomes stable on increasing α. For Fig. 6.5(a), we keep $f_1 = 4,\ \alpha = 0.18$ and remaining parameters same as of Fig. 6.3 for which system have a

periodic solution. As we increase α to 0.2, the oscillations are wiped out, and the solution approaches the zooplankton free equilibrium. Accordingly, we can say that a rise in the inhibitory effect may result in the extinction of both the zooplankton population and periodic fluctuations. Thus the defence mechanism of phytoplankton can help to control the plankton blooms by removing the periodic oscillations in the non-seasonal model. This deliberates the benefit of using Holling type IV response for handling the phytoplankton-zooplankton interaction.

Multistability is a substantial property of a non-linear model, which makes it flexible in an asymptotic way because a multistable system has more than one stable attractor. Due to this, different solutions with different initial conditions tend to their respective attractors. Our autonomous population model (6.1) also shows this character with three different stable attractors; stable interior equilibrium, stable limit cycle, and stable zooplankton free equilibrium. In Figs. 6.6(a)-6.6(c), we have portrayed the time-series graphs of zooplankton population from solutions with three different initial conditions (given in respective time-graphs). We can notice from these figures that as we change the initial conditions, the asymptotic destination changes correspondingly. In a 4-dimensional system, drawing the basin of attraction is not feasible, thus for our system (6.1), we keep the nutrient coordinate of initial condition as constant ($N(0) = 10$), and draw the basin by varying the remaining coordinates in Fig. 6.6(d).

Seasonal model

Now we do the simulations for analysing the behaviour of seasonally forced model (6.2). For simulation purpose, the following parameters are assumed to have sinusoidal form while other parameters are time-independent.

$$u(t) = u + u_0 \sin(wt),\ f(t) = f + f_0 \sin(wt),\ \delta(t) = \delta + \delta_0 \sin(wt),$$

where u_0 $(0 < u_0 < u)$, f_0 $(0 < f_0 < f)$, and δ_0 $(0 < \delta_0 < \delta)$ control the intensity related to seasonal forcing, and the values of these $u_0,\ f_0,\ \delta_0$ are assumed to be zero until mentioned in the text.

Now, we analyse the impact of adding seasonal forces in the non-seasonal model (6.1). For the parameters provided in Table 6.1, the interior equilibrium for model (6.1) is globally asymptotically stable (Fig. 6.2). As we introduce the seasonality by taking $w = 0.1,\ u_0 = 0.3$, for model (6.2), there is a rise of a positive periodic solution (Fig. 6.6) which is globally attractive in nature as three solutions started from different initial conditions converge to it. From Fig. 6.6(c), we can see that the solution of autonomous system with IC: [10, 4, 1.45, 1] is non-permanent as the zooplankton population extincts. But as we introduce the seasonality in this system by taking $\omega = 0.1,\ u_0 = 0.1$ and keeping all other parameters fixed as in Fig. 6.6(c), solution of this non-autonomous system with the same initial condition becomes permanent (Fig. 6.7(b)). Thus we can see that how the inclusion of seasonality in our system changes its

dynamics.

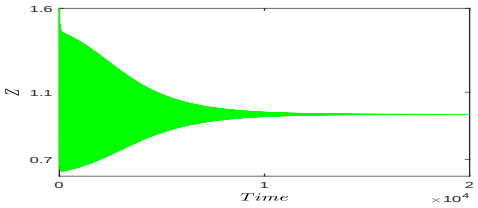

(a) IC: [10, 0.4, 1.6, 1].

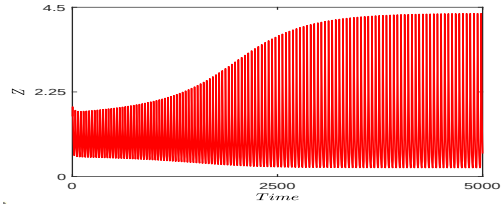

(b) IC: [10, 0.8, 1.6, 1].

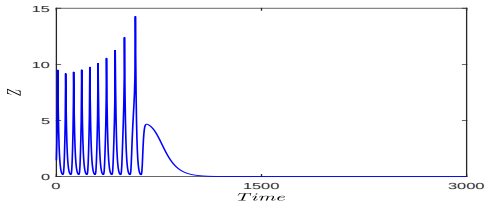

(c) IC: [10, 4, 1.45, 1].

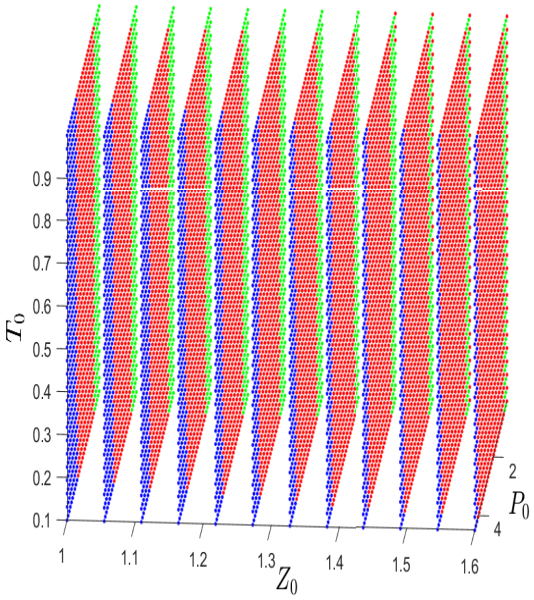

(d) Basins of attraction keeping $N(0) = 10$.

Fig. 6.6: In Figs. (a), (b), and (c), the solution started from three respective different initial conditions tend to stable interior equilibrium, stable limit cycle, and zooplankton free equilibrium. For the Basins of attraction in Fig. (d), green, red, and blue dots refers to initial conditions $(P(0) \in (0.1, 4.5), Z(0) \in (1, 1.6), T(0) \in (0.1, 1))$ from where the solution approaches interior equilibrium, limit cycle, and zooplankton free equilibrium, respectively, with $f = 1.267$, $\alpha = 0.1333$ and keeping other parametric values fixed from Table 6.1.

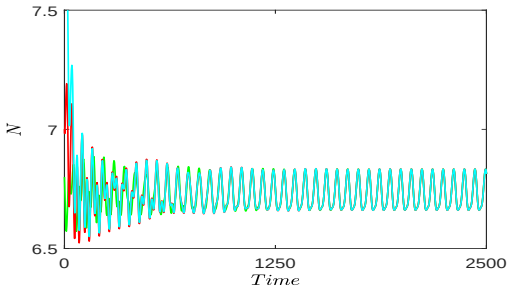

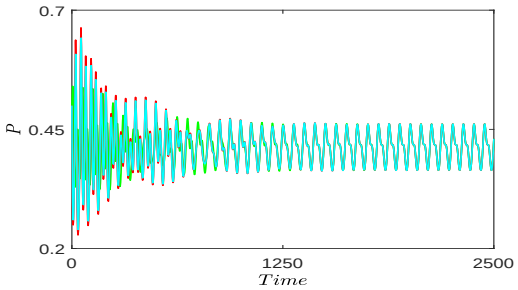

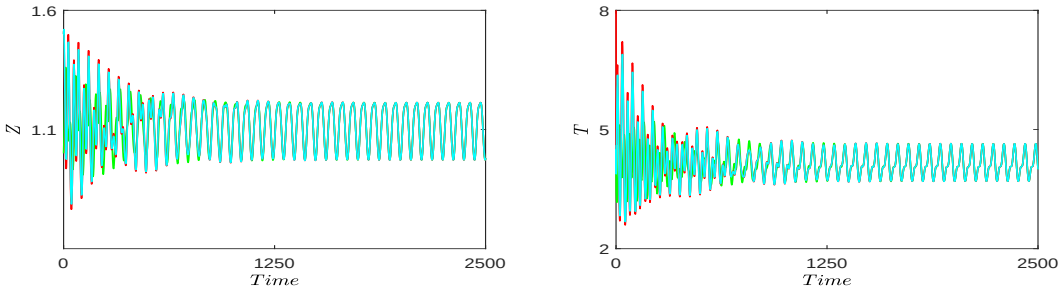

Fig. 6.6: This figure demonstrate the global stability of the periodic solution of system (6.2) for $w = 0.1,\ u_0 = 0.3$, and all other parameters from Table 6.1.

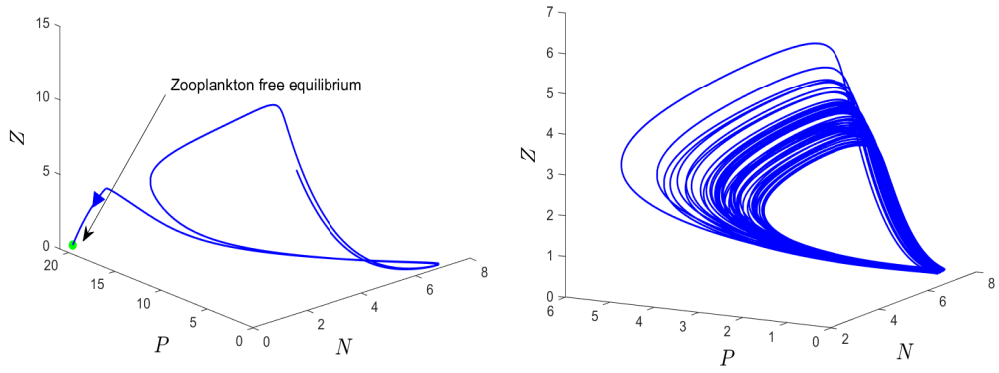

(a) Autonomous system is non-permanent.

(b) Non-autonomous system is permanent.

Fig. 6.7: With IC: [10, 4, 1.45, 1], in (a) solution of autonomous system is non-permanent whereas in (b) taking $\omega = 0.1,\ u_0 = 0.1$, solution of non-autonomous system is permanent.

Now, we further examine our seasonal model by changing the parameters and study some crucial qualities like; chaos and multistability, which are related to seasonal models [167]. For a particular set of parameters (provided in the respective figure), seasonal model (6.2) behaves chaotically. When a dynamical system becomes chaotic, predicting the future behavior of its solution is not feasible, as it becomes sensitive to initial conditions. Thus to corroborate the chaotic nature of this system, we perform sensitivity analysis by initiating two solutions from two different but closed initial conditions ([1, 1, 1, 1] and [1.001,1.001,1.001,1.001]) shown in Figs. 6.8(a)-6.8(d). From these figures, we can notice that these two closely started solutions diverge from each other as time passes which endorses the system's chaotic character. We have also drawn a 3-dimensional Poincare map (Fig. 6.8(e)) in PZT-space keeping $N = 5.5$, and the scattered distribution of points (magenta coloured) in this figure verifies the chaotic essence of our model.

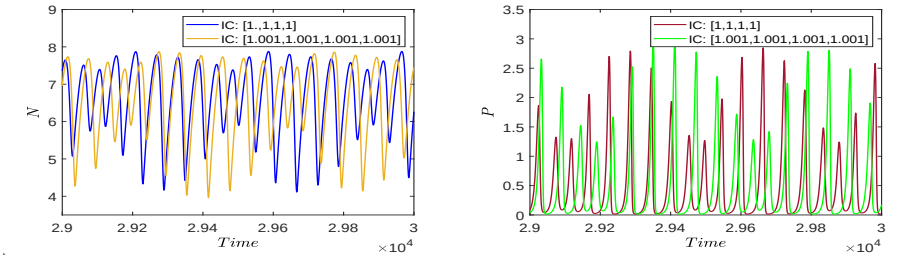

(a)

(b)

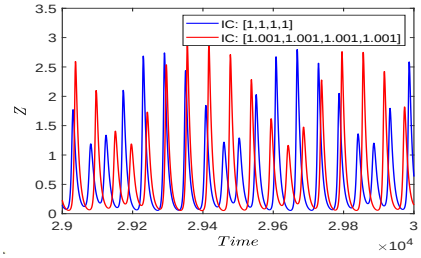

(c)

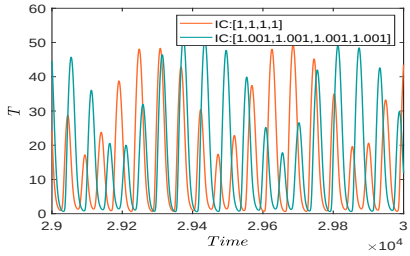

(d)

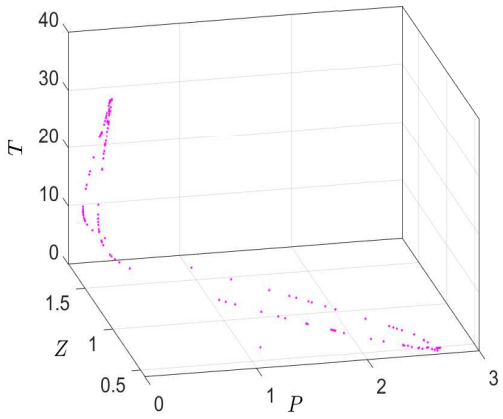

(e)

Fig. 6.8: Figs. (a)-(d) show the sensitivity of solution of non-autonomous model (6.2) with respect to initial conditions. Fig. (e) depicts Poincare map in PZT-space at $N = 5.5$, with parameters from Table 6.1 except $w = 0.1, u_0 = 1.3, f_0 = 0.9, \delta_0 = 0.001, f_1 = 4, \alpha = 0.12, l_1 = 17$.

As stated earlier, multistability is an appealing character in non-linear models. Our seasonal model (6.2) also exhibit this quality. From Fig. 6.9, we can see that for a set of parameters, model has the attribute of tristability between a limit cycle (L_1 which is around zooplankton free equilibrium), another stable limit cycle (L_2 around the interior equilibrium), and a chaotic attractor. In Fig. 6.9(a)-6.9(c), we have plotted time-series graphs for nutrient coordinate of three solutions started from three different initial conditions. Basins of attraction for all three

attractors (L_1, L_2, chaotic attractor) are also sketched in Fig. 6.9(d), in which green, blue, red dots represent the initial conditions in NPZ-space from where solution goes to L_1, L_2, chaotic attractor, respectively.

Taking $u_0 = 2$, $\delta_0 = 0.005$, and remaining parameters same as in Fig. 6.9, now our seasonal model shows tristability between period-1,2 and 4 limit cycles. To present this multistability, we provide time-series graphs of nutrient coordinate of the solution with three different initial conditions (mentioned in Fig. 6.10(a)-6.10(c)), from where the solution tend to different respective attractor. Again, we have have plotted the basins of attraction for these attractors in Fig. 6.10(d). If we compare the basin diagrams in Figs. 6.9(d) and 6.10(d) with basin diagram presented in Fig. 6.6(d), we can note that these basins of attraction are very complex and are scattered in a random way in the chosen domain. This behavior reflects the arise of complexity in the dynamics of the system due to addition of seasonal forces. We can observe that the presence of seasonal forcing in parameter δ contributes in manifesting the complex kind of multistablity and chaotic nature in the seasonal model. This reflects the significance of incorporating the nutrient-plankton dynamics in our system.

As the intrinsic growth rate (u) is an important seasonal parameter, thus we try to see the behavior of the seasonal model (6.2) on changing u in a particular range. In Fig. 6.11(a)-6.11(d), we have drawn the bifurcation diagrams for all the four populations of our model. From the figure, we can observe that the system switches its nature multiple times. From a chaotic regime, it reaches to periodic region while passing through multiple chaotic and periodic windows. We have also calculated the maximum lyapunov exponent (Fig. 6.11(e)) for the same range of u and keeping other parameters fix as for drawing the bifurcation diagrams. We see from Fig. 6.11(e) that the positive values of maximum lyapunov exponent validates the chaotic nature of non-autonomous system for this particular set of parameters. Thus one can say that the chaotic nature of this system can be controlled by varying u in a particular domain. In similar manner, we have drawn bifurcation diagram for varying $f \in (3.2, 4)$ in Fig. 6.12. From these figures, we can see that for the rightmost part of the interval $f \in (3.2, 4)$; there is a single peak for each value of f, which shows the existence of the period-1 limit cycle, i.e., the control of chaos.

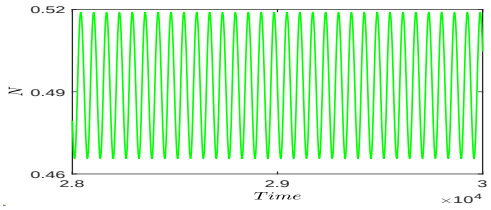

(a) L_1 with IC: [5, 15, 1, 1].

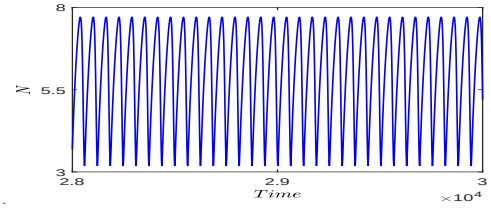

(b) L_2 with IC: [5, 5, 5, 1].

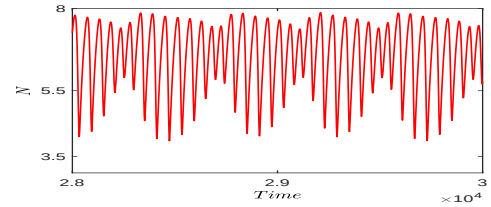

(c) Chaotic attractor with IC: [5, 5, 1, 1].

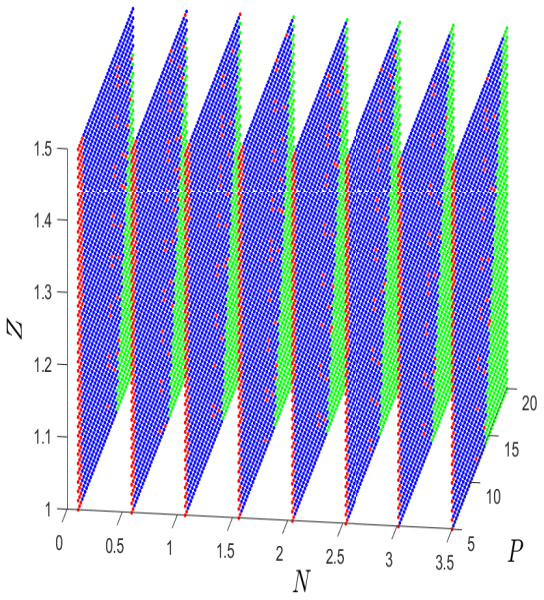

(d) Basins of attraction keeping $T(0) = 1$.

Fig. 6.9: In Figs. (a), (b), (c), the solution started from three different initial conditions ([5, 15, 1, 1], [5, 5, 5, 1], [5, 5, 1, 1]) tend to a stable limit cycle (L_1), another stable limit cycle (L_2), a chaotic attractor, respectively. For the Basins of attraction in Fig. (d), green, blue, red dots refers to initial conditions $(N(0) \in (0.1, 3.5), P(0) \in (5, 20), Z(0) \in (1, 1.5))$ from where the solution approaches L_1 L_2, and the chaotic attractor, respectively, with parameters from Table 6.1 except $w = 0.1, u_0 = 1.3, f_0 = 0.9, \delta_0 = 0.001, f_1 = 4, \alpha = 0.12, l_1 = 17$.

From the bifurcation diagrams presented in Figs. 6.11 and 6.12, we noticed how the kinetics of a system become complex after the introduction of seasonality. To view the complex dynamics of our seasonal model in more depth, we have sketched a bi-parametric bifurcation diagram in the uf-plane (Fig. 6.13). The combinations of u and f in this plane are divided into seven types, depicted with different respective colors, which are presented in the color bar given in the figure. Each color describes a periodic solution with a particular period. For example, the blue combination of u and f gives a solution of period-1, red gives period-2, and so on, whereas all the solutions in this figure are initiated from $[1, 1, 1, 1]$. This complex dynamics represented in this figure also agree with results delineated by Hossain et al. [167].

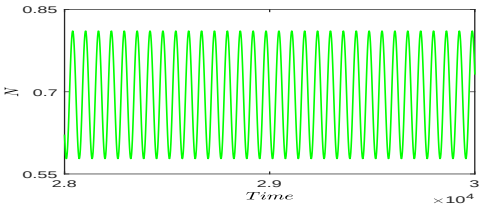

(a) Periodic-1 with IC: [15, 5, 5, 5].

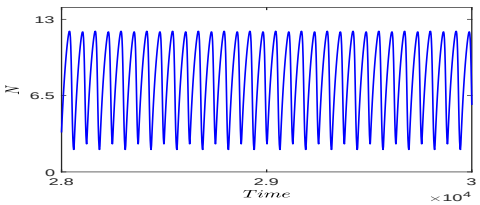

(b) Period-2 limit cycle with IC: [1, 5, 5, 5].

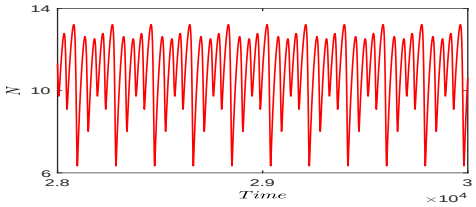

(c) Period-4 limit cycle with IC: [1, 1, 1, 5].

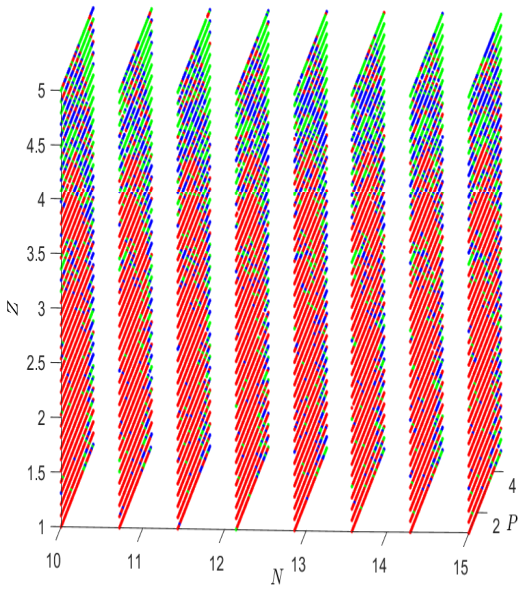

(d) Basins of attraction keeping $T(0) = 5$.

Fig. 6.10: In Figs. (a), (b), (c), the solution started from three different initial conditions ([15, 5, 5, 5], [1, 5, 5, 5], [1, 1, 1, 5]) tend to periodic-1, periodic-2, and periodic-4 limit cycle, respectively. For the Basins of attraction in Fig. (d), green, blue, red dots refers to initial conditions $(N(0) \in (10,15), P(0) \in (1,5), Z(0) \in (1,5))$ from where the solution approaches periodic-1, periodic-2, and periodic-4 limit cycle, respectively, with parameters from Table 6.1 except, $w = 0.1, u_0 = 2, f_0 = 0.9, \delta_0 = 0.005, u = 4, N_0 = 0.5, f_1 = 4, \alpha = 0.12, l_1 = 17$.

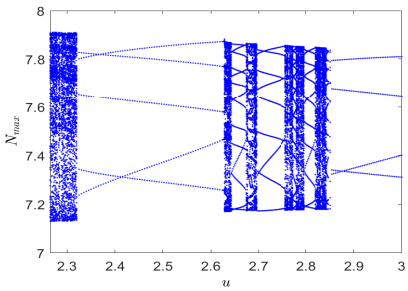

(a)

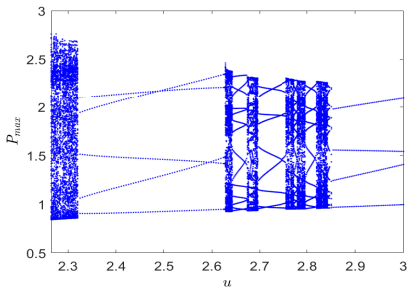

(b)

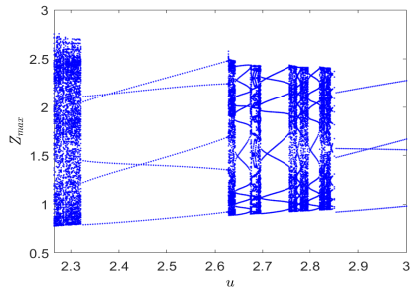

(c)

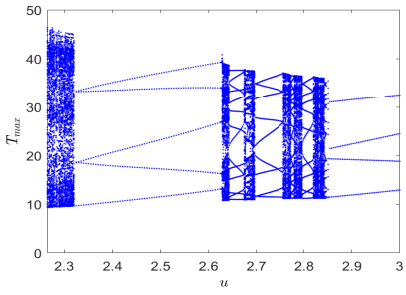

(d)

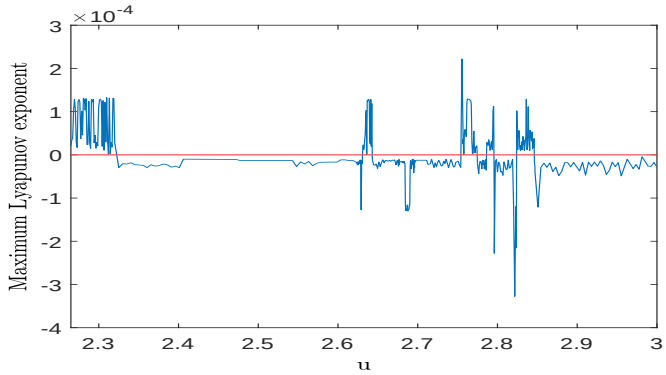

(e)

Fig. 6.11: Figs. (a)-(d) shows bifurcation diagrams for all four populations of model (6.2) whereas Fig. (e) gives the maximum Lyapunov exponent, with all other parameters from Table 6.1, except $w = 0.1, u_0 = 1.3, f_1 = 4, \alpha = 0.12, l_1 = 17$.

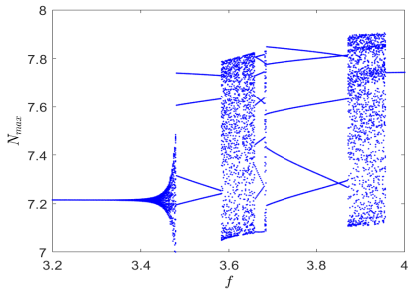

(a)

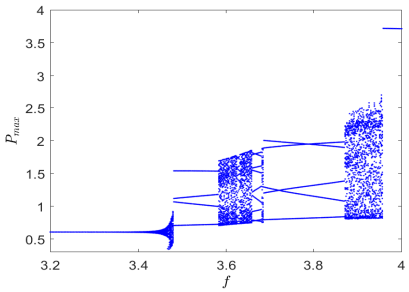

(b)

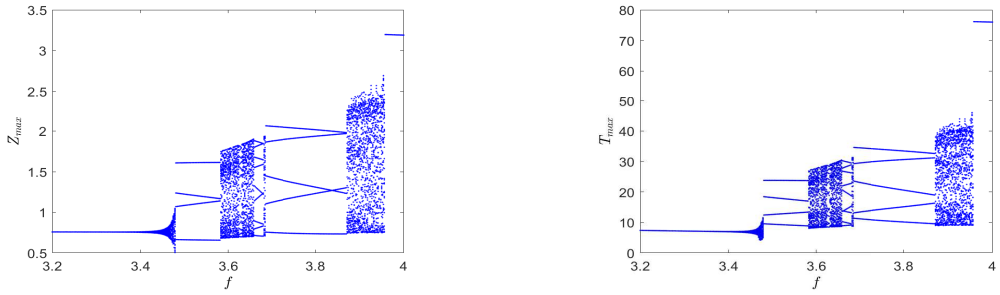

(c) **(d)**

Fig. 6.12: Bifurcation diagrams for all four populations of model (6.2), with all other parameters from Table 6.1, except $w = 0.1, u_0 = 1.3, u = 2.2, f_1 = 4, \alpha = 0.12, l_1 = 17$.

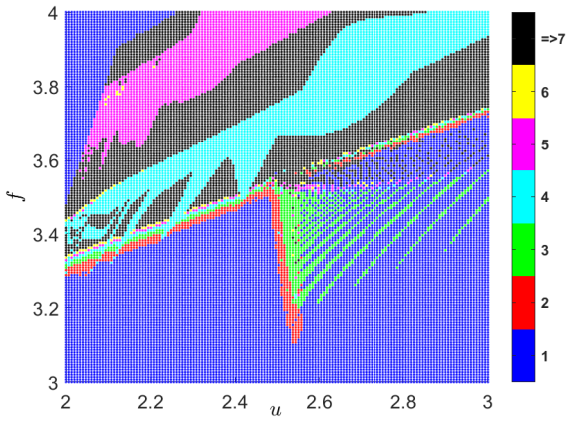

Fig. 6.13: Bi-parametric bifurcation diagram in uf-plane, with $w = 0.1, u_0 = 1.3, f_1 = 4, \alpha = 0.12, l_1 = 17$ and rest of parameters from Table 6.1.

6.4 Discussion and conclusions

The main purpose of mathematical modeling in evolutionary biology is to formulate the ecological interactions in the form of mathematical equations. In most of the works present in literature, authors have ignored the seasonality of the physical parameters involved in predator-prey interrelationships. However, recent works [46, 47] have incorporated this effect and developed the techniques to deal with such complex non-autonomous models. Inspired from these, we aspire to study a seasonal $NPZT$-model with group defence of phytoplankton against zooplankton.

Initialy we explained the formulation of our both autonomous and non-autonomous models with necessary assumptions. We assumed that phytoplankton absorb nutrients through Holling type II response whereas zooplankton consume phytoplankton via Holling type IV response. Firstly, we provided the analysis for system (6.1) and then for system (6.2). We established uniqueness and boundedness results for the autonomous model. Existence of equilibrium points

and stability analysis of the system around these feasible equilibria are investigated next. Further, we drived the condition for Hopf-bifurcation with respect to parameter A. In Section 6.2, we did the mathematical analysis regarding to the non-autonomous model. This comprises of driving the conditions for its permanence, existence of oscillatory solution, and its global stability.

Next, through numerical simulation, we saw that system (6.1) undergoes Hopf bifurcation for parameters f_1 and A. We observed that as long as both these parameters are less than some threshold values, the system remained stable and after which there is the rise of oscillations. We also examined the trend of change in N, P, Z, T as we vary f_1 and A (see Tables 6.2 and 6.3). Phytoplankton's inhibitory effect parameter (α) plays an observable role in the dynamics of model (6.1). As we raised α, the oscillation present in the system (Fig. 6.5(a)) are eliminated and zooplankton population went to extinction (Fig. 6.5(b)). Thus we can say that the defence system of phytoplankton against zooplankton is capable of wiping the oscillations present in the system and the zooplankton population. Our autonomous system (6.1) also showed the characteristic of multistability (Fig. 6.6) between three attractors; stable interior equilibrium, a stable limit cycle, and stable zooplankton free equilibrium. Further, we incorporated seasonality in model (6.1) to get model (6.2). In Fig. (6.6), we demonstrated the existence and global stability of periodic solution for non-autonomous system (6.2). The incarnation of seasonality in the autonomous system made it permanent (Fig. 6.7). Thus we can say that the seasonality promoted the coexistence of species in our system. For a particular set of parameters, system (6.2) manifested chaotic nature. To confirm the chaotic nature of this system, we have done the sensitivity analysis (Figs. 6.8(a)-6.8(d)). The sprinkled sampling points in the Poincare map (Fig. 6.8(e)) also support the presence of the chaotic attractor. Moreover, system (6.2) also exhibited multistability in complex ways. From Fig. 6.9, we can observe that the seasonal model is multistable with three types of attractors; a stable limit cycle (L_1), another stable limit cycle (L_2) and a chaotic attractor. Although, with some change in parameters it became multistable with; a period-1 limit cycle, a period-2 limit cycle and a period-4 limit cycle (Fig. 6.10). There is also switching in the stability (Fig. 6.11(a)-6.11(d)) when we vary the seasonal parameter u. We also calculated the maximum Lyapunov exponent (Fig. 6.11(e)) to verify the chaos and switching of stability which is pictured in the above bifurcation diagrams for u. The seasonal system showed a similar behaviour when we varied f (Fig. 6.12).

As we have extended the work of Mandal et al. [48], so we compare the model formulation and the results of this chapter with their work. In their research paper, they assume that zooplankton consume phytoplankton via Holling type II response and the reduction in zooplankton density due to toxicity of phytoplankton is governed by a function, $\frac{P^2}{\mu+P^2}$ (Holling type III response), where μ is half-saturation constant for the toxin release by phytoplankton. According to this assumption, even the low population density of phytoplankton contributes to

reducing the zooplankton density, although phytoplankton does not release toxic chemicals at low density. Thus to improve their model, we assume that zooplankton consumes phytoplankton via Holling type IV response. In this response, there is no decrement in functional response at the low density of phytoplankton. However, the response value decreases at high phytoplankton density, which abates zooplankton's density. Thus the response taken to deal with the phytoplankton-zooplankton interaction in the current work reflects the toxin-releasing mechanism of dense phytoplankton in a more realistic manner than the previous one. As nutrients play a vital role in plankton dynamics so to depict this role and make our model more comprehensive and realistic, we incorporated the nutrient-phytoplankton interaction in it. Therefore, we can observe that the current model is a more realistic and extensive version of the model given by [48].

One of the novel results in the non-seasonal model is that the defence mechanism of phytoplankton is capable of removing the oscillations present in the system, which can help in controlling the plankton blooms. Further, when we introduce seasonality in the non-seasonal model, chaos emerges for a set of parameters, making it more interesting to study. The non-seasonal, as well as seasonal models show different kinds of multistability, which demonstrate the noteworthy nature of the proposed work. To substantiate the results, we have also provided extensive numerical simulation work by drawing time series graphs, 1-D and 2-D bifurcation diagrams, basins of attraction, Poincare map, etc. All the above features, which are not discussed in previous study, make the present work more rigorous and reliable. This entire discussion captures the vibrant nature of the proposed work; as a result, it is anticipated that the work that has been put together will be able to help researchers to explore aquatic non-autonomous systems in more depth.

Conclusions and Future Directions

Conclusions

Mathematical modeling is an important tool for studying ecological interactions as it allows researchers to simulate and explore complex ecological systems in a quantitative manner. By using mathematical models, ecologists can develop a deeper understanding of how different species interact with one another and how they are influenced by various environmental factors. One of the primary benefits of mathematical modeling is that it allows researchers to make predictions about the behavior of ecological systems under different scenarios. By constructing models that reflect different aspects of ecological systems, researchers can explore the consequences of different assumptions and test the predictions of different ecological theories. In this thesis, we have attempted to study prey-predator (particularly phyoplankton-zooplankton) interactions with the inclusion of various physical parameters using the ordinary differential and delay differential equations.

In each model, we first proved the well-posedness of that model by demonstrating the positivity and boundedness of its solution. Then the existence of all possible equilibrium points is established, followed by their local and global stability analysis. Then we discussed all the possible bifurcations with respect to significant parameters involved in that particular model. Next, in the case of the delayed model, we did the local stability analysis for this. We did an extensive numerical simulation for each model to reflect its corresponding theoretical findings. In the numerical simulation, we drew various time-series graphs, different types of phase portraits, and bifurcation diagrams for non-chaotic as well as for chaotic systems; different kinds of basins of attractions are also drawn in case of multistabilities.

In Chapter 2, we put forth a prey-predator model that takes into account the influence of prey fear that the predator causes, as well as the prey's anti-predator behaviour in response to this fear. We observed that the rate of anti-predator behavior is an important parameter because the number of interior equilibrium points changes as the value of rate of anti-predator behavior varies. We studied the relationship between cost of fear and rate of anti-predator behavior. The non-delayed system in this chapter showed the property of bi-stability between two equilibrium points. We further noticed that, the delayed system suffered subcritical Hopf-bifurcation respect to both delays and underwent chaotic regime for high values of fear response delay.

In Chapter 3, categorising phytoplankton into the two groups of NTP and TPP, we investigated a phytoplankton-zooplankton system. To deal with zooplankton's interactions with TPP

and NTP, we choose generalised Holling type IV and Beddington-DeAngelis responses, respectively. When we change the TPP's inhibitory impact on zooplankton, it exhibits an unusual behaviour: an initial increase in its value promotes the proliferation of zooplankton species because less of the poisonous food is consumed. Because of the increased grazing pressure that zooplankton puts on NTP, this increase in zooplankton's population causes a decline in NTP population. However, as the zooplankton population depends entirely on NTP for survival, a further rise in this inhibitory impact results in a decrease in the population. The non-delayed system experienced Hopf and transcritical bifurcations with respect to different parameters. The interference parameter of the predator is also crucial to the system's dynamics. We notice that an increase in this interference causes zooplankton species' population densities to increase rather than decrease and this shift also helps regulate the periodic oscillations. By including two discrete delays, one to account for gestational delay and the other to assess the temporal lag caused by the TPP's cells maturing before they can release harmful chemicals, we further analyse the system's kinetics. A chaotic regime can be reached by increasing the second delay in a delayed system.

Chapter 4 is dedicated to a phytoplankton-zooplankton-fish system with increased fish food and anxiety of zooplankton due to fish. Holling type IV and type II responses handle the corresponding interactions. We observed that as fear rises to infinity, the fish population decreases until it reaches a point at which the coexistence equilibrium remains constant. Increasing the additional food quality can also help manage chaos at low levels of fear. This system demonstrated the relationship of multistability between a positive and a planner equilibrium and displayed the paradox of enrichment while using phytoplankton carrying capacity as the control parameter.

In Chapter 5, by combining both the characteristics linked to fear and its carry-over effects with all the necessary assumptions, we worked on the non-delayed and delayed PZF-population models. Simplified Holling type IV and II functional responses are postulated to govern the corresponding PZ and ZF interaction. We have theoretically demonstrated that the fish species saturates to a limited positive value for the carry-over effect parameter. The increase in zooplankton's PGR is the reason for the rise in the fish population. The non-delayed model flips its stability twice and passes through several periodic and chaotic windows before stabilizing, as seen by the variation of the COE parameter. Our non-delayed system exhibits the character of enrichment of paradox suffered and transcritical bifurcation. Because there is a latency and the carry-over effects are not immediate. We introduced a COE delay to make the non-delayed model more realistic and applicable. Most studies find that adding delay to a model makes it chaotic or periodic. However, there are rare cases when the presence of delay in an oscillatory system can render it stable by AD (amplitude death). In our approach, delay aids in chaos control by stabilizing it through the AD phenomenon.

In Chapter 6, we studied a seasonal $NPZT$-model with group defence of phytoplankton against zooplankton. We assumed that phytoplankton absorbs nutrients through the Holling type II response, whereas zooplankton consumes phytoplankton via Holling type IV response. We did a thorough analysis of the autonomous as well as non-autonomous models. Phytoplankton's inhibitory effect parameter played an observable role in the dynamics of the autonomous model. When this parameter increases, the oscillation in the system was eliminated, and the zooplankton population become extinct. Thus, the defence system of phytoplankton against zooplankton can wipe out the oscillations present in the system and the zooplankton population. Our autonomous system also showed the characteristic of multistability between three attractors; stable interior equilibrium, a stable limit cycle, and stable zooplankton-free equilibrium. The incarnation of seasonality in the autonomous system made it permanent. Thus we can say that seasonality promoted the coexistence of species in our system. For a particular set of parameters, a non-autonomous system manifested chaotic nature. The non-autonomous system exhibited multistability between different attractors. We noticed that our model is very complex and comprehensive as we have included the nutrient-phytoplankton interaction. We also showed that the seasonality in our model makes it permanent. Due to seasonality, the emergence of chaos in our model made it more interesting to study. Our model also demonstrated different kinds of multistability.

Future Directions

In this thesis, we worked on some ecological model by incorporating several important physical parameters. We investigated the complex kinetics of these models and have obtained significant outcomes. Future developments of our work can go in the following directions.

- In this thesis, we have worked on different kinds of local bifurcation, which are of codimension-1 basically; in the future, higher codimension and global bifurcations can also be explored.
- In this thesis, we have worked on temporal models, and in the future, this work be extended in spatial-temporal direction also.
- In the future more biological factors like; the Allee effect and predator taxis can be incorporated into the models. The predator taxis will make us learn new tools related to functional analysis.

Bibliography

[1] T. R. Malthus, *An Essay on the Principle of Population as it Affects the Future Improvement of Society, with Remarks on the Speculations of Mr. Goodwin, M. Condorcet, and Other Writers*. The Lawbook Exchange, Ltd., 1798.

[2] P.-F. Verhulst, "Notice sur la loi que la population suit dans son accroissement", *Correspondance Mathematique et Physique publiee par a*, vol. 10, pp. 113–126, 1838.

[3] A. J. Lotka, "Elements of physical biology", *Williams and Wilkins Company, Baltimore, 1925*,

[4] V. Volterra, *Variazioni e fluttuazioni del numero d'individui in specie animali conviventi*. Venezia, C. Ferrari, 1927.

[5] A. A. Berryman, "The orgins and evolution of predator-prey theory", *Ecology*, vol. 73, no. 5, pp. 1530–1535, 1992.

[6] J. Beddington, C. Free, and J. Lawton, "Dynamic complexity in predator-prey models framed in difference equations", *Nature*, vol. 255, no. 5503, p. 58, 1975.

[7] E. Venturino, "Epidemics in predator–prey models: Disease in the predators", *Math. Med. Biol.*, vol. 19, no. 3, pp. 185–205, 2002.

[8] C. Jost, O. Arino, and R. Arditi, "About deterministic extinction in ratio-dependent predator–prey models", *Bull. Math. Biol.*, vol. 61, no. 1, pp. 19–32, 1999.

[9] R. Gupta and P. Chandra, "Bifurcation analysis of modified Leslie–Gower predator–prey model with Michaelis–Menten type prey harvesting", *J. Math. Anal. Appl.*, vol. 398, no. 1, pp. 278–295, 2013.

[10] B Dubey, P. Chandra, and P. Sinha, "A model for fishery resource with reserve area", *Nonlinear Anal. Real World Appl.*, vol. 4, no. 4, pp. 625–637, 2003.

[11] X. Liu and L. Chen, "Complex dynamics of Holling type II Lotka–Volterra predator–prey system with impulsive perturbations on the predator", *Chaos, Solitons Fractals*, vol. 16, no. 2, pp. 311–320, 2003.

[12] Y. Huang, F. Chen, and L. Zhong, "Stability analysis of a prey–predator model with Holling type III response function incorporating a prey refuge", *Appl. Math. Comput.*, vol. 182, no. 1, pp. 672–683, 2006.

[13] S. J. Ali, N. M. Arifin, R. K. Naji, F. Ismail, and N. Bachok, "Analysis of ecological model with Holling type IV functional response", *Int. J. Appl. Math. Comput. Sci.*, vol. 106, no. 1, pp. 317–331, 2016.

[14] J. P. Tripathi, S. Abbas, and M. Thakur, "Dynamical analysis of a prey–predator model with Beddington–DeAngelis type function response incorporating a prey refuge", *Nonlinear Dyn.*, vol. 80, pp. 177–196, 2015.

[15] A. Kumar and B. Dubey, "Modeling the effect of fear in a prey–predator system with prey refuge and gestation delay", *Int. J. Bifurc. Chaos*, vol. 29, no. 14, p. 1 950 195, 2019.

[16] J. P. Tripathi, S. Tyagi, and S. Abbas, "Global analysis of a delayed density dependent predator–prey model with Crowley–Martin functional response", *Commun. Nonlinear Sci. Numer. Simul.*, vol. 30, pp. 45–69, 2016.

[17] Z. Tian-Wei-Tian, "Multiplicity of positive almost periodic solutions in a delayed Hassell–Varley-type predator–prey model with harvesting on prey", *Math. Methods Appl. Sci*, vol. 37, no. 5, pp. 686–697, 2014.

[18] F. Chen, L. Chen, and X. Xie, "On a Leslie–Gower predator–prey model incorporating a prey refuge", *Nonlinear Anal. Real World Appl.*, vol. 10, no. 5, pp. 2905–2908, 2009.

[19] B. Dubey, A. Kumar, and A. P. Maiti, "Global stability and hopf-bifurcation of prey-predator system with two discrete delays including habitat complexity and prey refuge", *Commun. Nonlinear Sci. Numer. Simul.*, vol. 67, pp. 528–554, 2019.

[20] B. Dubey and A. Kumar, "Dynamics of prey–predator model with stage structure in prey including maturation and gestation delays", *Nonlinear Dyn.*, vol. 96, no. 4, pp. 2653–2679, 2019.

[21] M. Banerjee and Y. Takeuchi, "Maturation delay for the predators can enhance stable coexistence for a class of prey–predator models", *J. Theor. Biol.*, vol. 412, pp. 154–171, 2017.

[22] Y. Kuang, *Delay Differential Equations*. University of California, 2012.

[23] S. Gakkhar and A. Singh, "Complex dynamics in a prey predator system with multiple delays", *Commun. Nonlinear Sci. Numer. Simul.*, vol. 17, no. 2, pp. 914–929, 2012.

[24] L. Perko, *Differential Equations and Dynamical Systems*. Springer Science & Business Media, 2013, vol. 7.

[25] A. Hastings, C. L. Hom, S. Ellner, P. Turchin, and H. C. J. Godfray, "Chaos in ecology: Is mother nature a strange attractor?", *Annu. Rev. Ecol. Evol. Syst.*, vol. 24, no. 1, pp. 1–33, 1993.

[26] D. Jana, "Chaotic dynamics of a discrete predator–prey system with prey refuge", *Appl. Math. Comput.*, vol. 224, pp. 848–865, 2013.

[27] S. L. Lima and L. M. Dill, "Behavioral decisions made under the risk of predation: A review and prospectus", *Can. J. Zool.*, vol. 68, no. 4, pp. 619–640, 1990.

[28] T. Caro, *Antipredator defenses in birds and mammals*. University of Chicago Press, 2005.

[29] L. B. Kats and L. M. Dill, "The scent of death: Chemosensory assessment of predation risk by prey animals", *Ecoscience*, vol. 5, no. 3, pp. 361–394, 1998.

[30] X. Wang, L. Zanette, and X. Zou, "Modelling the fear effect in predator–prey interactions", *J. Math. Biol.*, vol. 73, no. 5, pp. 1179–1204, 2016.

[31] R. P. Kaur, A. Sharma, and A. K. Sharma, "Impact of fear effect on plankton-fish system dynamics incorporating zooplankton refuge", *Chaos Solitons Fractals*, vol. 143, p. 110 563, 2021.

[32] D. Barman, J. Roy, H. Alrabaiah, P. Panja, S. P. Mondal, and S. Alam, "Impact of predator incited fear and prey refuge in a fractional order prey predator model", *Chaos Solitons Fractals*, vol. 142, p. 110 420, 2021.

[33] N. Pati, S. Garai, M. Hossain, G. Layek, and N. Pal, "Fear induced multistability in a predator-prey model", *Int. J. Bifurcat. Chaos*, vol. 31, no. 10, p. 2 150 150, 2021.

[34] B. K. Das, D. Sahoo, and G. Samanta, "Impact of fear in a delay-induced predator–prey system with intraspecific competition within predator species", *Math. Comput. Simul.*, vol. 191, pp. 134–156, 2022.

[35] P. K. Tiwari, M. Verma, S. Pal, Y. Kang, and A. K. Misra, "A delay nonautonomous predator–prey model for the effects of fear, refuge and hunting cooperation", *J. Biol. Syst.*, vol. 29, no. 04, pp. 927–969, 2021.

[36] J. Ghosh, B. Sahoo, and S. Poria, "Prey-predator dynamics with prey refuge providing additional food to predator", *Chaos Solitons Fractals*, vol. 96, pp. 110–119, 2017.

[37] P. Srinivasu, B. Prasad, and M Venkatesulu, "Biological control through provision of additional food to predators: A theoretical study", *Theor. Popul. Biol.*, vol. 72, no. 1, pp. 111–120, 2007.

[38] S. Nazmul, P. K. Tiwari, Y. Kang, and S. Pal, "A nonautonomous model for the interactive effects of fear, refuge and additional food in a prey–predator system", *J. Biol. Syst.*, vol. 29, no. 01, pp. 107–145, 2021.

[39] C. M. O'Connor, D. R. Norris, G. T. Crossin, and S. J. Cooke, "Biological carryover effects: Linking common concepts and mechanisms in ecology and evolution", *Ecosphere*, vol. 5, no. 3, pp. 1–11, 2014.

[40] J. C. Touchon, M. W. McCoy, J. R. Vonesh, and K. M. Warkentin, "Effects of plastic hatching timing carry over through metamorphosis in red-eyed treefrogs", *Ecology*, vol. 94, no. 4, pp. 850–860, 2013.

[41] M. De Block and R. Stoks, "Fitness effects from egg to reproduction: Bridging the life history transition", *Ecology*, vol. 86, no. 1, pp. 185–197, 2005.

[42] D. J. Marshall and S. G. Morgan, "Ecological and evolutionary consequences of linked life-history stages in the sea", *Curr. Biol.*, vol. 21, no. 18, R718–R725, 2011.

[43] D. R. Norris, "Carry-over effects and habitat quality in migratory populations", *Oikos*, vol. 109, no. 1, pp. 178–186, 2005.

[44] D. R. Norris, P. P. Marra, T. K. Kyser, T. W. Sherry, and L. M. Ratcliffe, "Tropical winter habitat limits reproductive success on the temperate breeding grounds in a migratory bird", *Proc. Royal Soc. B.*, vol. 271, no. 1534, pp. 59–64, 2004.

[45] M. C. Runge and P. P. Marra, "Modeling seasonal interactions in the population dynamics of migratory birds", *Birds of Two Worlds: The Ecology and Evolution of Migration(eds R. Greenberg & P.P. Marra), pp. 375– 389. Johns Hopkins University Press, Baltimore*, 2005.

[46] H. Li and Y. Takeuchi, "Dynamics of the density dependent and nonautonomous predator-prey system with beddington-deangelis functional response", *Discrete Contin. Dyn. Syst. Ser. B*, vol. 20, no. 4, p. 1117, 2015.

[47] D. Bai, J. Yu, M. Fan, and Y. Kang, "Dynamics for a non-autonomous predator-prey system with generalist predator", *J. Math. Anal. Appl.*, vol. 485, no. 2, p. 123 820, 2020.

[48] A. Mandal, P. K. Tiwari, S. Samanta, E. Venturino, and S. Pal, "A nonautonomous model for the effect of environmental toxins on plankton dynamics", *Nonlinear Dyn.*, vol. 99, no. 4, pp. 3373–3405, 2020.

[49] S. Biswas, P. Kumar Tiwari, and S. Pal, "Effects of toxicity and zooplankton selectivity on plankton dynamics under seasonal patterns of viruses with time delay", *Math. Methods Appl. Sci.*, vol. 45, no. 2, pp. 585–617, 2022.

[50] B. Mondal, S. Roy, U. Ghosh, and P. K. Tiwari, "A systematic study of autonomous and nonautonomous predator–prey models for the combined effects of fear, refuge, cooperation and harvesting", *Eur. Phys. J. Plus*, vol. 137, no. 6, p. 724, 2022.

[51] B. R. Moss, *Ecology of Fresh Waters: Man and Medium, Past to Future*. John Wiley & Sons, 2009.

[52] C. Holling, "The functional response of predators to prey density and its role in mimicry and population regulation", *Mem. Ent. Soc. Can.*, vol. 97, no. S45, pp. 5–60, 1965.

[53] J. F. Andrews, "A mathematical model for the continuous culture of microorganisms utilizing inhibitory substrates", *Biotechnol. Bioeng.*, vol. 10, no. 6, pp. 707–723, 1968.

[54] N. K. Thakur and A. Ojha, "Complex dynamics of delay-induced plankton–fish interaction exhibiting defense", *SN Appl. Sci.*, vol. 2, pp. 1–25, 2020.

[55] M. Kot, *Elements of mathematical ecology*. Cambridge University Press, 2001.

[56] R Arditi and H. Akçakaya, "Underestimation of mutual interference of predators", *Oecologia*, vol. 83, pp. 358–361, 1990.

[57] J. R. Beddington, "Mutual interference between parasites or predators and its effect on searching efficiency", *J. Anim. Ecol.*, pp. 331–340, 1975.

[58] C. Bandle and W. Reichel, "Solutions of quasilinear second-order elliptic boundary value problems via degree theory", *Stationary Partial Differential Equations, in: Handb. Differ. Equ*, vol. 1, pp. 1–70, 2004.

[59] J. Muscat, *Functional Analysis: An Introduction to Metric Spaces, Hilbert spaces, and Banach algebras*. Springer, 2014.

[60] K. Gopalsamy, *Stability and Oscillations in Delay Differential Equations of Population Dynamics*. Springer Science & Business Media, 2013, vol. 74.

[61] R. E. Gaines and J. L. Mawhin, *Coincidence Degree and Nonlinear Differential Equations*. Springer, 2006, vol. 568.

[62] S. Ahmad and M. R. M. Rao, *Theory of Ordinary Differential Equations: With Applications of Biology and Engineering*. Affiliated East-West Private Lmt., 1999.

[63] D. Xue, "Differential equation solutions with matlab®", in *Differential Equation Solutions with MATLAB®*, De Gruyter, 2020.

[64] P. Panday, N. Pal, S. Samanta, and J. Chattopadhyay, "Stability and bifurcation analysis of a three-species food chain model with fear", *Int. J. Bifurcat. Chaos.*, vol. 28, no. 01, p. 1 850 009, 2018.

[65] A. Das and G. Samanta, "Modeling the fear effect on a stochastic prey–predator system with additional food for the predator", *J. Phys., A*, vol. 51, no. 46, p. 465 601, 2018.

[66] S. Creel, D. Christianson, S. Liley, and J. A. Winnie, "Predation risk affects reproductive physiology and demography of elk", *Science*, vol. 315, no. 5814, pp. 960–960, 2007.

[67] E. L. Preisser and D. I. Bolnick, "The many faces of fear: Comparing the pathways and impacts of nonconsumptive predator effects on prey populations", *PLoS One*, vol. 3, no. 6, e2465, 2008.

[68] L. Y. Zanette, A. F. White, M. C. Allen, and M. Clinchy, "Perceived predation risk reduces the number of offspring songbirds produce per year", *Science*, vol. 334, no. 6061, pp. 1398–1401, 2011.

[69] P. Panday, S. Samanta, N. Pal, and J. Chattopadhyay, "Delay induced multiple stability switch and chaos in a predator–prey model with fear effect", *Math. Comput. Simul.*, vol. 172, 134–158, 2020.

[70] C. J. Barnard, *Animal behaviour: ecology and evolution*. Springer Science & Business Media, 2012.

[71] A. R. Ives and A. P. Dobson, "Antipredator behavior and the population dynamics of simple predator-prey systems", *Am. Nat.*, vol. 130, no. 3, pp. 431–447, 1987.

[72] H. Matsuda, P. A. Abrams, and M. Hori, "The effect of adaptive anti-predator behavior on exploitative competition and mutualism between predators", *Oikos*, vol. 68, pp. 549–559, 1993.

[73] J. Liu and X. Zhang, "Stability and Hopf bifurcation of a delayed reaction–diffusion predator–prey model with anti-predator behaviour", *Nonlinear Anal. Model. Control*, vol. 24, no. 3, pp. 387–406, 2019.

[74] K. Chakraborty, S. Haldar, and T. Kar, "Global stability and bifurcation analysis of a delay induced prey-predator system with stage structure", *Nonlinear Dyn.*, vol. 73, no. 3, pp. 1307–1325, 2013.

[75] L. Deng, X. Wang, and M. Peng, "Hopf bifurcation analysis for a ratio-dependent predator–prey system with two delays and stage structure for the predator", *Appl. Math. Comput.*, vol. 231, pp. 214–230, 2014.

[76] K. Li and J. Wei, "Stability and Hopf bifurcation analysis of a prey–predator system with two delays", *Chaos, Solitons Fractals*, vol. 42, no. 5, pp. 2606–2613, 2009.

[77] M. Liao, X. Tang, and C. Xu, "Bifurcation analysis for a three-species predator–prey system with two delays", *Commun. Nonlinear Sci. Numer. Simul.*, vol. 17, no. 1, pp. 183–194, 2012.

[78] C. Xu and P. Li, "Dynamical analysis in a delayed predator-prey model with two delays", *Discrete Dyn. Nat. Soc.*, vol. 2012, 2012.

[79] X.-P. Yan and Y.-D. Chu, "Stability and bifurcation analysis for a delayed Lotka–Volterra predator–prey system", *J. Comput. Appl. Math*, vol. 196, no. 1, pp. 198–210, 2006.

[80] X. Wang and X. Liu, "Stability and Hopf bifurcation of a delayed ratio-dependent eco-epidemiological model with two time delays and Holling type III functional response", *Int. J. Nonlinear Sci.*, vol. 23, no. 2, pp. 102–108, 2017.

[81] S Nakaoka, Y Saito, and Y Takeuchi, "Stability, delay, and chaotic behavior in a Lotka-Volterra predator-prey system", *Math. Biosci. Eng.*, vol. 3, no. 1, p. 173, 2006.

[82] K. D. Prasad and B. Prasad, "Qualitative analysis of additional food provided predator–prey system with anti-predator behaviour in prey", *Nonlinear Dyn.*, vol. 96, no. 3, pp. 1765–1793, 2019.

[83] B. D. Hassard, B. Hassard, N. D. Kazarinoff, Y.-H. Wan, and Y. W. Wan, *Theory and Applications of Hopf Bifurcation*. CUP Archive, 1981, vol. 41.

[84] Y. Song and J. Wei, "Bifurcation analysis for chen's system with delayed feedback and its application to control of chaos", *Chaos Solitons Fractals*, vol. 22, no. 1, pp. 75–91, 2004.

[85] G. A. Bocharov and F. A. Rihan, "Numerical modelling in biosciences using delay differential equations", *J. Comput. Appl. Math.*, vol. 125, no. 1-2, pp. 183–199, 2000.

[86] A. Bellen and M. Zennaro, *Numerical Methods for Delay Differential Equations*. Oxford University Press, 2013.

[87] A. M. Edwards and J. Brindley, "Oscillatory behaviour in a three-component plankton population model", *Int. J. Struct. Stab. Dyn.*, vol. 11, no. 4, pp. 347–370, 1996.

[88] A. M. Edwards, "Adding detritus to a nutrient–phytoplankton–zooplankton model: A dynamical-systems approach", *J. Plankton Res.*, vol. 23, no. 4, pp. 389–413, 2001.

[89] J Chattopadhyay, R. R. Sarkar, and A El Abdllaoui, "A delay differential equation model on harmful algal blooms in the presence of toxic substances", *Math. Med. Biol.*, vol. 19, no. 2, pp. 137–161, 2002.

[90] S. Roy, S. Bhattacharya, P. Das, and J. Chattopadhyay, "Interaction among non-toxic phytoplankton, toxic phytoplankton and zooplankton: Inferences from field observations", *J. Biol. Phys.*, vol. 33, no. 1, pp. 1–17, 2007.

[91] A Barreiro, C Guisande, I Maneiro, A. Vergara, I. Riveiro, and P Iglesias, "Zooplankton interactions with toxic phytoplankton: Some implications for food web studies and algal defence strategies of feeding selectivity behaviour, toxin dilution and phytoplankton population diversity", *Acta. Oecol.*, vol. 32, no. 3, pp. 279–290, 2007.

[92] R. Pal, D. Basu, and M. Banerjee, "Modelling of phytoplankton allelopathy with Monod–Haldane-type functional response—a mathematical study", *BioSystems*, vol. 95, no. 3, pp. 243–253, 2009.

[93] T. Zhang and W. Wang, "Hopf bifurcation and bistability of a nutrient–phytoplankton–zooplankton model", *Appl. Math. Model.*, vol. 36, no. 12, pp. 6225–6235, 2012.

[94] R. K. Upadhyay, A. Patra, B Dubey, and N. Thakur, "A predator–prey interaction model with self-and cross-diffusion in aquatic systems", *J. Biol. Syst.*, vol. 22, no. 04, pp. 691–712, 2014.

[95] J. T. Turner and P. A. Tester, "Zooplankton feeding ecology: Copepod grazing during an expatriate red tide", in *Novel Phytoplankton Blooms*, Springer, 1989, pp. 359–374.

[96] M. Schultz and T. Kiørboe, "Active prey selection in two pelagic copepods feeding on potentially toxic and non-toxic dinoflagellates", *J. Plankton Res.*, vol. 31, no. 5, pp. 553–561, 2009.

[97] L. Dionisio Pires and E Van Donk, "Comparing grazing by dreissena polymorpha on phytoplankton in the presence of toxic and non-toxic cyanobacteria", *Freshw. Biol.*, vol. 47, no. 10, pp. 1855–1865, 2002.

[98] S. Chakraborty, S. Bhattacharya, U. Feudel, and J Chattopadhyay, "The role of avoidance by zooplankton for survival and dominance of toxic phytoplankton", *Ecol. Complex.*, vol. 11, pp. 144–153, 2012.

[99] M. Javidi and B. Ahmad, "Dynamic analysis of time fractional order phytoplankton-toxic phytoplankton-zooplankton system", *Ecol. Modell.*, vol. 318, pp. 8–18, 2015.

[100] T. Chowdhury, S. Roy, and J. Chattopadhyay, "Modeling migratory grazing of zooplankton on toxic and non-toxic phytoplankton", *Appl. Math. Comput.*, vol. 197, no. 2, pp. 659–671, 2008.

[101] M. Banerjee and E. Venturino, "A phytoplankton–toxic phytoplankton–zooplankton model", *Ecol. Complex.*, vol. 8, no. 3, pp. 239–248, 2011.

[102] H. Freedman and P. Waltman, "Persistence in models of three interacting predator-prey populations", *Math. Biosci.*, vol. 68, no. 2, pp. 213–231, 1984.

[103] M. Kuwamura and H. Chiba, "Mixed-mode oscillations and chaos in a prey-predator system with dormancy of predators", *Chaos*, vol. 19, no. 4, p. 043 121, 2009.

[104] Q. Gan, R. Xu, and P. Yang, "Bifurcation and chaos in a ratio-dependent predator–prey system with time delay", *Chaos Solitons Fractals*, vol. 39, no. 4, pp. 1883–1895, 2009.

[105] J. Wang and W. Jiang, "Bifurcation and chaos of a delayed predator-prey model with dormancy of predators", *Nonlinear Dyn.*, vol. 69, no. 4, pp. 1541–1558, 2012.

[106] J. Banerjee, S. K. Sasmal, and R. K. Layek, "Supercritical and subcritical hopf-bifurcations in a two-delayed prey–predator system with density-dependent mortality of predator and strong allee effect in prey", *BioSystems*, vol. 180, pp. 19–37, 2019.

[107] M. Rehim and M. Imran, "Dynamical analysis of a delay model of phytoplankton–zooplankton interaction", *Appl. Math. Model.*, vol. 36, no. 2, pp. 638–647, 2012.

[108] A. Misra, P. Tiwari, and P. Chandra, "Modeling the control of algal bloom in a lake by applying some external efforts with time delay", *Differ. Equ. Dyn. Syst.*, pp. 1–30, 2017.

[109] X. Liu and Q. Huang, "The dynamics of a harvested predator–prey system with Holling type–IV functional response", *Biosystems*, vol. 169, pp. 26–39, 2018.

[110] R. S. Cantrell and C. Cosner, "On the dynamics of predator–prey models with the Beddington–DeAngelis functional response", *J. Math. Anal. Appl.*, vol. 257, no. 1, pp. 206–222, 2001.

[111] R. K. Upadhyay, N. Thakur, and V. Rai, "Diffusion-driven instabilities and spatio-temporal patterns in an aquatic predator–prey system with Beddington–Deangelis type functional response", *Int. J. Bifurc. Chaos*, vol. 21, no. 03, pp. 663–684, 2011.

[112] Y. Wang, H. Wang, and W. Jiang, "Hopf-transcritical bifurcation in toxic phytoplankton–zooplankton model with delay", *J. Math. Anal. Appl.*, vol. 415, no. 2, pp. 574 –594, 2014.

[113] J. E. Havel, "Predator-induced defenses: A review", *Predation: Direct and Indirect Impacts on Aquatic Communities*, pp. 263–278, 1987.

[114] Z. M. Gliwicz, "Relative significance of direct and indirect effects of predation by planktivorous fish on zooplankton", *Hydrobiologia*, vol. 272, no. 1, pp. 201–210, 1994.

[115] F. Hua, K. E. Sieving, R. J. Fletcher Jr, and C. A. Wright, "Increased perception of predation risk to adults and offspring alters avian reproductive strategy and performance", *Behav. Ecol.*, vol. 25, no. 3, pp. 509–519, 2014.

[116] J. Wang, Y. Cai, S. Fu, and W. Wang, "The effect of the fear factor on the dynamics of a predator-prey model incorporating the prey refuge", *Chaos*, vol. 29, no. 8, p. 083 109, 2019.

[117] B. Dubey, Sajan, and A. Kumar, "Stability switching and chaos in a multiple delayed prey–predator model with fear effect and anti-predator behavior", *Math. Comput. Simul.*, vol. 188, pp. 164–192, 2021.

[118] B. Prasad, M. Banerjee, and P. Srinivasu, "Dynamics of additional food provided predator–prey system with mutually interfering predators", *Math. Biosci.*, vol. 246, no. 1, pp. 176–190, 2013.

[119] B. Sahoo and S. Poria, "The chaos and control of a food chain model supplying additional food to top-predator", *Chaos Solitons Fractals*, vol. 58, pp. 52–64, 2014.

[120] S. Samaddar, M. Dhar, and P. Bhattacharya, "Effect of fear on prey–predator dynamics: Exploring the role of prey refuge and additional food", *Chaos*, vol. 30, no. 6, p. 063 129, 2020.

[121] J. E. Marsden and M. McCracken, *The Hopf Bifurcation and its Applications*. Springer Science & Business Media, 2012, vol. 19.

[122] M. Gao, H. Shi, and Z. Li, "Chaos in a seasonally and periodically forced phytoplankton–zooplankton system", *Nonlinear Anal. Real World Appl.*, vol. 10, no. 3, pp. 1643–1650, 2009.

[123] K. Pyragas, "Control of chaos via extended delay feedback", *Phys. Lett. A*, vol. 206, no. 5-6, pp. 323–330, 1995.

[124] R. K. Upadhyay, S. Iyengar, and V. Rai, "Chaos: An ecological reality?", *Int. J. Bifurcat. Chaos.*, vol. 8, no. 06, pp. 1325–1333, 1998.

[125] S. Boccaletti, C. Grebogi, Y.-C. Lai, H. Mancini, and D. Maza, "The control of chaos: Theory and applications", *Phys. Rep.*, vol. 329, no. 3, pp. 103–197, 2000.

[126] A. K. Misra, R. K. Singh, P. K. Tiwari, S. Khajanchi, and Y. Kang, "Dynamics of algae blooming: Effects of budget allocation and time delay", *Nonlinear Dyn.*, vol. 100, no. 2, pp. 1779–1807, 2020.

[127] Sajan and B. Dubey, "Chaos control in a multiple delayed phytoplankton–zooplankton model with group defense and predator's interference", *Chaos*, vol. 31, no. 8, p. 083 101, 2021.

[128] R. Motro, I. Ayalon, and A. Genin, "Near-bottom depletion of zooplankton over coral reefs: III: Vertical gradient of predation pressure", *Coral Reefs*, vol. 24, no. 1, pp. 95–98, 2005.

[129] S. K. Sasmal, "Population dynamics with multiple allee effects induced by fear factors–a mathematical study on prey-predator interactions", *Appl. Math. Model.*, vol. 64, pp. 1–14, 2018.

[130] A. Ojha and N. K. Thakur, "Exploring the complexity and chaotic behavior in plankton–fish system with mutual interference and time delay", *BioSystems*, vol. 198, p. 104 283, 2020.

[131] N. K. Thakur, A. Ojha, D. Jana, and R. K. Upadhyay, "Modeling the plankton–fish dynamics with top predator interference and multiple gestation delays", *Nonlinear Dyn.*, vol. 100, pp. 4003–4029, 2020.

[132] Z. Jiang, X. Bi, T. Zhang, and B. Pradeep, "Global hopf bifurcation of a delayed phytoplankton-zooplankton system considering toxin producing effect and delay dependent coefficient", *Math. Biosci. Eng*, vol. 16, no. 5, pp. 3807–3829, 2019.

[133] K. Sarkar and S. Khajanchi, "Impact of fear effect on the growth of prey in a predator-prey interaction model", *Ecol. Complex.*, vol. 42, p. 100 826, 2020.

[134] D. Schaeffer and J. W. Cain, *Ordinary Differential Equations: Basics and Beyond*. Springer, 2018.

[135] H. Zhang, Y. Cai, S. Fu, and W. Wang, "Impact of the fear effect in a prey-predator model incorporating a prey refuge", *Appl. Math. Comput.*, vol. 356, pp. 328–337, 2019.

[136] M. L. Rosenzweig, "Paradox of enrichment: Destabilization of exploitation ecosystems in ecological time", *Science*, vol. 171, no. 3969, pp. 385–387, 1971.

[137] M. E. Gilpin and M. L. Rosenzweig, "Enriched predator-prey systems: Theoretical stability", *Science*, vol. 177, no. 4052, pp. 902–904, 1972.

[138] J. P. Grover, "Competition, herbivory, and enrichment: Nutrient-based models for edible and inedible plants", *Am. Midl. Nat.*, vol. 145, no. 5, pp. 746–774, 1995.

[139] S. Roy and J Chattopadhyay, "The stability of ecosystems: A brief overview of the paradox of enrichment", *J. Biosci.*, vol. 32, no. 2, pp. 421–428, 2007.

[140] G. Harris, *Phytoplankton Ecology: Structure, Function and Fluctuation*. Springer Science & Business Media, 2012.

[141] C. E. Cressler, A. A. King, and E. E. Werner, "Interactions between behavioral and life-history trade-offs in the evolution of integrated predator-defense plasticity", *Am. Nat.*, vol. 176, no. 3, pp. 276–288, 2010.

[142] J. S. Brown and B. P. Kotler, "Hazardous duty pay and the foraging cost of predation", *Ecol. Lett.*, vol. 7, no. 10, pp. 999–1014, 2004.

[143] W Cresswell and J. Quinn, "Faced with a choice, sparrowhawks more often attack the more vulnerable prey group", *Oikos*, vol. 104, no. 1, pp. 71–76, 2004.

[144] S. Creel and D. Christianson, "Relationships between direct predation and risk effects", *Trends Ecol. Evol.*, vol. 23, no. 4, pp. 194–201, 2008.

[145] W. Cresswell, "Predation in bird populations", *J. Ornithol.*, vol. 152, no. 1, pp. 251–263, 2011.

[146] S. K. Sasmal and D. Ghosh, "Effect of dispersal in two-patch prey–predator system with positive density dependence growth of preys", *Biosystems*, vol. 151, pp. 8–20, 2017.

[147] S. H. Strogatz, "Death by delay", *Nature*, vol. 394, no. 6691, pp. 316–317, 1998.

[148] A. Koseska, E. Volkov, and J. Kurths, "Transition from amplitude to oscillation death via turing bifurcation", *Phys. Rev. Lett.*, vol. 111, no. 2, p. 024 103, 2013.

[149] S. K. Sasmal and Y. Takeuchi, "Modeling the allee effects induced by cost of predation fear and its carry-over effects", *J. Math. Anal. Appl.*, vol. 505, no. 2, p. 125 485, 2022.

[150] K. H. Elliott, G. S. Betini, and D. R. Norris, "Fear creates an allee effect: Experimental evidence from seasonal populations", *Proc. Royal Soc. B*, vol. 284, no. 1857, p. 20 170 878, 2017.

[151] Sajan, S. K. Sasmal, and B. Dubey, "A phytoplankton–zooplankton–fish model with chaos control: In the presence of fear effect and an additional food", *Chaos*, vol. 32, no. 1, p. 013 114, 2022.

[152] S. K. Sasmal and Y. Takeuchi, "Dynamics of a predator-prey system with fear and group defense", *J. Math. Anal. Appl.*, vol. 481, no. 1, p. 123 471, 2020.

[153] S. Mondal and G. Samanta, "A comparison study of predator–prey system in deterministic and stochastic environments influenced by fear and its carry-over effects", *Eur. Phys. J. Plus*, vol. 137, no. 1, pp. 1–31, 2022.

[154] A. Huppert, R. Olinky, and L. Stone, "Bottom-up excitable models of phytoplankton blooms", *Bull. Math. Biol.*, vol. 66, no. 4, pp. 865–878, 2004.

[155] P. B. Tchounwou, C. G. Yedjou, A. K. Patlolla, and D. J. Sutton, "Heavy metal toxicity and the environment", *In: Luch, A. (eds) Molecular, Clinical and Environmental Toxicology. Experientia Supplementum*, vol. 101, pp. 133–164, 2012.

[156] B Dubey and J Hussain, "Modelling the interaction of two biological species in a polluted environment", *J. Math. Anal. Appl.*, vol. 246, no. 1, pp. 58–79, 2000.

[157] S. Rana, S. Samanta, S. Bhattacharya, K. Al-Khaled, A. Goswami, and J. Chattopadhyay, "The effect of nanoparticles on plankton dynamics: A mathematical model", *BioSystems*, vol. 127, pp. 28–41, 2015.

[158] S. Ruan, "Persistence and coexistence in zooplankton-phytoplankton-nutrient models with instantaneous nutrient recycling", *J. Math. Biol.*, vol. 31, no. 6, pp. 633–654, 1993.

[159] T. K. Kar and A. Ghorai, "Dynamic behaviour of a delayed predator–prey model with harvesting", *Appl. Math. Comput.*, vol. 217, no. 22, pp. 9085–9104, 2011.

[160] J. Shukla and B Dubey, "Modelling the depletion and conservation of forestry resources: Effects of population and pollution", *J. Math. Biol.*, vol. 36, no. 1, pp. 71–94, 1997.

[161] S. Chakraborty, P. Tiwari, A. Misra, and J Chattopadhyay, "Spatial dynamics of a nutrient–phytoplankton system with toxic effect on phytoplankton", *Mathematical Biosciences*, vol. 264, pp. 94–100, 2015.

[162] P. K. Tiwari, S. Roy, A. K. Misra, and R. K. Upadhyay, "Effect of seasonality on a nutrient–plankton system with toxicity in the presence of refuge and additional food", *Eur. Phys. J. Plus*, vol. 137, no. 3, pp. 1–24, 2022.

[163] B Mukhopadhyay and R Bhattacharyya, "Modelling phytoplankton allelopathy in a nutrient-plankton model with spatial heterogeneity", *Ecological modelling*, vol. 198, no. 1-2, pp. 163–173, 2006.

[164] A. Sharma, A. K. Sharma, and K. Agnihotri, "Analysis of a toxin producing phytoplankton–zooplankton interaction with holling iv type scheme and time delay", *Nonlinear Dynamics*, vol. 81, pp. 13–25, 2015.

[165] P. Panja, S. K. Mondal, and D. K. Jana, "Effects of toxicants on phytoplankton-zooplankton-fish dynamics and harvesting", *Chaos Solitons Fractals*, vol. 104, pp. 389–399, 2017.

[166] N. K. Thakur, A. Ojha, P. K. Tiwari, and R. K. Upadhyay, "An investigation of delay induced stability transition in nutrient-plankton systems", *Chaos Solitons Fractals*, vol. 142, p. 110 474, 2021.

[167] M. Hossain, S. Pal, P. Kumar Tiwari, and N. Pal, "Bifurcations, chaos, and multistability in a nonautonomous predator–prey model with fear", *Chaos*, vol. 31, no. 12, p. 123 134, 2021.

List of Publications

Published/ Accepted

1. B. Dubey, **Sajan** and A. Kumar, Stability switching and chaos in a multiple delayed prey–predator model with fear effect and anti-predator behavior, *Mathematics and Computers in Simulation*, **188**:164–192, 2021.
   (Impact Factor **3.601**, Indexed in **SCI**, Q2)
   (https://doi.org/10.1016/j.matcom.2021.03.037)

2. **Sajan** and B. Dubey, Chaos control in a multiple delayed phytoplankton-zooplankton model with group defence and predator's interference, *Chaos*, **31**:083101, 2021.
   (Impact Factor **3.741**, Indexed in **SCI**, Q1)
   (https://doi.org/10.1063/5.0054261)

3. **Sajan**, S.K. Sasmal and B. Dubey, A phytoplankton-zooplankton-fish model with chaos control: In the presence of fear effect and an additional food, *Chaos*, **32**:013114, 2022.
   (Impact Factor **3.741**, Indexed in **SCI**, Q1)
   (https://doi.org/10.1063/5.0069474)

4. **Sajan**, B. Dubey and S.K. Sasmal, Chaotic dynamics of a plankton-fish system with fear and its carry over effects in the presence of a discrete delay, *Chaos, Solitions & Fractals*, **160**:112245, 2022.
   (Impact Factor **9.922**, Indexed in **SCI**, Q1)
   (https://doi.org/10.1016/j.chaos.2022.112245)

5. **Sajan**, A. Kumar and B. Dubey, Stability Switching in a Cooperative Prey-Predator Model with Transcritical and Hopf-bifurcations, In: S. Banerjee and A. Saha, *Nonlinear Dynamics and Applications, Springer Proceedings in Complexity, Springer*, 987-1000, 2022.
   (https://doi.org/10.1007/978-3-030-99792-2_84)

6. Massom Bhargava, **Sajan** and B. Dubey, Trade-off and chaotic dynamics of prey-predator system with two discrete delays, *Chaos*, **33**:053120, 2023.
   (Impact Factor **3.741**, Indexed in **SCI**, Q1)
   (https://doi.org/10.1063/5.0144182)

7. **Sajan**, K.K. Chaudhary and B. Dubey, A non-autonomous approach to study the impact of environmental toxins on nutrient-plankton system, *Applied Mathematics and Computation*, **458**:128236, 2023.
   (Impact Factor **4**, Indexed in **SCI**, Q1)
   (https://doi.org/10.1016/j.amc.2023.128236)

Workshops/Conferences

1. National Conference on Modeling, Analysis & Simulation (MAS-2019), Department of Mathematics, IIT (ISM) Dhanbad, India, (16-18 Dec. 2019).

2. A Seven-Day Workshop on Academic Writing, Department of Humanities and Social Sciences, BITS Pilani, Pilani Campus, (5-11 April 2019).

3. International Conference on Advances in Differential Equations and Numerical Analysis (ADENA-2020), Department of Mathematics, IIT Guwahati, India, (12-15 Oct. 2020).

4. Workshop on Bio-Mathematics (WoBM-2020), IIT Patna, India, (8-11 Dec. 2020).

5. International Conference on Nonlinear Dynamics and Applications (ICNDA-2022), Department of Mathematics, Sikkim Manipal Institute of Technology, Sikkim Manipal University, (9-11 March 2022).

6. International Conference on Advances in Biomathematics (ICABM-2022), Amity School of Applied Sciences, Amity University, Lucknow Campus, India, (21-23 July 2022).

Brief Biography of the Supervisor

Prof. Balrarn Dubey is Professor and Former Head of the Department of Mathematics, Birla Institute of Technology & Science, Pilani, Pilani Campus, India. He earned his Bachelor's Degree (B.Sc. Hons) with first rank of merit from Bhagalpur University, Bhagalpur, India in 1988. He received his Master's degree in 1990 and Ph.D. degree in 1994 from Department of Mathematics, Indian Institute of Technology Kanpur. Kanpur, India. He was Research Associate in IIT Kanpur from 1994-1995 and later he joined IIT Kanpur as visiting faculty during 2000-2002. He was awarded with "Best Teaching Award" for tutorship in MATH1102 in 2001 at IIT Kanpur. Prof. Dubey served as Lecturer and Senior Lecturer in Department of Mathematics, Tezpur University, India during 1995-2000. There he guided two students. In 2002 he joined Department of Mathematics, Birla Institute of Technology & Science, Pilani, Pilani Campus as an Assistant Professor. He got promoted to Associate Professor in August 2010 and Professor in February 2013. His research interests are Mathematical Biology, Mathematical Ecology, Ecotoxicology, Soil Erosion and Conservation, Epidemiology, Mathematical Immunology, and Applications of ODEs & PDEs in Real world Problems. As a result of his research accomplishment, he has published more than 100 research articles in national and international journals of repute. He is also the author of the book "Introductory Linear Algebra", Asian Books, Pvt. Ltd. 2007. He has successfully guided 5 Ph.D. students.

Brief Biography of the Candidate

Sajan earned his Bachelor's and Master's degree in Mathematics from Chaudhary Devi Lal University, Sirsa, Haryana in 2015 and 2018, respectively. After completing Master's, he got admission to Ph.D. program in Department of Mathematics, Birla Institute of Technology & Science, Pilani, Pilani Campus, India in January 2019 under the guidance of Prof. Balram Dubey. He has published five articles in peer reviewed international journals and presented three papers in national and international conferences. He has qualified CSIR NET-JRF exam in June 2018. At present, he is a Senior Research Fellow under CSIR, New Delhi, India.